AUTHOR: ADEGBOTOLU, U.V.

TITLE: Demulsification and recycling of spent oil based drilling fluid as nanofiller for polyamide 6 nanocomposites.

YEAR: 2016

URENNA VIVIAN ADEGBOTOLU

DEMULSIFICATION AND RECYCLING OF SPENT OIL BASED DRILLING FLUID AS NANOFILLER FOR POLYAMIDE 6 NANOCOMPOSITES

SCHOOL OF ENGINEERING

PhD THESIS

SCHOOL OF ENGINEERING

PhD THESIS

URENNA VIVIAN ADEGBOTOLU

Demulsification and Recycling of Spent Oil Based Drilling Fluid as Nanofiller for Polyamide 6 Nanocomposites

Supervisors:

Dr. Kyari Yates
Dr. James Njuguna
Dr. Kerr Matthews

September 2016

This thesis is submitted in partial fulfilment of the requirements for the Degree of Doctor of Philosophy

Declaration

I hereby declare that the research reported in this thesis is original and have been completed independently by myself (Urenna Vivian Adegbotolu), under the supervision of Dr Kyari Yates, Dr James Njuguna and Dr Kerr Matthews. This PhD thesis has not been submitted for the award of any other degree or professional qualification.

Where other sources are quoted full references are given.

Urenna Vivian Adegbotolu

September, 2016

Dedication

"Seek ye first the kingdom of God and His righteousness, and all these things shall be added unto you". Matthew 6:33 (The Holy Bible, King James Version)

This PhD research is dedicated to God Almighty – My Lover and Friend, who makes all things possible

Acknowledgement

I would like to give my most special thanks to our God Almighty, my Strength, my Deliverer and my Friend. I would like to express my heartfelt thanks to my supervisors, Dr Kyari Yates, Dr James Njuguna and Dr Kerr Matthews for their excellent academic supervision, advice, encouragement and constant support throughout this PhD. I wish to thank other lecturers, technicians and students as well as for their assistance, review and comments on the study.

I am thankful to all my colleagues in the School of Engineering, School of Pharmacy and Life Sciences especially Prof Pat Pollard (former supervisor (retired)) and University of Cracow Polymer Technology Research group (Prof Krzysztof Pielichowski, Dr Agnieszka Leszczynska, and Dr Tomasz Majak) for their support.

Sincere thanks also go to all my friends inside and outside the university for all their support, encouragement and love prior and during my research study. I appreciate the support of Prof Edward Gobina, Prof Babs Oyeneyin, Beth, Njideka, Izu, Bruno Agochukwu, Kristof Starost, Shohel Siddique, Laud Ochei, Sarah Nwinee, Lorraine Bakah-Kwoffie, Kofi Addae-Afoakwa, Maureen Ani, Elizabeth Wuyep, Roland Tebowei, Blessing Onyemejor, Mrs O. Okerinde, Mrs A. Crown, Joseph and Joshua Crown.

I appreciate the support and prayers of my pastor, Femi Labeodan and the family of RCCG, Montrose Tabernacle for All Nations. To all my friends and families too numerous to mention, I appreciate all your support.

My profound gratitude goes to all my parents, Sir and Lady Dr (Mrs) M.N.A. Ekeh and Mrs Josephine Adegbotolu, my siblings Obinna, Uchechi, Chikezie and Chibuike, other family members and in-laws Femi and Dotun Adegbotolu, Uche Ekeh and their families for their prayers wise words and assistance. I deeply thank my blessed husband, Oladipo Adegbotolu and my blessed children, Ifeoluwa and Samuel Adegbotolu for their love, considerations, encouragement, tolerance and for being my constant sources of inspiration. They were my encouragers; I would not have the opportunity to finish this study without their support.

My special appreciation goes to Petroleum Development Technology Fund (PTDF) Nigeria for funding this PhD research and to the Executive Secretaries (Past and Present) and the staff for their assistance and support throughout the duration of this research.

Abstract

Spent oil based drilling fluid and cutting wastes are global liabilities due to their hazardous hydrocarbon content which impacts negatively on flora, fauna, and global carbon footprint. The formulation of two demulsifiers to ensure chemically enhanced phase separation of this waste into oil, water and solid components was successfully carried out in addition to recycling the solid phase into PA6 nanocomposite materials. Initial characterisation of the untreated waste was carried out by Fourier Transform Infra Red (FTIR) for total petroleum hydrocarbon (TPH) analysis, Inductively coupled plasma optical emission spectrometry (ICPOES) for quantitative elemental analysis and Energy dispersive xray analysis (EDXA) for qualitative elemental composition amongst other characterisation methods. The analysis showed that the sample had a high hydrocarbon load of 662,500mg/kg and a high heavy metal load for Pb of 122mg/kg. No As, Cd, Hg were detected. The demulsifier formulations were composed of isopropanol, sodium dodecyl sulphate, poloxamer, sodium chloride, chitosan in 0.2M acetic acid and deionised water for demulsifier S4 and addition of phosphoric acid for demulsifier S3. Hydrocarbon reduction on the extracted solid phase nanofiller S3 and nanofiller S4 was 98.6% and 98.5% respectively after demulsification. The demulsified spent oil based drilling fluid solid extracts were below OSPAR regulation of <1% oil on cutting by weight. However, recycling of the recovered solid was carried out in order to achieve environmentally sustainable management of the waste in Polyamide 6 (PA6) nanocomposite manufacture/fabrication. The formulation of different blends of PA6 nanocomposite materials from untreated, demulsifier treated and thermally treated drilling fluid and cuttings was successfully achieved. Nanocomposite leaching test showed Pb immobilisation. The flexural and compressive - modulus and strength of the PA6 were markedly improved in the presence of the nanofillers and glass fibre. This was attributed to the reinforcement, exfoliating, stiffening, rigidity effect of the nanofillers. S6 (untreated drilling fluid) nanofillers significantly improved the mechanical properties of PA6. This was attributed to the increased interfacial bonding between the fillers and the polymer matrix as a result of the petroleum hydrocarbon present in the sample. The Thermogravemetric analysis (TGA) results showed that nanocomposites PA6/S3 and PA6/S3/GF30 had improved the thermal stability of PA6 by 13.6% and 38.8% respectively compared to PA6/S2 and PA6/S2/GF30 (simulated commercial nanocomposite materials) that improved PA6 by 9.7% and 35.8% respectively.

KEYWORDS: environment, oil based drilling fluid, drill cuttings, demulsification, surfactant, recycling, polyamide 6, nanocomposite material

Table of Contents

Table of Figures

List of Tables

List of Appendices

List of Abbreviations

APP	Amidopenthyl polyphosphate
API	American Petroleum Institute
ATR	Attenuated total reflection
BAT	Best Available Treatment
BATRRT	Best Available Treatment, Recovery and Recycling
BEC	Base Exchange Capacity
BPEO	Best practicable environmental option
BP	British petroleum
BTEX	Benzene, toluene, ethylbenzene and xylene
C	Centrifugation
CEFAS	Centre for Environment, Fisheries and Aquaculture Science
CIWM	Chartered Institute of Waste Management
COSHH	Control of substances hazardous to health regulations
DEFRA	Department for environment, food and rural affairs
DF	Drilling fluid
DI	Deionised water
DTI	Department for Trade and Industry
EA	Environment agency
EDXA	Energy Dispersive X-ray Analysis
EEC	European Economic Community
EIA	Environmental impact assessment
E&P	Exploration and Production
EMS	Environmental Management System
EU	European Union
EWC	European Waste Catalogue

FUND	International convention on the establishment of an international fund for compensation for oil pollution damage
FTIR	Fourier Transform Infra-Red
GF	Glass fibre
ISP	Isopropanol
ICPOES	Inductively coupled plasma optical emission spectrometry
IPPC	Integrated pollution prevention and control
IR	Infra-Red
LDS	Low-density solids
LED	light-emitting diode
LGS	Low-gravity solids
LMWC	Low molecule weight chitosan
MARPOL	Marine pollution
MCT	Mercury cadium telluride
mg/L	Milligram per litre
MMT	Montmorillnite
MSDS	Material Safety Data Sheet
NC	Nanocomposite(s)
NF	Nanofiller(s)
NS	Not significant
O&G	Oil & Gas
OBM	Oil based drilling mud
OBMC	Oil based drilling mud and cuttings
OCNS	Offshore Chemical Notification scheme
ODF	Oil based drilling fluid
ODFC	Oil based drilling fluid and cuttings

OGP	Oil and Gas producers
OMMT	Organophlisied montmorillonite
ONCS	Offshore Chemical Notification Scheme
OSPAR	Oslo and Paris commission
OPRC	Convention on oil pollution preparedness, response and co-operation
OWR	Oil/water ratio
O-W	Oil-Water
PA6	Polyamide 6
PA6/GF30	Polyamide 6/Glass fibre 30%
PA6/S2	Polyamide 6/pure bentonite
PA6/S2/GF30	Polyamide 6/pure bentonite/Glass fibre 30%
PA6/S3	Polyamide 6/demulsifier S3 treated spent drilling fluid and cutting
PA6/S3/GF15	Polyamide 6/demulsifier S3 treated spent drilling fluid and cuttings/Glass fibre 15%
PA6/S3/GF30	Polyamide 6/demulsifier S3 treated spent drilling fluid and cuttings/Glass fibre 30%
PA6/S4	Polyamide 6/demulsifier S4 treated spent drilling fluid and cutting
PA6/S4/GF30	Polyamide 6/demulsifier S4 treated spent drilling fluid and cuttings/ Glass fibre 30%
PA6/S5	Polyamide 6/thermally treated spent drilling fluid and cuttings
PA6/S5/GF30	Polyamide 6/thermally treated spent drilling fluid and cuttings/ Glass fibre 30%
PA6/S6	Polyamide 6/untreated spent drilling fluid and cuttings
PA6/S6/GF30	Polyamide 6/untreated spent drilling fluid and cuttings/Glass fibre 30%
PAH(s)	Poly Aromatic Hydrocarbon(s)

PSA	Particle size analysis
p-value	Calculated probability
QC/QA	Quality control and quality assurance
RCF	Relative centrifugal force
REACH	Registration, evaluation, authorisation and restriction of chemicals
RT	Relative turbidity
S	sonication (pre-centrifugation)
s+c	sonication + centrifugation (post-centrifugation)
S	Significant
SD	Standard deviation
SDS	Sodium dodecyl sulphate
SEM	Scanning Electron Microscope
SEPA	Scottish Environmental Protection Agency
TEO	Total extractable organics
TPH	Total petroleum hydrocarbon
TPHC	Total petroleum hydrocarbon concentration
THPS	Tetrakis hydroymethyl phosphonium sulphate
UKCS	United Kingdom Continental Shelf
UNEP	United Nations Environmental Protection
UV	Ultraviolet
$\overline{X}$	Mean
XRD	X-ray Diffraction
TEO	Total Extractable Organics
RCF	Relative Centrifugal Force

Chapter 1

Introduction

1.1 Background

Oil based drilling fluid (ODF), also called oil based drilling mud or non-aqueous drilling fluid, is a mixture of base oil, water, bentonite clay, lime, barite and/or other chemical additives used for oil and gas exploration (Caenn, Darley and Gray 2011). Drilling fluids (DF) are used to remove and bring to the surface cuttings generated by the drilling bits as the well is drilled.

Drilling fluids have become a potential source of environmental contamination and pollution; resulting in disease and death of humans (Hanrahan 2012, Vilavert et al. 2011) and flora (Adegbotolu et al. 2014; Ekeh-Adegbotolu et al. 2012; Montaño et al. 2011; Kennedy 2011). As a result, the European waste catalogue (2002) classified oil and gas wastes as hazardous waste under the European Union (EU) directive of dangerous substances (Directive 79/831/EEC); as their content pollute the air, land and water (Eur-lex 2013). The danger oil and gas wastes pose on the environment are attributed to poor handling (treatment, management or disposal).

Oil and gas industries have over the years been faced with the problem of identifying and using strategies or methods for proper management and disposal of drilling wastes. Research shows that different methods have been adopted for the purpose of oil waste management strategies by oil and gas industries including landfilling, land/farm spreading and demulsification / chemical washing of oily solid from drilling waste (Abbe, Grimes and Fowler 2011). It has been observed that some of these methods are harmful to the environment and negatively impact on the wellbeing of living organisms. For instance, demulsification which involves chemical washing of oil based drilling waste thenceforth referred to as spent or used drilling fluid; is currently one of the most prominent methods of drilling waste management (McCosh, Addicks and Gallo 2008; Fernandez et al. 2008). However, this method is hazardous when toxic chemicals such as benzene, xylene, toluene and their derivatives are employed in the formulation of the demulsifiers (Makhonin, Petrov and Borisov

1982). In addition, the demulsified solid residues may contain heavy metals if not removed during the treatment could be harmful to the environment.

Given the fact that demulsified solid residues may contain hazardous chemical substances/materials, OGP (2005) suggested recycling as the best option in managing demulsified oil solid residues. Recycling of oil wastes involves converting the wastes into useful resources. In view of the harmful effects of most of the current methods of drilling fluid management, the need for the development of a novel demulsification method for proper management of oil-based drilling residues becomes paramount.

1.2 Aim and objectives

The aim of this thesis is to develop an improved understanding in the development and formulation of chemical demulsifiers for better phase separation, extraction of oil efficiently from spent (used) drilling fluid, and improve the thermal properties of polyamide 6 through demulsifier modified fillers; and to recycle the solid residue present in the treated and untreated drilling fluid into useful and valuable engineering materials.

The above aim will be achieved through the following objectives:

i. To conduct a critical literature review of drilling fluid and current waste management technologies.
ii. To study the effect of existing chemical treatments on phase separation of spent oil based drilling fluid and cuttings as a pathway for the formulation of two demulsifiers.
iii. To develop a chemical process for the phase separation of oil, water and solids from spent oil based drilling mud and surface modification of the solid residues.
iv. To recycle the extracted solid residues from drilling solid waste in the manufacture of polyamide 6 nanocomposites, and investigate the effect of the treated (demulsifier and thermally) solid residues and untreated spent oil based drilling fluid in the manufacture of polyamide 6 nanocomposites.
v. To evaluate and benchmark the thermal and mechanical properties of the manufactured novel polyamide 6 nanocomposites.

1.3 Motivation

Current methods adopted by the oil and gas industry for the management of oily waste are limited in their capability to protect the ecosystem. There is a need for alternative methods which are mild, more eco-friendly and environmentally sound for use in managing oil-based waste and recycling treated oil-based drilling fluid solid residues. In addition, for economic and environmental reasons, oil and gas producers and waste management companies are currently seeking alternative uses for the solid residue from drilling mud and drill cuttings. This is due to increasing pressure from the government and environmental regulators to achieve zero waste and reduce landfilling of solid residue from drilling mud and drill cuttings.

The purpose of this research was to study the viability of treating oil based drilling fluid waste and recycling the treated residues into useful engineering materials. This involved identifying potential eco-friendly chemicals: (polymer) surfactants and co-solvents for demulsifier formulations to improve phase separation of oil based drilling fluid constituents. It also involved studying the influence of factors such as time, mechanical methods on the efficiency of demulsification. Additionally, it involved the assessment of the impact of thermal and mechanical changes to the PA6 material investigated.

In Figure 1.1 the knowledge gap that was explored in this research was shown. The first aspect involved phase separation of oil, water and solids from the drilling fluid using the formulated demulsifiers. The second aspect involved the manufacture of the PA6 nanocomposite materials and understanding the science associated with the novel PA6 engineering materials. In previous research, the solid residue has been used in the manufacture of concrete blocks, glass materials and interlocking tiles (Zhang et al. 2016; Abbe et al. 2009). However, the demulsifier washed solid residues have not been investigated as potential filler with the ability to improve mechanical and thermal properties of Polyamide 6 (PA6).

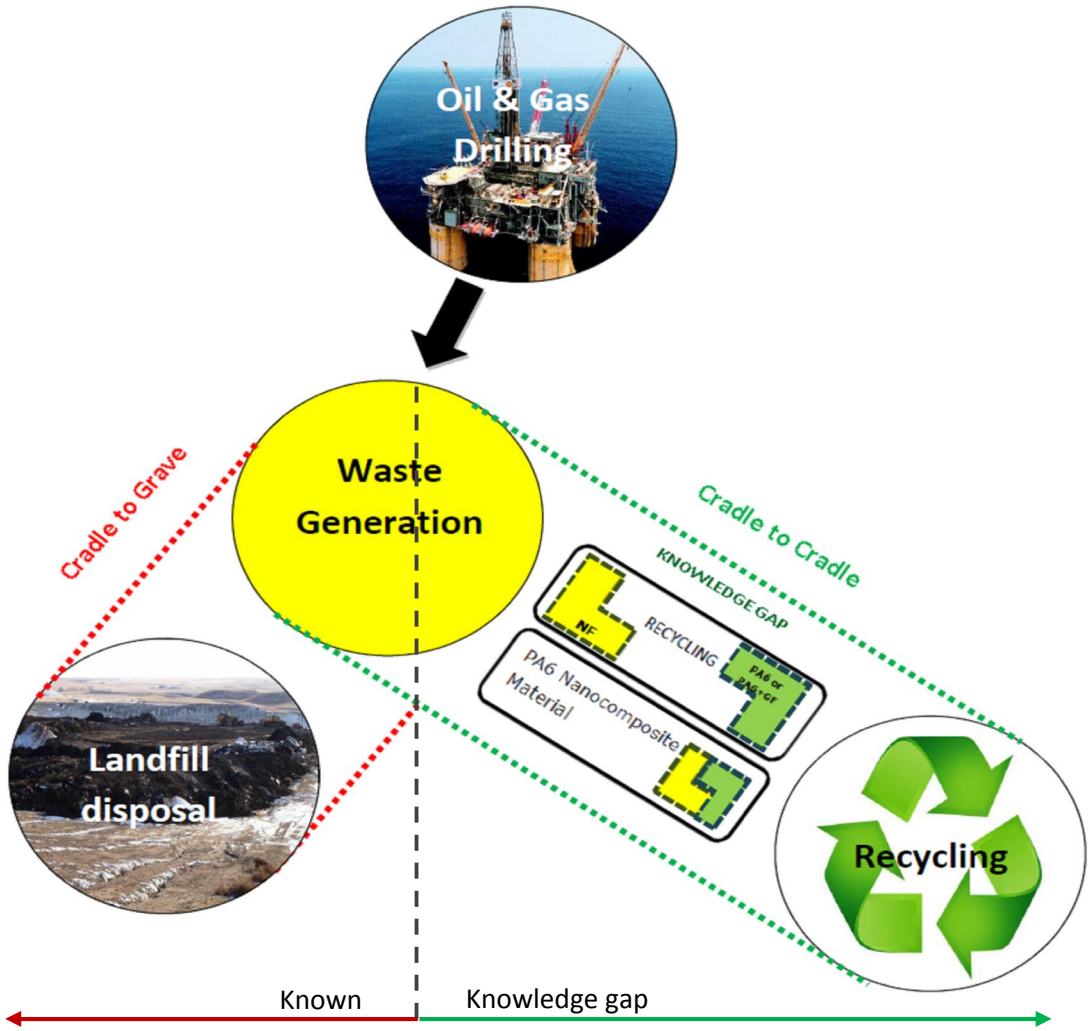

Figure 1.1 Schematic diagram illustrating the known practice and knowledge gap in drilling solid waste management. The knowledge gap explores the recycling of the drilling solid residues as fillers in PA6 nanocomposite fabrication in a 'waste to want' approach which entails further recycling or reuse of the novel PA6 nanocomposites (cradle to cradle approach) as opposed to landfilling

1.4 Methodology

The study methodology involved an extensive literature search, which was followed by the characterisation of the spent (used) drilling fluid. The initial steps offered understanding of the science of spent fluid and highlighted areas of potential research. Knowledge gaps include a need for non-toxic demulsifiers that meet Oslo and Paris commission (OSPAR) and offshore chemical notification scheme (ONCS) standards; a need to stop landfilling of drilling waste due to their effect on groundwater system and the environment. According to SEPA (2016 b),the Waste Framework Directive, there is a need to effectively recycle and reuse waste as a potential resource and subsequently there is a possibility to manufacture high-end value engineering material by using solid phase residue of the treated drilling fluid as nanofillers. The research, therefore, focuses on investigating the chemo-remediation potential of a novel demulsifier and the propensity for the recovered solids from drilling waste to be used as fillers in PA6 material. The demulsifier-led phase separation investigations encompass the consideration of potential challenges with treatment conditions, hydrophobicity, steric effect and surface charge of treatments with respect to their interactions with water, oil and solid phases (Quintero and Pietrangeli 2013; McCosh, Addicks and Gallo 2008; Ese et al. 2000). The thermo-mechanical investigations of novel PA6 nanocomposite materials encompass the consideration of potential challenges with material behaviour and failure mode (Njuguna, Mouti and Westwood 2015; Gendre et al. 2015; Silva et al. 2013).

This study further investigates the impact of the thermo-mechanical factors on the durability of the material. These factors include the effect of flexure and compression on the failure and damage mode of the new materials. This research leads to the provision of procedures for improving current PA6 prototypes for advanced mechanical/thermal properties as well as proposes new leads on drilling waste management (see Figure 1.2 and Figure 1.3).

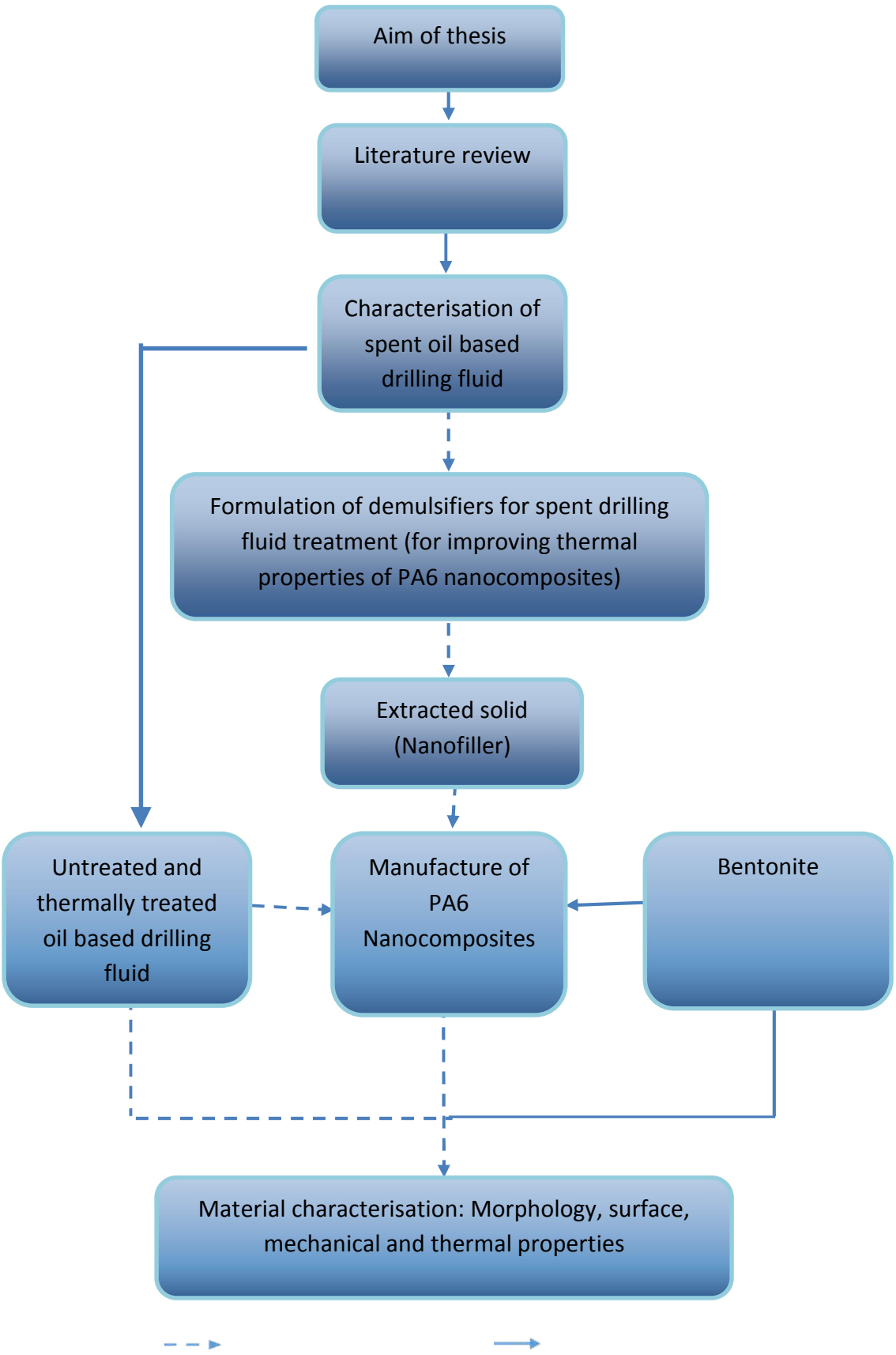

Figure 1.2 Methodology overview showing knowledge gap and known knowledge

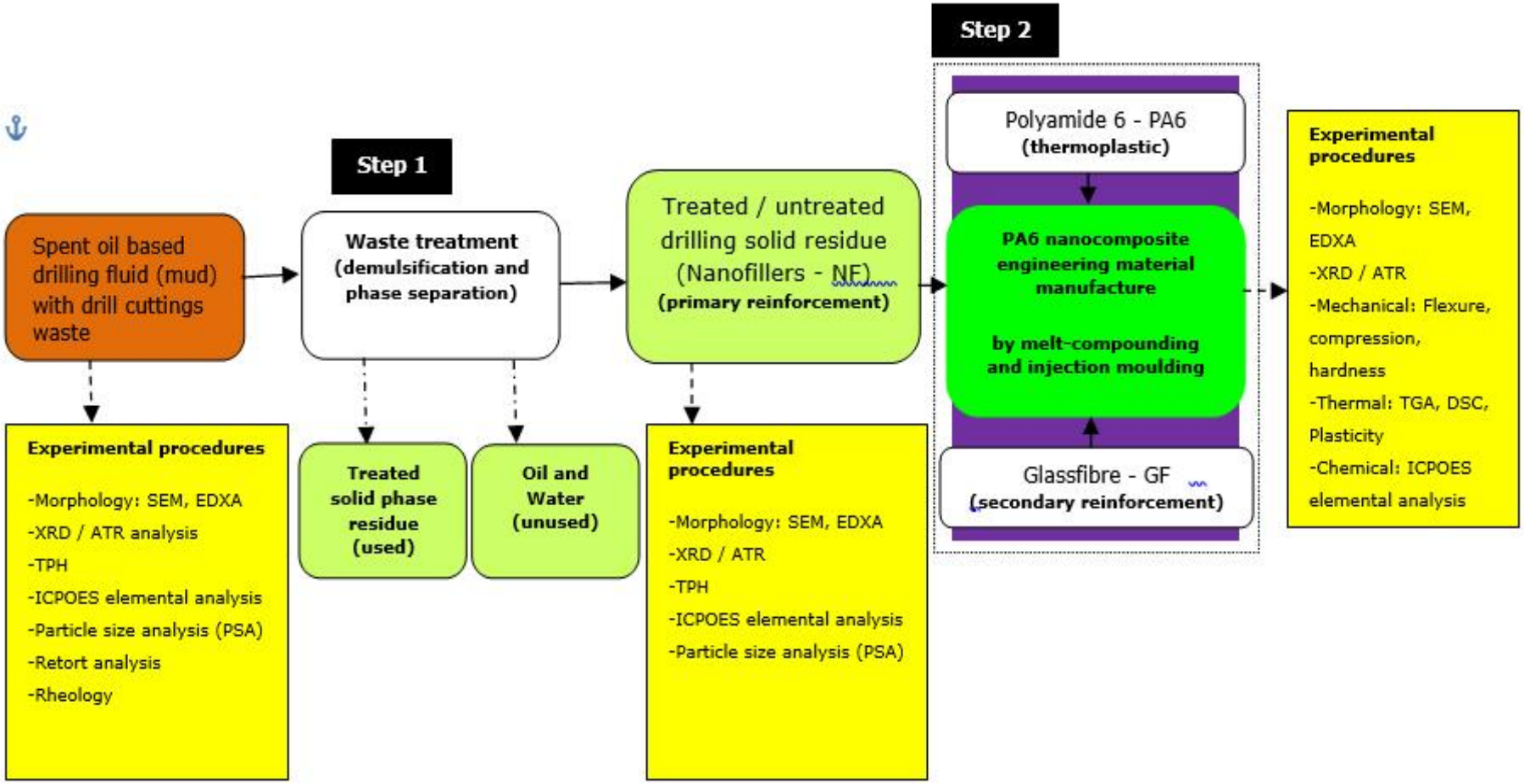

Figure 1.3 Workflow of the research showing the sample progression and experimental procedures

1.5 Thesis structure

Chapter 1 is the introduction. It gives information about the general background to the research, aim, objective, motivation and thesis structure. The key interest concerns oily waste demulsification and recycling. The key legislations driving oily drilling waste management are mentioned to emphasise the importance of the current work in the oil and gas industry.

Chapter 2 presents an extensive literature review carried out to present the current oil-based drilling waste treatment/management and gaps in knowledge. Drilling fluid and drill cuttings are discussed, including their impact on the environment. This is followed by techniques for their disposal and recovery operations based on the European Union legislation/the waste management framework. Waste treatment via demulsifier utilisation was introduced. Recycling of residual waste to a commercial product and engineering nanocomposite materials was discussed.

Chapter 3 assesses the characteristics of the spent drilling wastes using different analytical methods employed for the morphological, surface, physical and chemical characteristics of the samples in this research. This chapter emphasises the potential effect of waste characteristics as a decision-making tool for demulsifier treatment.

Chapter 4 focuses on the demulsification of spent oil based drilling mud and drill cutting (a multiphase system). The development of a phase separation method and the development of the demulsifier formulation using solvents, biological and chemical surfactants (treatments), and validating the demulsifiers efficacy through analytical investigation was carried out. It contains experimental analysis undertaken to ascertain the suitability of individual treatment for use in the formulation of the demulsifier.

Chapter 5 investigates the use of the treated solid phase as nanofiller in the synthesis and manufacture of different blends of novel Polyamide 6 (PA6) nanocomposite material. This study will also look into the characterisation of the new PA6 composite materials.

Chapter 6 discusses the mechanical properties of the novel materials. Properties such as flexural, compression and hardness will be investigated and discussed

within the context of industrial application. Chapter 7 focuses on the analytical investigation of the thermal properties of the novel materials. The thermal analytical studies for the determination of the melting point, crystallisation temperature, glass transition, decomposition temperature, melt flow index (MFI) and decomposition properties of the new materials, using Differential Scanning calorimetry (DSC), thermogravimetric analysis (TGA) and plasticity melt flow rate will be reported.

Chapter 8 summarises and concludes the PhD research thesis. It gives insight into the achievements of the project in treating and recycling drilling waste into a resource. The research challenges are mentioned and further work suggestions were made.

Chapter 2

Literature review

2.1 Introduction

This chapter introduces the different concepts associated with spent/used oil based drilling fluid, its application in the oil and gas industry and what waste management processes entail. It offers knowledge about drilling fluids and their importance to the oil and gas industry; the different types of drilling fluid available in the industry, the waste streams generated from their use, current methods of treatment, recycling/reuse, management and disposal. The chapter explores the theories associated with drilling fluid demulsification and phase separation as well as define some keywords related to demulsification and phase separation. An empirical study on the formulation of demulsifier for the treatment of spent drilling fluid, and recycling. The formulation of nanocomposite materials from the solid residue obtained from the demulsification of the spent oil based drilling fluid was also undertaken.

DF also referred to as drilling mud, is very important for well construction. The drilling fluid used is based on the formation (drilled geological rock) types, environmental consideration and cost. The drilling fluids could be non-aqueous, aqueous or pneumatic. The fluid in this research is a special chemical formula of oil and water emulsion with suspended solids. It is a unique slurry of base oil (petroleum), water, bentonite clay or lime, barite and other chemical additives used for oil and gas exploration and production (Caenn, Darley and Gray 2011).

Due to the risk involved in drilling very deep and narrow wells, drilling fluid is employed to aid the process of drilling oil and gas wells. Drilling fluid is used to suspend, remove and bring to the surface cuttings generated by the drilling bit as the well is drilled. As shown in Figure 2.1, drilling fluid is pumped down a hole through the drill string and used to move drill cuttings from the well to the Earth's surface. Drilling fluid is also utilised in the control of pressure in the well formation. This prevents blowouts originated by pressurised formation fluids. This minimises harmful industrial/environmental impact that can arise from oil spill due to well blowout. It maintains the stability of the wellbore, aiding casing,

cementing and installation. It helps seal permeable producing geological formation to reduce or prevent formation damage. The drilling fluid cools and lubricates drilling bits as well as supports the weight of the drilling assembly. It also transmits hydraulic energy to tools and bits which aid mud motor function. It provides the platform for formation evaluation via data collection from measurement-while-drilling (MWD), and logging-while-drilling (LWD), obtained through cuttings analysis. Depending on the drilling fluid type, use of oil based mud can aid corrosion control of the drilling assembly.

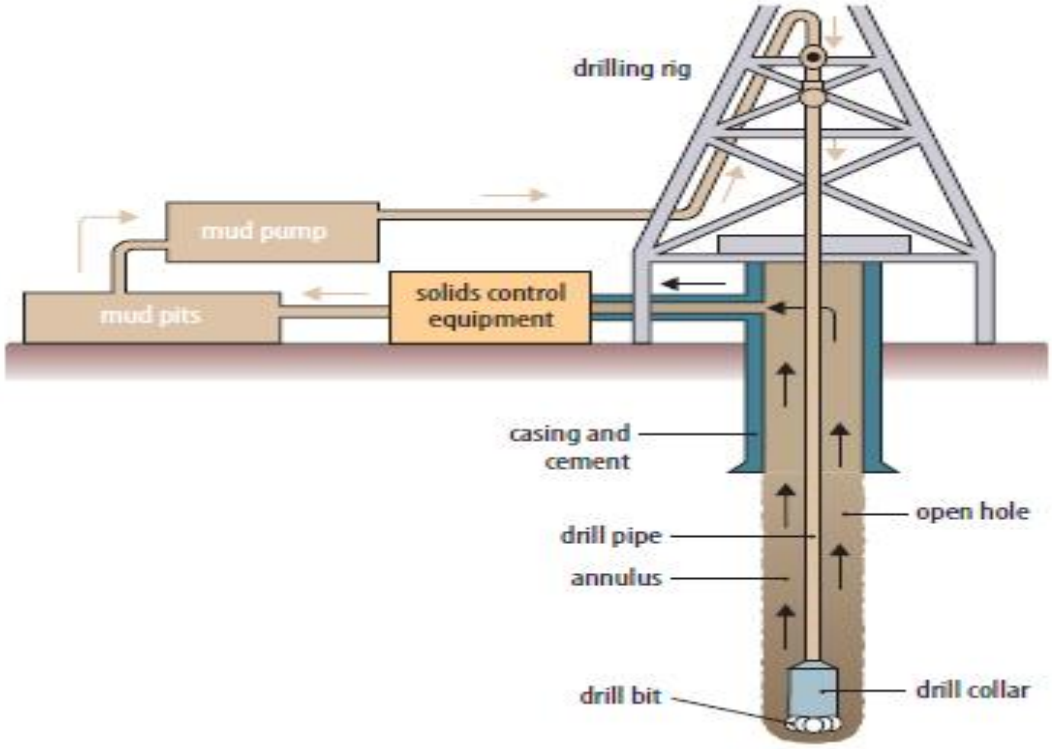

Figure 2.1 Movement of drilling fluid in drilling operations. Drilling fluid flows down the drill string and is carried up the annulus (OGP 2009)

2.2 Types of drilling fluids

The main types of drilling fluids are non-aqueous drilling fluid (oil), aqueous (water) based muds (WBMs), synthetic muds and formate brines (OGP 2003). Figure 2.2 illustrates a broader classification of drilling fluids as water based drilling fluid and non-aqueous drilling fluid.

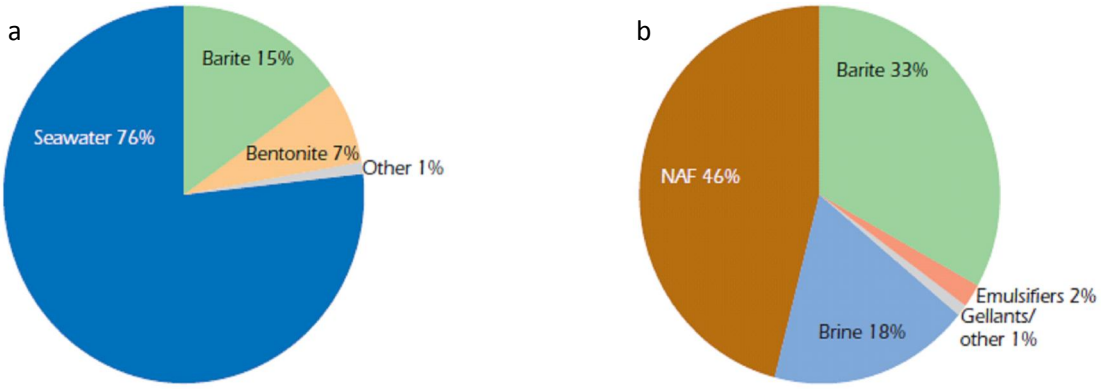

Figure 2.2 Drilling fluid compositions (a) Aqueous (water) based and (b) Non-Aqueous fluid (NAF) or oil based (OGP 2003)

The non-aqueous (oil based) drilling fluids, unlike the aqueous (water) based drilling fluids, have the potential to cause negative environmental impact after use. This is due to their bio-available nature, chemical content and high base oil (non-aqueous fluid, NAF) content required to formulate the oil based drilling fluid. There are two main types of non-aqueous drilling fluids - oil-based drilling fluids and synthetic-based drilling fluids.

Type 1 non-aqueous drilling fluid is made up of Class 1 and Class 2 oil based drilling fluids. Class 1 drilling fluid is mainly made up of diesel base oil which could have a polycyclic aromatic hydrocarbon (PAH) value of ~ 2 - 4% w/v and aromatic hydrocarbons of about 25%. Within this class, there are some drilling fluids made using conventional mineral oil which is refined/distilled crude oil. Mineral oil has a lower PAH content of ~ 1 - 2% (OGP 2003). Class 2 non-aqueous drilling fluid is made up of highly refined crude oil with a PAH range between 0.001 and 0.35% w/v and an aromatic content of 1 - 5%. Class 2 drilling fluid was developed due to the adverse environmental effect caused by the high PAH content of the diesel based drilling fluid such as carcinogenesis, teratogenesis and mutagenesis of flora and fauna in the environment.

Table 2.1 Composition of non-aqueous drilling fluid

Drilling fluid composition	**Examples**
Weighting agents	Barite – $BaSO_4$, hematite – Fe_2O_3
Lubricants	Diesel, asphaltic, aliphatic and synthetic oils
Scale inhibitors	Methyl phosphoric acid
Corrosion inhibitors	Zinc oxide, iron oxide, hexamine
Viscosifiers	Starch, guar gum, glycol, xanthan gum
Flocculants	Polyacrylate
Surfactants	Alkanolamide, alkyl polyglycosides
Dispersants	Polyoxyethylene
Biocides	Glutaraldehyde, Tetrakis hydroxymethyl phosphonium sulphate (THPS)

Type 2 non-aqueous drilling fluid is made using synthetic base fluids generated from chemical reactions and plant sources. They include olefin, paraffin and esters. They contain less than 0.001% PAH and 0.5% aromatic content. They are said to be environmentally friendly because they contain negligible amounts of aromatic hydrocarbons and can be biodegraded faster than the other classes (OGP 2003).

In addition to the base oil, other components are used to formulate the different types of drilling fluids as seen in Figure 2.2. The composition of oil based drilling fluid is shown in Table 2.1.

One of the benefits of OBM is its thixotropic potential which enables suspension of drill cuttings in static conditions, that is, when drilling operations have been suspended. It also lubricates the drill bits and makes drilling much faster and easier compared to other drilling fluids. It also aids the drilling of high-

temperature, high-pressure wells where water based drilling fluid (water based mud) often dry out (Fink 2012).

2.2.1 Spent Oil Based Drilling Fluids

Spent oil based drilling fluid is any used or waste oil based drilling fluids set aside for treatment, reused/recycled or disposal. There are three main types of wastes emanating from waste oil based drilling fluid. They include: spent oil based mud (slop), oil based drill cutting and spent emulsion.

Spent oil based drilling mud (slop) is made up of the waste drilling fluid, which in most cases contains low-density cuttings as well as high-density cuttings and chemical additives. Oil based drilling cuttings are large rock particles coated with drilling fluids which are extracted from the Earth's crust during drilling. The high-density drill cuttings are separated from the slop using the shale shaker solid control system. The spent emulsion, on the other hand, is comprised of the oil water emulsion from drilling fluid and low-density solid particulates.

Although the use of oil based drilling fluid is cost intensive, they have several advantages in drilling. In drilling shales (smectite) i.e. water soluble formations (e.g. limestone) that swell, they dissolve into water-based muds unlike the oil based drilling fluid. In addition, this type of drilling fluid does not dehydrate when drilling high-temperature wells in contrast to water-based muds.

On the other hand, oil based drilling fluids have become a potential source of pollution thereby increasing the environmental footprint. Some of the environmental contaminants or toxic substances in drilling fluids include heavy metals, biocides and PAHs. Currently, the chemistry of PAHs, for example, benzo(α)pyrene, found in oil (petroleum hydrocarbon) is responsible for some of the hazardous effects the drilling fluids have on the environment. PAHs are toxic and highly flammable hydrocarbon. Under the European Union directive for dangerous substances (Directive 79/831/EEC); amended from Directive 67/548/EEC; EU Regulation 1907/2006 - (Registration, evaluation, authorisation and restriction of chemicals) (REACH) information on substances notified under Directive 67/548/EEC and Dangerous substance and explosives atmosphere regulation (DSEAR, 2006), where petroleum oil is described as carcinogenic, mutagenic and toxic due to PAH presence (Eur-lex 2013).

PAHs are commonly found components of crude oil as well as coal tar. In humans, it is introduced into the body by ingestion, inhalation or direct contact with the skin. In the body, benzo(α)pyrene is recognised as a foreign body (toxin) which can be transformed into soluble forms in xenobiotic phase one and two reactions (i.e. hydroxylation and conjugation respectively) in order for it to be excreted. Benzo(α)pyrene is chemically inactive but reacts with xenobiotic metabolising enzymes (cytochrome P450, epoxide hydrolase) to form the active destructive metabolic intermediate – Benzo(α)pyrene-7,8-dihydrodiol-9,10-epoxide. The epoxide reacts as a free radical (electrophile) with the DNA (a cellular nucleophile) to form an irreversible covalent bond (Trush 2008) hence interfering with transcription and causing the formation of abnormal cells which may further result in the multiplication of cancerous cells.

Table 2.2 gives an example of different chemicals used with drilling fluids in the oil and gas industry and their acute toxicity effects on selected organisms. Non-aqueous drilling fluids contain both organic and inorganic substances. The composition of the drilling fluid determines its toxicity or harmful effect on the environment (Terzaghi et al. 1998, Benka-Cokerand Olumagin 1996, Reis 1996). The toxicity could be either acute or chronic. For instance, the leakage of drilling fluid into the sea would have some impact on the aquatic environment as reported by (Holdway 2002). Algae, brine shrimp, and microtox are some selected analyses used for the acute EC50 test (test for the concentration of test substance in dilution water that has a toxic effect on 50 percent of a test population throughout constant exposure over a short period of time).

The uses of these organisms are for different reasons. Algae is located on the surface of marine habitat, thus, would be best for monitoring surface hydrocarbon contamination. Shrimp (Artermia *salina*) have great adaptability in estuarine, and hypersaline aquatic environments thus it can be used in quite extreme conditions. It is located in the benthic region (the ecological area at the lowest level, the bottom of the waterbody) thus would be best used for pollution monitoring. Microtox is a very rapid and sensitive bio-pollution monitoring test which utilises the photoluminescence of a bacterium, *Vibrio fischeri* to ascertain

the level of pollution. This microbe is found in sediments, thus is best suited for marine sediment toxicity tests.

Table 2.2 Acute toxicity of chemicals used in oil and gas processes (Adapted from Holdway 2002)

Chemical type Acute toxicity EC50 (mg/L)	**Algae (*Skeletonem acostatum*)**	**Brine shrimp**	**Microtox (*Vibrio fischeri*)**
Corrosion inhibitor	-	>20–25	15–50
Scale inhibitor	60	1000	>1000
Demulsifier	20	30	2.1–112
Flocculent	>1000	>15,000	>15,000
Anti-foam	120	150	9
Biocide	-	-	15.2–33.7

2.2.2 Environmental Legislation

Waste disposal in the oil and gas industry has evolved over the years from ocean dumping to landfill disposal. This waste disposal evolution has been driven by environmental legislations. For instance, in the early days, ocean dumping of drilling fluid and cuttings waste was highly acceptable. On the other hand, the negative impact of ocean dumping such as water pollution, disease and death of flora and fauna led to abolishing of this practice. Currently, the use of landfill disposal is the norm. However, this practice has posed several negative impacts such as an increase in land heavy metal content and groundwater pollution. Interestingly, the legislations tend to differ between countries. As already established, drilling product (petroleum) and by-products (produced water, spent/used drilling fluid and sludge) have short and long term hazardous effects. Hence, in the interest of global health, environmental, economic and social

sustainability, different treaties, legislation and regulations have been passed at international, regional, national and local government levels for implementation. In summary, there are international and regional agreements that translate into national regulations and legislation as well as legislation originating from national issues. Appendix A.1 is a summary of international and regional agreements pertaining to the offshore oil and gas industry enacted globally by the United Nations (UN) and International Maritime Organisation (IMO), and regionally by OSPAR commission and the UN. Appendix A.2 is a comparison of regulations pertaining to the oil and gas industry which affect waste management.

In September 1992, the Oslo and Paris convention (OSPAR) was set up to advise countries associated with the North Sea on environmental policies and legislations (OSPAR Commission 2013a), agreed to establish the OSPAR directive 92 which prohibits the discharge of select drilling waste offshore [e.g. Oil (Non-aqueous) based drilling fluid]. The review by OSPAR on the acceptable concentration of oil in water for discharge by the oil and gas industry led to the reduction of permissible oil in water from 40 to 30 mg/L as at January 2007 (OSPAR Commission 2010a). According to the OSPAR north-east Atlantic environmental strategy, there will be a move towards the termination of all discharge, emission and loss of hazardous substances by the year 2020 (OSPAR Commission 2010b). OSPAR decisions 92/2 and 2000/3 set restrictions on the marine discharge of oil based drilling fluid cuttings (OBMC) retaining over 1% by weight ratio of oil to cuttings (Al-Ansary and Al-Tabbaa 2007). On the other hand, a critical review of the limit of oil on cutting ratio by weight should be carried out with the intention of having a fixed limit in mg/kg of oil on cutting as opposed to a ratio which may vary in actual concentration from one cutting oil-extraction procedure to another. This would also ensure that no excess oil, over the environmentally tolerable oil introduced into the ecosystem.

According to Ormeloh (2014), polluter tax principle and the OSPAR precautionary principle are important in combating environmental pollution and monitoring waste. In addition, the use of the best available techniques (BAT) as well as best environmental practices (BEP) is encouraged to reduce pollution. Best practice include substitution of hazardous components of the drilling fluid so as to reduce

negative environmental impact, such as the switch from non-aqueous drilling fluid to water based drilling fluid

The EU Waste Framework directive is a piece of legislation by the EC which is aimed at reducing waste generation and promoting recycling and reuse. According to the European Parliament, under Article 4 of the EU Waste Framework Directive (WFD) (2008/98/EC) the waste management hierarchy for waste prevention and management involve the following: prevention, preparing for re-use, recycling, recovery, e.g. energy recovery, and disposal.

In line with common practice in waste management, waste is sorted, separated and treated for impurity removal before recycling. For spent drilling fluids, the major components need to be separated (by treatment) for reuse. In open loop recycling of drilling fluids, drilling fluid solids can be used for the production of cement/concrete building blocks, road cover and interlocking tile (Gonzalez, Crawley and Patton 2008; Page et al. 2003).

The oil can be reused as fuel, formulation of lubrication oil and new drilling fluid (Seaton et al. 2006). The obtained water within the fluid or that arising from clean up can be treated using appropriate technology and can be reintroduced into the ecosystem or used for other industrial processes. Closed-loop recycling of drilling fluid where all components of old drilling fluid are used to make new drilling fluid is not presently practised. Recycling is a method of waste management in the waste minimisation process of the WFD waste management hierarchy as shown by the waste triangle in Figure 2.3.

Recycling is one of the key ways the UK oil and gas industry can reduce its carbon footprint. Recycling of drilling fluids is a way of minimising waste to the environment. It is carried out to ensure that drilling fluid can be converted into other products for further use.

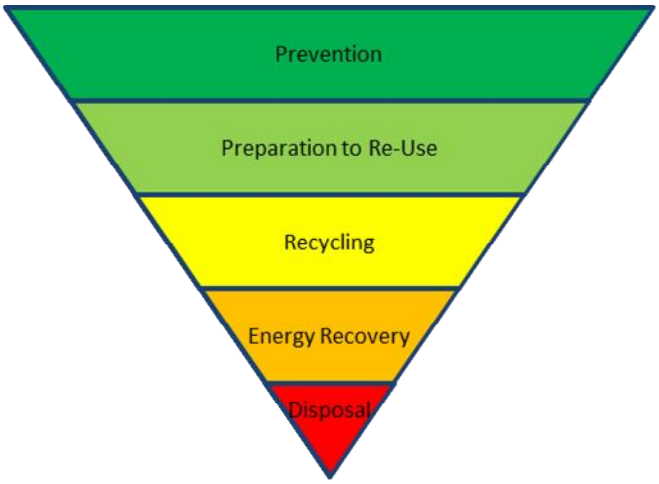

Figure 2.3 Waste management hierarchy (Letsrecycle 2014)

Recycling of drilling fluid ensures the safe use of drilling fluid as a product, according to CIWM (2014) from 'cradle to cradle' rather than 'cradle to grave' which discourages and minimises the use of the landfill disposal option. The raw waste material (spent drilling fluid) may require waste separation, treatment and modification before it can be reutilised (Page et al. 2003). Therefore, it serves as base (raw) materials for the production of other products (Denison and Ruston 1990).

In hazardous waste management, prevention is the top priority in the waste framework directive (WFD) which entails the absolute prevention of waste creation. Thus, the creation of waste oily water emulsions and oily solids such as drilling fluids should be prevented (Ghazi et al. 2011; Shuixiang et al. 2011; Caenn, Darley and Gray 2011; Sadiq et al. 2004; Caenn and Chillingar 1996). Waste prevention could be achieved by reducing the amount of spent drilling fluids and drill cuttings generated by drilling narrower wells, utilising or inventing other technologies as alternatives to drilling fluids (Page et al. 2003), for instance, producing and using smart or 'super drilling fluids' that are eco-friendly, free of rheology loss and with improved drilling fluid properties. Hazardous waste prevention can be reduced by replacing formulation chemicals cited in the European Waste Catalogue as hazardous with non-hazardous substitutes (OSPAR Commission 2013b) - for instance: replacement of

halogenated solvent based degreasers; use of techniques that separate potential waste stream at the source.

One of the challenges associated with the environmental regulations and legislation for drilling waste management is the difference in regulations amongst different countries and sometimes regions in a country. This is due to the fact that the regulations are driven by social, economic and political factors prevalent in the different countries (Garland et al. 2008). On the other hand, there seems to be discrepancies in the analytical results provided by regulatory bodies that are then utilised as recommendations and employed by the government for law making. For instance, the United States environmental protection agency (USEPA) and American petroleum institute (API) heavy metal analysis using similar analytical methods for drilling fluid produced water and associated wastes, showed inconsistency in the results for pH and elements such as barium, lead and chromium (Holliday and Deuel 1990). In addition, Holliday and Deuel (1990) reported that analytical test carried out on the same samples by independent bodies did not correlate with results provided by regulatory bodies. However, the toxicity limits obtained from the analytical tests by regulators influence the disposal threshold adopted for operators to follow.

Alternative waste management options will be considered as a matter of stringent compliance necessity and the oil and gas companies' value on its image and corporate responsibility. Current legislations do not propose best practice or alternative methods of disposal or reuse of drilling fluid and cuttings waste on companies but simply, impose the regulations on the operators. This could result in some companies utilising environmentally devastating methods of waste management to achieve compliance. One such instance concerns the current and prevalent use of a thermal desorption treatment method for drilling waste which results in increased emission of greenhouse gases. There is a need for legislations that stipulate to the operators and waste management companies, ways to recycle, reduce or prevent drilling wastes.

In the UK, the current landfill tax charge is £56/tonne for hydrocarbon contaminated waste such as spent oil drilling fluid, and £2/tonne for inert and

uncontaminated waste. These taxes are aimed at minimising landfill disposal. In conclusion, the cost of landfilling could be further increased to prevent landfilling of this toxic waste. (See Appendix A.2 for different environmental regulations associated with the oil and gas industry).

2.2.3 Methods of treatment, management and disposal of spent oil based drilling waste

During E&P activities, the drilling fluid and cuttings generated are brought back to the surface which is also called the top-side of the platform. At this location, the drill cuttings are separated from the drilling fluid using the solids control equipment before it is tested for rheology and reused for further drilling activities. Figure 2.4 illustrates the fate of the used drilling fluid during and/or after the drilling process.

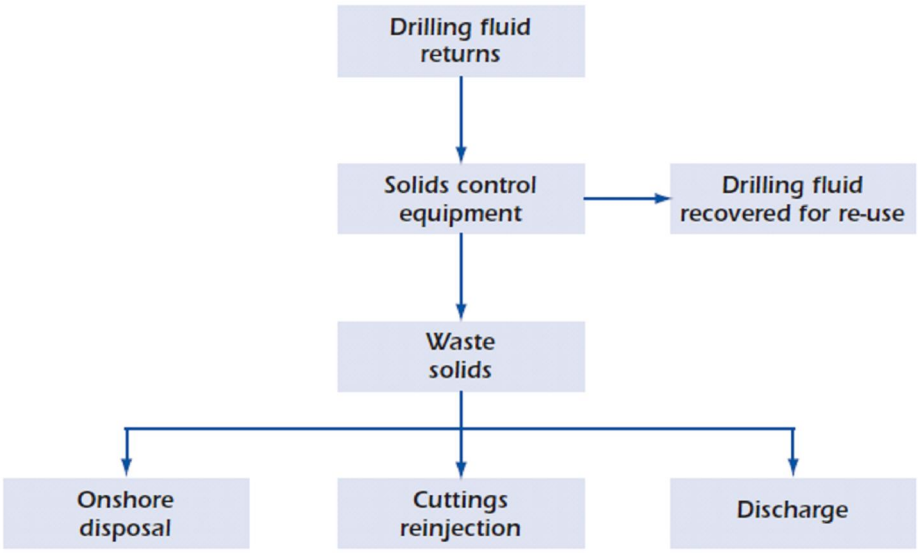

Figure 2.4 Fate of the used drilling fluid (OGP 2003)

Waste generated from exploration and production processes via the solid control system can subsequently be managed by the methods now described. The landfill is one of the most widely used processes in the waste management of drilling fluids. This involves the burying of spent oil based drilling fluid waste matter into landfill sites which are covered or left open and without underlining, as is the case in underdeveloped countries (Sedman et al. 2012; Ray et al. 2005;

Jha et al. 2008; Rafizul and Alamgir 2012). The landfills allow for the decomposition of some of the waste components via natural attenuation, but the leachates generated can be toxic and introduce pollutants into the land and groundwater in that environment (Elshorbagy and Alkamali 2005; Sánchez-Chardi and Nadal 2007). For the open (uncovered) landfills, greenhouse gases escape into the atmosphere which is the cause of air pollution and microbes are generated which cause air-borne diseases (Mari et al. 2009).

Road spreading is a means of reusing used drilling fluid. It involves the spreading of DF wastes on roads. It is sometimes applied to simulate road covers like coal tar (Gonzalez, Crawley and Patton 2008). In some cases, these wastes may not be treated. However, the danger here is that this untreated oil and gas waste can contaminate the soil with heavy metals, hydrocarbons and radioactive elements (Bansal and Sugiarto 1999). In addition, when organisms feed on plants cultivated in or near these polluted soils, it could harm the plants and the organisms feeding on these plants (Kisic et al. 2009; Lewis 1995; Nfon, Cousins and Broman 2008; OSPAR Commission 2007) as well as harm to the environment results (Ladousse, Tallec et al. 1996).

Ocean dumping involves the disposal of partly treated and untreated wastes into the ocean as well as other water bodies like aquifers, rivers, and streams. This is a source of immense environmental pollution. Often, this may be discovered as an oily sheen near offshore platforms or may be discovered on the water surface above the dump site. Water body waste dumping is associated with the destruction of living organisms *e.g.* coral reefs on the seabed (Wills 2000, Stevens et al. 2012).

Thermal separation techniques involve the application of thermal treatments such as incineration with energy recovery, gasification and thermal desorption of spent OBM and drill cutting wastes to reduce the waste to a stable ash (solid content) for disposal or reuse (Jones, Sanders and Chambers 2002) The cost of acquiring and maintaining a thermal desorption unit is very high and the energy consumption, and the high greenhouse emission from the use of this method makes it disadvantageous, however, the oil could be used to generate power (Li, Zhu and Zhang 2012).

Subsurface drilling waste reinjection involves the transport of pressurised drilling wastes underneath the Earth's surface. This is used to increase pressure necessary for extracting hydrocarbons from the reservoir. Drilling cuttings are also re-injected into the Earth crust or seabed, but this must be carried out in such a manner as would not cause harm to the ground water system. These wastes must be treated (Caenn, Darley and Gray 2011).

The mechanical method involves the use of mechanical equipment to separate the components of the oily drilling fluids wastes. Some of the equipment used includes shale shakers for drill cutting removal, hydrocylones for oil and water removal (Yang et al. 2010; Caenn, Darley and Gray 2011). Some other mechanical methods include gravity separation, using interceptor and settling tanks, where spent oil based drilling fluid or produced water is decanted into a settling tank for the solids such as bentonite clay, limestone and drill cuttings sink to the bottom for collection. The major disadvantage of the lone use of mechanical processes is an inadequate separation of oil from solid residues and an aqueous phase.

The biological method of treating the spent drilling fluid involves the use of plants (phytoremediation) and microbial organisms (bioremediation), often enhanced by natural factors such as climatic conditions, to treat oil and gas wastes. Plants can degrade pollutants naturally within the soil rhizosphere via biosurfactants produced. They can also phytoextract, accumulate and volatilise (phytotranspiration) the waste components (Ekeh-Adegbotolu; Ekeh and Wegwu 2012; Sun et al. 2010; Khan 2005; Fitz and Wenzel 2002; Macek et al. 2008; Gan, Lau and Ng 2009; Lin and Mendelssohn 2009; Li, Kang and Zhang 2005; Millar, Goodman and Dobrai 2013). In bioremediation, the drilling waste (OBM) could be sent to a facility (ex-situ) where microbial treatments are applied on the wastes to decrease and degrade the hydrocarbon and other toxic components into simpler compounds (Peng et al. 2009; Radwan et al. 1998; Huang et al. 2005). The major disadvantage of the biological method is that it can spread pollutant especially due to feeding on polluted plants.

Stabilisation and solidification of drilling cuttings involve the encapsulation/engulfing of waste matter so as to reduce or stop its mobility in

the ecosystem. Due to the toxicity of drilling fluid, various researchers have sought ways of solidifying and stabilising this waste type. Leonard and Stegemann (2010a) worked on stabilisation of the heavy metal by $CaCO_3$ reaction. Work has been undertaken on the solidification of drilling waste in Portland cement (Nguyen et al. 2008) and also on the stabilization/solidification of γ-radionuclide polluted soils using Portland cement (Falciglia et al. 2014). Abbe et al. (2009) also carried out a novel work of stabilising and vitrifying oil well drill cuttings for use in producing sintered glass-ceramics. The challenge of this method is that heavy metals could leach from the stabilising or solidification matrix such as cement, limestone, and glass.

The chemical method of waste management involves the use of chemicals to wash, demulsify or flocculate oily drilling fluid waste components. Some of the chemicals used are solvents and surfactants, which could be inorganic, organic, synthetic or biological based (Fink 2012; Urum and Pekdemir 2004; Pabon and Corpart 2002; Bhatnagar, Khandelwal and Rao 2010). This method does not involve the use of a lot of energy or power nor does it generate greenhouse gases relative to mechanical methods. However, these conventional chemicals (including benzene, xylene and toluene) have been found to be hazardous to the environment and agencies such as centre for environment, fisheries and aquaculture science (CEFAS) via its offshore chemical notification scheme (OCNS) has highlighted the need to phase them out in line with OSPAR Recommendation 2006/3 because of their persistence, bioaccumulation and toxicological properties. There is a need to provide environmentally friendly chemicals for oily drilling fluid waste management. This approach is, therefore, the basis for the current study.

2.3 Demulsification and phase separation

Oil based drilling fluid is an emulsion of water in oil having a suspended solid phase. Ideally, an emulsion has dispersed droplets and particles/solid substances which remain uniformly dispersed in the continuous phase without losing its original properties, colour, appearance and consistency. Demulsification is a process of destabilising emulsions *i.e.* separating the emulsion into phases of oil,

water and solids (if present). Emulsions are naturally unstable but are stabilised through the use of emulsifiers. During demulsification, there are different mechanisms of emulsion instability that can be caused by the chemical treatment and/or mechanical techniques for emulsion destabilisation to occur. The mechanism adopted by a chemical treatment for demulsification of OBM can be as a result of its chemical properties, type, functional groups and concentration.

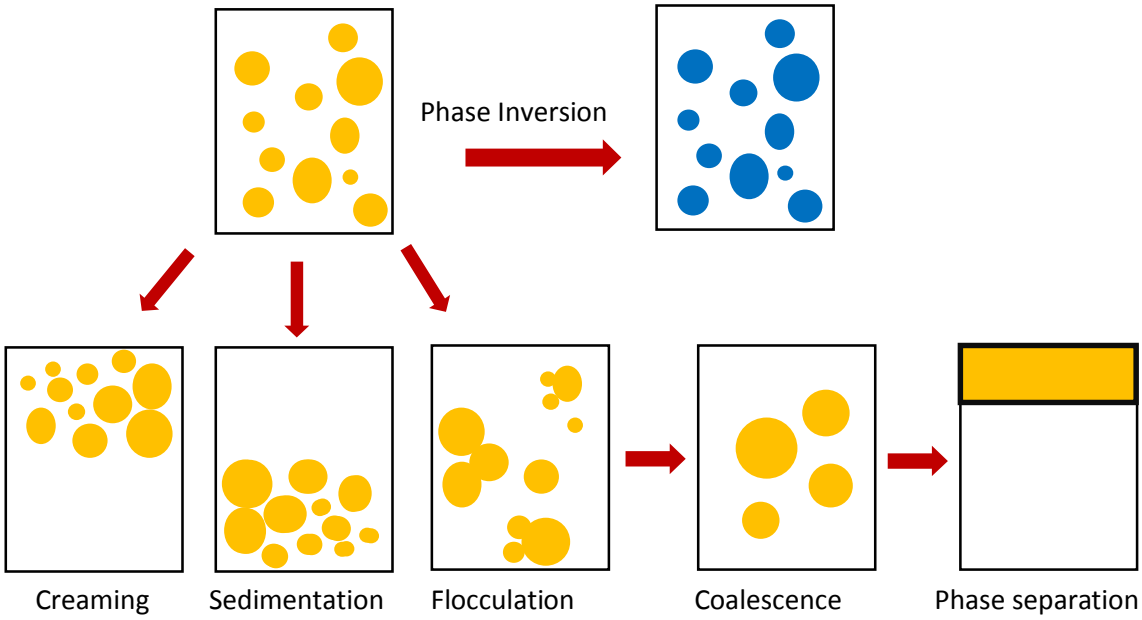

Figure 2.5 Mechanisms of emulsion instability (Salager 2006; Sjoblom, Fordedal and Skodvin 1996)

Emulsion instability mechanisms include creaming, sedimentation, flocculation, coalescence and phase inversion (Hargreaves 2003; Sjoblom, Fordedal and Skodvin 1996) (see Figure 2.5). The demulsification process utilised in this study is designed to cause the phase separation of oil, water and solids from the spent oil based drilling fluid and drill cutting slurry, so that the individual phases can be recovered and reused (Salager 2006). In the oil and gas industry, demulsification is defined as the breakdown of crude oil emulsion into oil and water to facilitate oil recovery. Thus, demulsifiers are also used to improve the quantity of extracted oil from the solid and water phases of oil based drilling mud (McCosh, Addicks and Gallo 2008). Several published studies have shown the utilisation of

chemical treatments which involve two main classes of treatments: organic (easily biodegradable and non-easily biodegradable) and inorganic (non-biodegradable) (Laha, Tansel and Ussawarujikulchai 2009; Khalladi et al. 2009; Paria 2008; Mulligan, Yong and Gibbs 2001). Research by Mishra, Sonawane and Shimpi (2009) and Lee and Tiwari (2012) have shown that chemical treatment will also enhance adhesion between the treated solid phase particles and the hydrophobic polymer matrix in polymer nanocomposite manufacture. Some typical chemical treatment processes include enzyme, silane, alkali-polymer, polymer, microemulsion, saponification, esterification, surfactant and biosurfactant treatments (Ali 2012; Koshelev et al. 2000; Brugnerotto et al. 2001; Abdul-Raheim et al. 2013). Hence, the addition of the demulsifier consists of different surface active agents to the oil based drilling mud, results in different kinds of chemical and physical events such as wetting, dissolution, flocculation, deflocculation, hydrolysis and lipolysis.

Generally, chemical demulsification can be caused by the use of ionic emulsifying surface-active agents with opposite charge to the emulsified material (OBM) resulting in a neutralising effect due to the incompatibility of anionic and cationic chemical agents. The use of sodium dodecyl sulphate (SDS) facilitates destabilisation of water in oil emulsion (Fernandez et al. 2008). Thus, the use of ionic surfactant can result in a flocculated or deflocculated system based on the charge of the particles. When particles and surfactant have opposite charges, neutralisation of particle charge occurs - leading to emulsion destabilisation. When a higher charge density is imparted to the suspended particles, deflocculation occurs. Flocculating agents such as chitosan, a cationic surfactant, promotes flocculation of oil in oily water remediation (Hosny et al. 2016).

Wetting agents such as poloxamer (polyoxyethylene/polyoxypropylene copolymers), sodium dioctyl sulfosuccinate, and lecithin promote reduction in interfacial tension between both liquids, and liquids with solids. Non-ionic wetting agents can lead to deflocculation because of the reduction of solid-liquid interfacial tension of the hydrated, hydrophilic layer around the individual solid particles which forms a mechanical barrier that prevents aggregation. Non-ionic wetting agents could also form a flocculated system of phase separation by adsorbing onto more than one particle and forming a loose flocculated structure.

Additives such as alcohol will reduce interfacial tension at the water-oil interface, penetrating loose agglomerates, displacing air from the pores of individual particles and promoting dispersion, thus allowing wetting to occur. The addition of alcohol to the demulsifier formulation could result in the precipitation of hydrophilic colloids. In some cases, these hydrophilic colloids such as bentonite have a tendency of acting as protective colloids by coating hydrophobic particles to impart a hydrophilic nature to the hydrophobic particle so as to enhance wetting and used to produce a deflocculated system (Billany 2007). Changes in pH can result in the breaking of an emulsion, particularly when sodium soaps react with acids. This is possible at low to neutral pH while alkaline pH could lead to a soap stabilised emulsion.

Oxidation by chemical addition, atmospheric oxygen and microbial action could result in demulsification. Microbial contamination of OBM could result in changes to its physicochemical properties. This is as a result of the production of microbial biomass and enzyme release into the OBM at favourable conditions of nutrients, temperature and pH (Yan et al. 2012). Temperature changes can influence demulsification and freezing of the emulsion aqueous phase will result in the production of ice crystals which exert unusual pressures on the dispersed globules and their adsorbed layer of demulsifier. While some emulsifying agents may precipitate at low temperature, dissolved electrolytes may concentrate in the unfrozen water, thus changing the charge density on the globules, allowing easy dissociation from the oil and emulsifying agents. At high temperature, the rate of creaming increases, leading to a decrease in the viscosity of the continuous phase. An increase in the temperature would cause an increase in the kinetic energy of dispersed droplets and associated emulsifying agent(s) at the water-oil interface. A consequent decrease in the association energy of the disperse phase and increased collision between globules would occur (Billany 2007).

On the other hand, research by Christian et al. (2009); Newman, Lomond and McCosh (2009); McCosh, Addicks and Gallo (2008); Quintero et al. (2008) have shown physical/mechanical emulsion destabilisation using techniques such as centrifugation, ultrasonication, vortexing, shaking and brushing to assist chemicals in the demulsification of spent oil based drilling fluid. Yan et al. (2012)

investigated the effect of mechanical stirring speed on the remediation of oil-based drill cuttings to reduce total extractable organics (TEO) *i.e.* hydrocarbon concentration of the drill cutting. Their findings show that as stirring speed is increased from 100 to 350 revolutions per minute (rpm), TEO percentage increased from greater than 40 to 80%. McCosh, Addicks and Gallo (2008) applied the use of a heated centrifuge, spun at 1800 relative centrifugal force (RCF) at 85^0C for 60 minutes to achieve demulsification of spent oil based drilling fluid.

As established earlier, demulsification leads to phase separation. Phase separation is the partitioning of a mixture into phases based on the density of the individual material making up each phase. Thus, the addition of the demulsifier could result in a deflocculated system where the dispersed particles remain as discrete units, forming a compact structure on sedimentation, or deflocculated where the dispersed particles remain associated with the liquid phase forming a loose structure on sedimentation (Billany 2007). Hence, the stability or instability of a suspension is normally measured by its rate of sedimentation, final volume or height of the sediment. This measurement is achieved by obtaining a ratio of V_f which is volume or height of sediment and V_o the volume or height of the suspension (OBM slurry). A plot of V_f/V_o against time can be obtained to ascertain the rate of sedimentation. It is important to note that when there is no measurable sedimentation, $V_f/V_o = 1$. V_f/V_o is called the flocculation value (f-value) or the sedimentation volume ratio (Fell 2007).

Phase separation studies by Azim et al. (2011) were carried out to ascertain optimum demulsifier concentration resulting in maximum % aqueous phase separation. Their phase separation study involved comparing demulsifier with treated, and untreated petroleum sludge mechanically stirred at 800 rpm for 5 minutes, both left to separate for 6 hours. In the phase separation study by McCosh, Addicks and Gallo (2008), carried out by use of a heated centrifuge, spun at 1800 RCF at 85^0C for 60 minutes, for oil recovery, it was found that the combination of the demulsifier and mechanical processes enhanced phase separation of the OBM based production waste (see Table 2.3). Without the demulsifier, only 40% water separation was achieved.

Table 2.3 Composition of production waste. (Adapted from McCosh, Addicks and Gallo (2008)

Demulsification method	**Oil (%)**	**Emulsion (%)**	**Water (%)**	**Solids (%)**
Centrifugation	40	35	25	Trace
Demulsifier and Centrifugation	45	-	54	1
Retort (Control method)	45	0	54	1

2.3.1 Formulation of demulsifier

Several chemical formulas have been developed for the demulsification of crude oil emulsion, oil based drilling fluid and oily sludge. As mentioned earlier, an emulsion is a mixture of two immiscible liquids *i.e.* oil and water while a suspension is a mixture of a solid in a liquid *e.g.* bentonite in water / oil (colloidal suspension). While emulsions are thermodynamically unstable, colloidal suspensions tend to be thermodynamically stable. Oil based drilling mud is a combination of a suspension and an emulsion (a complex slurry). Surfactants, emulsifiers and solvents can be used to produce a very low interfacial tension between aqueous and non-aqueous/organic phases which encourages mixing that continues to possess a degree of thermodynamic instability (Childs et al. 2005)s. The objective of the demulsifier treatment is to remove oil from the bentonite and other solid residues whilst encouraging the separation of oil and water. The desired interconnected events to be achieved by the demulsifier would include creation of very low interfacial tension between phases, high oil solubilisation, dispersion of solids phase, to increase oil extraction from solid surfaces and demulsifier surface (organo-) modification of the solid phase (Quintero, Jones and Pietrangeli 2012). Emuchay et al. (2013) formulated demulsifiers of surfactants, flocculants and solvents using different concentrations of coconut oil, D-limonene, liquid soap, starch, camphor, calcium hydroxide and paraffin wax. Using a bottle test analysis carried out at 40^0C, they found that 100mL crude oil emulsion was best demulsified using 0.6mL and 1.0ml formulation blends D and E which contained 5g camphor, 30mL of liquid soap, 30mL of starchy distilled water and 10mL coconut oil; and 2g camphor,

20mL of liquid soap, 15mL of distilled water with 20g starch, 10mL coconut oil and 5g petroleum wax respectively. They also found that the combination of demulsification and treating methods such as gravity sedimentation and heat enhances the demulsification process. Studies by Wang et al. (2010) and Zhang et al. (2005) showed the use of polyamidoamine (PAMAM), amphiphilic copolymer and polypropylene oxide-polyethylene oxide (PPO-PEO) polyether dendrimers for the demulsification of crude oil emulsion. The demulsification efficiency improved with increasing dendrimer generation as well as the terminal functional group *e.g.* amine used to synthesise the dendrimers. Microemulsion has been used for the solubilisation of non-aqueous fluid (base oil) in oil based drilling fluid filter cake and oily sludge. Microemulsion formulation by Quintero, Jones and Pietrangeli (2012) comprised of a brine-surfactants-oil microemulsion system, which includes co-solvents (*e.g.* methanol, isopropanol, butanol), salt *(e.g.* $CaCl_2$, NaCl), optional acid and linkers. Results showed that formulations with 5%NaCl, 5%vol alcohol co-solvent at 85^0C promoted the best phase separation; it was also observed that optimal phase separation could take place without salt using 5%vol alcohol co-solvent at 200^0C. On the other hand, other additives could be added to demulsifiers for additional functions besides emlusion instability *e.g.* Phosphorous. The presence of phosphorus in a demulsifier would increase solid residue phosphorus. Yan et al. (2015) suggested that the sorption of phosphorus to soil can be increased in the presence of organo-Al(Fe) complexes; which spent oil based drilling fluid and cuttings would contain due to the presence of petroleum hydrocarbon and Al and Fe. Phosphorus is known to assist in dewaxing, degumming and sedimentation of solid residues in suspension (Kusum and Bommayya 2011; Shiver 1984, Chin and Wong 1981), and reduce combustion or thermal degradation of polymers when the solid phase is used as filler (Chen and Wang 2006; Almeras et al. 2003).

In summary, the different chemicals *e.g.* bio-surfactants, synthetic surfactants, solvents could be used in the production of demulsifiers. However, demuslifier efficiency is also dependent on chemical dosage, temperature, time and mechanical process utilised.

2.4 Polyamide 6 (PA6) glass fibre reinforced nanocomposites

2.4.1 Polyamide 6 (PA6)

Polyamides are a class of engineering polymers. They are a popular and cheap polymer used in various engineering applications with a repeated molecular structure and weight of 113.16g/mol. PA6 also known as Nylon6 is a chemical substance which belongs to a class of high molecular weight polyamides. It is a semi-crystalline material. Physically, it comes in the form of rods, plates, pellets, disc, tubes and rings. It has no odour. Chemically, it is a product of the chemical reaction of diacids and diamines to produce amides and water (see Figure 2.6). It has a density of 1.15g/cm^3 at 23^{O}C [ISO 1183], melting point of 220^{O}C, glass transition of 47-50^{O}C, self-ignition temperature of >400^{O}C [ASTM D1929], thermal decomposition of >300^{O}C and crystallisation temperature of about 17.6 ^{O}C (Katoh and Okamoto 2009). It is also considered to be biodegradable (Mecking 2004). It has been used in different applications including textile (Bourbigot et al. 2002), food packaging (Quintavalla and Vicini 2002), barrier technology - rigid package (Lange and Wyser 2003) and it is used in the manufacture of automobile parts such as gears, oil pans and fittings (Mouti et al. 2012).

PA6 contains excellent toughness at equilibrium moisture content as well as chemical resistance and oil resistance. This is due to low permeability and good barrier potentials for liquids and gases. They have good heat resistance at continuous temperature applications between 80°C and 150°C. It is worth noting, however, that PA6 has low resistance to strong acids and strong bases, which for instance, acid led protonation distorts the polyamide structure to form an N-protonated amide, while base led deprotonation (N-ionisation) leads to alkali salt formation in presence of alkali metals (Moiseev and Zaikov 1987). Due to the crystalline and melting (phase changing) properties, PA6 is easily reinforced with other materials. Some of those materials include natural fibre, silica, glass fibre and montmorillonite. Studies show that reinforcement of PA6 with other materials provides a material with superior, thermal and mechanical properties (elastic modulus and strength). Amongst Polyamides, PA6 contains the highest water absorption rate of 8% and more. PA6 can be further modified with special chemicals or materials to enhance and specialise its qualities. Thus,

PA6 could be advanced to possess electric conductive and flame-resistant as well as self-extinguishing properties (Zhang et al. 2013, Morgan and Wilkie 2007).

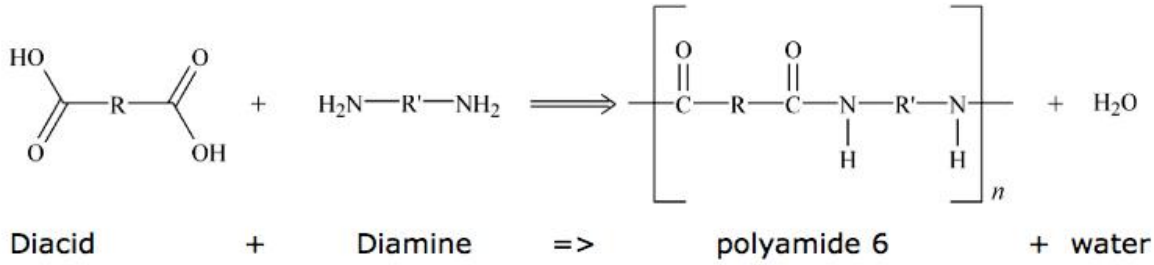

Figure 2.6 General formula for the production of polyamides

On the other hand, PA6 has some disadvantages. Some of them include high absorbance to moisture. Due to its semi-crystalline nature, its polymer chains are not packed in a highly ordered (lattice) structure, thus it is less dense and has a higher permeability which allows for the diffusion of colouring (dyes) into its matrix. This can also be advantageous in the manufacture of a nano-micro phased composite material. Again, although it is classified as a semi-crystalline material, it is more amorphous and thus it is susceptible to mechanical failures such as permanent compression as a result of regular or periodic pressure (poor recovery properties).

2.4.2 Glass fibre (GF)

Glass fibre is a material made up of many fine fibres or filament of glass. It is produced by heating and drawing glass into thin fibres of small diameters. There are different kinds of glass fibre. The most common glass fibre used in glass reinforcement of thermoplastics is called E glass fibre. It is made up of alumina borosilicate glass and 1% w/w alkali oxides, and has electric resistance (Vlasveld et al. 2005; Vlasveld, Bersee and Picken. 2005). R glass fibre is similar to E glass fibre but without CaO and MgO for higher mechanical property of reinforcement; S glass fibre is similar to E-glass fibre but including MgO and excluding CaO for high tensile strength (Hewak et al. 1994). Another glass fibre made up of alkali lime glass with negligible or no boron oxide is called A glass fibre. C glass fibre used for insulation is made up of alkali-lime glass and high boron content. E-CR glass is made up of alumina lime silicate glass and 1% w/w alkali oxides and

known for electrical and chemical resistance especially high acid. D-glass fibre is made up of borosilicate glass and known for its low dielectric constant (Henckens, Driessen and Worrell 2015; Fitzer et al. 2000).

Glass fibre is used as reinforcement in different materials such as plastic, textile, concrete to produce high strength, corrosion or heat resistant materials. It can also be used to produce thermal, electrical or sound insulation materials. It is currently used to reinforce materials for automobile bodies, transparent roofing sheets, sports equipment (*e.g.* hockey sticks), and medical casts.

Issues associated with glass fibre include material brittleness, weak abrasive-resistance, moisture association and airborne fibre impact on asthmic people.

2.4.3 Montmorillonite

Montmorillonite is a natural mineral which occurs as a hydrated aluminosilicate of sodium that might also contain calcium, magnesium, iron and other solids such as respirable crystalline silica. Bentonite is a type of montmorillonite used in the oil and gas sector as a component of drilling fluid to improve drilling fliud viscousity.

Montmorillonite is a layered silicate with about 2 nm thickness and with a large surface area and negatively charged by either O^{2-} or $(OH)^{-}$ (see Figure 2.7). Its layer lattice are formed from oxygen ion-covalent bonds which shows two kinds of structural units: tetrahedral units of a central silicon with four surrounding oxygen ions ($Si_4O_{10}(OH)_2$) called a silica layer, and octahedral units of central aluminium or magnesium ion surrounded by six hydroxyl ions – [$Al_4(OH)_6$ and $Mg_6(OH)_6$] called gibbsite layer and brucite layer respectively (Pavlidou and Papaspyrides 2008). Montmorillonite has an adsorbed or adhering layer where very strong interaction with water via H_3O^+ bonding takes place, as the water immigrates to and beyond the adsorption (absorbed) layers (perhaps due to excess water), the bonds weaken until the clay becomes fluidised.

When clay is in liquid suspension, forces of attraction or repulsion could act. Forces of attraction by van der Waals occur when particles are brought together due to a decrease in adsorbed layer thickness resulting from Base Exchange Capacity (BEC), thereby causing flocculation. When the water content is low,

only occupying the adsorbed layer, the clay particles exert strong forces of attraction on each other which generates an internal tension (cohesive force) amongst clay particles. As the water content increases, the cohesion, suction or binding effect amongst the particles decreases until there is sufficient water present to permit particles to slide off each other without internal cracks. This is called plastic limit. Continued addition of water causes the mixture to flow freely as liquid bringing the mixture to its liquid limit. Montmorillonite has high swelling, shrinking and plastic potentials amongst clays, and thus, can be easily dispersed and separated from mixtures (Whitlow 1995).

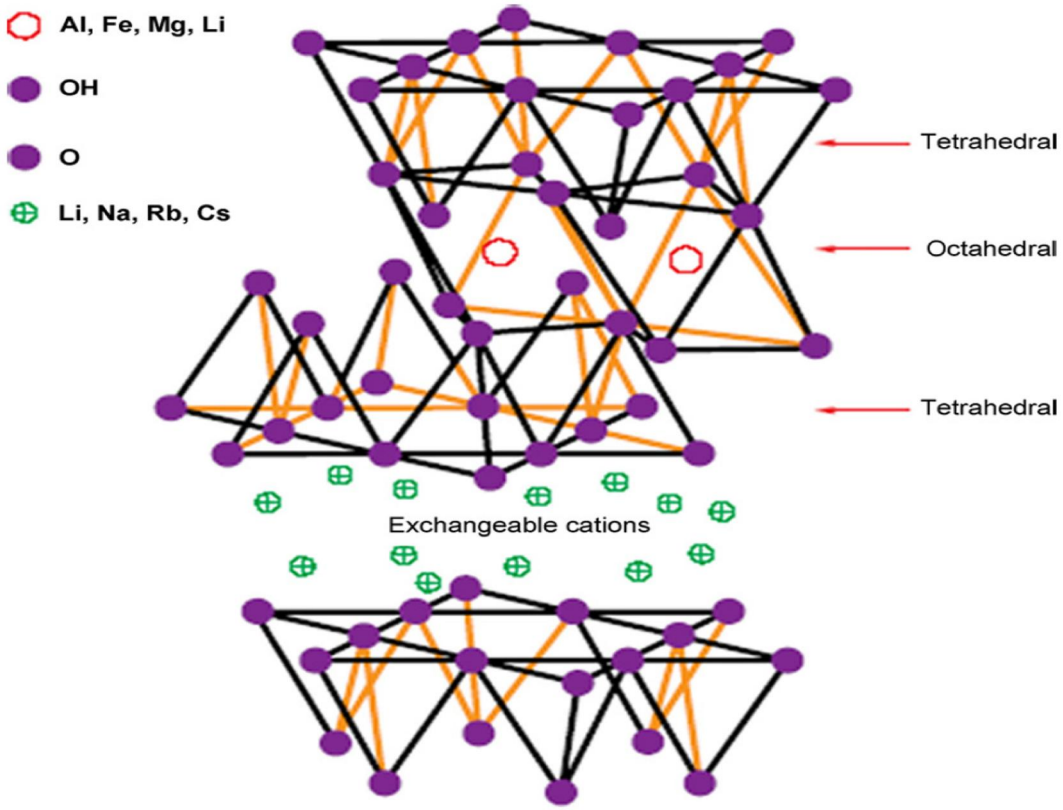

Figure 2.7 Structure of montmorillonite showing arrangement of functional groups and site of exchangeable ions (Pavlidou and Papaspyrides 2008)

2.4.4 Surface modification of montmorillonite

Nanocomposites with nanoparticles enhance the mechanical and thermal properties of thermoplastic materials. However, the filler interaction or association with the polymer is dependent on dispersion process as well as filler treatment or surface modification. On the other hand, surface modification has been used to enhance interfacial bonding between the filler and the polymer

matrix; for instance, the use of coupling agents, and organo-modifiers such as long-chain alkyl ammonium ions (Theng and Yuan 2008) (see Figure 2.8).

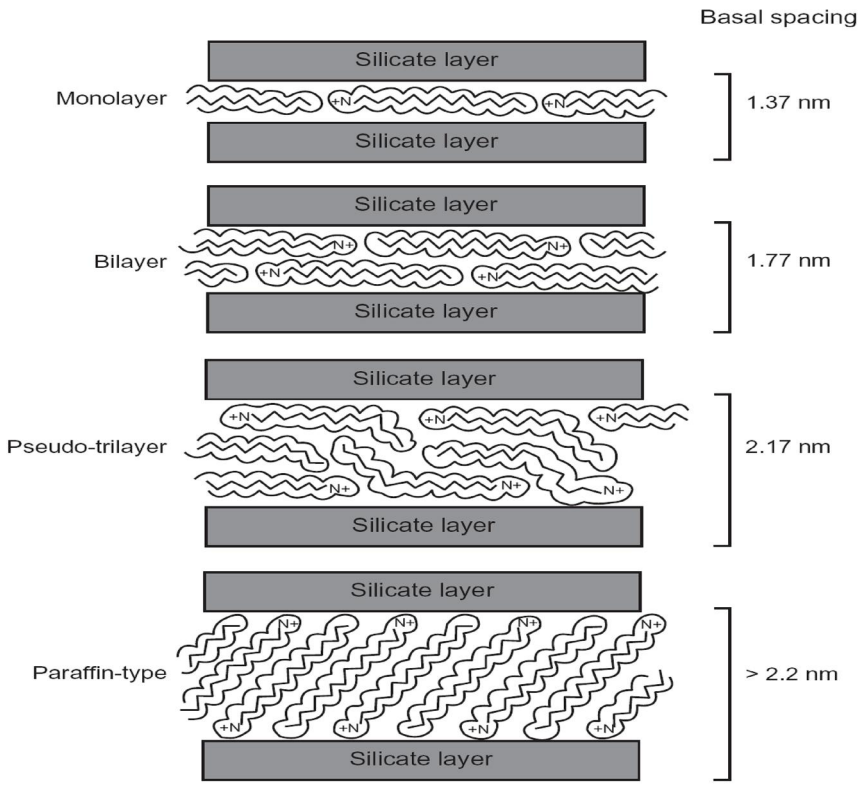

Figure 2.8 Potential organisations of long-chain alkyl ammonium ions in the interlayer space of montmorillonite, indicating basal spacing of different organoclays. (Theng and Yuan 2008).

In some cases, nanoparticles can form agglomerates within the polymer matrix. This particle agglomeration resulted in non-uniform stress concentration and led to a decrease in nanocomposite material properties (Rong, Zhang and Ruan 2006; Bansal et al. 2005).

Surface modification, in general, is employed to enhance filler-matrix interaction by increasing the interfacial bonding of filler and polymer. In some cases, surface modification could result in a change in hydrophilicity of polymers or change in filler charge which improves bonding. For instance, organic chemicals have been used in the surface modification /organic synthesis of fillers which converts montmorillonite (MMT) to organo-montmorillonite (OMMT) as well as with maleic acid. Some methods for surface modification include silage, enzyme and alkaline

treatment, benzoylation (Zhu et al. 2013) and some of these are briefly described below:

- **Acetylation**: Acetylation is an esterification method used to improve moisture resistance and dimensional stability. Here, the acetic anhydride such as butanetetracarboxylic acid (BTCA) reacts with reactive hydroxyl groups (OH) of the filler. This improves the flexural strength of composites by 18%. Acetylation has the potential effect of increasing the basal space of a filler (Zhu et al. 2013).
- **Alkali treatment:** The alkali treatment of filler is another surface modification process (Motawie et al. 2014). This treatment changes in surface morphology and chemical compositions of fillers which reduces the thermal degradation of fillers. The presence of alkali in the crude oil and demulsifier could lead to alkali treatment on the OBM solid residues (filler).
- **Benzoylation treatment:** In this surface modification method, benzoyl chloride is employed. The treatment involves the addition of the benzoyl group to the natural fibre filler. This reduces the hydrophilic nature of the filler, thus, making it polymer matrix friendly. This decreases composite material water absorption as well as an increase in strength properties. The addition of benzene and its derivatives to fillers could also be achieved using untreated oil based drilling fluid which contains crude oil.
- **Enzyme treatment:** Enzymes are the catalyst of chemical modification. Lipase is used to catalyse the hydrolysis of fats, oil and hydrocarbons to produce hydrocarbon radicals. The use of enzymes could result in oxidation of functional groups to form radicals on the filler, thereby making the filler suitable for use.
- **Stearic acid and SDS treatment:** Stearic acid ($CH_3(CH_2)_{16}COOH$) and SDS ($C_{11}H_{23}CH_2SO_3Na$) treatment of fillers increases hydrophobicity of fillers. In rubber with montmorillonite clay filler, Stearic acid treatment increased rubber intercalation into the clay (Das et al 2011). These treatments also expanded the interlayer space of montmorillonite, improving exfoliation of fillers and intercalation of the polymer matrix. It also improves the mechanical properties of nanocomposites (Gonzalez et al. 2013; Das et al 2011, Wang et al. 2004; Liu et al. 2005)

2.4.5 Polymer Nanocomposites

Polymer composites are multiphase materials consisting of one or more fillers within a polymer matrix. Polymer nanocomposite materials contain fillers having a particle size in nanometers.

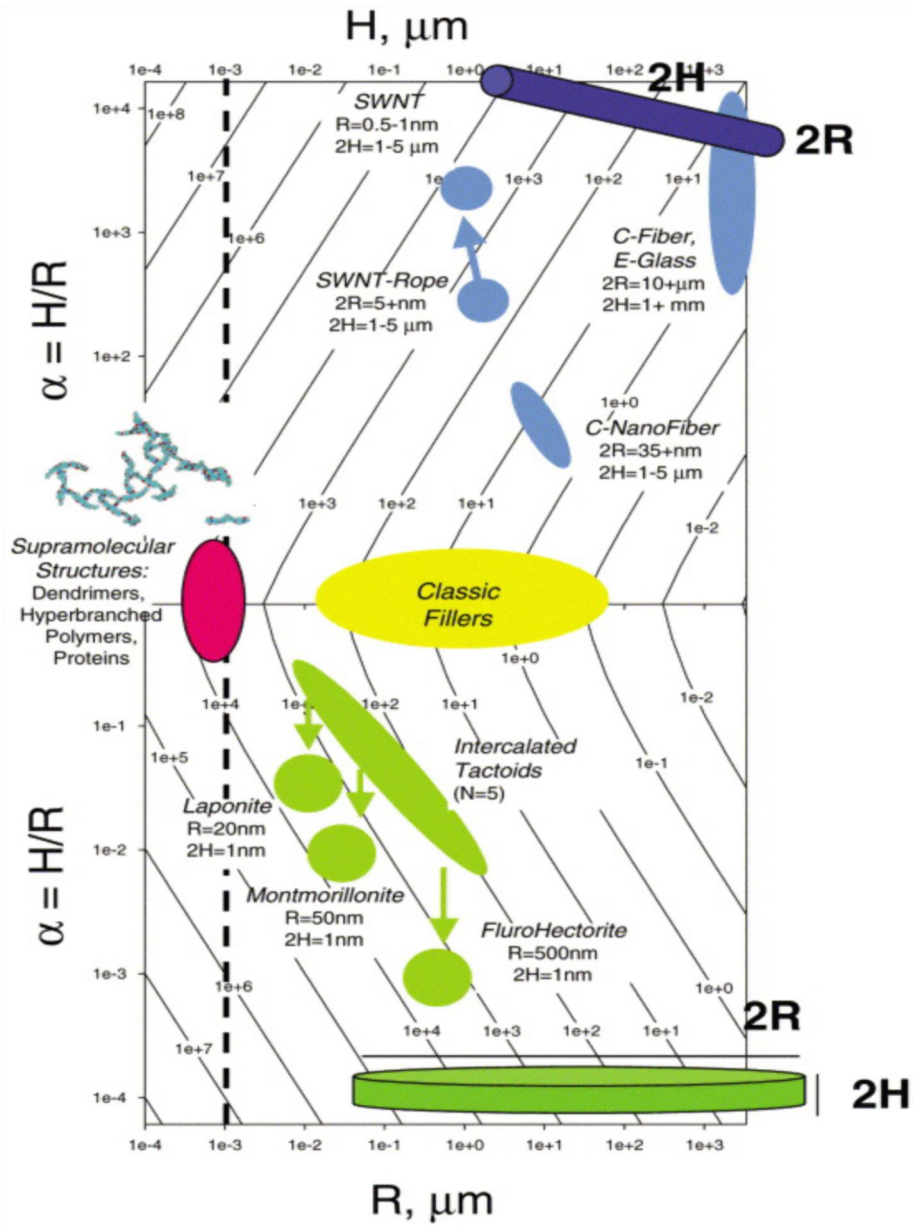

Figure 2.9 Logarithmic isolines of interfacial (surface) area / volume of particles (µm1 = m^2/mL) showing different sizes and shapes of polymer fillers and reinforcement materials. (Vaia and Wagner 2004)

In polymer nanocomposites, nanofillers are used to enhance polymer properties due to their large surface-to-volume ratio. Nanofillers vary in shapes such as

nanoplates (nano clay), nanoparticles (nano barium sulphate), nanofibres (chitosan), nanotubes (carbon nanotubes) and nanorods (calcium sulphate) (see Figure 2.9). Nanofillers dispersed in polymer matrixes offer higher interfacial area than macrofillers. Other factors that influence the quality of a polymer nanocomposite aside from the filler size and shape include the polymer properties, filler dispersion and the manufacturing process adopted.

The importance of layered fillers is in their ability to form well intercalated and exfoliated composites (see Figure 2.10). The layered nature of nanoplates causes the polymer molecules to be 'sandwiched' between these layers. This morphological distribution enhances the mechanical properties of the composite. In exfoliated and intercalated composites, there is a random distribution or dispersion of the filler in the polymer matrix. This results in increased (original) material strength and modulus. However, exfoliated composites possess more enhanced mechanical properties than intercalated composites as a result of higher dispersion of fillers within the polymer matrix. In intercalation composites, there is the agglomeration of filler(s) which does not allow for easy exfoliation. Thus, some composite materials could have both intercalation and exfoliation.

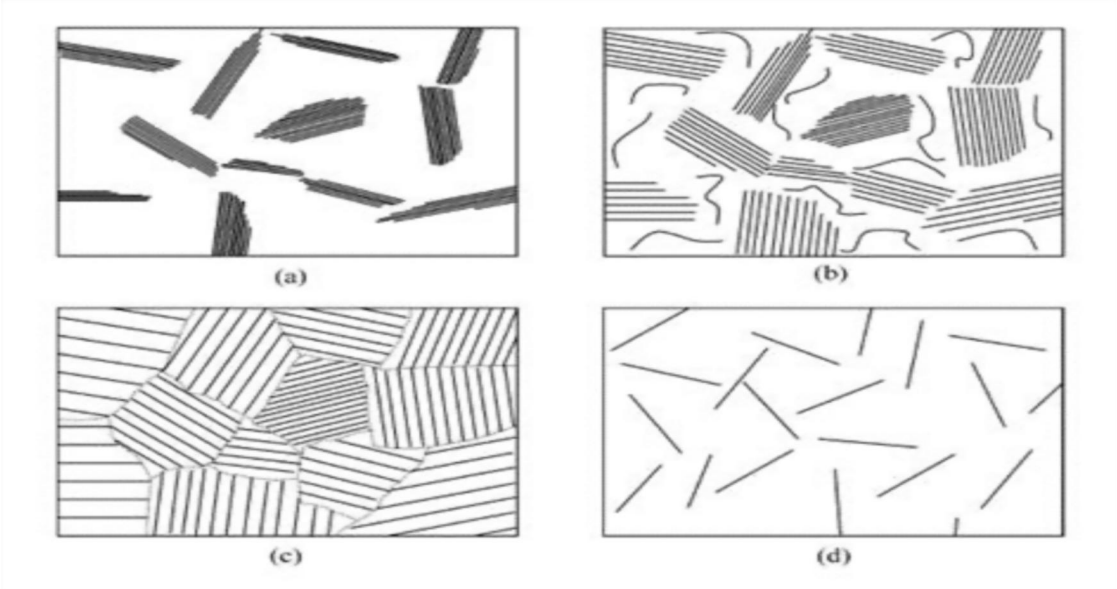

Figure 2.10 Morphology of polymer and filler interaction (e.g. nanoclay composite) showing (a) conventional miscible, (b) partially intercalated, (c) intercalated and dispersed and (d) exfoliated and dispersed (Luo and Daniel 2003)

Figure 2.11 shows that the use of fillers also helps to enhance compatibility and reduce dispersive space between blended and non-blended polymers. This is discussed by Khatua et al. (2004) where organo-clay aids domain size reduction of EPR elastomer phases. In PA6 matrix organo-clay interactions with the polymer give rise to more polymer-polymer interactions thus improving the properties of the previously incompatible polymer chains. Organo-clay achieved this as a result of the organo (organic) functionalisation of the clay (MMT) by a surfactant such as $(R\text{-}NH_3^+)\text{-}Cl^-$ (dipolyoxyethylene alkyl (coco) methylammonium cation) to make the organoclay easily interact with hydrophobic polymers (Li and Shimizu 2004).

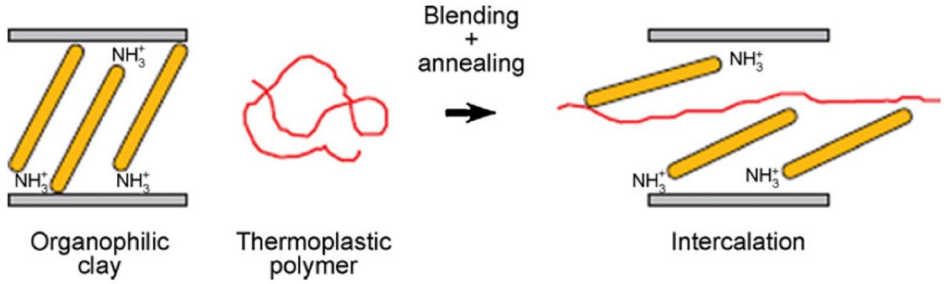

Figure 2.11 Melt intercalation process of blending PA6 thermoplastic polymer with organophillic filler

Study by Li and Shimizu (2004), organo-clay acted to reduce the interfacial tension between PA6 and polypropylene oxide (PPO) polymer chains. Thus, as the filler volume (% weight) was increased, PPO (of high melt viscosity) was found to have a lesser (finer) domain size within the PA6 matrix. This increased polymer-polymer interaction due to the ability of the organoclay to reduce coalescence of PPO moiety. It also resulted in the thinning of the PA6 phase (reduced coalescence) through the PA6 exfoliation of the layered clay platelets. Wilkinson et al. (1999) reported this in their investigation of phase structure in blends of PP/ PA6/ SEBS (Polypropylene/Polyamide6/(poly[styrene-b-(ethylene-co-butylene)-b-styrene]). The increase in SEBS increased interaction of PP and PA6 as well as decreased yield stress.

The use of fillers may change the phase behaviour of a composite material from that of the precursor polymers. A good example was seen in the use of nanoclay

in the reinforcement of PA6. The nanoclay leads to the formation of the γ-crystalline phase of PA6 rather than the more stable α-crystaline phase. The phase transition from γ to α phase in PA6 occurred at a temperature of 160^{O}C in nanocomposite compared to 120^{O}C in neat PA6 as shown in XRD diffractogram study by Liu and Wu (2002). Thus, PA6 nanocomposite has a higher phase transition temperature than neat PA6. Thermal analysis of the samples by Liu and Wu (2002) showed that PA6 nanocomposite melt started at 190^{O}C with a T_m of 219^{O}C which was initiated by the presence of the γ-crystalline while PA6 started melting at 210^{O}C with a T_m of 223^{O}C which was initiated by the presence of α-crystalline PA6 phase. However, this ability of filler property to enhance melting could be based on the treatment of the filler (e.g. nanoclay or silica) prior to use and the chemical reaction that takes place as a result of heating the material.

In plastics such as PA6, glass fibre has been used extensively so as to enhance mechanical strength and thermal stability. Khan and Ahmed (2015) carried out a comparative study on PA6 composites of clay (MMT) at 5% and glass fibre at 25%, and PA6. The findings showed that PA6/MMT and PA6/GF had improved tensile modulus of 460% and 148% respectively compared to pure PA6. On the other hand, PA/GF did not show the polymorphic phase of PA6, while PA6/MMT showed both polymorphous phases, α and γ-phases of PA6.

Research by Tan, Wang and Wu (2015) highlighted that the length of glass fibre was a determinant for improved mechanical properties. They found that by increasing interfacial adhesion of long glass fibre to PA6 matrix, the impact properties were more improved than the short glass fibre. Wan et al. (2013) investigated the mechanical and thermal properties of multiphase reinforcement of PA6 with short glass fibre (SGF) and nanoclay. Their findings revealed that the synergy of PA6/Clay/SGF produced materials of higher viscosity, an increase in glass transition temperature, T_g, increase in storage modulus and higher yield stress than that of individual fillers. The combustion reduction / fire retardance properties were improved because clay improved the char formation and fire retardance (combustion reduction) was increased with increasing glass fibre content.

Silva et al. (2014) showed that multiple reinforcements or fillers had an impact on the tensile properties of PA6 and Polypropylene (PP) nanocomposite materials. The results also showed that the presence of multiple fillers within a matrix lowered the crystallinity of the material. The differences in tensile modulus of PA6/ GF compared to PA6/GF/SiO, PA6/GF/MMT and PA6/GF/GS were 4.34%, 10.15%, and 24.64% respectively. However, PP composites had a reduction in tensile modulus of 10.6, 10.6% and 13.64% for PP/GF/SiO, PP/GF/MMT and PP/GF/GS respectively compared to the tensile modulus of PP/ GF which was 6.6GPa.

For PA samples PA6/GF/SiO, PA6/GF/MMT and PA6/GF/GS, there was the percentage change in transverse extension of 1.7%, -0.1% and -0.4% compared to PA6/GF of 5.2%. Percentage changes in transverse elongation of PP composites were 0.1%, -0.4% and -1.5% for PP/GF/SiO_2, PP/GF/MMT and PP/GF/GS respectively, while PP/GF had an extension of 2.8%. This showed that SiO_2 in PA6/ GF/GS and PA/GF/SiO composites had an impact on improving the tensile modulus and elongation properties of PA6/GF composites respectively.

Nanoclays were first used in polymer nanocomposites by Toyota in 1993 (Okada and Usuki 2006, Deguchi, Nishio and Okada. 1993). Polymer nanocomposites such as polyamide have found applications in engineering such as aerospace, medical and automotive sector *e.g.* automotive applications on Figure 2.12. Nanoclays are the most frequently used nanofillers for polyamide nanocomposites to improve their mechanical and thermal properties.

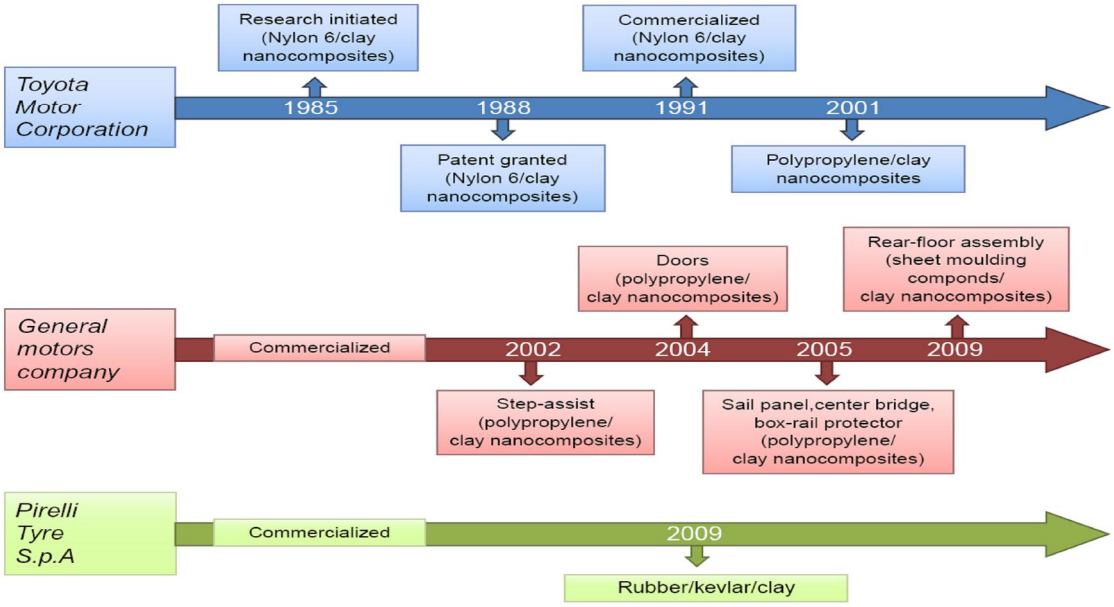

Figure 2.12 Polymer nanocomposite applications developed in the automotive industry. (Galimberti, Cipolletti and Coombs 2013)

2.5 Conclusions of the literature review and scope of the thesis in the light of literature review

This literature review focused on oil based drilling fluid, their treatment methods especially via demulsification and phase separation as well as the use of treated and untreated solid residue of spent oil based drilling fluid for the manufacture of PA6 nanocomposite materials.

The key finds of the literature review are

- Oil based drilling fluid and cutting wastes are global liabilities. This is due to their nature as oil hazardous waste and their impacts on flora, fauna, and global carbon footprint. The use of mechanical and thermal methods for the clean-up and treatment of these oily waste types have proven insufficient due to residual oil on the dry waste surface. The development of demulsifiers to ensure chemically enhanced phase separation of these wastes into oil, water and solid components is therefore of particular importance due to the chemistry of individual treatments. These wastes have potential as useful minerals.

- Bentonite used in the oil and gas sector as drilling fluid contain stabilisers, preservatives, solvents, gases or liquids. Within the drilling fluid, in the presence of barium sulphate-bentonite-oil mixture, bentonite acts as an emulsion stabiliser, which is destabilised by organic surface active agents (Abend et al. 1998, Lagaly, Reese and Abend 1999a, Lagaly, Reese and Abend 1999b).

- Nanofillers are sometimes particularly important because of their inertness, stability and unique rheological properties, as well as their chemical reactivity and catalytic activity.

- In clay-oil-water mixtures, oil adheres firmly to the clay adsorbed layer while water molecules have a secondary preference and adhere more to the oil (liquid). The surface of clay particles must become water wet for easy separation of oil from the clay absorbed layer. Thus, using surfactants and other chemicals, the oil could be flocculated from the clay.
- The recycling of treated drilling fluid into Polyamide composites has not been published.

This thesis will, therefore, focus on the characterisation of spent oil based drilling fluid (also known as OBM), demulsification and phase separation process to extract oil and recover solid residue for recycling into PA6 nanocomposite manufacture and the investigation into the surface, mechanical and thermal properties of the novel PA6 nanocomposite materials.

Chapter 3

Characterisation of spent oil based drilling fluid and low-density cuttings from the North Sea

3.1 Introduction

In this chapter, the characterisation of oil based drilling fluid and cutting from the UK continental shelf of the North Sea is presented and discussed. The characterisation was carried out using a range of analytical techniques. Fourier transform infra-red (FTIR) was used for total petroleum hydrocarbon concentration, inductively coupled plasma optical emission spectroscopy (ICPOES) for metal and non-metal concentration, X-ray diffraction (XRD) for mineralogy and crystallinity, scanning electron microscopy (SEM) for morphology, and energy dispersive x-ray analysis (EDXA), and attenuated total reflectance – Fourier transform infra-red (ATR- FTIR) to study surface chemistry of the spent oil based drilling fluid.

Andrade et al. (2009) used SEM, XRD and ATR-FTIR to characterise petroleum sludge. The research findings suggest that SEM micrograph of dry oily petroleum sludge showed solid residues of irregular sizes. The XRD result showed the presence of crystalline materials including barite, quartz, zinc oxide, montmorillonite, magnesium oxide and calcite while the FTIR results showed the spectral bands at 1166 cm^{-1} were assigned to Si-O stretching of quartz as well as Si-O spectra bands at 1124 cm^{-1} and 1014 cm^{-1} from montmorillonite. Classic analytical methods for TPH include FTIR TPH and gas chromatography. Research by Perry and Griffin (2001) showed that although Mexican regulation stipulates that the oil on residue before disposal must be less than 1000ppm by infrared method (FTIR TPH), TPH of oil based drilling mud and associated cutting obtained by gas chromatography was 65,000ppm. Perry and Griffin (2001) showed that particle size analysis for the DF mud and cutting sample was carried out by sieve method and had an average particle size. However, the challenge with the sieving technique is the inability to analyse the nano-size particle which laser diffraction particle size analyser and zetasizer would show. Gbadebo, Taiwo and Eghele (2010) investigated elements in both oil based and water based drilling

fluid using atomic absorption spectrophotometry. The results showed the presence of Fe, Ca, Mg, Cr, Pb, Mn and Ni. Research by Adegbotolu et al. (2014) showed ICPOES analysis of oil based drilling fluid and cuttings. The result showed the presence of heavy and trace metals. Tehrani, Chapman and Fraser (2003) showed the use of rheology measurements to investigate thixotropy and barite sag of oil based drilling fluid. Retort analysis is used to obtain the percentages of oil, water and solids in drilling fluid as reported by Tyrone and Ulyasheva (2016) in the research on phase evaporation in oil based muds.

It was expected that the characterisation of this used oil based drilling fluid should give indications of method suitability for analyses of untreated and treated (cleaned up or remediated) samples, provide data for comparisons of different wastes characterisation methods or treatment methods, and more importantly provide data for the untreated sample which will be used as a baseline for assessing the efficiency of the treatment and further studies.

3.2 Experiment

3.2.1 Materials

Used oil based drilling fluid was obtained from a local oil and gas company, tetrachloroethylene (TCE) with purity of 99.5% was purchased from Sigma-Aldrich, UK, deionised water, element stock solutions of 10,000ppm Ba, Zn, Na, Al, Cu, Mg, Fe, Cr, Cd, Hg, Ni, Pb, As, Ca, Mn, K, P, Si, S and V in nitric acid, hydrochloric acid (analytical grade) and sodium sulphate (analytical grade) were obtained from Fisher Scientific Ltd, Loughborough, UK.

3.2.2 Characterisation

Scanning electron microscopy/energy dispersive x-ray analysis (SEM/EDXA)

The experiment was carried out using a Zeiss EVO LS10 variable pressure scanning electron microscope instrument. Dried samples of untreated oil based drilling mud and cutting were placed in the sample chamber for analysis. The system was set to chamber pressure of 50 Pa, different magnifications, a

working distance (WD) of 6.5mm, and accelerating potential of 25kV. Zeiss Smart SEM software was used to control the microscope and capture images.

The SEM images were obtained and thereafter the EDX analysis was carried out to determine the elemental composition of the used drilling mud and cutting samples through the automated collection of X-ray spectra over a predefined grid.

X-ray diffraction (XRD) analysis

X-ray diffraction (XRD) analysis was carried out following a methodology adapted from Andrade et al. (2009). The analysis was performed using a Philips Analytical X-ray diffractometer. An acceleration voltage of 40 kV and 25 mA applied using a CuKα radiation with wavelength λ = 0.154 nm. The diffractograms were obtained within the range of scattering angles (2θ) of 5° – 80° at a scan rate of 1°/min. Sample preparation involved introducing the dried sample into the XRD sample holder.

Attenuated Total Reflectance – Fourier Transform Infra-Red (ATR-FTIR) analysis

The ATR-FTIR analysis was carried out following a methodology described in Andrade et al. (2009). The measurements were performed using a Thermo Scientific Nicolet iS 10 FT-IR Spectrometer. It was used to obtain the infrared spectra of the dried used oil based drilling fluid. The spectrometer was set up in ATR mode using a diamond internal reflection element (IRE). The mid-infrared range across 4000–400 cm^{-1} was measured with a spectral resolution of 8 cm^{-1} and 32 scans. The air background was collected and then the sample spectra was collected and saved. The dry drilling waste sample was placed between the ATR stage and the diamond.

Total Petroleum Hydrocarbon (TPH) concentration analysis

The method used for the determination of total hydrocarbon content was obtained from The UK Department of Energy and Climate Change method for the determination of hydrocarbons (DECC 2014) using the Perkin-Elmer GX 2000 FTIR. Calibration standard solutions from 0 - 500 mg/L were prepared in

triplicate from a 1000mg/L stock solution of diesel in Perklone (tetrachloroethylene). The standards were then analysed on the FTIR using 10 scans and the peak area over 3100 and 2700 cm^{-1} was recorded. Drilling waste of 0.5g was weighed into a centrifuge tube and 15ml of tetrachloroethylene (TCE) solvent was added for the extraction of petroleum hydrocarbon from the sample through sonication for 15 minutes. The sonicated sample was centrifuged at 3500rpm for 10 minutes at room temperature. The organic solvent phase was decanted and 0.5g of anhydrous sodium sulphate was added to the hydrocarbon containing solvent phase to remove any excess water. The solvent portion was transferred into a 10mm cuvette for analysis as carried out for standards. The results based on spectrometer absorption reading were recorded and actual concentration values were deduced from diesel in TCE calibration graphs.

Inductively Coupled Plasma Optical Emission Spectroscopy (ICPOES) Analysis

Oil-based drilling fluid and cuttings sample of 0.5g was digested using an aqua regia-microwave digestion procedure for 30minutes. An Optima 2100 DV ICP-OES system was used to carry out the analyses. The ICP-OES system had the following operation parameters of Power: 1500 Watts, frequency: 40.68 MHz, nebuliser flow: 0.60 L/min, argon plasma flow: 15 L/min, Argon auxiliary Flow: 0.2 L/min, argon pump rate: 2.0 mL/min. A 100mg/L multi-element standard was prepared and used to prepare the elemental calibration of range 0.5 to 5mg/L. The elements in the multi-element standard were heavy metals: As, Cd, Cr, Ni, Zn, Pb, Hg; mineral elements: Ba, Ca, Na, Al, Fe, S, P, Si, Mg, K. The acid extract was analysed for the selected elements using ICPOES. The analytical results obtained were compared against OSPAR threshold guidelines.

Retort Analysis

This method was adapted from McPhee, Reed and Zubizarreta (2015). The oily drilling waste of 100ml was weighed and transferred into the retort apparatus. The apparatus was heated to 1200^{o}C and the water and oil portions were condensed and collected. The residual solid, water and oil were weighed and oil:water ratio and percentage of extracted phases calculated.

Rheology

A Brookfield rheometer with LV 64 spindle was set up and readings were taken at a temperature of 19^{o}C using 300mL of used drilling fluid and cuttings. The Brookfield LV 64 spindle has a working viscosity range of 15 to 6,000,000 cP. The sample viscosity, shear stress, shear rate and torque were measured at different speeds of 0.5, 1, 2, 4, 8 and 15rpm. The viscosity values were obtained at different speeds (rpm) versus analysis time to ascertain the fluid property.

Particle Size Analysis

A Malvern Mastersizer 2000 with a small sample liquid dispensing unit was used to carry out the particle size analysis for the microsized solid residues in the dried oil based drilling fluid with cuttings sample. Sample of 0.5g was suspended in deionised water. A background of the water was obtained as a blank using the Malvern particle sizer. The sample solution was passed through the laser. The results were recorded for sample particle size distribution. A Malvern zetasizer ZS was used to obtain the nanosize distribution of the sample. 0.5g of the sample was suspended in deionised water and centrifuged at 4500rpm for 10minutes at 23^{o}C to obtain the nanosized residues for the nano particle size determination.

3.3 Results and discussion

3.3.1 Morphology studies

The surface analyses were carried out using X-ray diffraction, FTIR-ATR and SEM for morphology. The SEM micrograph shows a variation of particle sizes in the oil based drilling mud and cutting sample. As shown in Figure 3.1, the particles are sized from a nanoscale to the microscale. Figure 3.1 micrograph showed some smaller sized layer structured platelets which are attributed to bentonite clay. The larger block like particles were suggested to be barite, calcite, sandstone and quartz based on references (Kodel et al. 2012; Bin Merdhah 2010).

Andrade et al. (2009) showed SEM micrograph similar to that obtained in this study for dry oily petroleum sludge. In their study, the SEM images of the dry

sludge showed the characteristic aggregation of flat plates with irregular shapes, boundaries and sizes as in this current study.

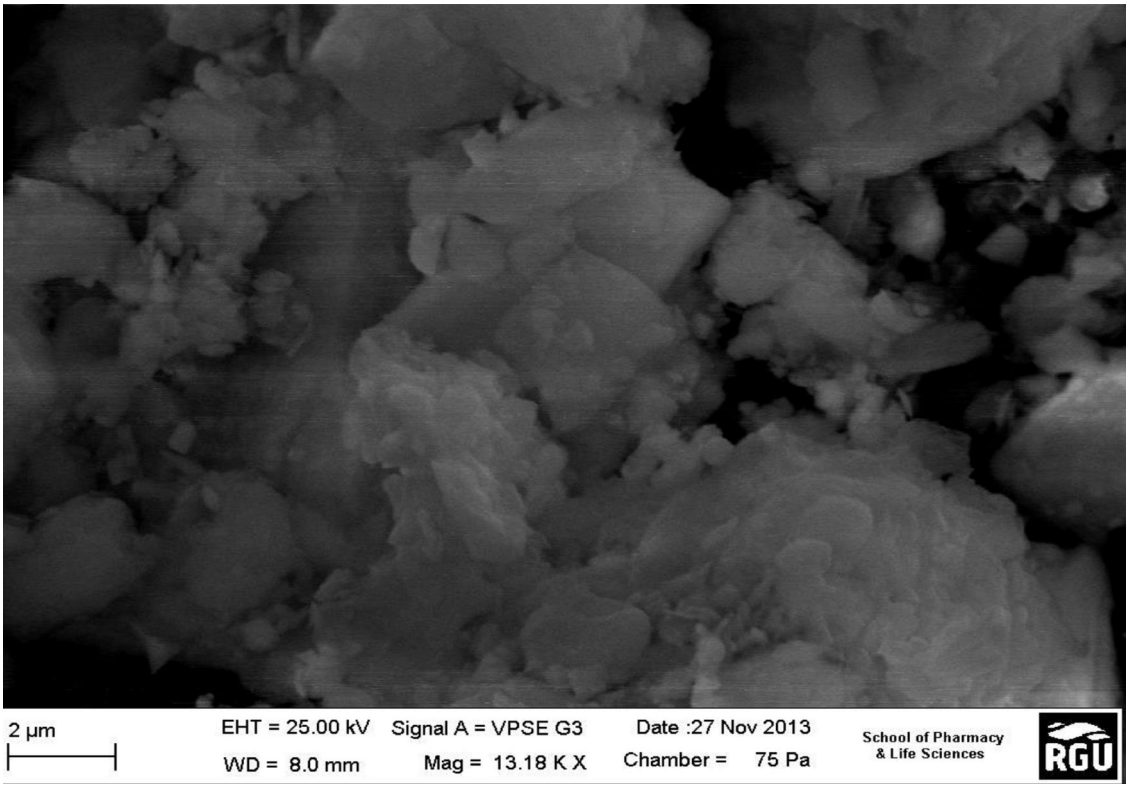

Figure 3.1 SEM image of spent oil based drilling fluid containing low-density cutting (magnification: 13.18 K X)

The XRD diffractogram of OBMC is shown in Figure 3.2. The results showed the presence of $BaSO_4$, $CaCO_3$, SiO_2, and MMT (bentonite clay). The diffractogram measured in the range of 2Theta (2θ) = 5^o – 80^o shows that the sample has both amorphous and crystalline properties. The broad amorphous peak starting from 2θ = 5^o – 19^o shows the presence of amorphous silica. This is suggested to be as a result of the clay content of the sample. On the other hand, the sharp peaks suggested the presence of crystalline materials in the samples. These crystalline materials include barite (2θ = 26.2^o(26^o), 29.1^o(29^o), 31.9^o and 43.5^o), quartz (2θ = 21.5, 23 and 26.0^o), zinc oxide (30-40^o), montmorillonite (6^o, 9^o, 12^o, 14^o, 18^o, 27^o, 30^o, 61^o), bentonite (6^o, 9^o, 12^o, 14.8^o, 18^o, 27^o, 30^o, 61^o), magnetite oxide (35.5^0) and calcite (29.6^o, 39^o). Kodel et al. (2012) and Andrade et al. (2009) showed the presence of similar crystalline phases as found in this

research, in their investigation of dry petroleum sludge and in the sludge samples heated at different temperatures under nitrogen.

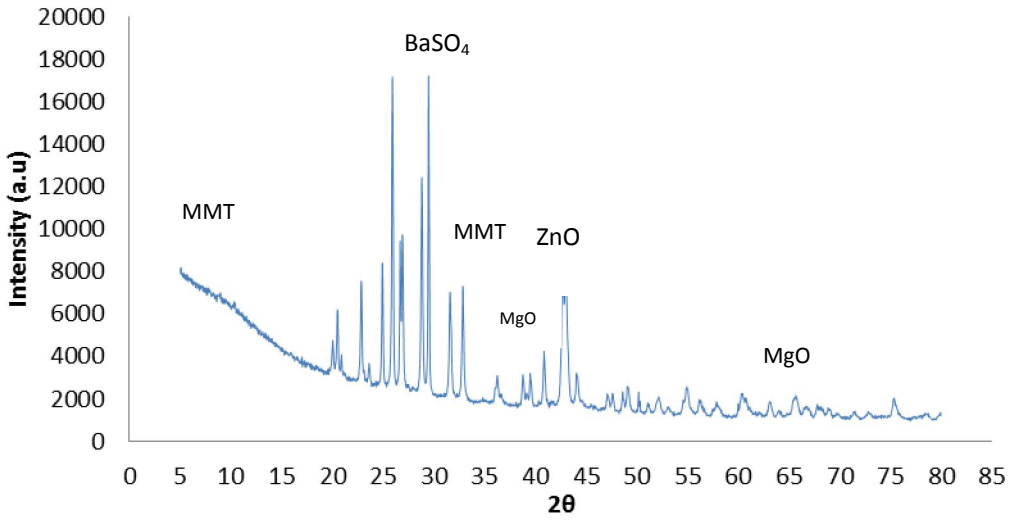

Figure 3.2 XRD diffractogram of oil based drilling fluid and cutting sample

ATR-FTIR spectroscopy confirmed the minerals observed in the X-ray diffractometry by showing the associated functional groups and organic matter content of compounds found in the X-ray diffractometry. In Figure 3.3, the broad band at 3500-3000cm^{-1} was assigned to the hydroxyl portion of water and indicates the presence of absorbed water. The ATR spectrum shows the presence of hydrocarbon due to bands between 3000-2700cm^{-1}. The band at 1630cm^{-1} was assigned to the hydroxyl group of water. Similar to Mukherjee and Srivastava (2006), the band at 1600 cm^{-1} was assigned to the adsorbed water molecules (bending mode). The bands between 800-900cm^{-1} and 1400-1500cm^{-1} are assigned to carbonate groups. The carbonate groups are suggested to arise from the presence of $CaCO_3$ in the sample. The bands at 1118-1106cm^{-1} are assigned to the presence of silicate groups from clay and shale (sand) due to Si-O stretching. The band at 1080 cm^{-1} was assigned to S–O bond stretching attributed to barite ($BaSO_4$). The bands at 1200-1300cm^{-1} were assigned to alkyl ether peaks which could be due to the presence of additives such as oilfield

chemicals in the sample.These findings are supported by that of Andrade et al. (2009).

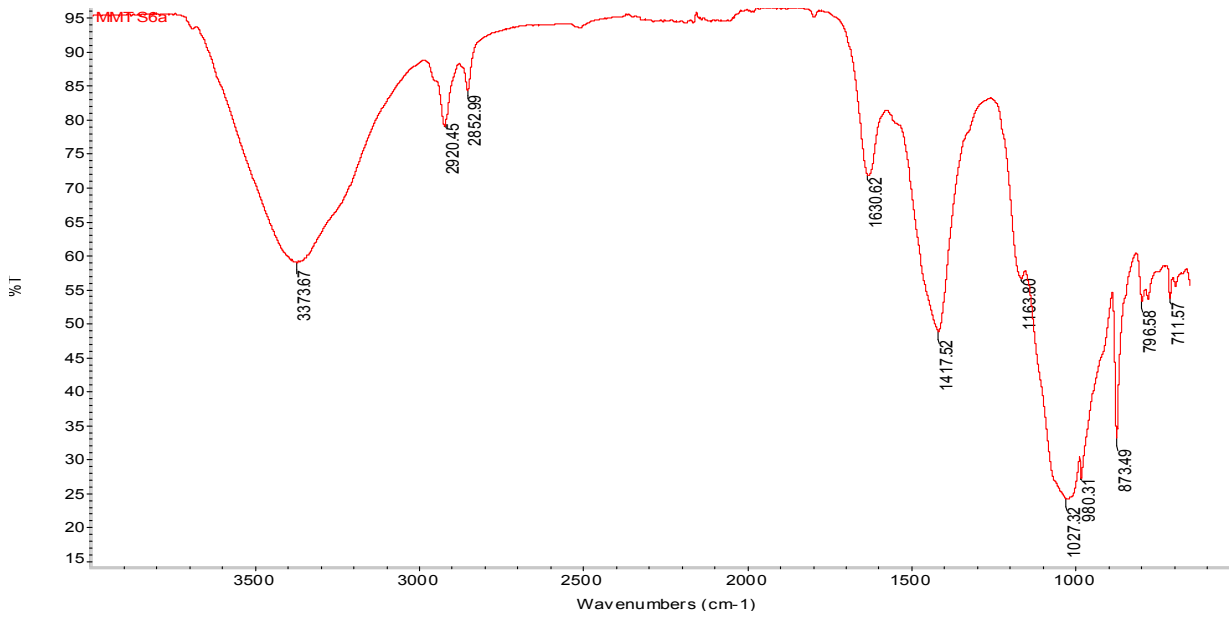

Figure 3.3 Infra-red spectrum of spent oil based drilling fluid and drill cuttings sample

3.3.2 Chemical analyses

The drilling muds and cuttings obtained from a forties drilling site in the United Kingdom was studied. General properties of the sample are shown in Table 3.1 summarises the data obtained from the THC analysis using FTIR and elemental composition using ICPOES. The elemental analysis was undertaken following the identification of specific elements in the EDX analysis.

The calibration graph of the concentrations of diesel in perklone ranged from 0 - 1000mg diesel per litre of perklone and was found to be linear with a correlation coefficient of 0.999 as shown in Figure 3.4. The FTIR TPH analysis showed that the used oil based drilling fluid and cutting sample had a total petroleum hydrocarbon value of 662,500mg/kg ± 50670 (66.2%w/w). This clearly exceeds the OSPAR regulation of 1%w/w oil on drill mud/cuttings (Al-Ansary and Al-Tabbaa 2007) and can be classified under the European waste catalogue, as hazardous waste with catalogue number 01 05 05* necessitating its clean up.

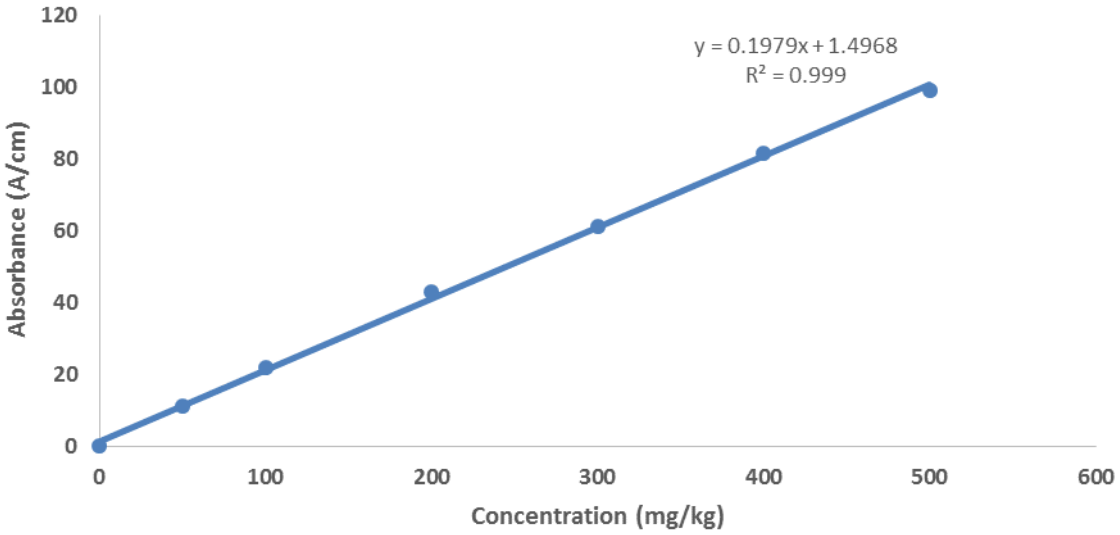

Figure 3.4 FTIR TPH calibration of diesel in perklone for spent oil based drilling fluid sample

Table 3.1 Properties of used oil based drilling fluid and cutting

Oil based mud drill cutting sample (n=3)		
Properties	**Concentration (mg/kg)**	**±SD**
TPH by FTIR	662,500 mg/kg	50670
Metals		
Ba	6026	2233
Na	3010	287
Al	5287	370
Mg	2099	106
Fe	11832	563
Ca	89140	6827
Mn	843	47
K	1548	87
As	Nd	Nc
Cr	23	2
Cd	Nd	Nc
Cu	43	1
Hg	Nd	Nc
Pb	122	5
Zn	162	9
Ni	10	0.4
P	85	2.8
Si	34	11
S	6618	335
V	6	1

*nd= not detected, *nc= not calculated

ICPOES was used to ascertain the elemental concentration of spent oil based mud and drill cutting sample (Table 3.1). The results showed that As, Cd and Hg were not detected. All the heavy metals: Cr, Cu, Ni and Zn were below the OSPAR threshold. However, the concentration of Pb was higher than the OSPAR limit of 5 -50 mg/kg (see Appendix A: Table A.3). The concentration of Ca was very high compared to other elements. The high Ca concentration suggested that the formation that was drilled was rich in Ca *i.e.* limestone formation.

The EDXA spectrum (Figure 3.5) shows the elemental composition of the sample. It gives evidence of the presence of elements such as barium, calcium, potassium, carbon, oxygen, manganese, chlorine, sulphur, iron, magnesium, sodium, aluminium and silica. Table 3.2 shows the percentage mass of elements present in the sample.

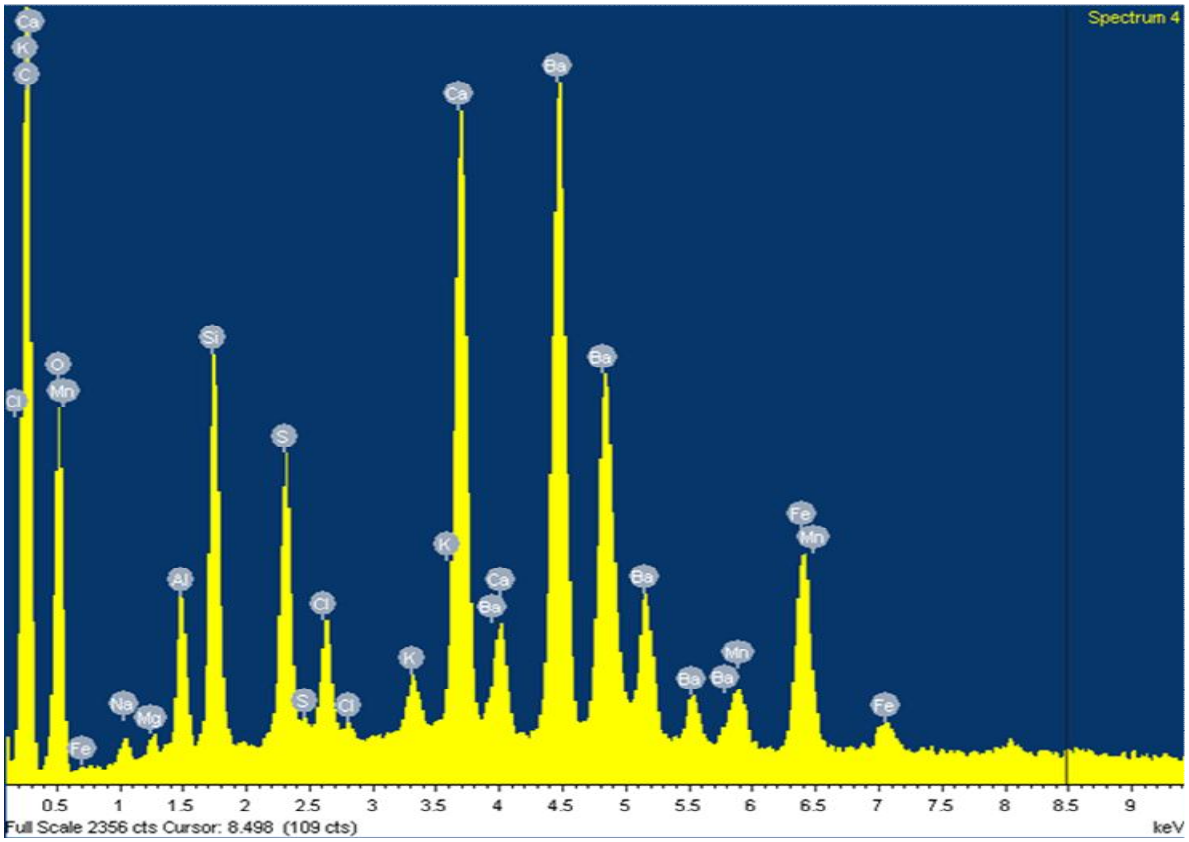

Figure 3.5 Energy dispersive X-ray spectrum of used drilling fluid and cutting sample

The silica was expected to be a component of sand or shale from the cutting as well as bentonite clay. Calcium was suggested to be present as a result of drilling

from limestone containing formations or drilling fluid additive. Iron and manganese is also suggested to be present as a result of the drilled formation. Possible sources of chlorine and sodium are suggested to be from the offshore salty water in the North Sea. Sodium, aluminium, magnesium and silica are possibly from the bentonite clay additive of the drilling fluid. Barium and sulphur contributions to the sample may be as a result of the drilling mud weighting agent, barite which typically accounts for 60% of the drilling fluid (OGP 2003). The hydrocarbon content of the sample and formation are thought to contribute the carbon and oxygen present as well as other metals and non-metal content such as sulphur. These findings are supported by those of Andrade et al. (2009) where a similar EDXA study of petroleum sludge showed that the petroleum sludge contained C, O, Na, Al, Si, S, Cl, K, Ca, Ti, Fe, Cu and Ba. Their results also showed that the presence of oil in the sample shielded Mg, Al, Si, Cl, K, Ca, Ti and Fe which was revealed by an increase in percentage (%) of mass and atomic weight of these elements upon heating and evaporation of the volatile hydrocarbons at 800^{o}C. This supports the oil shielding of some elements during the EDX analysis which were later revealed in acid-digested samples used in ICPOES elemental analysis. This finding informed the need for the advanced techniques such as ICPOES in the elemental composition study for this research.

Table 3.2 EDXA elemental composition of spent oil fluid showing percentage weight

Element	**Weight (%)**	**Atomic (%)**
C K	24.10	36.64
O K	43.46	49.61
Na K	0.61	0.49
Mg K	0.53	0.40
Al K	2.02	1.37
Si K	6.34	4.12
S K	2.79	1.59
Cl K	1.90	0.98
K K	0.29	0.13
Ca K	6.46	2.94
Mn K	0.15	0.05
Fe K	0.85	0.28

3.3.3 Physical properties

The physical analyses were carried out using particle size analysis, rheology and retort analysis. The retort analysis result of the used drilling mud sample is shown in Figure 3.6. The oil-water ratio was 70:30.

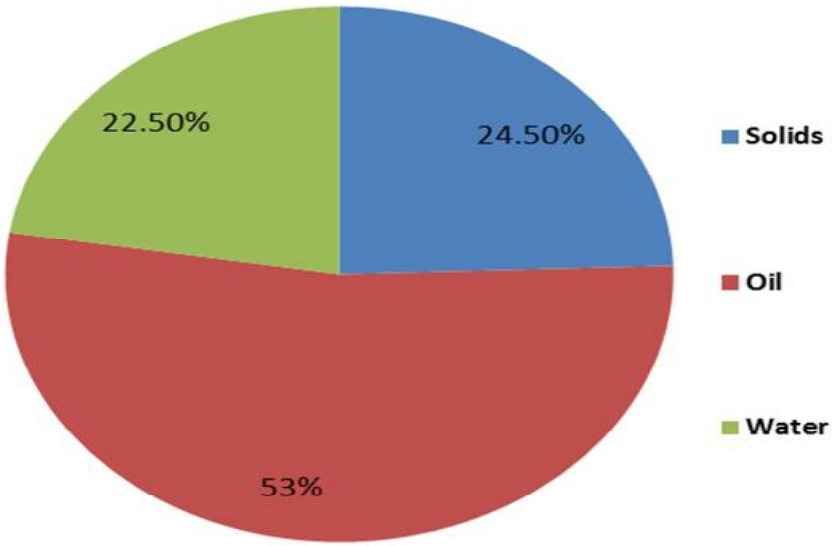

Figure 3.6 Composition of oil, water and solids ratio in spent oil based drilling mud sample

Table 3.3 shows a decrease of the viscosity of the used drilling fluid with increasing speeds which implies a non-Newtonian fluid behaviour (Brookfield 2001). The torque, which is the force required for the fluid to rotate was found to increase from 15.4 to 54.4% as the speed of the spindle increased from 0.5 to 15 rpm at 18^{o}C. This shows that the used drilling fluid sample to be treated was very viscous due to the increase in fine solids (low-density cutting of the formation) which trap water to form gels and cause the lowering of the free oil/water ratio (OWR) in the given sample (McCosh et al. 2007). According to Pham and Nguyen (2014), the bentonite clay mineral (a montmorillonite) absorbs water into its internal structure (between its unit layers) and this result in the swelling and increase in the volume of the drilling waste. Thus, the presence of clay usually reduces the amount of unbound water in the drilling

waste slurry with an increase in the actual solids volume fraction, which causes an increase in drilling waste slurry viscosity.

Table 3.3 Rheology of used drilling fluid sample for chemical treatment measured at 18.1°C

	Speed (rpm)					
	0.5	1	2	4	8	15
Viscosity (cP)	208155	124778	81283	53988	33368	21715
Torque (%)	15.4	21.1	28.1	36.5	44.1	54.4

Effect of time and speed on the viscosity of used drilling fluid was investigated as the viscosity of the fluid is inversely proportional to the speed of the spindle at a given time, t (Brookfield 2001). It was observed that fluid (sample) resistance occurred at speed 15 and 30 rpm for viscosity measurements taken at 10, 15 and 20 minutes. Thus, some experiments were therefore not carried out due to the risk of breaking the spindle as a result of fluid resistance.

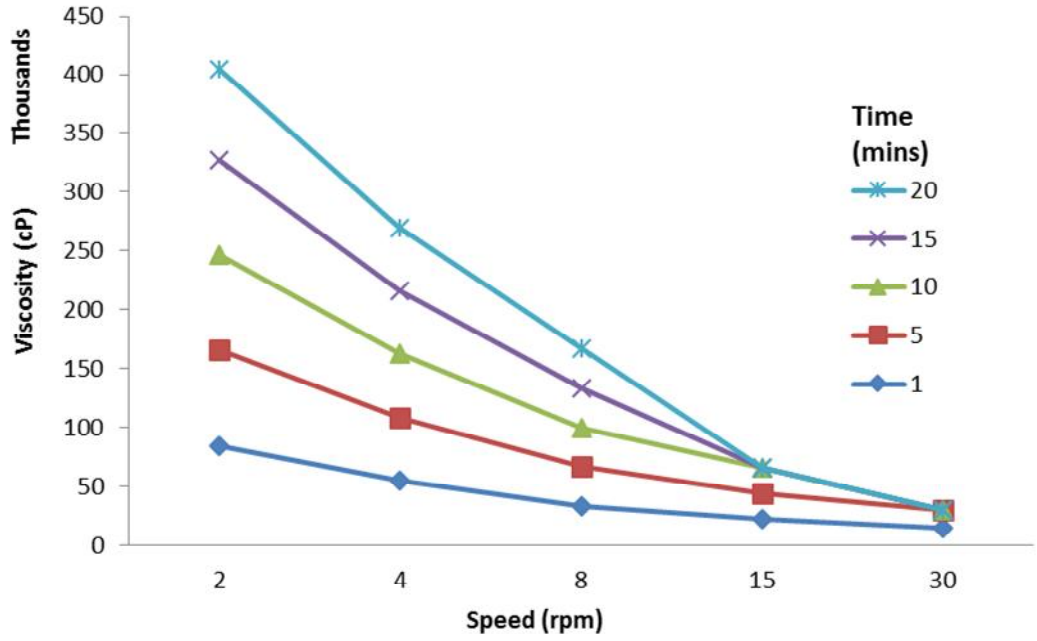

Figure 3.7 Effect of time and speed on the viscosity of used drilling fluid and cuttings sample

This characteristic time dependent non-Newtonian fluid behaviour is suggested to be as a consequence of its lost rheology (plasticity (elasticity) or Thixotropic effect). Thus, at a high viscosity, spindle speed diminished and at low viscosity the speed increased (Figure 3.7). The data also shows that high viscosity is due to the removal (skimming) of base oil on the surface of the used drilling fluid sample before treatment. The experiment could not be carried out at a high temperature due to concerns of remaining base oil evaporation which could affect the sample treatment.

Particle size analysis showed that the oil based drilling mud contained both nano and micro sized residues. The nano-sized residues had a range of 690–855nm. The micro-sized residues had a range of 1-259μm (See Table 5.3). This was similar to the figures reported by Darley and Gray (1988) which specified that drilling fluid (mud) had solids of three categories: colloids with particle size of 5 – 1000nm, silt and barite with particle size of 1 -50μm, and sand with particle size of 50 - 420μm (depending on shale shaker mesh size).

3.4 Conclusion

The sample was characterised based on 3 categories: the chemical properties, surface / morphological properties and physical properties. The chemical properties were investigated using FTIR for TPH analysis, ICPOES for quantitative elemental analysis and EDXA for qualitative elemental composition. The surface analyses were carried out using X-ray diffraction, FTIR-ATR and SEM for morphology. The physical analyses were carried out using particle size analysis, rheology and retort analysis. The characterisation analyses illustrated that the sample had a high hydrocarbon load of 662,500mg/kg as well as a high heavy metal load for Pb of 122mg/kg. The sample also has a high metal concentration for Ba, Ca, Fe of 6026, 89140 and 6618 mg/kg respectively; and high concentrations of S of 6618 mg/kg. From the ICPOES analysis it was observed there was no Sn, As, Cd or Hg. However, this sample could be made sustainably useful through closed or open recycling into DF or DF composite products respectively. This can be achieved after appropriate environmentally sustainable treatment to extract pollutants before recycling. The close recycling would focus

on reconditioning the drilling fluid for further use as a drilling fluid. The only downside to this operation is barite sag and the loss of fluid rheology due to the presence of a high volume of low-density solids. The open recycling would give more options of treating and converting the constituents of used oil based drilling fluid and cutting into other products.

Chapter 4

Demulsification and phase separation of spent oil based drilling fluid and cuttings: Surface modification and recovery of nanofillers for improved thermal stability of PA6

4.1 Introduction

An oil based drilling fluid is broadly a three phase mixture made up of oil, water and solids (Benka-Coker and Olumagin 1995; Tehrani, Chapman and Fraser 2003). When spent or after use in drilling, it can typically contain very fine low-density (gravity) solids of shale or formation rock particles (drill cuttings), as well as bentonite clay (montmorillonite), barium sulphate, oil emulsifiers and other chemical additives. This is dependent on the formulation (initial composition) of the drilling fluid used. The emulsion of oil based drilling fluid is mainly water in oil emulsion emulsified by asphaltenes (Langevin and Argillier 2016), may contain aromatic/heteroatomic organic molecules, resins (wax, paraffin) from the oil phase (Zhang et al. 2016); or sulphates or carbonates scales (Jiaojiao et al. 2011) or corrosion (ferrous sulphide) and microbial biomass (Xia et al. 2016; Yoshioka et al. 2015).

In order to separate and recover the different phases, a demulsifier can be used. Demulsifiers are chemical treatments utilised in breaking emulsions and emulsion based materials. Demulsifiers act by changing the stabilised emulsion characteristics. On the other hand, demulsification occurs via the synergy of factors such as chemical (surfactants, solvents), mechanical methods, and treatment time and temperature applied. Due to oil rig locations (*e.g.* offshore, subsea installations), the cost of drilling waste accumulation and extreme operational temperatures, demulsifiers could be formulated to enhance shorter treatment times, withstand operational temperatures and chemical influences on the treatment process (Urum et al. 2006; Urum, Pekdemir and Gopur 2003). Demulsifier formulations are made by blending different chemicals (solvent, emulsifying agent, flocculants, demulsifier *etc.*) to alter the balance of charges at the interface of oil and water that is critical to result in the destabilization of the emulsion. The use of flocculants such as chitosan, and coagulants in producing

the demulsifier formulation also aid flocculation and coagulation of oil and water (Pekdemir, Copur and Urum 2005; Ese et al. 2000). Similarly, the use of hydrophilic and lipophilic agents aids the attraction of energetically favourable group, thus, hydrophilic compounds (*e.g.* surfactants) attract hydrophilic molecules (of the waste) while the converse is true for lipophilic additives. The composition of the demulsification agent includes water, which is often used as a carrier and a universal solvent and electrolyte to enhance ionic interactions. In some cases, enzymes are used to catalyse the breakdown of complex polymers enhancing emulsion stability *e.g.* oil, polysaccharides - xanthan and peptides (Chabrand and Glatz 2009), while acids and alkaline products are used to change the pH of the emulsion system to enhance demulsification (Duke 1983).

The phase separation of a mixture of the oily slurry is complex. This is as a result of the interfacial bonding formed between the different phases of oil, water and solids as a result of emulsifying agents such as asphaltenes and wax. In order to extract the oil, suitable chemical compounds must be employed to cut through the oily slurry by lowering the surface tension of the oily/water, oil/solid matrix.

Current oil and gas demulsifying techniques mainly utilise chemicals such as polyglycols, xylene, toluene, alkylphenol formaldehyde resin alkoxylate (APFRA) - nonylphenol, epoxy resin/polyglycol derivatives as demulsifier bases (Fink 2012). Implementation of OSPAR decision 2000/2 and the offshore chemical regulation 2002, led to the department of trade and industry regulating the use and discharge of chemicals in the UK continental shelf. Hence, the OCNS indicates the toxicity and environmental impact of the chemicals used. This has led to the harmonised mandatory control system (HMCS) and assigning of OCNS categories to chemicals used in the formulation of demulsifiers and other oil and gas chemicals by the Centre for Environment, Fisheries and Aquaculture Science (CEFAS). This was important in choosing the environmentally acceptable chemicals to be blended in the formulation of the demulsifers in this chapter.

There are different methods for testing demulsifier efficacy, including the bottle/jar test, interfacial tensiometer and turbiscan (Liu et al. 2011). The bottle test was modified to make the phase separation tube test used in testing of the demulsifier and other chemicals. In this study, the experiments were designed

such that the acids, solvents and salt would aid dispersion due to their ionic nature. Sodium dodecyl sulphate (SDS) would be used as a solubilising agent for the hydrocarbons, and an oil flocculant (chitosan) would be used to aggregate the oil molecules. Wetting agents such as poloxamer would be introduced to lower the interfacial tension between oil, water and solids as well as that between the oily matrix and water/solid residue mixture. Phosphoric acid would be used to chemically separate the waste, enhance the sedimentation of the solid residues as well as modify the surface with the phosphorus moiety in order to enhance the thermal property of the solid residues recycling product. Such treatments should aid the removal of the oily layer of the solid particles.

Consequently, this chapter aims to formulate two demulsifiers (demulsifier S3 and demulsifier S4), investigate the use of a demulsification process for the separation of individual phases in spent oil based drilling fluid and modify the surface of the solid residue using demulsifier S3.

4.2 Experiment

4.2.1 Materials

Low molecular weight chitosan (LMWC) / deacetylated chitin with the degree of deacetylation of 70 - 85% and tetrachloroethylene with purity of 99.5% were purchased from Sigma-Aldrich, UK. SDS (general purpose grade), sodium chloride (analytical grade), isopropanol (HPLC grade) and acetic acid (HPLC grade), ortho-phosphoric acid (laboratory grade), sodium sulphate (analytical grade) were purchased from Fisher Scientific, Loughborough, UK. Poloxamer (PO) synperonic PE/L64 block copolymer of polyethylene and polypropylene glycol was purchased from Fluka, France. Spent oil based drilling fluid with low-density drill cuttings was donated by a local oil and gas company.

4.2.2 Formulation

The demulsifier formulation method was adapted from Quintero et al. (2012) for the spent oil based drilling fluid and cuttings demulsifier treatment. The demulsifier-S4 formula composition was made up of 60ml water with 1.56g NaCl, 20ml surfactant mixture of 75% SDS and 25% PO, 5ml isopropanol, and 15ml of 3ppm chitosan in 0.2M acetic acid and an addition of 5ml 0.2M phosphoric acid

for demulsifier S3, which was prepared in a beaker and stirred together for 20 minutes at speed 5 using a magnetic stirrer.

4.2.3 Treatments

The two demulsifiers prepared using materials in 4.2.1 above were subsequently applied for the treatment of oil based drilling fluid and drill cutting waste. Similarly, individual components of the demulsifier formulation were also used as controls. Briefly, 1.67g (1.5ml) of dried oil based drilling mud with cuttings was introduced into a graduated centrifugation tube, followed by the addition of 5ml of the required treatment with calculated dosages per sample. The mixture was sonicated for 5, 10, 15, 30 and 60 minutes using an ultrasonic bath at temperatures between 23-30^{o}C. The dispersion of the solid phase was measured in millilitres. Reading of separated oil, water and froth (where applicable) were taken with photo evidence collected. Thereafter, the mixture was centrifuged for 10 minutes at 3500 rpm. The photo images and volumes of the separated phases were recorded, while samples were collected for further analyses.

For the small scale single treatments, individual surfactants and solvents including low molecular weight acetylated chitosan (LMWC), SDS, poloxamer, isopropanol, acetic acid, phosphoric acid, sodium chloride and deionised water (control) were used for the treatment of the spent drilling fluid.

For scaled up batch treatments, the formulated demulsifier treatments, *i.e.* 100ml of the demulsifier treatment, and 5ml of 0.2M phosphoric acid were introduced into a mixer cup. Afterwards, 100ml of spent drilling fluid was added, and finally, 250ml of deionised water. These were mixed using a Hamilton mixer at 16,000rpm for 5 minutes. The treated spent drilling mud was then transfered to a 500ml measuring cylinder to observe the rate of sedimentation with time. The static phase separation readings *i.e.* sedimentation reading (ml) per time was taken using the graduations on the cylinder and a stopwatch. The dynamic phase separation was achieved using the centrifuge. Centrifugation was carried out at 2300rpm for 5 minutes for cylinder 1 (with demulsifier S3) and cylinder 2 (with demulsifier S4). The phase separation was not adequately signified by the absence of loose solids. Further centrifugation was carried out for cylinders 1 and 2 at 3500rpm for 10 minutes. Cylinders 3 (with demulsifier S3) and 2 (with

demulsifier S4) were centrifuged in the third run of centrifugation at 3500rpm for 10 minutes. Separated phases were collected for storage in glassware for oil and oil-water emulsion and in ceramic ware for the solids.

4.2.4 Phase Separation Method Development

Ultra-sonication and centrifugation treatment process were adopted. Ultra-sonication led to the vibration of the particles within the system and creating pores for the treatment to seep into the oily waste for treatment. The vibrations were ultrasonic and local, thus the glass walls of the centrifuge tube were kept clean throughout the treatment process and it became easier to obtain the phase reading after the first stage process. Ultrasonic cleaning has a fast and robust environmentally friendly cleaning process (Azim et al 2011; McCosh, Addicks and Gallo, 2008). The centrifugation is a well-known method for the separation of the mixture. In this experiment, it was used to cause a forced sedimentation of solids and to enhance the separation of oil and aqueous (water) phases. Ultrasonic times of 5, 10, 15, 30 and 60 minutes were chosen for the experiments to investigate the effect of time on demulsification.

The centrifugation step *i.e.* dynamic phase separation step was optimised as earlier mentioned in section 4.2.3. Thus, centrifugation was carried out at 3500 rpm for 10 minutes at 25^{o}C.

In this test, the following were to be determined: the best demulsifying agent for the sample demulsification and phase separation; surface modification of the sedimented solid residue for improved thermal properties of residue and PA6 nanocomposite fabrication; and oil extraction treatment.

Final phase separation procedure adopted for use involved sample preparation carried out by weighing in the desired weight of oily waste into a centrifuge tube and sealed before use; individual demulsifier component/demulsifier was prepared according to concentration requirement for each treatment; after individual demulsifier component/demulsifier preparation, it was poured into the centrifuge tube containing oily waste for treatment. The centrifuge tubes were then transferred into an ultrasonication bath (indirect method – where centrifuge tubes were first placed in a glass beaker with water) where the demulsifying agent and the mechanical vibratory forces led to the mixing of the waste and

treatments, and phase separation of oil from the water and solids in the mixture. After samples have been sonicated to desired sonication times (a = 5mins, b=10mins, c=15 minutes, d=30 minutes and e=60 minutes) between 25 -30°C, the samples were taken out of the sonic bath and photographed for phase separation evidence. The measurements of phase (e.g. oil, water and solid) volume (ml) were carried out. Thereafter, centrifugation of the mixture at 3500 rpm for 10 minutes at 25°C was carried out to enhance the phase separation of the oil, water and solids (Figure 4.1). Photo and phase measurements were obtained. Samples of the water and solid phases were collected for further analysis.

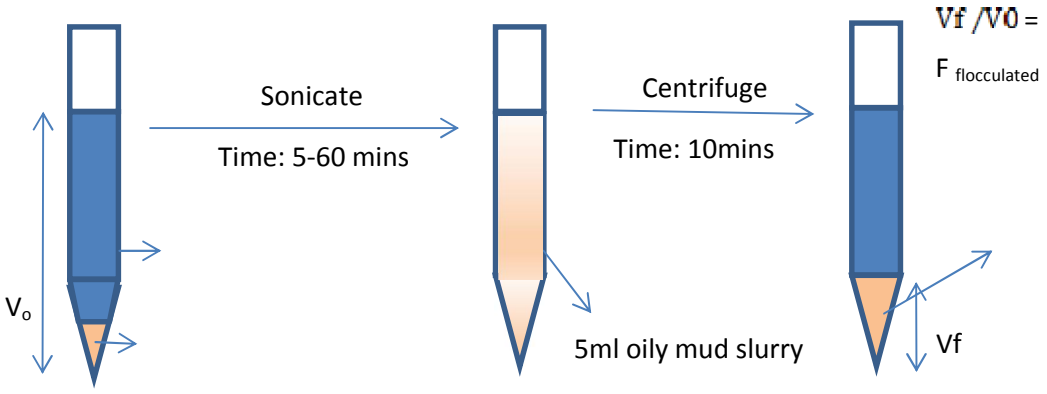

(a) F flocculated (chemically enhanced sedimentation: Phosphoric acid)

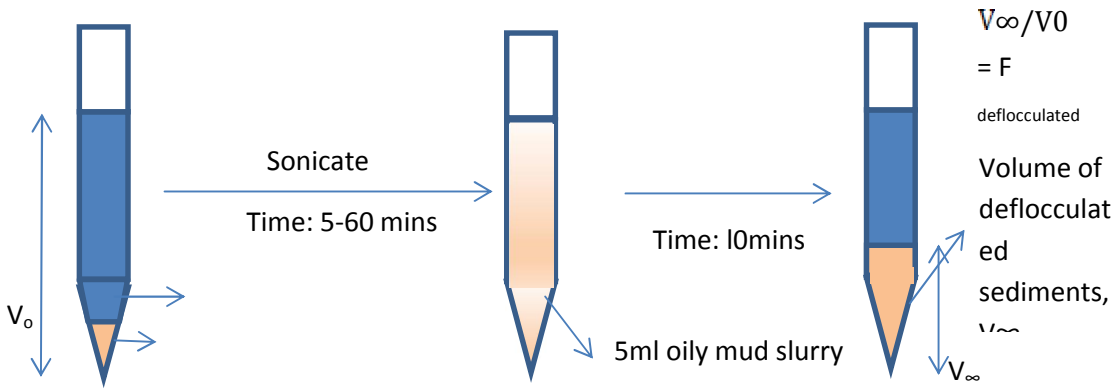

(b) F deflocculated (steric hindrance assisted suspension: ISP)

Figure 4.1 Centrifugation led phase separation: Rate of separation experiment using different treatments and demulsifiers

4.2.5 Characterisation

The FTIR TPH and ICPOES characterisation methods used in this chapter are described in chapter 3.2.2.

The surface tension of demulsifiers S3 and S4 were measured using the ring method using the Du Nouy tensiometer, Germany. Each measurement was undertaken at 20^{o}C and repeated five times and average results were reported. The critical micelle concentration (CMC) was determined by plotting surface tension as a function of demulsifier concentration (mg/l).

The drilling fluid and cuttings solid residue obtained from demulsifier and thermal treatment as well as bentonite will be used in the PA6 nanocomposite manufacture (Chapter 5).

4.3 Results and discussion

4.3.1 Demulsifier characterisation

Surface tension was observed to decrease with increase in demulsifier S4 concentration. When dispersed in water, hydrophilic monomer head groups of the demulsifier S4 accumulated at the interface. This showed demulisifier S4 would have sufficient affinity to oil at interface, to attract the non-polar groups of the oily waste to be demulsified. Surface tension dropped linearly to demulsifier concentration until 20mg/L in the logarithmic fit (Figure 4.2). When demulsifier S4 concentration was greater than 20 mg/L, surface tension dropped at a non-linear mode, and it was maintained at 0.050 to 0.065 mN/m. Thus, the point of first sharp surface tension linear drop was assumed to be the CMC of the demulsifier, S4. Therefore, the CMC of demulsifier S4 was taken to be 20 mg/L with the surface tension of 0.067mN/m.

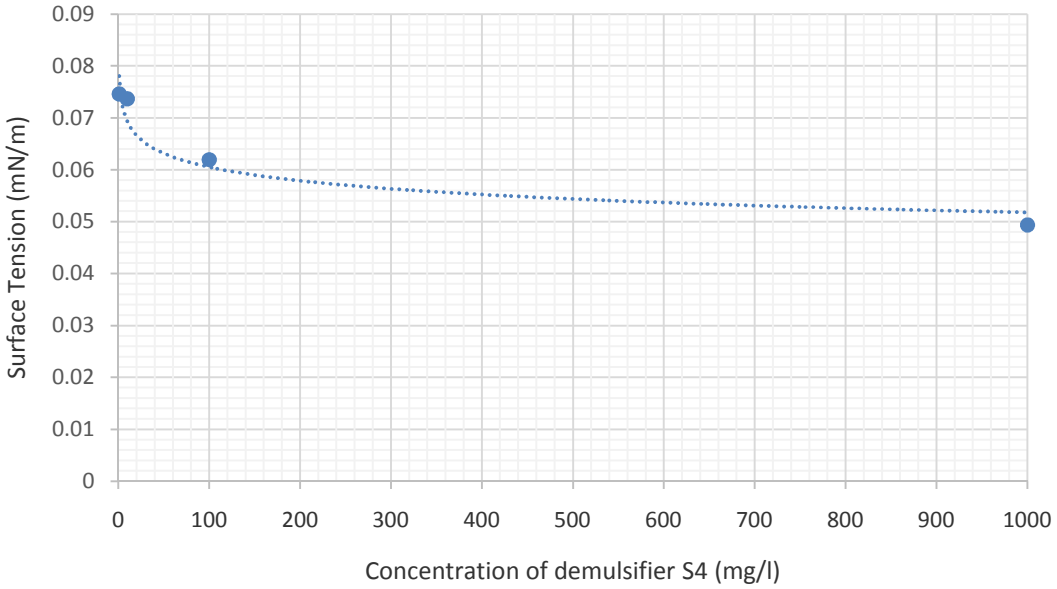

Figure 4.2 CMC determination of demulsifier S4

In demulsifier, S3, the phosphoric acid modified demulsifier, the surface tension was observed to decrease and increase with an increase in the concentration of demulsifier S3 (see Figure 4.3). This was due to the demulsifier nature which is acidic resulting in increasing the surface tension of water as the demulsifier concentration increased.

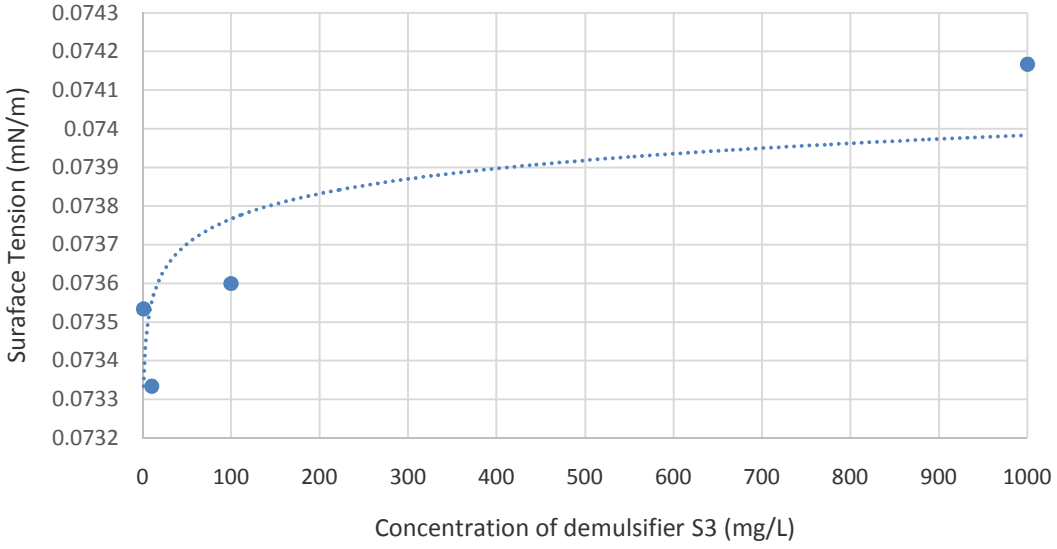

Figure 4.3 CMC determination of demulsifier S3

The pH of the demulsifiers S3 and demulsifier S4 were 4 and 7 respectively using pH paper. The acidity of demulsifier S3 was due to the presence of phosphoric acid.

The CMC determination of the demulsifier used in the treatment of spent oil based drilling fluid and cuttings is crucial to determining the optimum amount of demulsifier to be used for oil extraction. When dispersed in water, hydrophilic monomer head groups of the demulsifier S4 accumulated at the interface, which has sufficient affinity to water to drag non-polar groups into aqueous solutions. Surface tension dropped linearly to demulsifier S4 concentration until 20mg/L (Figure 4.2). This was due to the fact that at low concentration, the hydrophilic group of the demulsifier accumulated and formed a monolayer at the interface, which makes water have sufficient affinity and decreased the surface tension. When demulsifier S4 concentration was greater than 20 mg/L, surface tension dropped at a less non-linear mode, and was maintained at 0.050 to 0.065 mN/m. Thus, the point of first sharp surface tension linear drop was assumed to be the CMC of the demulsifier, S4 (Beckett, Stenlake 1976). Therefore, the CMC of demulsifier S4 was 20 mg/L with the surface tension of 0.067mN/m. The use of a lowered concentration below CMC would result in inadequate solubilisation of the oil and other emulsion stabilisation agents in the spent oil based drilling fluid.

The effect of the demulsifier components could not be overlooked as the addition of salt (NaCl), could have led to the raised surface tension (ST) of the water. This is because the surface layer was water due to the fact that salt resides more in the bulk solution thereby resulting in the lack of solute from the demulsifier components on the water surface (Beckett and Stenlake 1976). In the case of demulsifier, S3, surface tension increased with demulsifier concentration which meant the treatment had no or lower solute concentration on the surface than the bulk of the solution. This is because the phosphoric acid pulled most of the solutes from other components (SDS, isopropanol, chitosan, poloxamer) to the bulk solution due to deflocculating and sedimentation tendency of the phosphoric acid present (Figure 4.3). This indicated that surface excess was negative for demulsifier S3. Thus, no micelles could be formed. However, at a low concentration of 10mg/L, decrease in ST indicates the presence of solute from demulsifier S3 components which was absent at higher concentrations of

demulsifier S3 (see Figure 4.3). In the case of demulsifier S4, with the progressive increase in demulsifier concentration from 1mg/L to 1000mg/L, it was observed that the surface tension of water was lowered from 0.0748 to 0.0667mN/m. This showed that demulsifier S4 was distributed between the bulk and surface of the solution. At 0.0667m/Nm, the demulsifier molecules in the mixture began to aggregate to form micelles. Further increase in demulsifier S4 concentration from 0.0667mN/m had little effect on the surface tension as seen in Figure 4.2. Application of 20mg/L demulsifier S4 and above would result in effective solubilisation and demulsification of the spent oil based drilling fluid and cuttings.

4.3.2 Method for the demulsification of spent Oil Based Mud and drill cutting

The sedimentation study was carried out for the recovery of the solid phase. This study was adapted from Billany (2007). The F-values were obtained for sonicated (only) samples and represent the flocculated volume of the solid phase after chemical treatment. Mathematically, Vs (solid phase after sonication only)/Vo infinity (initial volume of slurry + demulsifying treatment). The hypothetical Vo is 6.5ml. Experimentally, F-values are expected to be less than 1. The β-value determined from the F-value, is a ratio of recovered treated solid phase in volume or percentage to the untreated sample. Mathematically, β-value = F_f (solid phase of treated sonicated samples)/ F_{df} (solid phase of treated sonicated and centrifuged samples). This value showed the effect of the chemical treatment on solid recovery. β-value is not shown in this study but it is always theoretically expected to be greater than 1. This means that the treatment is expected to bring about the expansion or dispersion by increased interaction with the mobile phase which could be (wash) water. This is important because an increase in dispersion of the oil based drilling fluid by the treatment could mean that the treatment has more access to the pore space / capillary spaces within the solid matrix to bring about a thorough cleaning or treatment of the sample. Experimentally, it was observed that some treatments (isopropanol, NaCl) would cause the dispersion of the clay-barite matrix observed by an increase in solid phase volume while others based on experimental conditions would lead to the compressed sedimentation of the solid phase observed by a decrease in solid phase volume.

4.3.3 Effect of sonication time on phase separation using different components of the demulsifier

The tests in Figure 4.4(i-ii) showed the percentages of the phase separated portions of solids, water and oil including froth after the application of different components of the demulsifier treatments at different sonication times (5-60 minutes) and constant centrifugation time (10 minutes). The research focused on solids recovery with the intention of recycling them as nanofillers for nanocomposite manufacture. The scope of this research did not include investigations into the presence of residual water in solid pore spaces, oil in the froth (colloid), oil in water phase or suspended solids in the water phase.

Deionised water was used as a control treatment in this study. As shown in Figure 4.4(i), this study showed that deionised water-induced demulsification was most efficient for maximum oil separation at a shorter treatment time of 5minutes. It was observed that as the sonication time of deionised water treated oil based drilling mud and cuttings slurry increased, the percentage volume of the solid phase increased from about 15-25%, while the oil phase percentage decreased from 8-2.5%.

This was attributed to the fact that prolonged sonication of the mixture aided mixing and association of the phases which increased solid phase percentage volume. This showed that more oil was extracted at a lower pre-sonication time of 5 minutes as opposed to the other times of 10, 15, 30 and 60 minutes. In addition, no solid (froth *i.e.* colloidal solid) was associated with oil and water. Sedimented solids of about 15% were observed and deionised water did not promote froth formation (clay/ colloid separation).

The treatment of the oil based drilling mud and cuttings with low molecular weight chitosan (LMWC) was characterised by the formation of froth, lower oil recovery, lower percentage water volume recovery and increased solid percentage volume. The percentage volumes of oil recovered in LMWC treated samples were lower and between 2-4.5%. The froth recovered was observed to be associated with oil during visual inspection. Thus, the treatment of froth would lead to increased oil recovery. The percentage volume of oil recovered increased with increase in sonication time at 10, 15 and 30 minutes. At

sonication time, 10 and 15 minutes, increased concentration of LMWC (200mg/L) led to a visible decrease in oil recovery compared to the concentration of 2mg/L and 20 mg/L respectively. The solid phase was assumed to have oil and water in the pore spaces, increasing the percentage volume of treated solids to a range of about 23-27% volume solid residue. This was also attributed to steric hindrance from organic groups coating the particles.

Organic acids influence the demulsification of water in oil emulsions (Fink 2015). In this study, it was observed that acetic acid increased dispersion of the solid minerals as observed in the formation of froth and solid phase range of 20-30%. The 5 minutes' sonication using the lowest concentration of acetic acid (0.02M) resulted in the best oil recovery of 9% followed by the highest concentration (2M) with 4.5% oil recovery during the 15 and 60 minutes sonication.

Phosphoric acid has been used to modify the surface of solids hence reducing thermal degradation of the solids and associated composite materials (Bureau et al. 2002). According to Fink (2015) phosphoric acid has been used to improve sedimentation of solid phase enhanced oil recovery. Phosphoric acid treated samples had best oil recovery at 5 minutes sonication time of 8, 7 and 8% for 0.2, 0.02 and 2M respectively. Thus, treatment time was an important factor for oil recovery. The highest concentration of 2M phosphoric acid promoted froth formation observed at all sonication times. However, at sonication time 30 and 60mins froth was formed by 0.2M phosphoric acid. This was attributed to the effect of increased sonication time of 30 and 60minutes on the sample. The solid phase recovered varied from 15-25% volume. Phosphoric acid was observed to result in the flocculation of the solid phases in the treated samples. The effect of time was inconsistent. However, the longer treatment time of 60minutes produced better results. This compression (flocculation) of the solid phase was similar to increased oil extraction by this treatment.

The treatments using sodium dodecyl sulphate (SDS) showed a reduction of froth formation which is important in nanocomposite manufacture. SDS treatments of 10, 15 and 30 minutes sonication had no froth except for 30 minutes sonication at low SDS concentration of 0.025%w/v. The 60 minutes sonication at all SDS concentrations produced froth. This showed that increased sonication at

60minutes led to froth (colloid) separation using SDS. The recovered water phase was cloudy as a result of suspended solids and oil present. Unlike LMWC, acetic acid, ISP, phosphoric acid and NaCl treatments, SDS has solid phase recovery of ≤20% across the different treatment packages. The oil recovery was in the range of 1-4%. This is unlike the results from Urum et al. (2005) that showed SDS caused oil recovery from oil contaminated soils to increase from about 65 to 90% as the SDS concentration increased from 0.0001 - ≥0.5% mass. This showed that the concentration of SDS should be increased above 1.0%w/v to enhance oil recovery. On the other hand, the particle sizes of their samples were between ≤0.06 - ≥2mm while this research had a particle size range of 249nm - ≤1000μm which possessed smaller pore spaces hindering effective washing/ treatment and oil recovery. In addition, Urum et al. (2005) used air sparging assisted stirred tank reactor as washing/treatment method which could have resulted in higher oil recovery as opposed to the sonication and centrifugation method used in this research.

The poloxamer (non-ionic surfactant) had the highest percentage volume of oil recovered amongst all treatments. This was attributed to the presence of nonionic triblock copolymers isomer of poly(ethylene oxide)-poly(propylene oxide)-poly(ethylene oxide) or PEO-PPO-PEO where acceptors react with PO moiety before the ethylene oxide (EO) moieties; hence increasing the degree of hydrophilicity, water coalescence and demulsification efficiency (Wu et al. 2005). It was observed that 5 minutes treatment at concentrations 1.25g/L and 4.2g/L, 10 minutes (37.5g/L), 15 minutes (37.5g/L), 30minutes (37.5g/L) and 60 minutes (4.2g/L and 37.5g/L) sonication treatment had the highest oil recovery amongst the poloxamer treatments. This could be attributed to the increasing agitation duration which led to enhanced particle-particle interaction for 10, 15, 30 and 60 minutes treatments; thus, requiring a higher poloxamer concentration to enhance the demulsification (Zolfaghari et al. 2016). However, treatment of poloxamer at concentration 4.2g/l using 5minutes sonication gave best oil recovery of 11%. However, the formation of 8% froth in sample 10 minutes (4.2g/L) showed that the percentage of the sedimented solid phase would be low. The sedimented solid phase percentage volume varied from 15% for 5 minutes sonication to ≥ 25% amongst the other poloxamer treated samples.

Zolfaghari et al. (2016) have highlighted the need for higher concentration of poloxamer to improve phase separation and oil recovery in the oily waste.

Isopropanol (co-solvent) was also used to aid dispersion within the DF sample. According to Fink (2015), isopropanol aids oil recovery. The addition of alcohol co-solvents improves the efficiency of demulsifier formulation by reducing its viscosity and increasing the wettability of the solid phase. The surface of clay particles must become water wet for easy separation of oil from clay absorbed layer using surfactants and chemicals that can flocculate the oil clean from the clay surface. The result showed increased dispersion of the solid phase with the range of about 24-29% for the solid phase except for the 60 minutes sonication with a high concentration of isopropanol (ISP) with the least solid dispersion of 18%. This showed the increase in pore spaces allowing the association of and mobility of water and perhaps oil. The percentage volume of oil recovered varied across ISP concentrations especially. With 5 minutes sonication treatment, oil recovery improved from 2.5-7%. The increase in sedimented solid was suggested to be due to the steric hindrance caused by the adsorbed organic moieties on the solid phase.

The addition of NaCl as an electrolyte has been known to have enhanced surfactant induced oil extraction from the oily waste (Zhong, Mayer and Pope 2003). NaCl works by reducing the CMC of the surfactant, hence, increasing aggregation (Urum et al. 2005) and increasing demulsification effectiveness (Zolfaghari et al. 2016). In this study, NaCl treatment had the best oil phase recovery after 5minutes sonication. Froth formation was absent in lower concentrations of 7.8g/L and 15.6g/L; as the result confirmed high concentration of 30g/L led to froth formation. At higher sonication times of 30 and 60 minutes the use of 15.6g/L and 30g/L yielded froth. The solid phase showed a range of 15-25% recovery.

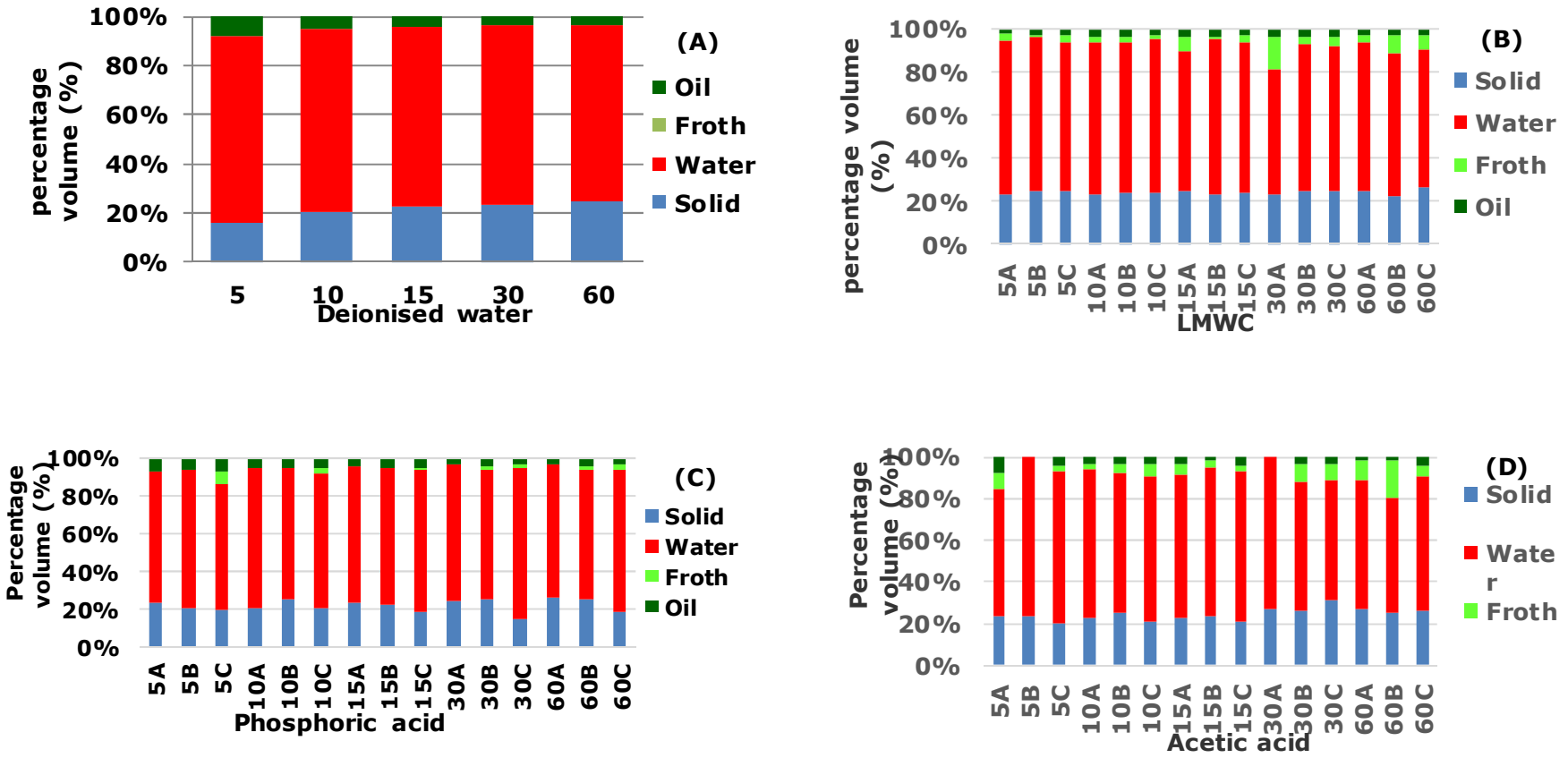

Figure 4.4 (i) Effect of sonication time on phase separation of spent oil based drilling fluid and cuttings treated with individual components of the demulsifiers (A) Deionised water treatment at varied sonication times 5-60minutes; (B) LMWC treatment of concentrations A- 2mg/L, B-20mg/L, C-200mg/L at varied sonication times 5-60minutes; (C) phosphoric acid treatment of concentrations A-0.02M, B-0.2M, C-2M at varied sonication times 5-60minutes; (D) acetic acid treatment of concentrations A-0.02M, B-0.2M, C-2M at varied sonication times 5-60minutes

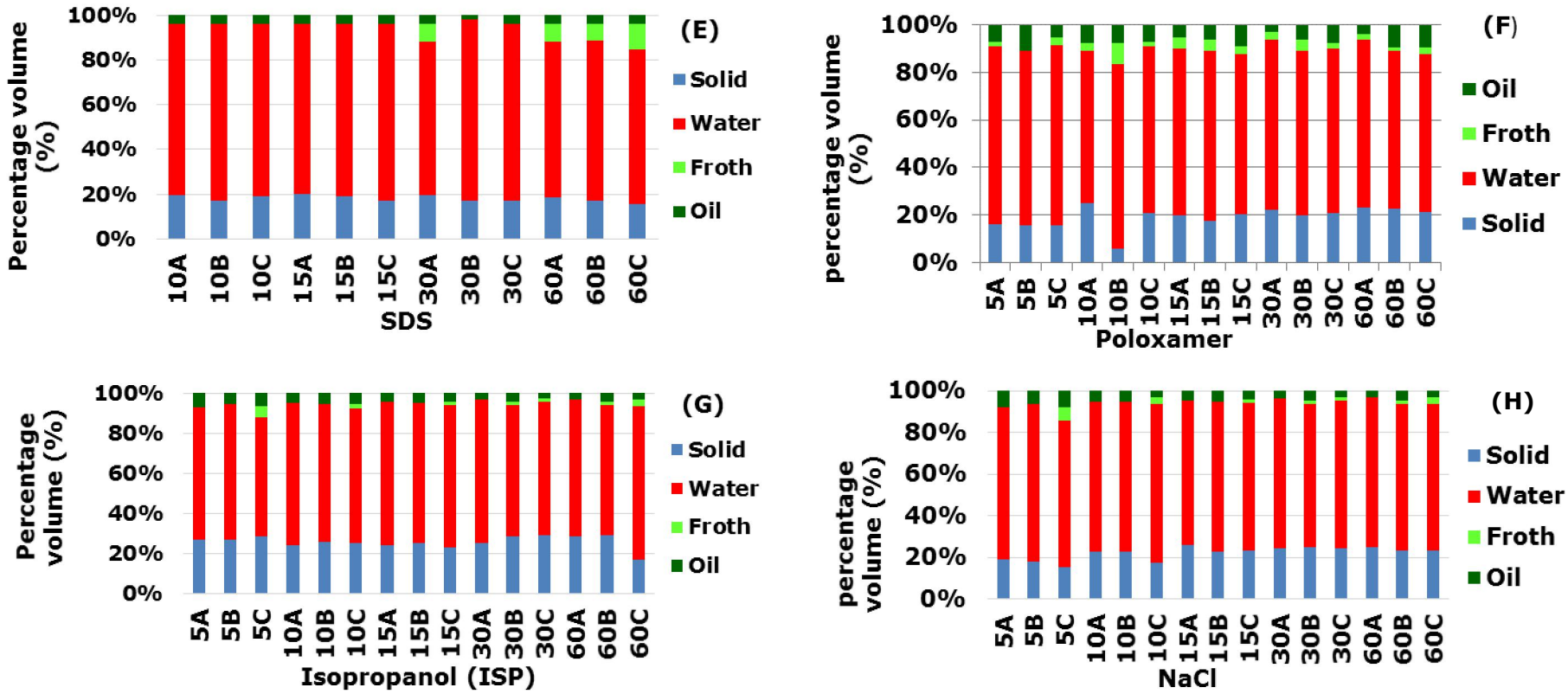

Figure 4.4 (ii) Effect of sonication time on phase separation of spent oil based drilling fluid and cuttings treated with individual components of the demulsifiers (E) SDS treatment of concentrations A- 0.025% w/v, B-0.05%w/v, C-0.1%w/v at varied sonication times 10-60minutes; (F) poloxamer treatment of concentrations A- 1.25g/L, B-4.2g/L C- 37.5g/L at varied sonication times 5-60minutes; (G) isopropanol treatment of concentrations A- 0.025 v/v%, B-0.05v/v%, C- 0.1 v/v% at varied sonication times 5-60minutes; (H) NaCl treatment of concentrations A- 7.8g/L , B-15.6g/L, C-30g/L at varied sonication times 5-60minutes.

There was no significant difference between (t-test; $p>0.05$) samples that were centrifuged and those that were sonicated (pre-centrifugation) when deionised water (used as a control), phosphoric and acetic acid, SDS and LMW chitosan were used for flocculation. However, when using isopropanol, NaCl solution and poloxamer, a significant difference was observed (t-test; $p>0.05$) on centrifugation (Table 4.1). Comparison of F-values for deionized water treated spent oil based drilling fluid samples before and after centrifugation showed that after centrifugation the recovered solids increased in volume compared to the sonicated sample mainly for deionised water, isopropanol and acetic acid. This is attributed to the steric hindrance by methyl groups of the organic treatment of acetic acid and isopropanol, and the formation of the emulsion in the deionized water treated samples. On the other hand, most poloxamer, phosphoric acid, NaCl treated samples were compressed due to the centrifugal force. This was attributed to the solid flocculating effect of phosphoric acid mainly at the lower concentrations and sonication times of 5, 10 and 15minutes. The significance of the changes in volumes after sonication (pre-centrifugation) and sonication + centrifugation (post-centrifugation) was assessed using a t-test. The result showed that the deionised water led demulsification had a better dispersion of solid phases after centrifugation.

In acetic acid treated samples, the lower sonication times showed the most compression of the solid phase. Further investigations of the oil and water phase volume would provide more information of the characteristic of the treatment. The phosphoric acid treatment functioned best using the highest concentration of 2M. The flocculation was also evident in the lowest concentration (0.02M) of phosphoric acid used unlike the medium concentration of 0.2M. The F-value result for poloxamer showed that the sample 10B treated for 10 mins at the medium concentration (4.2g/L) had the lowest F-value after sonication and after the centrifugation which follows sonication. The isopropanol had maximum dispersion when the highest concentration of 0.1%v/v was used. It was observed from the F-values that chitosan treated samples had best solid dispersion treatment at higher treatment time and concentration of 60minutes and 200mg/L. Comparison of F-values for NaCl treated spent oil based drilling fluid samples before and after centrifugation is shown in Figure 4.5 (i-ii).

Table 4.1 t-test analysis of difference in the effect of individual demulsifier additives on mean recovered solid phase f-value of spent oil based drilling fluid phase separation during pre-centrifugation (sonication) and post-centrifugation (sonication and centrifugation) - (t-test: p>0.05)

Demulsifier additives	**Mechanical Conditions**	$\overline{X}$	**SD**	**p-value**	**Crit.t**	**Remark**
Deionised water	pre-centrifugation	0.224	0.014	0.14	1.82	NS
	post-centrifugation	0.237	0.019			
Phosphoric acid	pre-centrifugation	0.24	0.085	0.64	0.48	NS
	post-centrifugation	0.228	0.037			
Acetic acid	pre-centrifugation	0.22	0.042	0.35	0.97	NS
	post-centrifugation	0.24	0.030			
LMWC (chitosan)	pre-centrifugation	0.248	0.015	0.22	1.27	NS
	post-centrifugation	0.243	0.010			
Isopropanol	pre-centrifugation	0.24	0.009	0.0016	3.91	S
	post-centrifugation	0.28	0.043			
SDS	pre-centrifugation	0.22	0.054	0.068	2.02	NS
	post-centrifugation	0.18	0.014			
NaCl	pre-centrifugation	0.245	0.022	0.0043	3.4	S
	post-centrifugation	0.224	0.033			
Poloxamer	pre-centrifugation	0.2082	0.034	0.011	2.93	S
	post-centrifugation	0.191	0.0449			

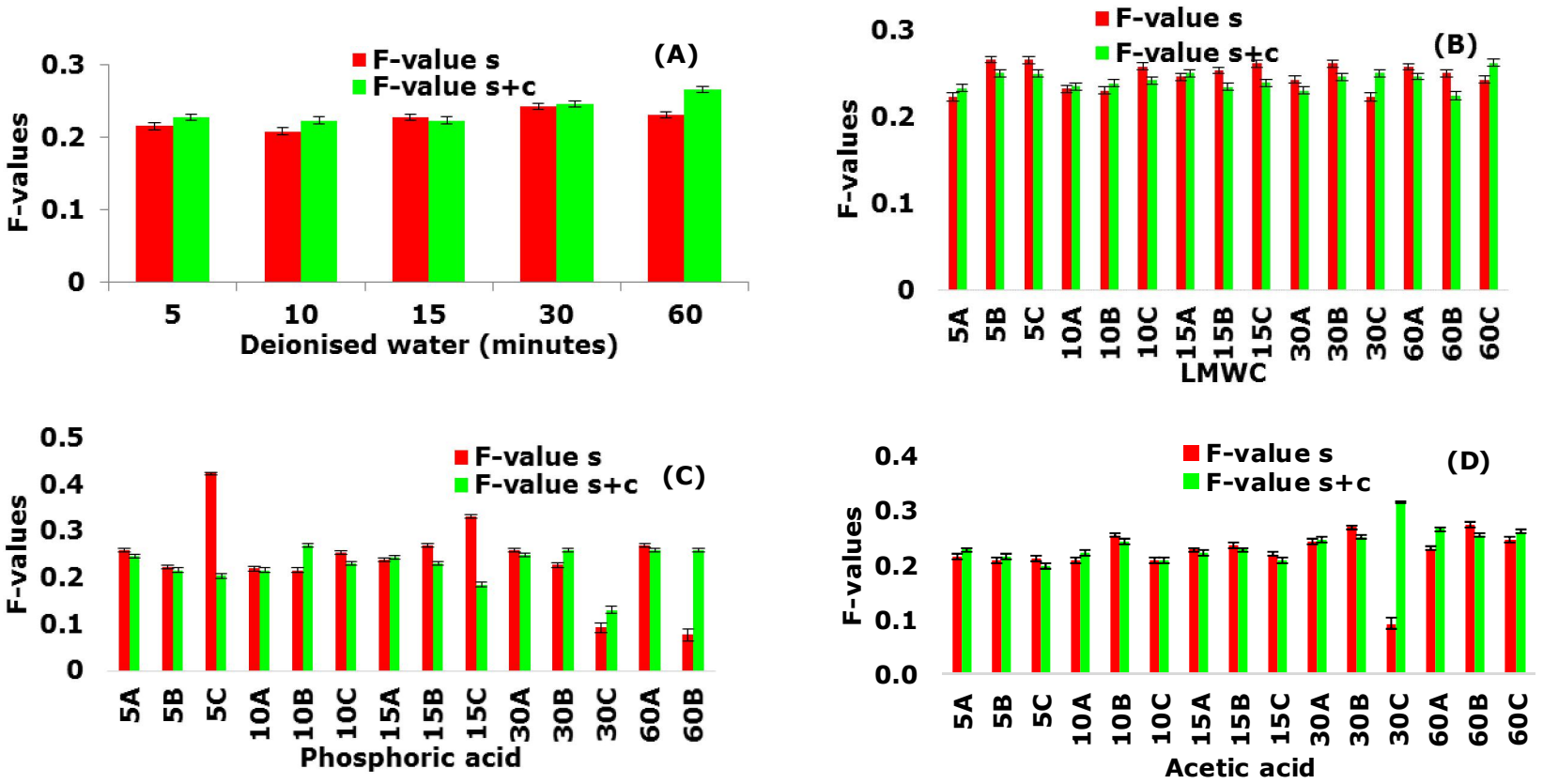

Figure 4.5 (i) Comparison of F-values for demulsifiers components treated spent oil based drilling fluid and cutting recovered solid residue by sonicaton (s) and sonication+centrifugation (s+c); (A) Deionise water treatment at varied sonication times 5-60minutes; (B) LMWC treatment of concentrations A- 2mg/L, B-20mg/L, C-200mg/L at varied sonication times 5-60minutes; (C) phosphoric acid treatment of concentrations A-0.02M, B-0.2M, C-2M at varied sonication times 5-60minutes; (D) acetic acid treatment of concentrations A-0.02M, B-0.2M, C-2M at varied sonication times 5-60minutes

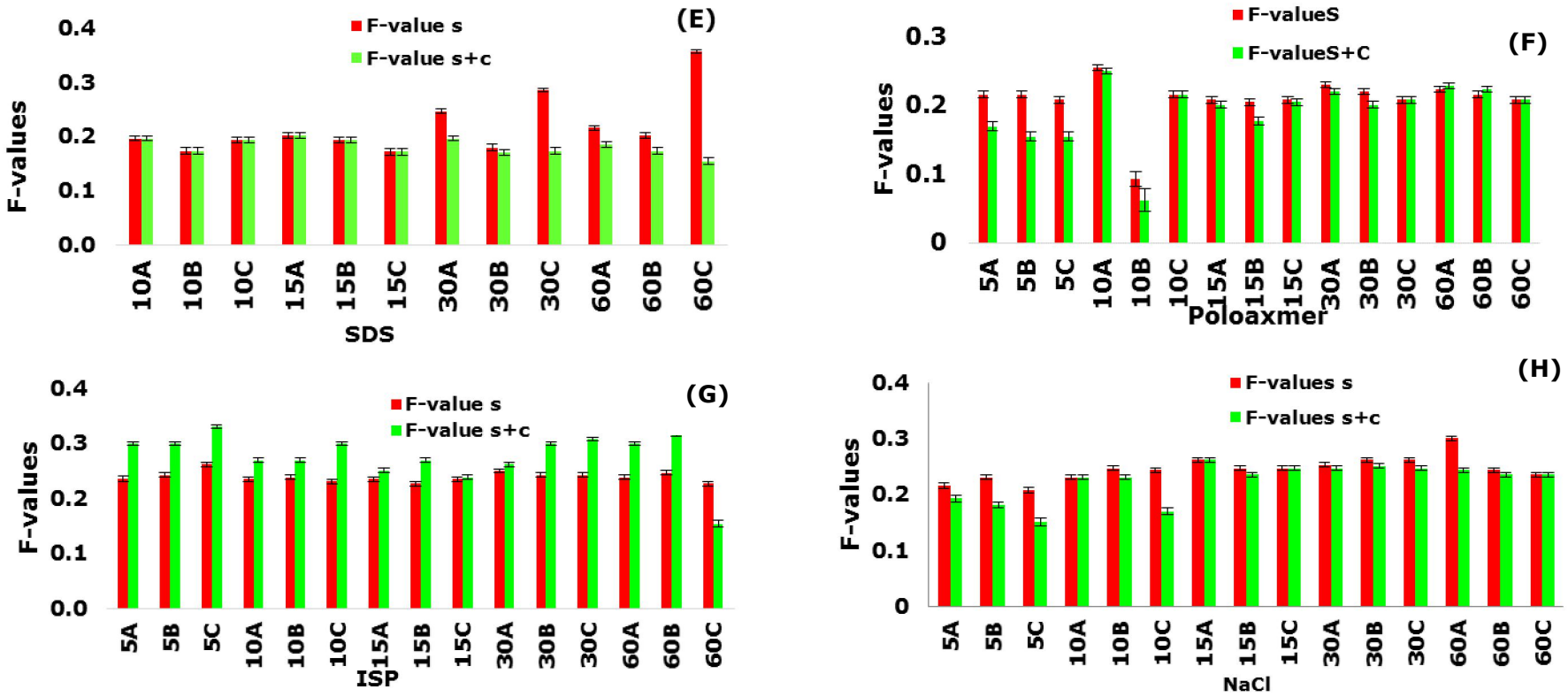

Figure 4.5 (ii) Comparison of F-values for demulsifiers components treated spent oil based drilling fluid and cutting recovered solid residue by sonicaton (s) and sonication+centrifugation (s+c); (E) SDS treatment of concentrations A- 0.025% w/v, B-0.05%w/v, C-0.1%w/v at varied sonication times 10-60minutes; (F) poloxamer treatment of concentrations A- 1.25g/L, B-4.2g/L C- 37.5g/L at varied sonication times 5-60minutes; (G) isopropanol treatment of concentrations A- 0.025 v/v%, B-0.05v/v%, C- 0.1 v/v% at varied sonication times 5-60minutes; (H) NaCl treatment of concentrations A- 7.8g/L , B-15.6g/L, C-30g/L at varied sonication times 5-60minutes.

Following the investigation of demulsifying potentials of individual components present in the demulsifier formulation, the two demulsifiers (demulsifier S3 and demulsifier S4) were tested for their phase separation and demulsification potentials. The results of the demulsification process are shown in Figure 4.6 and Table 4.2.

The optimum demulsifier formulations were composed of ISP - 2.5%v/v, SDS - 4.2 g/L, poloxamer - 1.3 g/L, NaCl - 1.7g/L, 3ppm LMWC in 0.2M acetic acid - 1.7%v/v for demulsifier S4 and an addition of phosphoric acid - 2.8%v/v for demulsifier S3. The demulsification result showed that demulsifier S4 treated DF had a more improved oil recovery following sonication and centrifugation of the samples at different sonication times compared to demulsifier S3 treatment which contained phosphoric acid. The reason for the poor oil recovery using demulsifier S3 is not fully understood. The difference in oil recovery is showed in the TPH results of the solid phase from S3 which has a TPH of 9844mg/kg while S4 had a TPH of 9591mg/kg (see Table 4.3).

Table 4.2 t-test analysis of difference in the effect of demulsifiers on mean recovered solid phase f-value of spent oil based drilling fluid phase separation during pre-centrifugation (sonication) and post-centrifugation (sonication and centrifugation) - (t-test: $p>0.05$)

Demulsifiers	**Mechanical conditions**	$\overline{X}$	**SD**	**p-value**	**Crit.t**	**Remark**
Demulsifiers S3	pre-centrifugation	0.20	0.034	0.005	5.597	S
	post-centrifugation	0.10	0.010			
Demulsifiers S4	pre-centrifugation	1.499	0.164	0.00012	14.96	S
	post-centrifugation	0.64	0.1010			

Demulsifiers S3 and S4 led phase separation per time are shown in Figure 4.6. F-values showed that the samples were compressed by centrifugal force in both the solids of S3 and S4. S4 treated samples, there was a significant difference between the pre-centrifugated (s) and centrifugated (s+c) samples (t-test: $p>0.05$).

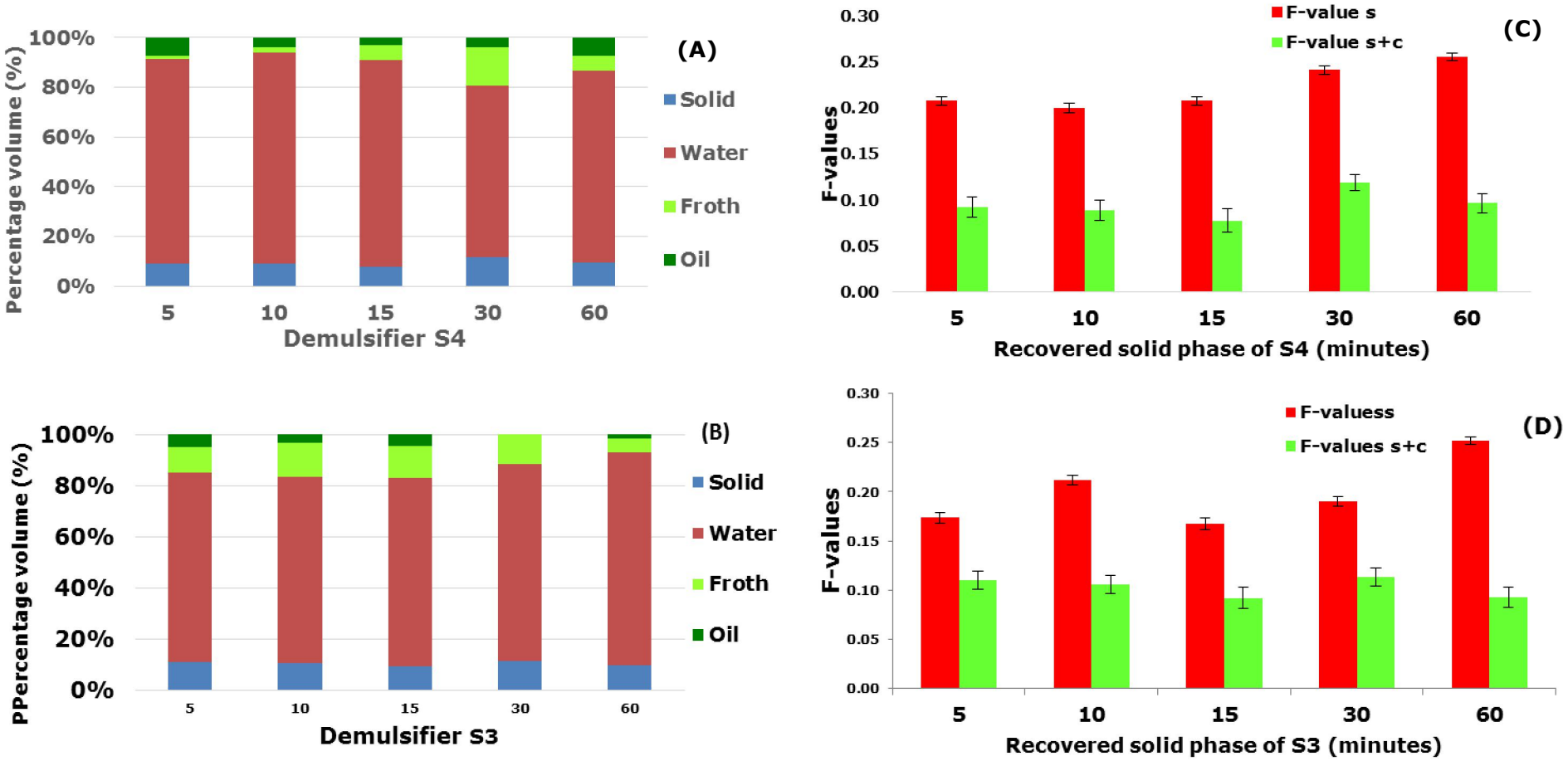

Figure 4.6 Effect of time on phase separation and sedimentation of spent oil based drilling fluid and cuttings treated using demulsifiers S4 (A) and S3 (B). Comparison of F-values of sedimented solids recovered using demulsifiers S4 (C) and S3 (D)

4.3.4 Effect of demulsifiers on solid phase characteristics compared to undemulsified spent oil based mud and cuttings samples (including bentonite and thermally treated sample): TPH and elemental concentrations

As shown in Table 4.3, S6 was the untreated oil based drilling fluid; S4 was the demulsifier S4 treated solid, S3 was the demulsifier S3 treated solid, while S2 was pure bentonite without hydrocarbon and S5 was the thermally treated oil based drilling fluid. The resultant solid matter, S4 of demulsifier S4 wash was solid particles with ~ 1.4% organic content from the crude oil and demulsifier components. The demulsifier contained SDS, poloxamer, chitosan, isopropanol (ISP), NaCl and water. The demulsifier S4 formula acted as a soap by lowering the surface tension between oil and water, and insoluble substances such as bentonite, barium sulphate, sand, calcium sulphate and calcium carbonate that leads to the separation of oil from their surfaces. As in the case of sodium stearate formation, oil, SDS and other additives form a sodium lauryl stearate during demulsifier treatment. According to Demirbas, Sari and Isildak (2006) bentonite and other particles are capable of adsorbing on the surface of the particle. This adsorption caused a surface modification of the solid particles to be used as fillers. It is important to note that the surface modification of stearate resulted in organo fillers. This is due to the oil soluble, non-polar hydrocarbon end of the SDS which coats the solid materials such as bentonite to form the organo-layered solid phase (see chapter 5.5.4). The organofilm is further stabilised by the presence of Isopropanol (Mishra, Chatterjee and Singh 2011) . The adsorption and stability of the organo-surface modification of bentonite, barium sulphate, sand, calcium sulphate and calcium carbonate are temperature, pH and salinity dependent Demirbas, Sari and Isildak (2006) and Mishra, Chatterjee and Singh (2011). In the above synthesis, due to higher pH, high surfactant and alcohol content as well as low temperature and low salinity of demulsifier treatment, a very stable emulsion of dispersed but highly suspended solids in the emulsion was formed after mechanical mixing. This stable emulsion was broken by a further mechanical process of centrifugation. This kind of surface modification could decrease the melting point or maintain (near) constant temperature as heat is absorbed by material as a result of the large latent heat capacity.

The presence of 0.2M orthophosphoric acid in demulisifer S3 produced a very dry texture solid residue, S3. The presence of phosphoric acid in demulsifier S3 had a flocculating effect on the solid particles. Therefore, the particles sediment after mixing with the demulsifier to produce 3 separated phases of oil, water rich emulsion and solids. Research by Dahiya et al. (2008) on the synthesis and study of the thermal properties of PA6-bentonite- ammonium phosphate composite highlighted that phosphate group (APP) layer on the solid enhance combustion reduction / fire retardancy and reduced charring of the synthesised nanocomposite material (in Chapter 5) as characterised by TG. However, it was also observed that the combined presence of the clay and APP/TP. Following the treatments with the various treatments assessed, the S3 and S4 treatments were taken selected as the optimal treatment conditions and hence the solids recovered from these were extracted and the hydrocarbon content measured as described in Chapter 3. The TPH results show a hydrocarbon reduction of over 98% by both demulsifiers (demulsifier S3 and demulsifier S4) (Table 4.3).

Table 4.3 TPH results of nanofillers showing hydrocarbon content of nanofillers recovered after demulsification and used in PA6 nanocomposite manufacture

Samples	**TPH concentration (n=3) mg/kg**	**± SD**	**Hydrocarbon reduction (%)**	**OSPAR limit of ≤ 1%w/w (%)**
S2 (bentonite only)	Nd	nc	100	0 (<1%)
S3 (demulsifier S3 treated)	9844	1088	98.5	0.98 (<1%)
S4 (demulsifier S4 treated)	9592	2148	98.6	0.96 (<1%)
S5 (thermally treated)	3391	1934	Lc	0.34 (<1%)
S6 (untreated sample)	662,500	50670	N/A	66.2 (>1%)

*nd – not detected, nc – not calculated, N/A – not applicable, Lc – from local company

The elemental analysis of the untreated and demulsified drilling fluid and cuttings, as well as the metal analyses of thermally treated drilling fluid and cuttings and bentonite (S2) used as a control is shown in Table 4.4. The result

showed the presence of different elements such as Ba, Cd, Cr, Cu, Ni, Pb, Zn, Al, Fe, Mg, Si, S and P. Initial studies of the untreated drilling fluid and cuttings showed that Hg was not present and As concentration was below the detection limit, thus, they were not analysed. Results showed that Ba concentration was highest in S3 the demulsifier S3 washed drilling fluid and cuttings (3831 mg/kg), followed by S5 (3720 mg/kg), then S4, demulsifier S4 treated drilling fluid and cuttings (1173 mg/kg). S2 (bentonite) had no Ba present, which confirmed it was Ba free. The concentration of P in the samples analysed was most abundant in S3 (981 mg/kg). This is due to the phosphoric acid added to the demulsifier which also modified the surface of the S3 solids. The increase in P increased the flame retardancy of the nanocomposite material PA6/S3 (see chapter 6 and 7). S4 had more Al and Mg than S3 due to the acid-influenced colloid removal (chapter 5 section).

Table 4.4 ICPOES elemental concentration (mg/kg) of treated oil based drilling fluid and cuttings samples and bentonite

Elements	S2 (n = 3)	±SD	S 3 (n = 3)	±SD	S4 (n =3)	±SD	S5 (n =3)	±SD
Mg	2810	416	1974	48	2000	125	3951	180
Al	12900	3104	3811.82	589	4451	506.55	12510	2894
Fe	9967	1233	15050.51	787	16333	464.61	25869	1393
Mn	407.95	4.76	771.55	37.65	791.41	14.12	2680	39.24
Zn	39.13	1.22	123.16	7.71	129.94	10.68	265.90	10.35
Ba	nd	nc	3830.88	966.06	1173	597.89	3720	3254
Ca	8367	756	75183	2407	75191	4045	64906	3286
Cu	4.70	0.82	31.95	1.75	35.81	2.46	97.98	3.45
Ni	0.79	0.71	12.31	n.c	5.20	5.04	27.62	2.29
Cr	6.53	0.97	223.88	n.c	228.27	7.87	432.03	34.27
Pb	17.96	0.66	89.93	n.c	89.98	6.58	157.28	7.31
Ti	116.57	60.35	463.81	n.c	483.28	142.63	1626	606.85
Co	nd	nc	nd	n.c	nd	nc	7.99	3.85
P	200.63	7.13	981.22	n.c	176.46	14.95	364.71	11.66
S	800.23	1111	128.36	n.c	78.85	28.88	1729	2820
Si	699.70	14.90	7792	n.c	10174	258.55	5433	890.85
Na	7903	1429	799	1132	735	543	3214	852

*nd= not detected, *nc=not calculated.

S5 had the highest concentrations of Fe, Zn, Cu, Ni, Cr, Pb, Ti, Co and S. this was attributed to the additives used for the drilling processes from which S5 was obtained and elements associated with the geological formation drilled. S2 had very low concentrations of the heavy metals including Zn, Ni, Pb, Cr and Cu. Comparing the demulsifier treated samples - S3 and S4, it was observed that S3 had the lowest concentration of the heavy metals. This suggested that the acid containing demulsifier S3 aided the removal of these elements from the solid phase. It also suggested that these elements could have more association or affinity for the colloidal solids which were removed from the solid phase by the acidified demulsifier washing.

4.4 Conclusion

Demulsification of spent oil based drilling fluid with cutting was carried out successfully. The formulation of the demulsifiers for spent oil based drilling fluid demulsification using more environmentally acceptable chemical additives compared to some current industry demulsifier additives such as benzene derivatives (xylene, toluene) was achieved. The optimum demulsifier formulation was composed of ISP - 2.5%v/v SDS - 4.2 g/l, poloxamer - 1.3 g/l, NaCl - 1.7g/l, 3ppm LMWC in 0.2M acetic acid - 1.7%v/v for demulsifier S4 and an addition of phosphoric acid - 2.8%v/v for demulsifier S3. Hydrocarbon reduction on the extracted solid phase nanofiller S3 and nanofiller S4 was 98.6% and 98.5% respectively after demulsification. The demulsified spent oil based drilling fluid solid extracts were below OSPAR regulation of <1% oil on cutting by weight.

However, the carbon footprint of the demulsification treatment process applied in this research could be less compared to the thermal treatment applied to nanofiller S5 which could have resulted in the release of noxious gases (SOx and NOx), and greenhouse gases. None the less, the true measurement of CO_2 footprint from demulsifier and thermal treatments could form the scope for further studies.

On the other hand, ISP was observed to be a good dispersant of the sedimented solid phase while poloxamer was observed to extract more oil than the other individual components of the demulsifiers. Generally, the short treatment time of

5 minutes had the best oil recovery. The study finding was in agreement with the findings of Balson (2003), that demulsification in some cases is best at shorter retention (treatment) times. There was a significant difference (effect) in sonication times used in the demulsification process when demulsifier additives such as poloxamer, isopropanol and NaCl were tested.

Elemental concentrations varied as a result of demulsifiers applied in the treatment of the spent oil based drilling fluid. While demulsifier S3 treated samples had less of Si, Al, Mg, Fe, Mn, Zn, Cu, Cr and Ti than S4. On the other hand, S3 had more Ba, Ni, P and S of 69%, 57%, 82% and 38% respectively; and 23% less Si than S4 nanofiller. Whereas As, Cd, Hg and Co were not detected in both nanofillers. The solid residues (nanofillers) recovered after demulsifier treatments were below or within the OSPAR threshold for Zn, Cu and Ni with exception to Cr and Pb that were above OSPAR thresholds. The surface modification of solid residues S3 by phosphorus was successfully achieved. The results in Table 4.4 showed that S3 had the highest concentration of phosphorus (981mg/kg) compared to the other solid residues investigated.

Chapter 5

Synthesis and Manufacture of Nanocomposite Materials from Oil Based drilling mud and cuttings from the North Sea

5.1 Introduction

As the world moves rapidly and consciously towards environmental sustainability, various aspects of life and technology are being put into maximum use to achieve the great expectation of little or no environmental pollution. In order to achieve this global goal, various plans, policies, protocol, procedures, guidelines, regulations and legislations have been put in place. One of such legislations is the waste management hierarchy (EU 2014), which outlines potential management steps for hazardous and non-hazardous wastes generated internationally. The steps in the waste management hierarchy include prevention, reduction, reuse, recycling, recovery (energy) and landfill disposal. While prevention of waste generation is the most favourable strategy for waste management, landfill disposal is the least favourable. Waste researchers show that various wastes can be complex due to their composition and as such may contain different phases of matter such as gas, liquid, solids and even colloids (Shon et al. 2016; Jimenez et al. 2015; Aguilera, Broitman and Thiel 2016; Liu et al. 2016). Therefore, waste could require segregation into various phases to recover and effectively treat the recovered phases for reuse. The Scottish Environmental Protection Agency (SEPA) guideline for waste also prevents irresponsible or illegal disposal of waste in the environment (SEPA 2016 a; SEPA 2016 b; SEPA 2016 c). Drilling mud and drill cutting are classified as hazardous waste by the European Waste Catalogue (European Union 2002).

In this research, oil based drilling fluid, a hazardous waste generated from oil and gas exploration process was obtained, treated and separated into the solid, water and oil phases using a demulsifier discussed in chapter 4. The recovered water could be tested for purity and further treated where necessary while oil recovered could be potentially reused in making new drilling fluid (Seaton et al. 2006) energy generation or resold for capital.

The recovered solids were composed mainly of barite, bentonite clay and low-density cuttings. These recovered solids of the drilling fluid were obtained for use as nanofillers in the manufacture of polyamide (PA6) plastic nanocomposite material to promote the reuse of waste drilling solids and prevent landfilling of the recovered solid which is the current practise (Figure 5.1). Thus, the solid phase is utilised in open recycling for the production of new engineering nanocomposite materials. From an environmental perspective, PA6 acts as a matrix for the stabilisation and solidification of the solid material from the waste recycling, while from a material and structural viewpoint, the nanofiller is used to improve the mechanical and thermal properties, quality and the performance of the matrix material, PA6.

The aim of this chapter was to produce a novel engineering material based on PA6 with improved mechanical properties whilst promoting environmental sustainability through the immobilisation of heavy metal rich waste solids in polyamide 6.

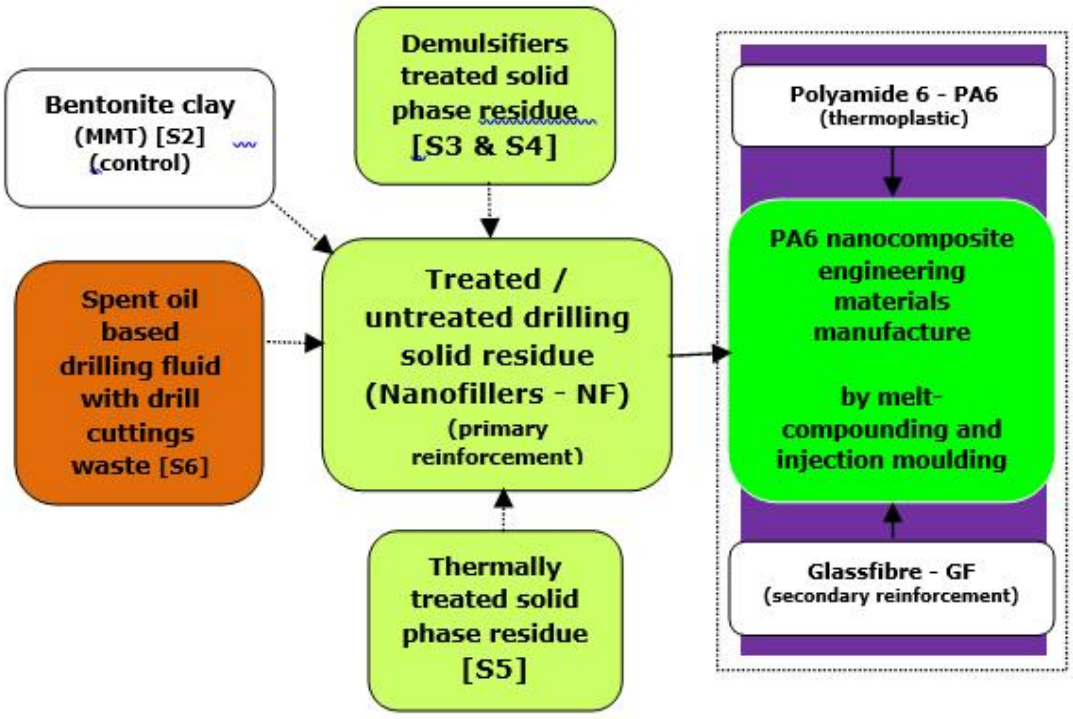

Figure 5.1 Fabrication of PA6 nanocomposite materials: recycling of spent oil based drilling fluid

5.2 Components for the formulation of nanocomposite materials

There are three main components used in the manufacture of Polyamide 6 (PA6) nanocomposites. They are nanofillers, polymer - polyamide 6 and glass fibre (GF). Previous studies have demonstrated the use of different natural and synthetic fillers percentage by weight of fillers to PA6 for enhancing the mechanical, thermal, electrical properties of Polyamide 6. For example, Mészáros et al. (2013) worked on the use of basalt (volcanic rock) nanocomposite for improving the flexural property of PA6. Jiang et al. (2005) used 0.1, 0.2, 0.3 and 0.5% clay as filler for PA6. The research findings showed increased flexural strength of PA6 by 35%. Chow and Mohd Ishak (2007) suggested the use of 2.5% wt. of MMT (clay) filler to PA6 for best mechanical properties.

5.2.1 Nanofillers

Nanofillers are reinforcement materials used to enhance the mechanical and thermal properties of (plastic and elastic) polymers (Wypych 2016; Jiang et al. 2005). Fillers S2 is composed of bentonite clay (MMT) while DF fillers S3 to S6 (Table 5.1) are composed of barite ($BaSO_4$), bentonite clay (MMT), sand, quartz, shale (low-density solids) and calcium carbonate ($CaCO_3$).

5.3 Formulation of Nanocomposite Materials

The novel nanocomposite materials formulated in this research contain nanofillers which have MMT and barite as part of the solid components. (see section 4.3.4: Table 4.4). The novel nanocomposite formula was 97.5% PA6 and 2.5% nanofiller for the 2-phase nanocomposites, while the 3-phase nanocomposites contained 2.5% nanofiller, 15% or 30% glass fibre for improved mechanical and thermal properties and the appropriate weight% of polyamide 6 (PA6) (see Table 5.1).

The nanocomposite materials were formulated based on previous studies by Liu, Qi and Zhu (1999) which showed that about 2.5 – 3% MMT was required to produce PA6 nanocomposite with best mechanical properties because increasing the filler % composition led to a decline in the mechanical properties.

Table 5.1 Matrix of PA6 composite blending and synthesis: PA6 and PA6 formulated nanocomposites and controls:

Polymer	**Label**	**PA6 wt.%**	**Filler wt.%**	**glass fibre (GF) wt.%**
Polyamide6	PA6	100	-	-
Polyamide6 + untreated spent drilling fluid and cuttings	PA6/S6	97.5	2.5	-
Polyamide6 + pure bentonite	PA6/S2	97.5	2.5	-
Polyamide6 + demulsifier S3 treated spent drilling fluid and cuttings	PA6/S3	97.5	2.5	-
Polyamide6 + demulsifier S4 treated spent drilling fluid and cuttings	PA6/S4	97.5	2.5	-
Polyamide6 + thermally treated spent drilling fluid and cuttings	PA6/S5	97.5	2.5	-
Polyamide6 + glass fibre	PA6/GF30	67.5	2.5	30
Polyamide 6 + untreated spent drilling fluid and cuttings + glass fibre	PA6/S6/GF30	67.5	2.5	30
Polyamide 6 + pure bentonite + glass fibre	PA6/S2/GF30	67.5	2.5	30
Polyamide 6 + demulsifier S3 treated spent drilling fluid and cuttings + glass fibre	PA6/S3/GF15	82.5	2.5	15
Polyamide 6 + demulsifier S3 treated spent drilling fluid and cuttings + glass fibre	PA6/S3/GF30	67.5	2.5	30
Polyamide 6 + demulsifier S4 treated spent drilling fluid and cuttings + glass fibre	PA6/S4/GF30	67.5	2.5	30
Polyamide 6 + thermally treated spent drilling fluid and cuttings + glass fibre	PA6/S5/GF30	67.5	2.5	30

The use of glass fibre in PA6 composite manufacture is to enhance the mechanical strength and modulus of PA6 as well as increase its heat resistance. Studies have reported that 30% glass fibre gave the best mechanical property for PA6 (Wu et al. 2001). Therefore, the nanocomposite materials were manufactured using PA6 as the matrix material, the nanofillers as the primary fillers and glass fibre as the secondary filler.

The result of this study should provide useful information for the redevelopment, recycling and reuse of the waste as a measure to sustainably reduce offshore ocean dumping and land filling of the waste. Therefore, this chapter aims to evaluate the characteristics of the nanocomposite components and how these potentially influence any chemical or physical changes in the characteristic of the novel formulated nanocomposite materials.

5.4 Experiment

5.4.1 Materials

Polyamide 6 (PA6) was obtained from Tarnamid T30, Zaklady Azotowe in Tarnow - Moscice, Poland. The spent oil based drilling fluid was donated by an oil and gas company (S6); thermal desorbed oil based drilling fluid (S5) was donated by an oil and gas company, while commercial bentonite (MMT) used as nanofiller, S2 Commercial montmorillite (pure bentonite) was obtained from Thronton and Ross, UK. It was used as a control sample in this experiment to compare the performance of the novel nanofillers with the chemically and thermally derived nanofillers. S2, pure bentonite had a TPH concentration was 0mg/L. The particle size distribution was an average of 301.1nm for nanosized residues.

S6 - untreated spent drilling fluid and cutting slurry: The spent drilling fluid used to produce this nanofiller was not treated, either by thermal or demulsifier treatment. The resultant solid matter was uncrushed particles obtained by drying the drilling waste under ambient conditions. Thus, had a high hydrocarbon content of 662500 mg/kg compared to S3, S4, S5 and S2 which had hydrocarbon percentage reduction of 98.5, 98.6, 99.5 and 100% respectively compared to S6. The used untreated drilling fluid consists of weighting agents,

base oil - diesel, mineral oil; shale inhibitors; corrosion inhibitors; viscosifers; flocculants; surfactants; dispersants; biocides and rock particles often called cuttings (Li et al. 2015; Hermoso, Martinez-Boza and Gallegos 2014). This complex mixture is used in this study to understand the effect of the cuttings on the PA6 nanocomposite material thermal and mechanical properties. The particle size was an average of 790nm for nanosized residues.

S3 – Demulsifier S3 treated spent oil based drilling fluid / drilling mud: the spent drilling fluid used to produce this nanofiller was treated by the same demulsifier treatment used for S4 but with 0.2M ortho-phosphoric acid added during the demulsifier formulation. The formulation mechanism of demulsifier S3 was similar to that of S4 but differs by the addition of 0.2M ortho-phosphoric acid. The particle size was an average of 248.9nm for nanosized residues. The resultant solid matter was uncrushed particles with 1.45% TPH content from demulsifier surface modification of the nanofiller. As mentioned earlier in section 4.2.2, demulsifier S4 was composed of SDS, poloxamer, chitosan, ISP, NaCl and water. The particle size of the S4 nanofillers was an average of 312.7nm for nanosized residues.

S5 – Thermal treated spent drilling fluid: the spent drilling fluid used to produce this nanofiller (S5) was treated through the use of a thermal desorption unit or the Hammersmith thermal units. This method was used to extract oil and water from recovered drilling fluid and drill cutting wastes and the resultant solid matter was crushed solid particles with about 1% unrecovered oil. The particle size was an average of 345.4nm for nanosized residues. Silane coated glass fibre specific for polyamide (Gu et al. 2000) was donated by University of Krakow, Poland - polymer technology department.

5.4.2 Sample preparation

This involved the preparation / acquisition of nanofillers, the premixing of nanofiller and polymer, and the extrusion (melt compounding) and injection moulding of the melt compounded pellets (Pielichowski et al. 2013) (see formulation summary Table 6.1). The equipment used in the sample preparation were Twin co-rotation screw extruder Thermo Scientific Rheomex PTW 16/25 XL, cooling tank of ZAMAK, granulator- ZAMAK G-16/325, injection moulding

instrument ZAMAK WT12. The processing conditions for sample preparation and equipment are given in Table 5.1 and 5.2 for the nanocomposite materials.

Table 5.2 Manufacturing equipment operating conditions for PA6 and its nanocomposite samples preparation

Twin co-rotating screw extruder								
Flow rate [%]	Rotational speed [1/min]	Heating zones						
0.3	150	1	2	3	4	5	6	Die
Temperature [^{0}C]		250	250	250	250	255	250	250
Atmospheric venting		-	-	-	-	YES	-	-
Length of zones [mm]		80	60	60	64	60	76	23
Length/Diameter (L/D)		5.00	3.75	3.75	4.00	3.75	4.75	-
Cooling tank								
Length of cooling surface [mm]		1500						
Tank volume [dm^3]		27						
Height of bath [mm]		1081						
Water temperature [^{0}C]		18						
Granulator								
Size of pellets [mm]		1						
Rotational speed [1/s]		12						
Injection Moulding machine ZAMAK WT12								
Temperature of cylinder [^{0}C]		233						
Temperature of Mould [^{0}C]		80						
Injection pressure [Bar]		10						

5.4.3 Material characterisation and testing methods

Microscopy

The material characterisation has been carried out using SEM microscopy, X-ray diffraction (XRD) analysis, FTIR-ATR. The experimental study has been carried out on untreated and treated spent oil based drilling fluid/cutting nanofillers, bentonite clay nanofiller, PA6, PA6 glass fibre reinforced nanocomposites and PA6 nanocomposites. The characterisation methods have been earlier discussed in section 3.2.2

5.5 Results and discussion

5.5.1 Visual inspection

Visual inspection in Figure 5.2(a-f) showed that the manufactured nanocomposite materials were of the following dimensions: length – 80mm; width – 10mm; and

height – 4mm. It was observed that some of the nanocomposite materials such as PA6/S3, PA6/S4, PA6/S5 and PA6/S6 had shrunk by ±0.1mm in length from 80mm. This was attributed to the fact that PA6 has a shrinkage factor of 0.14% due to loss of absorbed moisture as stated in the PA6 T-30 MSDS, 2009 (see Appendix E Figure E.1).

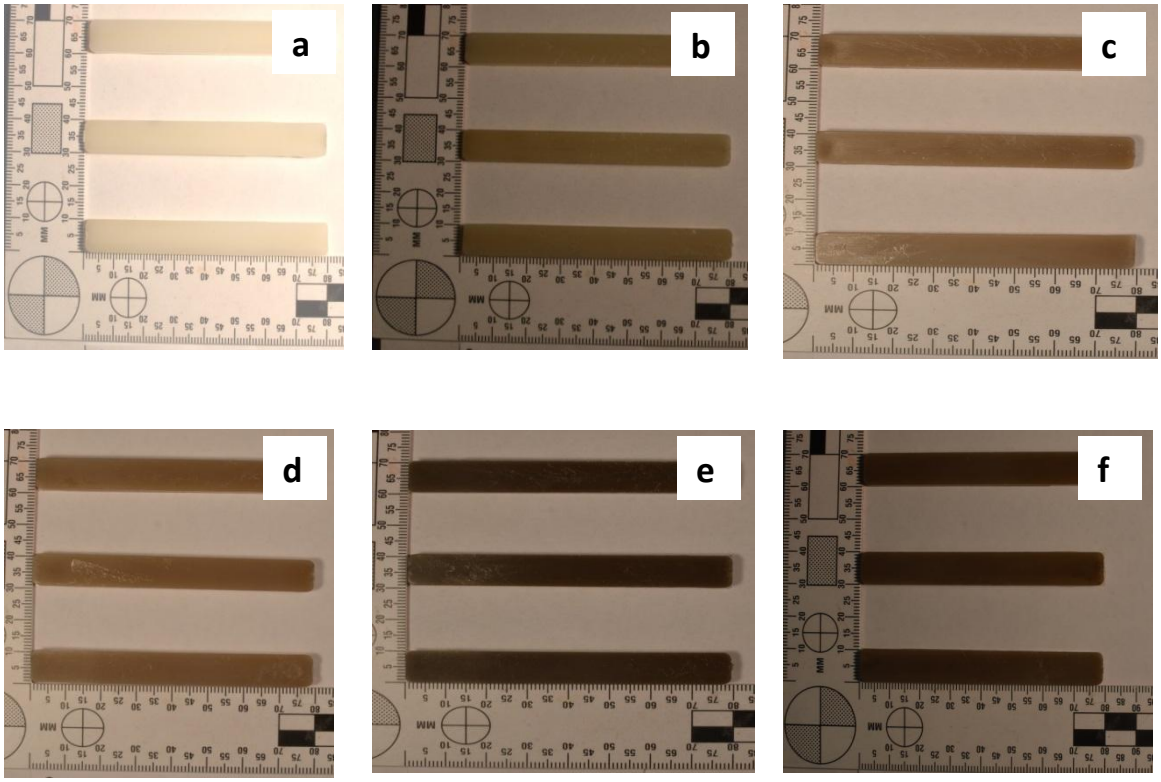

Figure 5.2 (a-f) Photographic images of PA6 and PA6 nanofiller only filled nanocomposite materials (a) PA6 (b) PA6/S2 (c) PA6/S3 (d) PA6/S4 (e) PA6/S5 (f) PA6/S6

Similar to Figure 5.2, visual inspection in Figure 5.3(a-f) showed that the manufactured PA6 glass fibre reinforced nanocomposite materials were of the following dimensions: length – 80mm; width – 10mm; and height – 4mm. It was observed that some of the nanocomposite materials such as PA6/S4/GF30, PA6/S5/GF30 and PA6/S6/GF30 had shrunk in length due to water loss.

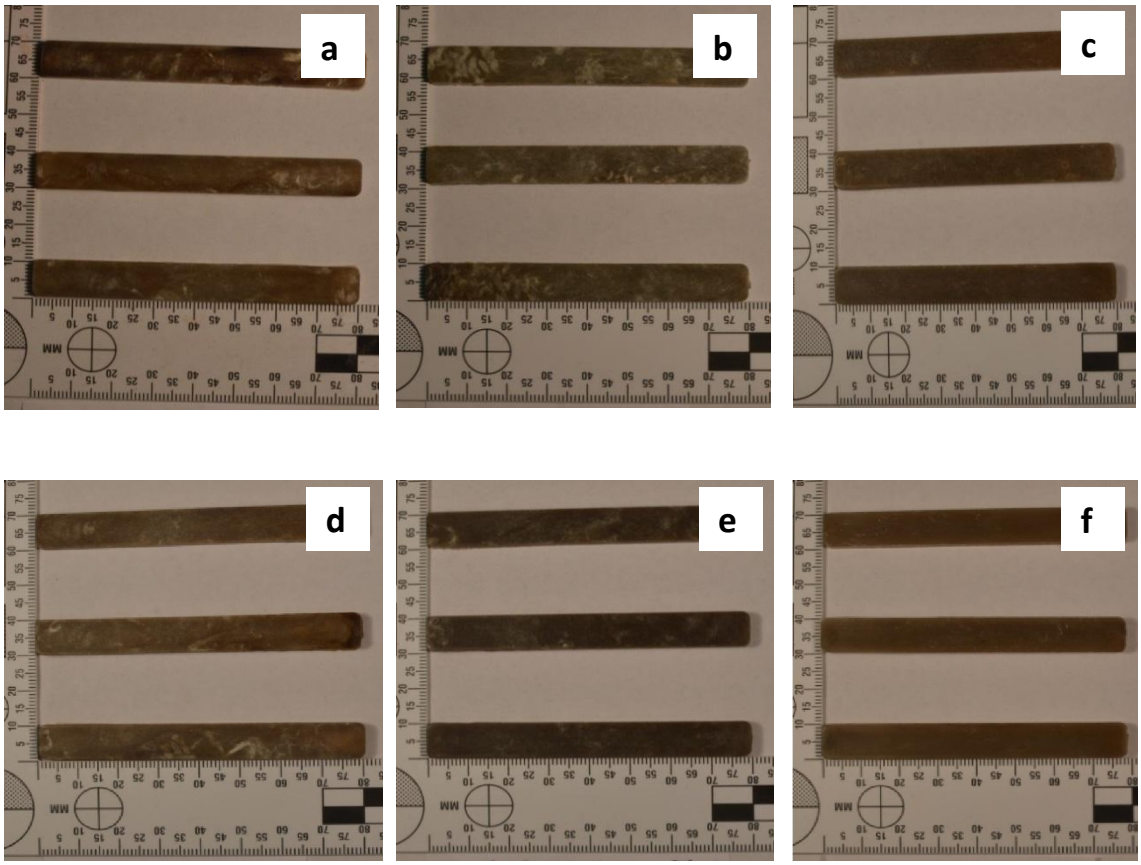

Figure 5.3 (a-f) Photographic images of PA6 glass fibre reinforced nanocomposite materials. (a) PA6/GF30 (b) PA6/S2/GF30 (c) PA6/S3/GF15 (d) PA6/S3/GF30 (e) PA6/S5/GF30 (f) PA6/S6/GF30

5.5.2 Morphology studies

Morphological studies were carried out to understand the form and structure of the nanomaterials produced. It involved the use of different scientific experimental methods to break down the nanomaterial into essential components thereby understanding how it was formed and expected to perform based on possible nanofiller agglomeration, nanofiller distribution and glass fibre distribution and alignment (unidirectional or multidirectional).

The nanofillers and nanocomposites were investigated using SEM. To understand the integration of PA6 and the different nanofillers, scanning electron micrographs of the nanofillers generated for nanocomposite material manufacture are represented in Figure 5.4a to 5.4e. In Figure 5.6a, the micrograph of the untreated spent drilling fluid and cutting slurry showed densely stacked large irregular shaped particles within a layered structure. In Figure

5.4b, the micrograph of the commercial MMT (pure bentonite) was evidently different from the other samples; it showed presence of many minute particles (loosely) coagulated together. It showed large layers with agglomerates of small particles (flakes) of bentonite on top. In Figure 5.4c, the micrograph of the demulsifier S3 treated DF (with phosphoric acid) showed a layered structure of irregularly shaped particles of smaller sizes compared to Figure 5.4d, while it is the micrograph of demulsifier S4 treated DF (without phosphoric acid). It was suggested that the phosphoric acid content of the demulsifier S3 treatment led to the further weathering and fragmentation of particles (clay) in Figure 5.4c compared to particles in Figure 5.4d. Figure 5.4e is a representation of thermally treated spent drilling fluid (S5); its micrograph showed tightly packed/ stacked spherically shaped looking particles. The particles consist of <200 – 1000nm.

At magnification of 47KX, the SEM micrographs showed some similarity in texture between the chemically treated DF or OBM nanofillers followed by the thermally treated DF nanofiller sample. The untreated DF nanofiller showed a characteristic feature of less fragmentation in its particles when compared to the other nanofiller samples. This is attributed to the presence of hydrocarbon or oil which acted as a bind and subsequently not evidently revealing the spaces in between the particle layers.

Particles generated by the Hammersmith thermal desorption unit (TDU) technique (Figure 5.4e) showed the presence of layered (sheet like) particles associated with bigger particles similar to the untreated (oil rich) based drilling fluid and drill cutting (Figure 5.4a). The smaller particles of size between 50-900nm were attributed to be the clay due to their layered nature. The bigger particles were attributed to the presence of barium sulphate which are micro sized. The nanocomposite material was manufactured using the S5 nanofiller (Figure 5.4e). Figure 5.4f showed the fillers (S5 and glass fibre) in the glass fibre reinforced nanocomposites materials. The particles consisted of 50 nm - >100µm which suggested the presence of nanoclay, shale rock (cuttings), sand, calcium carbonate (limestone) and barium sulphate. However, it was observed that some of the particles formed were an agglomeration or coagulation of the smaller particles. The particle size analysis by Malvern particle sizer and Zetasizer showed the particle size ranges for nano and microsized particles (Table 5.3).

Table 5.3 Nanofiller size range in nm and µm

Nanofiller samples	Description	Nanosize range (nm)	Microsize range (µm)
S2	Pure bentonite	299.6-302.3	1 – 9.0
S3	Demulsifier S3 treated DF	247.1-251.5	1-190.8
S4	Demulsifier S4 treated DF	287.9-327.7	1-555.7
S5	Thermal treated DF	337.4-354.7	1-351.5
S6	Untreated DF	690.1-855.2	1-259.0

The glass fibres were exfoliated in nature, scattered and less often arranged within the PA6 matrix. SEM micrograph Figure 5.4a and 5.4e showed that the solid residue shapes varied dependant on the filler and its mineral composition.

SEM micrograph of PA6 showed a fibrous material with spaces. The micrograph of nanocomposites with primary reinforcement showed that injection moulded PA6 had no nanofillers present while the other samples from Figure 5.5 (b-f) had nanofillers present. It was observed that they were dispersed in between layers and some samples had nanofiller particles of unequal size due to agglomeration of some nanofiller particles (Figure 5.5).

The SEM micrograph of nanocomposites with secondary reinforcement shows that injection moulded nanocomposite materials were exfoliated samples. The glass fibres alignment with the primary nanocomposite materials were multi-directional (Figure 5.6). Energy dispersive x-ray analysis (EDXA) showed the presence of elements such as carbon, oxygen, silicate, barium, sulphur and calcium (Figure 5.7). This can be attributed to the chemical composition of the fillers and polymer matrix. The EDXA samples were gold (Au) sputtered to enhance the analysis, hence, the presence of gold (Au) in the EDXA results.

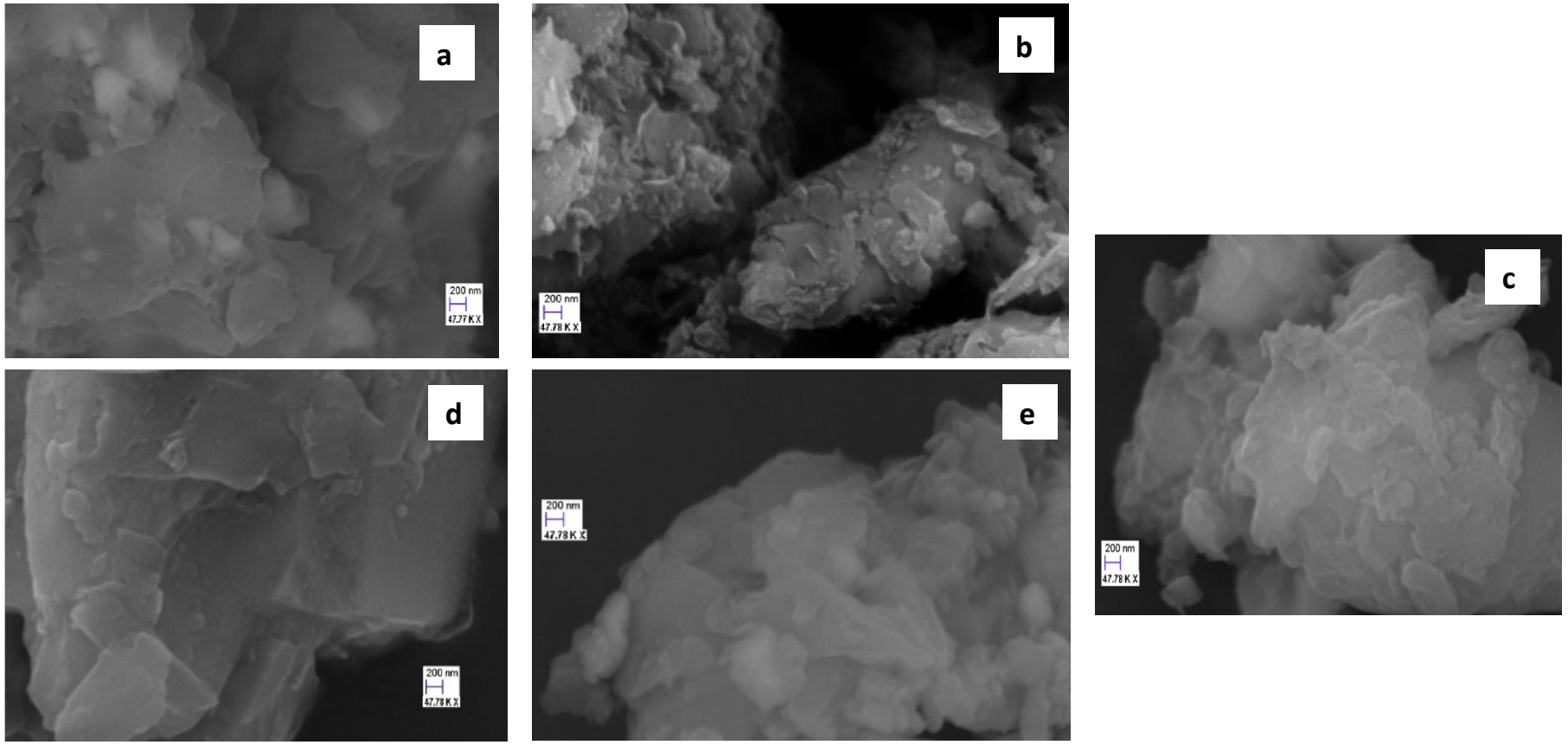

Figure 5.4(a-e) SEM micrograph of nanofiller showing their shapes and sizes (a) S6: Untreated DF (b) S2: pure bentonite (c) S3: demulsifier S3 treated DF (d) S4: demulsifier S4 treated DF (e) S5: Thermally treated DF

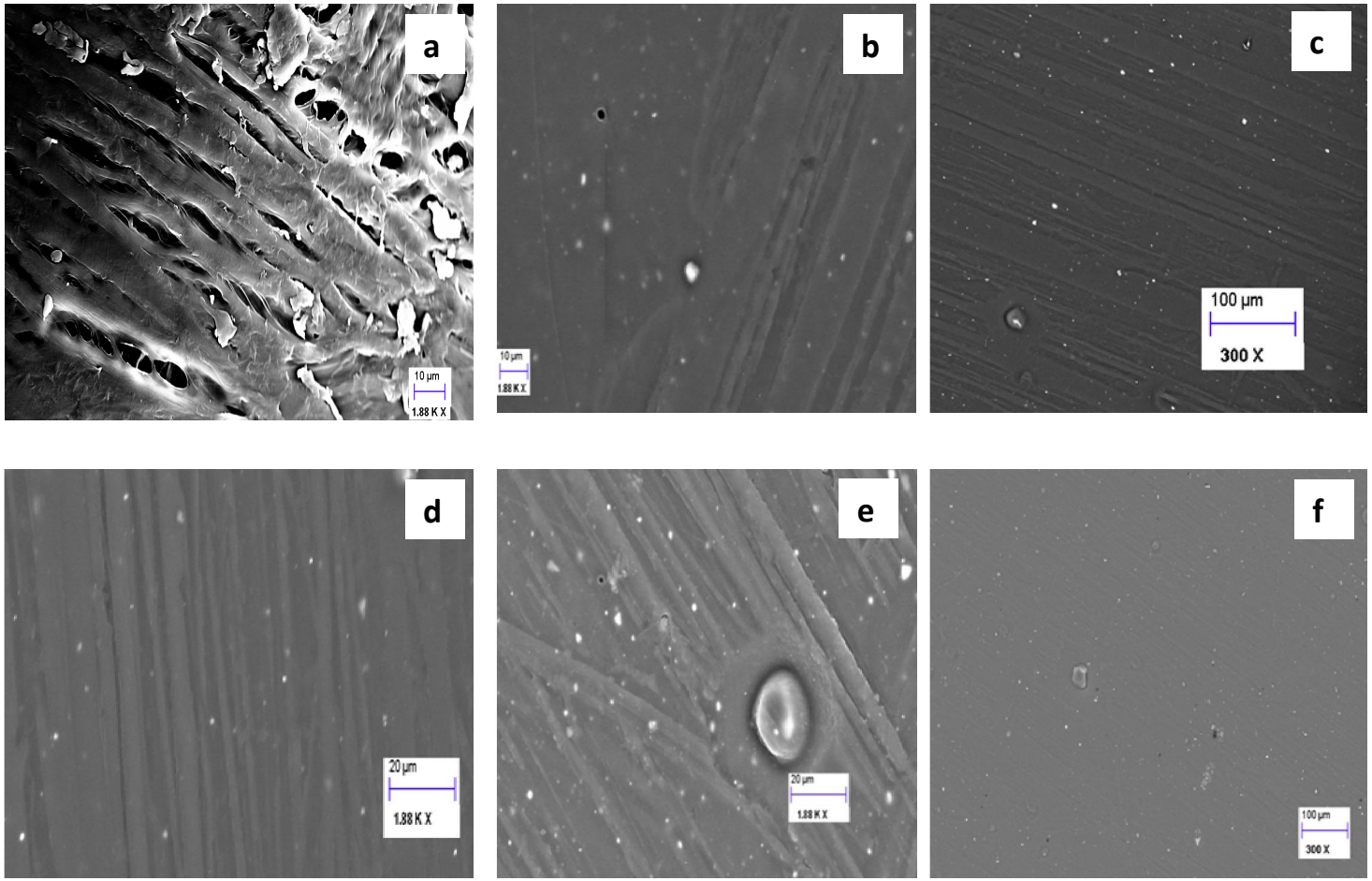

Figure 5.5 (a-f) SEM micrograph of PA6 and nanocomposites with primary reinforcement (a) neat Polyamide PA6 (b) PA6/S2 (c) PA6/S3 (d) PA6/S4 (e) PA6/S5 (f) PA6/S6 untreated sample

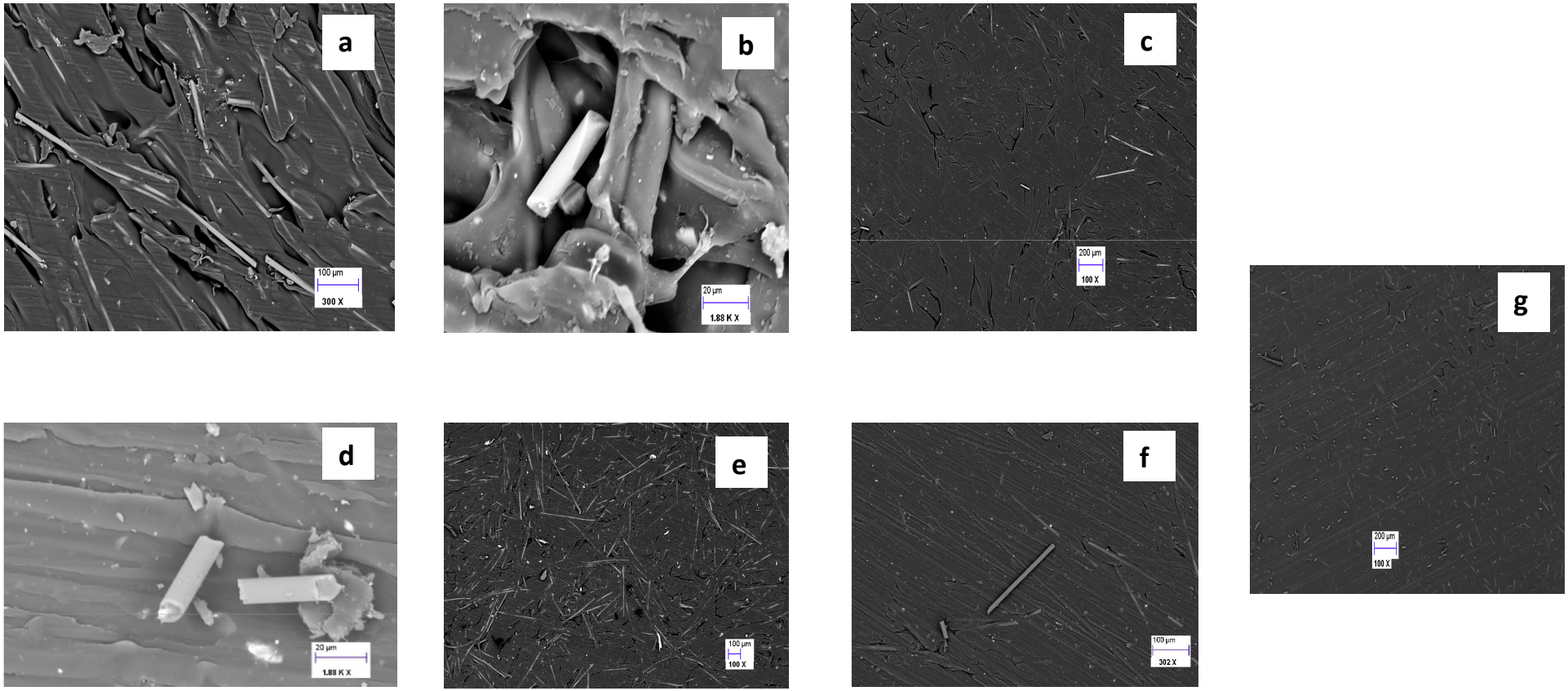

Figure 5.6 (a-g) SEM micrograph of PA6 and nanocomposites with secondary (glass fibre) reinforcement (a) PA6/GF30 (b) PA6/S2/GF30 (c) PA6/S3/GF15 (d) PA6/S3/GF30 (e) PA6/S4/GF30 (f) PA6/S5/GF30 (g) PA6/S6/GF30

EDXA results of Nanocomposites

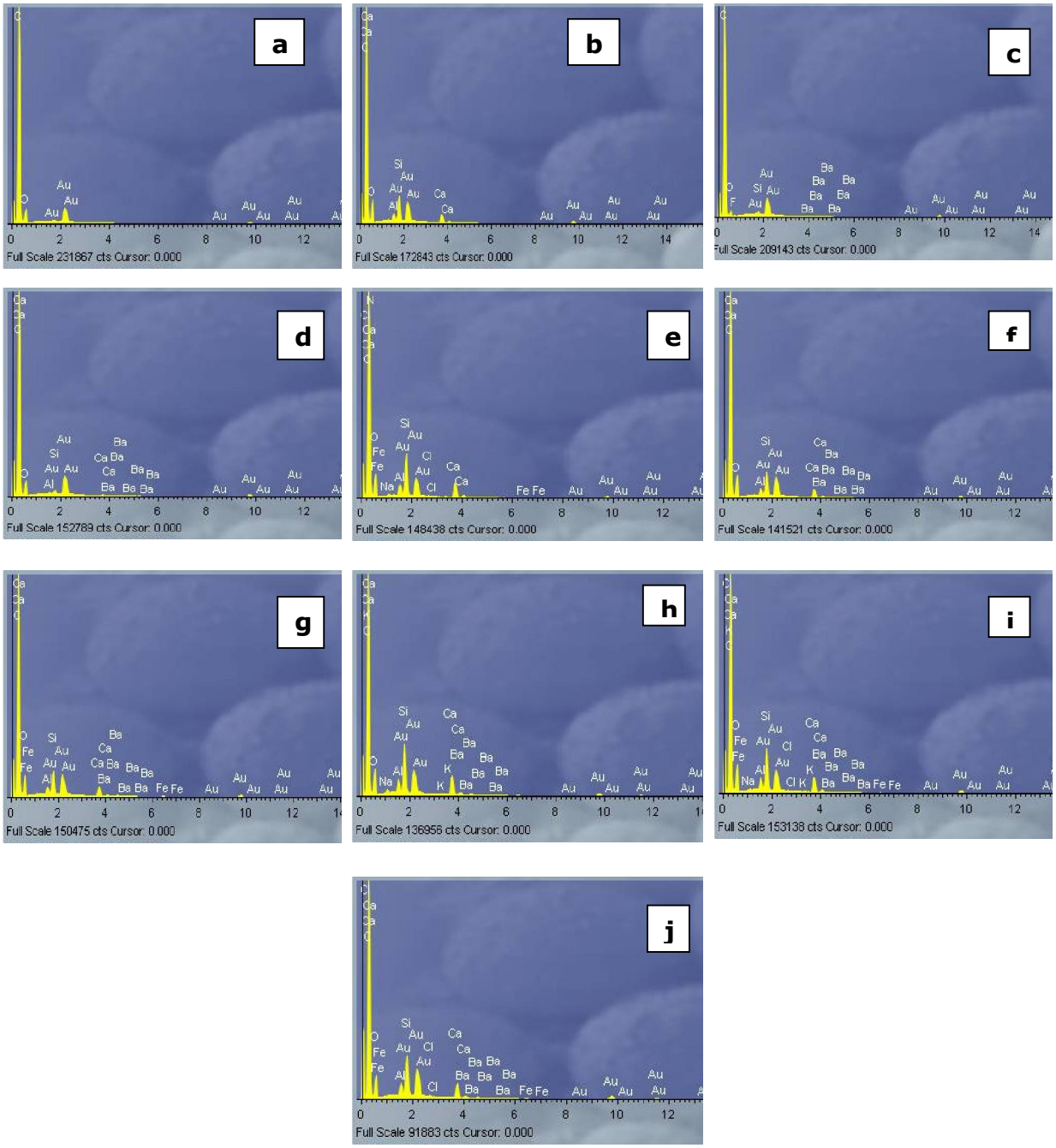

Figure 5.7 (a-j) EDXA of the nanocomposites showing their elemental compositions (a) PA6 (b) PA6/S2 (c) PA6/S3 (d) PA6/S4 (e) PA6/S2/GF30 (f) PA6/S3/GF15 (g) PA6/S3/GF30 (h) PA6/S4/GF30 (i) PA6/S5/GF30 (j) PA6/S6/GF30

5.5.3 X-Ray Diffraction of nanofillers and PA6 nanocomposites

The diffractogram of the nanofiller shown in Figure 5.8 showed a marked difference between S2 (bentonite clay) and the rest of the samples. S6, S3, S4, and S5 had similar mineralogy. The main constituent of the fillers S6, S3, S4,

and S5 were Barite ($BaSO_4$), quartz (SiO_2), Calcite ($CaCO_3$) and bentonite ($Al_2O_3.4(SiO_2).H_2O$). On the other hand, the result also showed the presence of NaCl in S3 and S4 arising from the demulsifier used in treating the spent oil based drilling fluid samples. Amongst the nanofiller samples, S5 had the highest quantity of SiO_2 which could be due to a high drill cuttings loading.

While S2 had a broad peak at about 2θ= 7°, S3 and S4 showed high intensity for Barite. This observation was similar to that of Shon et al (2016) with exception to their finding of Kalonite instead of bentonite in this case.

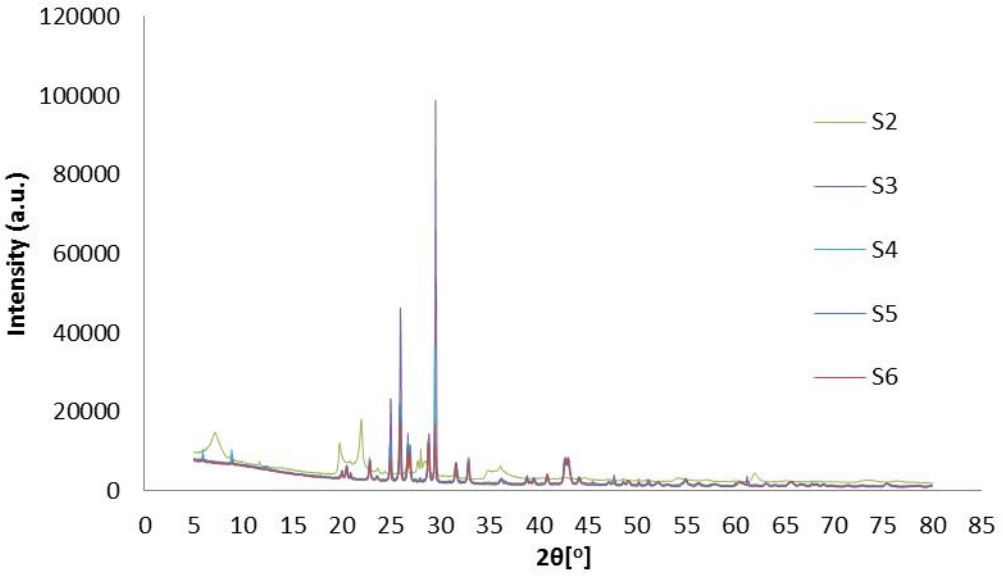

Figure 5.8 XRD of nanofillers used in the manufacture of spent oil based drilling fluid and cutting PA6 nanocomposites

Polyamide is a semi amorphous material. The diffractograms of the manufactured PA6 and PA6 nanocomposites were shown in Figure 5.9(a-f). The diffractogram which was measured in the range of 2Theta (2θ) = 3° – 30° showed that the samples had crystalline properties as depicted by the peaks. The highest peak situated at 2θ = 21° showed the presence of γ-phase of PA6. PA6 had 2 forms/phases: α and γ phases (Katoh and Okamoto 2009; Fornes et al. 2002; Liu, Qi and Zhu 1999). The γ-phase might have been as a result of the development of γ-crystals in the polymer which was due to high shear, high cooling rate and the presence of nanofillers during the nanocomposite manufacture (Liu and Wu 2002; Mathias, Davis and Jarrett 1999). On the other

hand, the low intensity peaks were suggested to be due to the presence of crystalline materials in the nanofillers such as barite, quartz, calcite and bentonite.

The peak of the injection moulded PA6 had a significantly high intensity of about 42000a.u. at about 21^{o}. The nanocomposites with nanofillers showed a decrease in peak intensity at 21^{o} which differed for different nanocomposites. It suggested that PA6 crystalline lattice became microcrystalline due to the introduction of the nanofillers, therefore decreasing the degree of intensity observed in the formulated nanocomposites. PA6/S6, the nanocomposite material with untreated df (hydrocarbon rich) nanofiller had an intensity of 5,400 a.u. PA6/S5 containing the thermal treated df (S5), PA6/S4 containing the demulsifier S4 treated df (S4), PA6/S3 containing the demulsifier S3 treated df (S3) and PA6/S2 containing pure bentonite (S2) had intensities of 3291 a.u., 4845 a.u., 4420a.u. and 11717 a.u. respectively. However, the nanofiller constituents were assumed to have influenced the differences in intensities observed in the different PA6 nanocomposites. It was observed that the addition of the glass fibres (secondary filler) brought about a further increase in the microcrystalinity of PA6 starting material as well as a further decrease in the degree of intensity in the characteristic PA6 peak at about 21^{o}. Amongst the glass fibre reinforced PA6 nanocomposites: PA/S2/GF30, PA/S3/GF15, PA/S3/GF30, PA/S4/GF30, PA/S5/GF30, PA/S6/GF30, they had intensities of 719 a.u., 1123 a.u., 739 a.u., 623 a.u., 1360 a.u. and 811a.u. respectively.

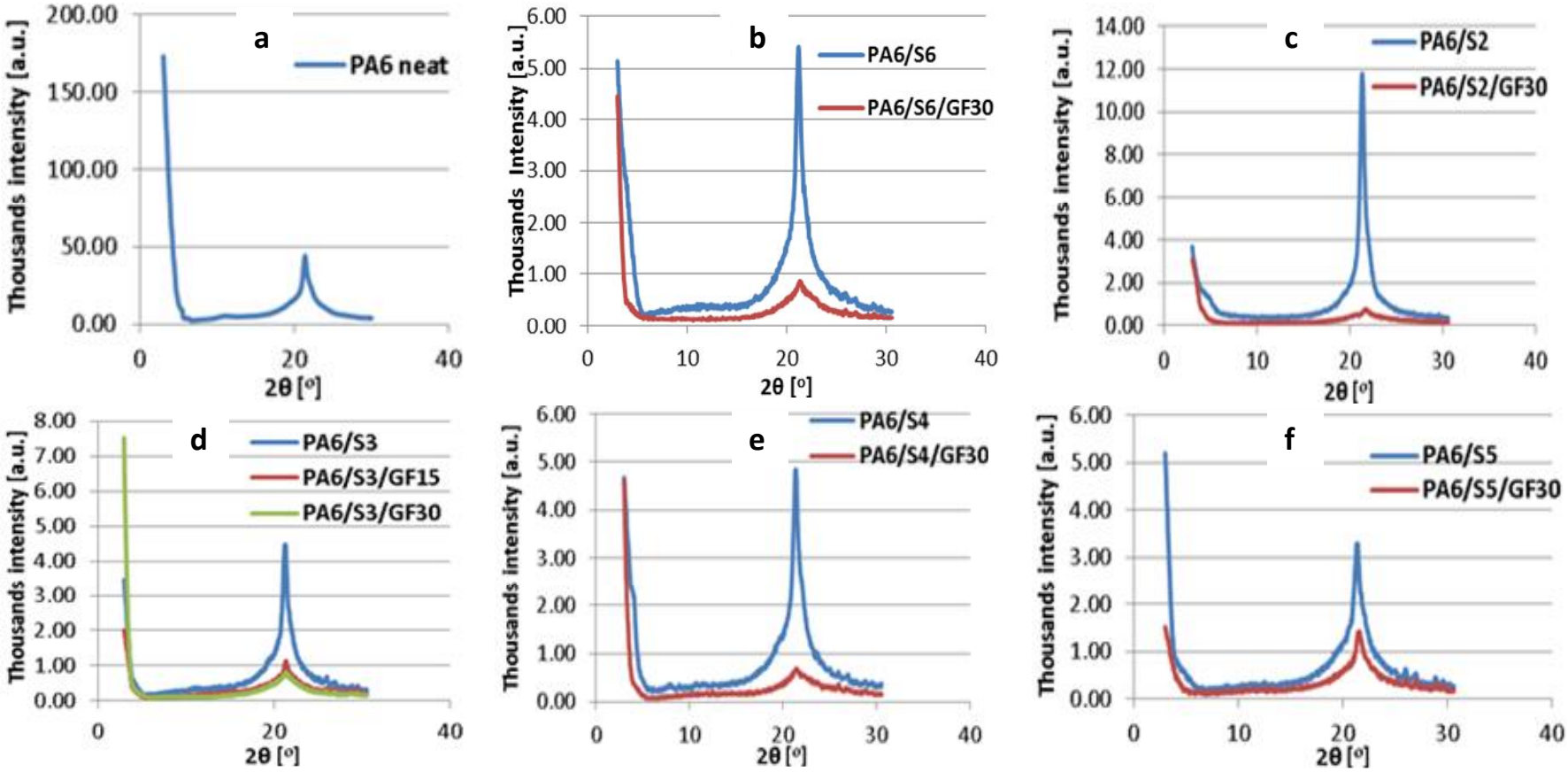

Figure 5.9 (a-f) XRD diffractograms of nanocomposites (a) PA6 (b) PA6/S6 and PA6/S6/GF30 (c) PA6/S2 and PA6/S2/GF30 (d) PA6/S3, PA6/S3/GF15 and PA6/S6/GF30 (e) PA6/S4 and PA6/S4/GF30 (f) PA6/S5 and PA6/S5/GF30

The increased intensity of PA6/S3/GF15 could be due to the increase in PA6% present in the composite. It was observed that the PA6 glass fibre reinforced nanocomposites did not have a similar trend to the nanofiller (only) filled PA6 nanocomposites.

5.5.4 FTIR-ATR Spectroscopy of nanofiller and PA6 nanocomposites

FTIR-ATR analysis was used to identify the functional groups in the nanofillers and nanocomposite materials. The nanofillers spectra for the five nanofillers investigated showed significant absorbance at different regions.

As shown in Figure 5.10, S6 had a broad band at 3500-3000cm^{-1} which was assigned to the hydroxyl group of water. This large water peak was much reduced in S2 - S5.

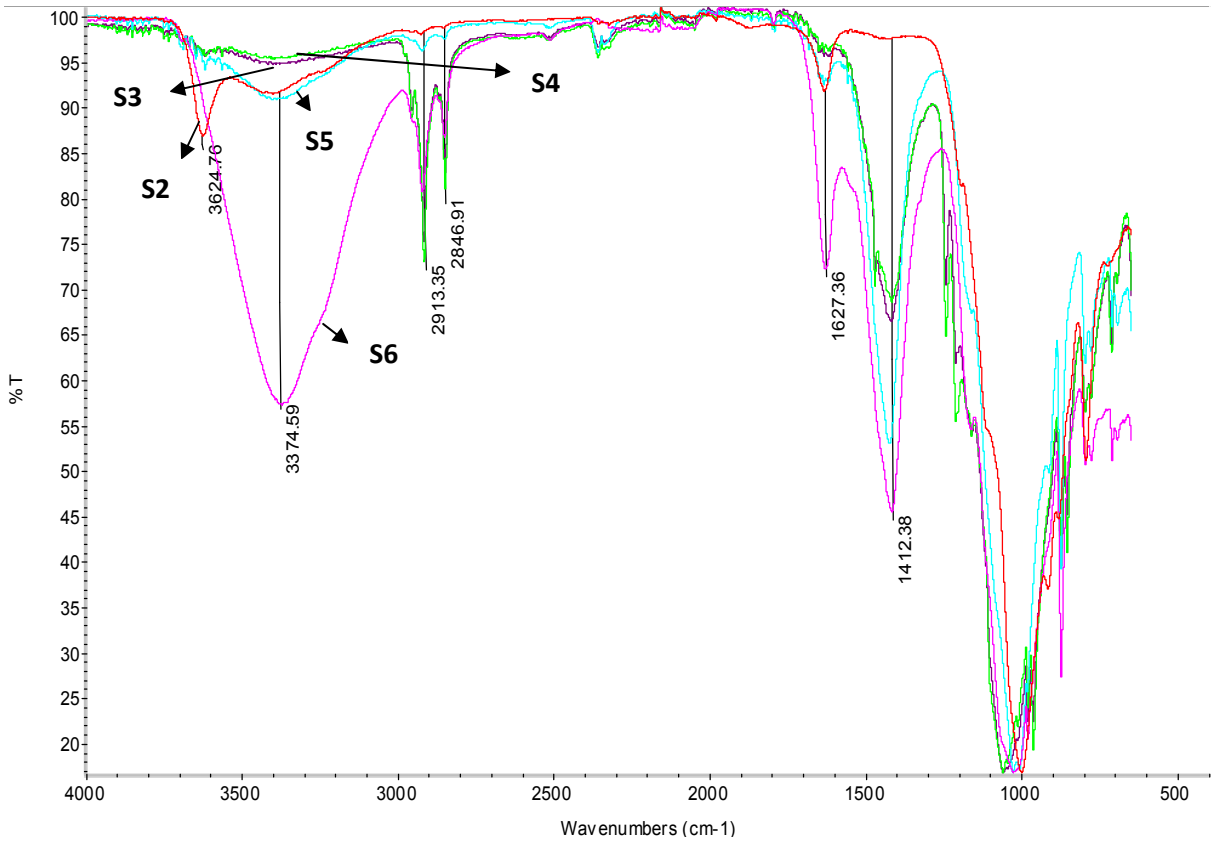

Figure 5.10 FTIR-ATR spectra of nanofillers measured between 4000 - 600cm^{-1} wavenumber (a) S2 in red (b) S3 in purple (c) S4 in green (d) S5 in light blue (e) S6 in pink

As mentioned earlier in section 4.3.4, the untreated drilling waste (S6) contained petroleum hydrocarbon of 662,500 mg/kg while the treated drilling waste – S3 and S4 had lower TPH concentrations of 9844 mg/kg and 9592 mg/kg. The spectra of S3, S4 and S6 showed bands between 3000-2700cm^{-1} which is assigned to the presence of hydrocarbon suggesting that the peaks of aliphatic and aromatic C-H bonds vibrations observed in that region could have arisen from surface modification mainly by the demulsifier used for oil extraction treatment in S3 and S4, and petroleum hydrocarbon for S6, the untreated spent drilling fluid. S3 and S4 showed presence of sulphate ion at the region of 1080-1000cm^{-1} from SDS present in the demulsifiers. On the other hand, the absence and reduced intensities of these characteristic hydrocarbon bands at 3000-2700cm^{-1} suggested the absence and low concentration of hydrocarbon in nanofillers S2 and S5 respectively. However, absence and reduced intensity of hydrocarbon peaks in S2 and S5 were further investigated by TPH which showed that S2 was not organo-modified and did not have any TPH content while S5 had TPH of 3391mg/kg. During thermal treatment S5 had lost the most volatile and alkyl hydrocarbon due to high temperature TDU treatment of over 700^{o}C (Seaton et al. 2006, Stephenson et al. 2004). At 1500cm^{-1}, smaller bands were observed in S3, S4, S5 and S6 which further suggested the presence of hydrocarbons.

The band between 1600-1700cm^{-1} (the band at 1630 cm^{-1}) in S2 was present in the spectra of clay minerals. It is assigned to the bending mode of adsorbed water molecules (Mukherjee and Srivastava 2006). However, the band between 1600 -1700cm^{-1} in S6 was assigned to the presence of carbonyl group or C-C bonds from the organic residues. The bands at 1600-1700cm^{-1} were of lower intensities in S3, S4 and S5. The bands between 800-900cm^{-1} and 1400-1500cm^{-1} were assigned to carbonate groups present in all the nanofillers investigated. The carbonate group was attributed to the presence of $CaCO_3$ in the sample. The bands at 1090, 1118-1106, 1166 and 790 cm^{-1} in S2 - S6 were assigned to the presence of silicate groups from clay and shale (sand), thus, suggesting that the organosiloxane (Si-O-C) stretching was as a result of quartz (Andrade et al. 2009). The bands at 1014 cm^{-1} and 1124 cm^{-1} from montmorillonite resulted from Si-O stretching as a result of quartz. The presence of bands at 1200-1300cm^{-1} was assigned to alkyl ether peaks which could be due to the presence

of additives in the sample. S3 and S4 had slightly visible bands at about 1122cm^{-1} which suggested the presence of sulphates from SDS. The bands at 1080 cm^{-1}-1250cm^{-1} were assigned to S–O bond stretching from barite ($BaSO_4$). These S-O bands were absent in S2, but visible in S3, S4, S5 and S6. The band at 1070cm^{-1} is attributed to phosphate in S3, which would contribute to its flame retardancy property (see chapter 7).

PA6 has a characteristic peak at 3291cm^{-1} which is attributed to the N-H stretching, a peak at 2925cm^{-1} and 2856cm^{-1} which is attributed to C-H stretching, 1630cm^{-1} carbon double bond and 1535cm^{-1} N-H bending. The intercalation of the PA6 matrix, fillers and glass fibre were observed in the region of 1100-900cm^{-1} of PA6/S2/GF30 (see Figure 5.11 a). Similar observations were made for S4 reinforced PA6 nanocomposites (see Figure 5.11 b) and other PA6 nanocomposites.

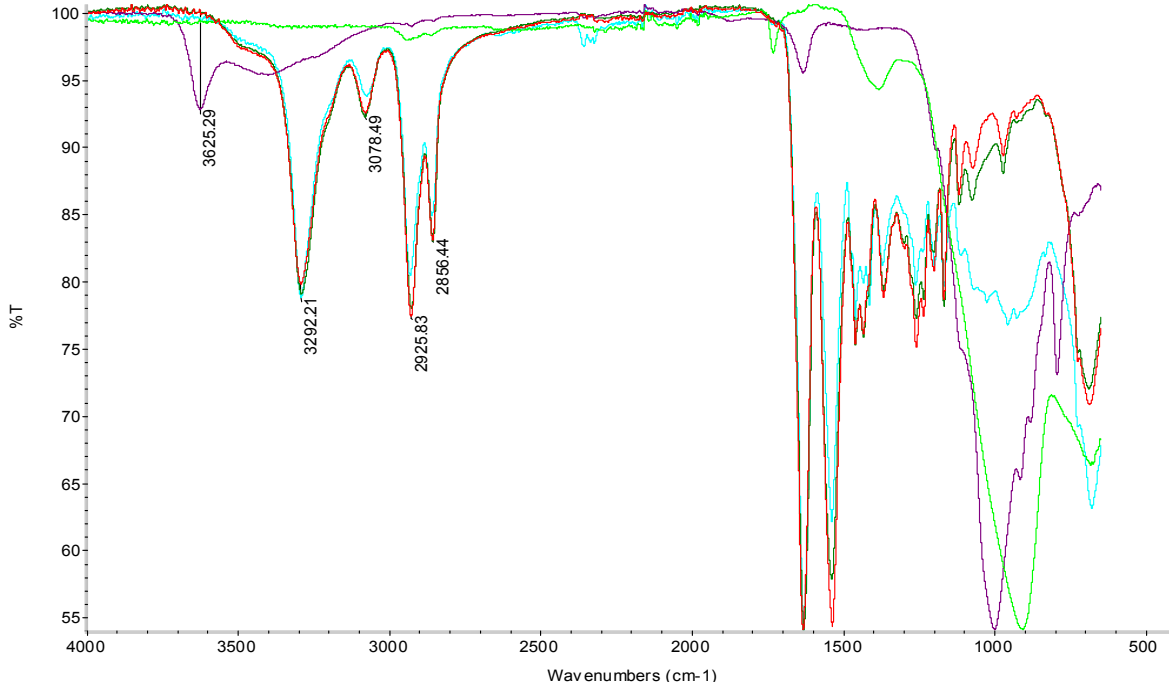

(a) S2 and its PA6 nanocomposites

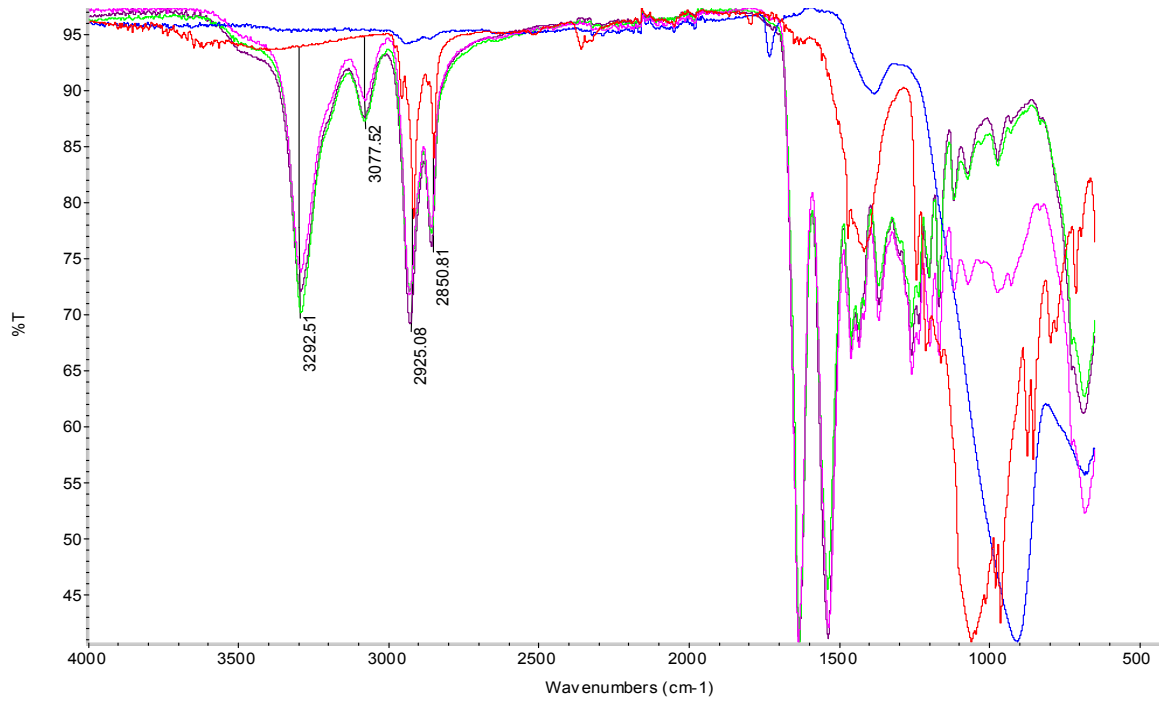

(b) S4 and its PA6 nanocomposites

Figure 5.11 FTIR-ATR spectra of S2 and S4 reinforced nanocomposites measured between 4000 - 600cm^{-1} wavenumber (a) S2 and its PA6 nanocomposites (i) showing PA6/S2/GF30 in light blue (ii) showing PA6/S2 in dark green (iii) showing PA6 in red (iv) showing S2 in purple (v) showing GF in light green (b) S4 and its PA6 nanocomposites (i) showing PA6/S4/GF30 in pink (ii) showing PA6/S4 in green (iii) showing PA6 in purple (iv) showing S4 in red (v) showing GF in blue

5.5.5 Effect of surface modification on the nanofillers

Nanofillers S6, S3, S4 and S5 were surface modified due to their origin (S6), demulsifier wash treatment (S3 and S4) and thermal treatment (S5). S6 was the untreated nanofiller derived from the used oil based drilling fluid. It was coated with crude oil. Crude oil is a complex mixture of different hydrocarbon substances such as PAHs, paraffin, as well as heavy metals which are environmentally toxic (Adewole, Adewale and Ufuoma 2010; Benka-Coker and Olumagin 1996; Reis 1996). Chemically, oil is a non-polar substance but the presence of napthalic and carboxylic groups could make oil react as a negatively charged substance. Generally, oil has a higher affinity or adherence to clay than water by capillary action and viscosity in the adsorbed layer, and also due to the organo-chemical nature of oil. Therefore, water was quite easily displaced which made filler S6 hydrophobic.

S4 was hydrophobic as shown by FTIR-ATR results (Figure 5.10) where the band assigned to hydroxyl group (of water) at 3500 – 3000cm^{-1} had a low intensity. The source of its hydrophobicity is attributed to the demulsifier organic constituents such as sodium dodecyl sulphate (SDS) and unextracted drilling fluid base oil. The presence of SDS would also give the nanofiller an anionic charge on its surface. These two properties could enhance the interfacial bonding of S3 nanofiller and the polymer PA6. On the other hand, due to the presence of non-ionic surfactant Poloxamer used in the demulsifier formulation, it was possible that the Poloxamer could remain in bulk solution or form a coating around the sodium dodecyl sulphate engulfed filler as suggested by Barker (2013) and Billany (2007).

On the other hand, demulsifier S3 treatment to obtain S3 nanofiller suggested that phosphate would influence the surface charge of filler S3 due to the presence of phosphoric acid in demulsifier S3. It is important to note that the charge of the filler (solid phase) during demulsification resulted in its flocculation. According to Barker (2013), SDS losses its emulsifying potential and emulsion stability in acidic conditions and this supports the observed flocculation of drilling fluid. However, the emulsion potential of SDS was observed in the system as seen in the oil-water phase. The presence of SDS adsorption to the filler was also shown by the FTIR-ATR results. Further adsorption experiments would give a

detailed understanding of the chemical mechanism involved. Nevertheless, the S3 filler was hydrophobic which would have enhanced the polymer and filler interfacial bonding.

S5 filler which was collected from a 'To landfill disposal batch' was known to contain some oil residue which is permissible by OSPAR requirement for oil and gas companies for disposal of drilling waste at a landfill site (with TPH concentration of 3391mg/kg). This suggests that the S5 filler was also hydrophobic. The presence of hydrocarbon on the filler made it hydrophobic in nature. However, it was less hydrophobic than S3 and S4 (with higher TPH values) due to its high thermal treatment which had desorbed most of the hydrocarbon content from S5. This hydrophobic nature is very important for polymer and filler interaction.

5.5.6 Effect of leaching on the nanocomposites

Leaching test was carried out on all the PA6 nanocomposite samples using deionised water. The test was carried out by ICPOES to ascertain the elemental release of heavy metals and some elements into the environment in the case of the nanocomposite's water content. The results obtained were for 1-hour and 24-hour (see Appendix C). The result showed that P, Cr, Cd and Cu were not detected in all the samples as compared to the other elements (Zn and Ba). Cd was tested but was not detected as expected because the fillers did not have Cd present (see section 3.3.2). It was concluded, that PA6 was good for stabilising Pb (toxic heavy metal). This is because Pb did not leach out of the nanomaterials during the 1-hour and 24-hour test. No leaching of Ba was observed in the 1-hour test. This was attributed to the insoluble form of $BaSO_4$ in the nanocomposite samples. Further work on the chemical bonding between PA6 and Pb would be investigated in future as well as investigation into PA6 bonding with radioactive elements such as uranium. Leaching studies by Leonard and Stegemann (2010b) and Al-Ansary and Al-Tabbaa (2007) on solidification and stability of drilling wastes using binders showed element leaching. On the other hand, while the studies of Leonard and Stegemann (2010b) and Al-Ansary and Al-Tabbaa (2007) focused on acidic and alkaline pH respectively, this study focused on neutral pH.

5.6 Conclusion

The manufacture of advanced nanocomposite polyamide material using solid residues from spent oil based drilling fluid and drill cutting was demonstrated. The use of drilling fluid and drill cutting (low-density solids) in the formulation of different blends of PA6 nanocomposite materials from untreated, chemically treated and thermally treated drilling fluid and cuttings was successfully achieved. A good understanding of the nanofillers characteristics should enhance the understanding of their chemical, mechanical and thermal potential to influence chemical and physical changes in the novel formulated nanocomposite materials.

The SEM images revealed nanometer and micrometer sizes of the nanofillers in nanocomposites. EDXA results showed presence of Ba, Al, Si, Fe and some other elements present in the PA6 nanocomposites from the nanofillers. As shown by XRD diffractograms, the presence of fillers produces a more amorphous material especially in the presence of 30% wt. glass fibre. FTIR-ATR results showed the intercalation of the nanofillers and glass fibre in the PA6 matrix.

15% glass fibre (GF15) was used to investigate the effect of glass fibre on the mechanical and thermal properties of PA6 nanocomposite materials. The 15% glass fibre was added to only the PA6 S3 containing nanocomposite because S3 showed the best stress resistance properties amongst the nanocomposites and a need to understand the effect of only 15% GF on PA6/S3/GF15 stress-strain behaviour as compared to PA6/S3.

This novel waste management method would reduce the volume of spent drilling fluid and drill cuttings going to the landfill as it was found useful in polymer enhancement. The leaching test confirmed that the manufacture of spent oil based drilling fluid and cuttings – PA6 nanocomposites could be a promising method for immobilising heavy metals such as Pb present in this kind of hazardous waste. The result from this study should provide useful information for the redevelopment, recycling and reuse of drilling waste as a measure to sustainably prevent offshore ocean dumping and landfilling of the spent oil based drilling fluid and cuttings waste.

Chapter 6

Mechanical Properties of Novel Polyamide 6 Nanocomposite Materials

6.1 Introduction

Polyamide is a widely used engineering polymer. It has been used extensively in the automotive (Mouti et al. 2012), packaging (Quintavalla and Vicini 2002), textile (Bourbigot, Devaux and Flambard 2002) and construction industries (Ferreira and Branco 2007). In recent times, polyamide has been used in the oil and gas industry for the production of umbilical and pipe applications (Fogg 2011; Ito and Nagai 2008). A major advantage of polyamide compared to other polymers is its hydrogen bonding capability which enhances its compatibility with fillers and higher thermal and mechanical stability.

In the manufacture of advanced materials, fillers and reinforcement materials are included to improve the mechanical strength of the original polymer. These advanced materials could be known as composites or nanocomposites, a classification based on the size of the fillers. Some fillers used for PA6 include clay (montmorillonite - MMT and organophilised-montmorillonite - OMMT), titanium oxide, talc, carbon nanotubes and glass fibre (Wan et al. 2013; Zhou et al. 2015; Silva et al. 2014). Research shows that the use of nanosized fillers greatly improves the mechanical strength of materials whilst nanofillers such as nanoclay and melt compounding improved the intercalation of fillers in PA6 (Liu, Qi and Zhu 1999). This improved the mechanical properties of the PA6 such as flexure and impact especially at lower quantity of nanofiller.

In the North Sea due to high temperature and high pressure well drilling, oil based mud is often used. However, after a while the drilling mud and drill cuttings become part of the waste generated (Adegbotolu et al. 2014; Caenn, Darley and Gray 2011). Under the European Waste Catalogue, these wastes are classified as hazardous wastes due to the presence of heavy metals and hydrocarbons including PAHs. Various remedial techniques have been reported for the treatment of such oil polluted waste. This includes phytoremediation

(Ekeh-Adegbotolu, Ekeh and Wegwu 2012), constructed wet land (Eke and Scholz 2008), bioremediation, chemical treatment (McCosh et al. 2009) thermal desorption (Seaton et al. 2006).

Preliminary chapters have discussed the remedial treatment for oil based drilling mud by demulsification to recover oil, water and solid phase which consists mainly of nanoclays (bentonite), barium sulphate and calcium carbonate (see chapters 2, 3 and 5). The aim of this chapter is to investigate the mechanical properties of the novel PA6 engineering material manufactured in chapter 5.

6.2 Experiment

6.2.1 Materials

The materials used in this chapter are described in section 5.4.1.

6.2.2 Sample preparation

The nanocomposite samples were prepared in two sets. The first set was a weighed combination of 97.5% polyamide and 2.5% dry filler. The second set was mainly a combination of 67.5% polyamide, 2.5 % dry filler and 30% glass fibre (see Table 5.1). The manufacture process involved melt compounding using a Thermo Scientific Rheomex PTW 16/25 XL twin screw extruder with 6 heating zones and die with an operating temperature of 250^{o}C and a rotation speed of 150 rpm. The extruded material was pelletized and injection moulded at 230^{o}C with a pressure of 10 bar using ZAMAK WT12 injection moulding instrument to manufacture 80mm x 10mm x 4mm test specimen. The use of 30% glass fibre is recommended by the thermoplastic and material manufacture industry to improve mechanical and thermal properties of thermoplastic materials (Gu et al. 2000). Table 5.1 shows the samples studied.

6.2.3 Mechanical testing

Flexural tests were carried out on the specimens studied in this paper. The test specimens (samples) were conditioned based on the ISO 291 standard at 23^{o}C for 88 hours and transferred to a desiccator prior to testing. The specimen dimension was also determined by use of an engineering steel ruler and calliper. The flexural test was carried out according to ISO 178:2010+A1:2013 standard

using Instron 3382 electro-mechanical equipment. Three samples were tested per material at the rate of 2 mm/min for flexural properties of the materials. The flexural modulus and flexural strength values were obtained through the test.

Compression tests were carried out on the specimens studied in this chapter. The test specimens (samples) were conditioned based on ISO 291 (for conditioning and testing plastics) at 23^{o}C for 88 hours and transferred to a desiccator prior to testing. The specimen dimension was determined by use of an engineering steel ruler and calliper. The compression test was carried out according to ISO 604 standard using Instron 3382 electro-mechanical equipment. Three samples were tested per material at the rate of 1 mm/min for compression modulus and 5mm/min for compression strength for materials that yield, and compared against specimens tested at 2 mm/min for compression modulus and strength.

Hardness tests were carried out on the test specimens (samples) which had been conditioned based on ISO 291 standard. The hardness test was carried out according to DIN EN 2039-1 equivalent of ASTM D575 test standard 604 standard using Zwick 3106 material testing hardness tester. The test was carried out to determine the indentation hardness of plastic materials using a force of 358N.

6.3 Results and discussion

Mechanical properties of the PA6, PA6 nanocomposites and PA6 glass reinforced nanofiller material samples were determined.

6.3.1 Flexural performance

The fundamental importance for material application is their strength and elastic properties. Reinforcement fibres have the elastic properties until rupture while the polymer matrixes are characterised by their viscoelastic properties. The results of mechanical tests for composites reinforced with nanofillers and short glass fibre are presented in this section. Figure 6.1 showed the flexural load versus extension graphs for materials PA6, PA6/S2, PA6/S3, PA6/S4, PA6/S5 and PA6/S6. The neat PA6 was used as a control sample. The results showed that PA6 had undergone a maximum flexural load of 114N and has maximum

extension of 10.6mm. In contrast to the other samples, PA6/S6 has undergone a maximum flexural load of 132N and has maximum extension of 10.3mm. This 15.8% improvement in load bearing compared to PA6 could be attributed to the higher nanoclay content than PA6/S3 with 10.5% and PA6/S4 with 12.3% whose clay content was reduced by the demulsification process in chapter 4. On the other hand, PA6/S5 which was thermally treated had an improved load bearing of 7.9% than PA6. PA6/S2, containing bentonite clay, a common industrial filler for PA6 has undergone a maximum flexural load of 130N and has maximum extension of 10.7mm, having an improved load bearing of 14% compared to PA6. However, PA6/S6 was observed to have a more improved load bearing potential than PA6/S2 of 1.3%.

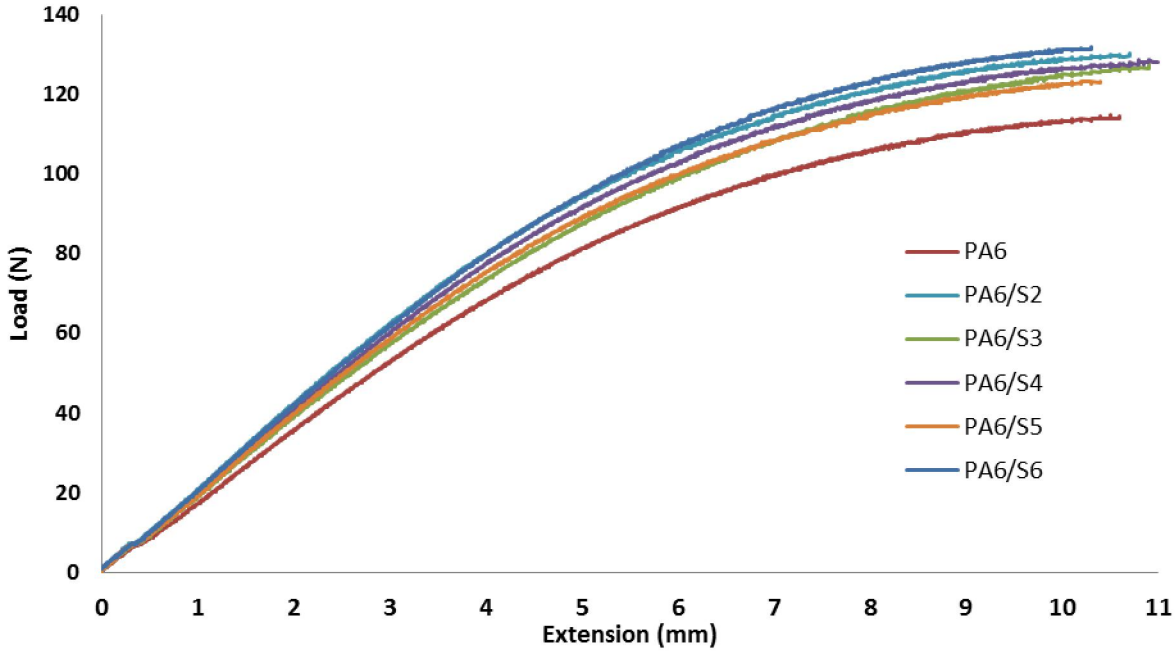

Figure 6.1 Load vs Extension graphs of PA6 and PA6 nanocomposites

A closer look at the flexure stress-strain graphs for PA6 and the PA6 nanocomposites in Figure 6.2 showed that there was a trend in flexural properties of PA6, PA6/S5, PA6/S3 and PA6/S4 that remained similar to their load-extension graph in Figure 6.1. In contrast to the trends in figure 6.1 and 6.2, PA6/S2 in Figure 6.3 showed higher strain and stress resistance than PA6/S6. This could be attributed to a difference in filler distribution in samples

tested as shown by the flexural modulus results in Figure 6.2(b) were PA6/S6 is seen to have a higher standard deviation from PA6/S5.

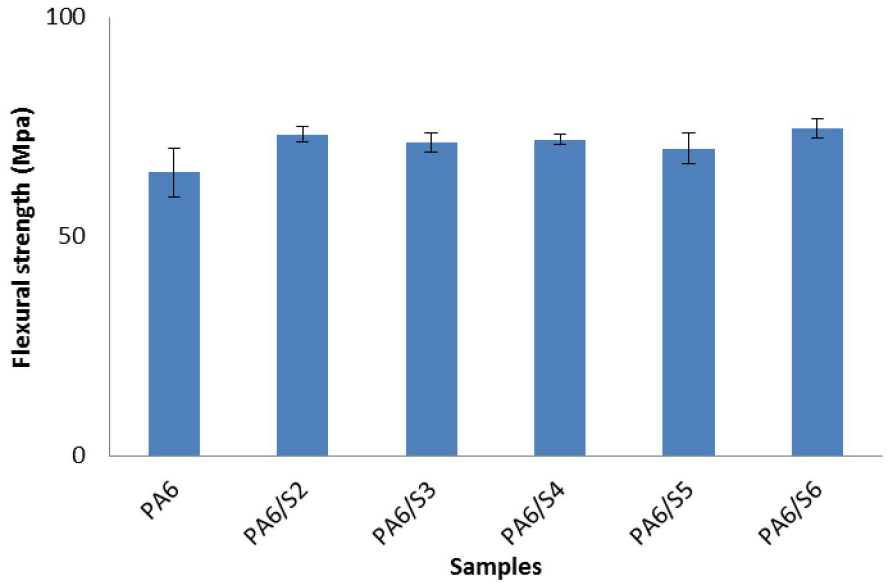

(a) Flexural strength PA6 and PA6 nanocomposites

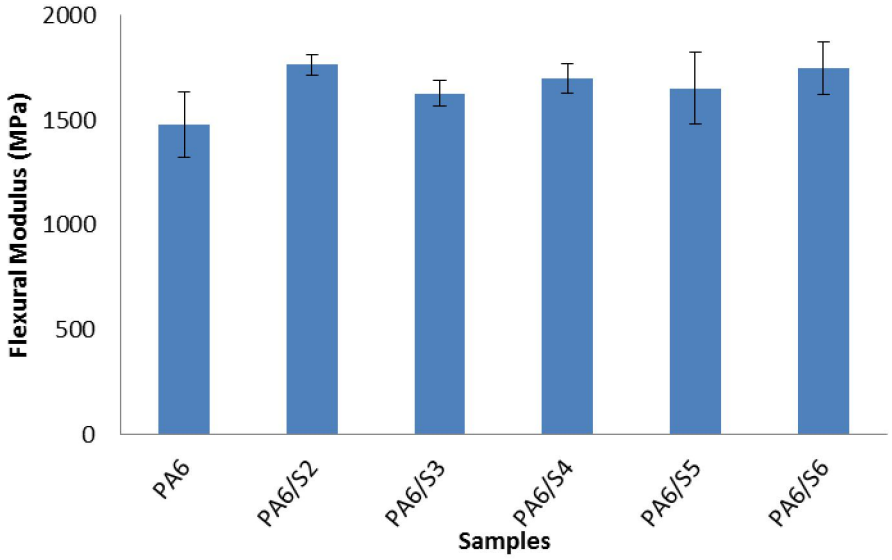

(b) Flexural modulus of PA6 and PA6 nanocomposites

Figure 6.2 Effect of fillers on flexural (a) strength and (b) modulus of PA6 nanocomposites and glass reinforced PA6 nanocomposites showing nanofiller effect in increasing flexural strength and modulus of PA6.

In terms of the extension, PA6/S4 had a highest % extension improvement of 3.77% compared to PA6. This was followed by PA6/S3 (2.8%) and PA6/S2 (0.9%) while PA6/S5 and PA6/S6 had lower extensions by 1.9% and 2.8% respectively.

The treatment of PA6/S3, PA6/S4 and PA6/S5 by demulsification and thermal processes seemed to influence their load and extension responses when compared to PA6/S6 which contained the untreated oil based drilling fluid nanofiller. Hence, it was observed that due to the treatments applied, PA6/S6 had improved load resistance than PA6/S3 by 4.8%, PA6/S4 by 3.13% and PA6/S5 by 7.31%. Thus, it was concluded that the demulsifier treatments of S6 nanofiller could have altered the mineral composition, residual petroleum hydrocarbon content and demulsifier-led surface modification of the resultant S3 and S4 nanofillers used in the manufacture of nanocomposites PA6/S3 and PA6/S4. As for PA6/S5, it could not be concluded that the thermal treatment could have been the only factor responsible for its low load bearing capacity, but, the fact that the drilling waste batch for S3 and S4 were different from S5 which could have resulted in variation of percentage mineral composition. This trend was similar to the flexure stress-strain relationship in Figure 6.3. However, treatment could have had an impact on the extension capabilities of the manufactured nanocomposites. According to TPH results in chapter 4, nanofiller S6 was known to have the highest TPH concentration of 662,500mg/kg while S4, S3 and S5 had TPH concentrations of 9592 mg/kg, 9844 mg/kg and 3391 mg/kg respectively. Irrespective of the higher TPH of S6, S4 which was treated with a demulsifier had a better strain resistance and improved extension than PA6/S6, PA6 and the other PA6 nanocomposites. PA6/S4 had improved extension than PA6 by 3.8% as earlier stated, PA6/S6 by 6.8%, PA6/S5 by 5.8%, PA6/S2 by 2.8%, PA6/S3 by the least value of 0.9% while PA6/S3 had improved extension than PA6/S2 by 1.9%. Thus, it was deduced that possible compounds in the demulsifier formula could have had plasticising effects and would have resulted in better strain resistance and improved extension in PA6/S4 as well as PA6/S3.

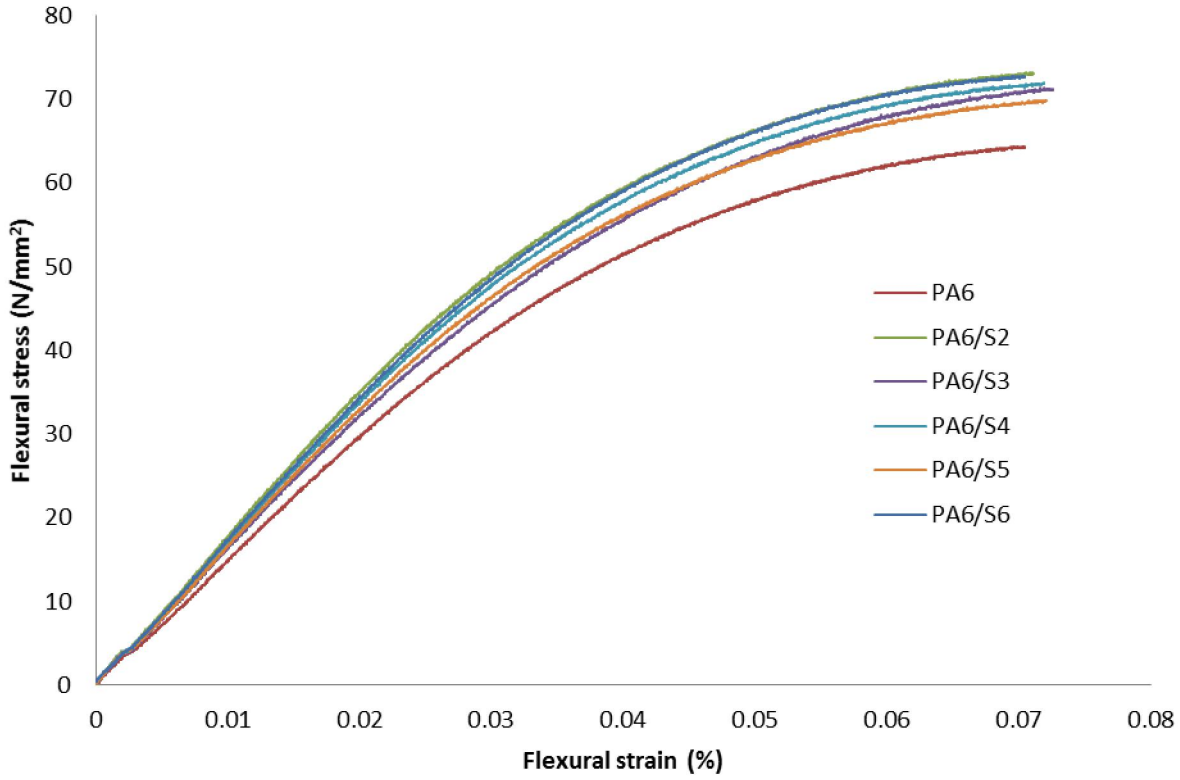

Figure 6.3 Flexure stress versus strain graphs of PA6 and PA6 nanocomposites showing addition of nanofillers improve PA6 stress strain relationship

PA6 and PA6 nanocomposites load-extension graph, Figure 6.1 and flexural stress-strain graph have shown that the gradient for PA6 was lower. Thus, in both figures a general trend was observed that the lower the gradient of a material, the lower its maximum load or stress and the higher the extension. However, PA6/S6 was an exception to this proportionality relationship. This was attributed to the S6 petroleum hydrocarbon content and its mineral composition.

Figure 6.4 shows the flexural load versus extension graph for materials PA6/GF30, PA6/S2/GF30, PA6/S3/GF15, PA6/S3/GF30, PA6/S4/GF30, PA6/S5/GF30 and PA6/S6/GF30. PA6/GF30 has not been filled with any nanofiller but only the glass fibre reinforcement materials, and it is used as a control sample. Samples PA6/GF30, PA6/S2/GF30, PA6/S3/GF30, PA6/S4/GF30 and PA6/S5/GF30 were more brittle than PA6/S3/GF15 and PA6/S6/GF30 which appeared to be more ductile materials. This brittle nature of the former samples was due to the presence of glass fibre reinforcement compared to PA6/S3/GF15

which had 50% less glass fibre composition than the other glass reinforced nanocomposites, and more PA6 resin (see Figure 6.5). On the other hand, PA6/S6/GF30 is a lubricated sample containing nanofiller with petroleum hydrocarbon surface modification which results in a more elastic material with a higher flexural extension of 10.5mm.

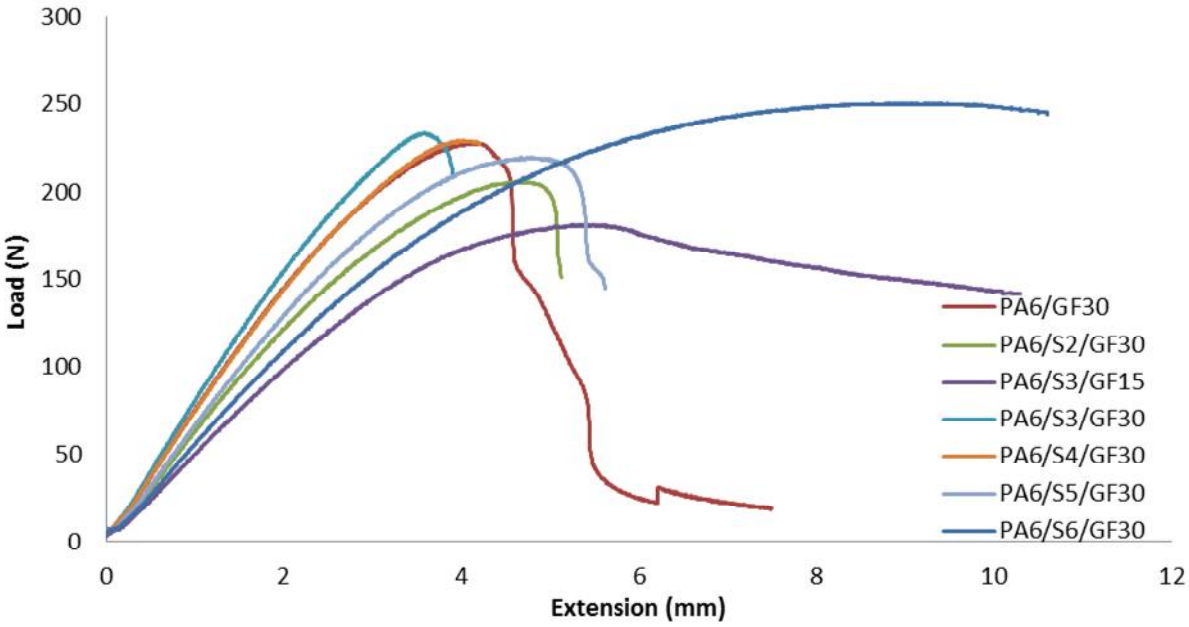

Figure 6.4 Load vs Extension graphs of PA6/GF30 and other glass reinforced PA6 nanocomposites showing the addition of glass fibre increased the flexural strength of PA6 by over 50% except for PA6/S3/GF15 with 15% less glass fibre compared to glass reinforced materials

Figure 6.4 also showed that the steeper the gradient of a material, the higher its maximum load as observed in PA6/S3/GF30 and the lower the gradient, the lower the maximum load as observed in PA6/S3/GF15.

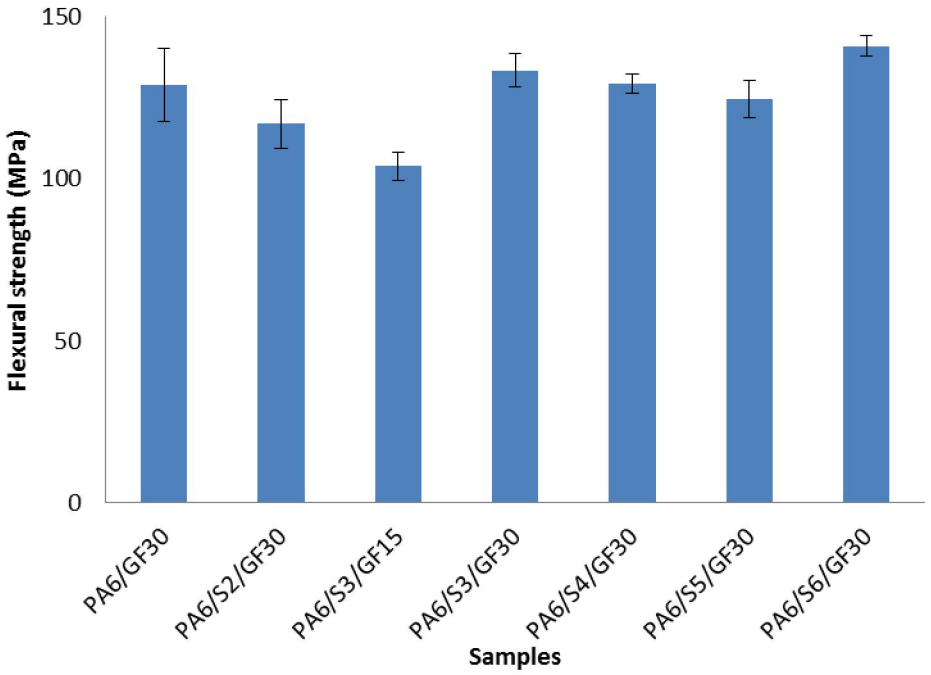

(a) Flexural strength of PA6/GF30 and PA6 glass reinforced nanocomposites

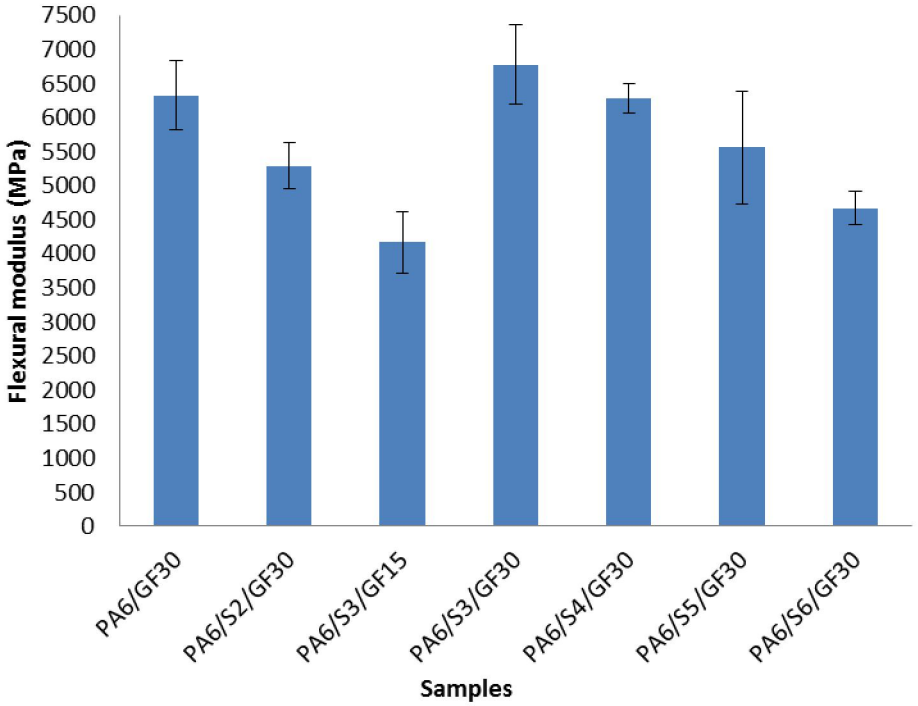

(b) Flexural modulus PA6/GF30 and PA6 glass reinforced nanocomposites

Figure 6.5 Effect of fillers and glass fibre on flexural (a) strength and (b) modulus of PA6 glass reinforced composites showing the effect of glass fibre percentage and surface modification on PA6 flexural strength and flexural modulus.

This showed that GF composition influences the nanocomposites material's load-extension and flexural stress-strain relationships (Figure 6.6). However, there was a lack of trend between the flexural load versus extension and flexure stress versus strain graphs as observed in the PA6 nanocomposite materials earlier discussed. For flexural load versus extension the trend was PA6/S3/GF30, PA6/S4/GF30, PA6/GF30, PA6/S5/GF30, PA6/S2/GF30 and PA6/S3/GF15 with exception to PA6/S6/GF30. For flexural stress versus strain the trend was PA6/S3/GF30, PA6/GF30, PA6/S5/GF30, PA6/S2/GF30, PA6/S3/GF15 and PA6/S4/GF30 with exception again to PA6/S6/GF30.

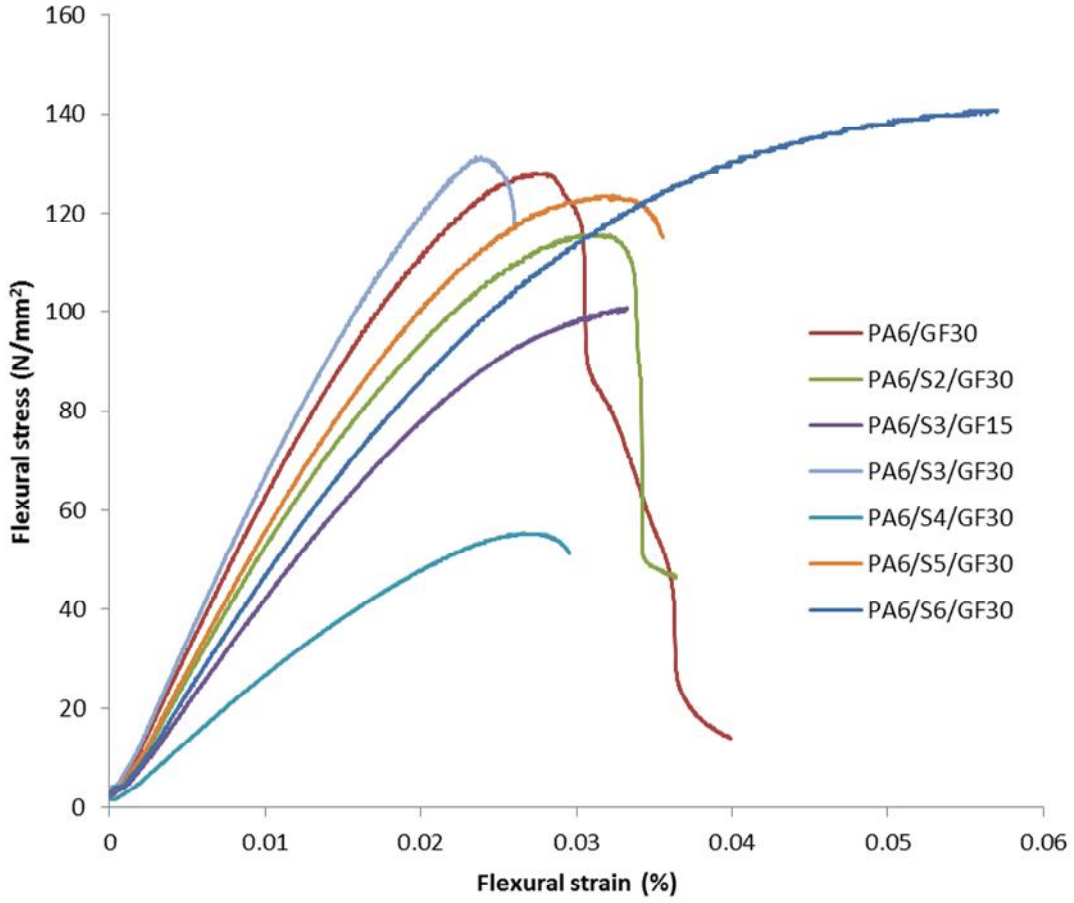

Figure 6.6 Flexure stress versus strain graphs of PA6/GF and PA6 glass fibre reinforced nanocomposites showing increased stress strain capacity of PA6/S6/GF30 as a result of increased interfacial bonding between nanofillers glass fibre and PA6 matrix.

In terms of PA6 flexural property percentage (%) improvement in both nanocomposites and glass fibre reinforced nanocomposites from the maximum

load of the flexural load-extension and flexural stress-strain graphs, and flexural modulus and strength percentage improvement, the following observation was made and summarised in Appendix E - Table E.1. It can be seen that glass fibre reinforcement had a significant influence on improvement of the PA6 and PA6 nanocomposites. However, it is important to note that only 2.5% of the nanofiller was used to achieve this level of improvement. Perhaps, an increase in nanofiller ratio to PA6 could show further improvement in PA6 flexural properties.

Figure 6.2 showed the graphs of flexural strength and modulus showed the effect of the fillers on the nanocomposite materials. The test specimens PA6/S2, PA6/S3 and PA6/S4 have much reproducible modulus than PA6/S1, PA6/S5 or PA6/S6. PA6/S2 sample is one of them which has a greater resistance to deformation under applied stress. The high interfacial adhesion contributes to the increase of the static flexural strength of PA6. Trend of changes to the maximum bending stress (Figure 6.3) for composites reinforced with S2-S6 was very similar to that presented in Figure 6.5(a). The highest flexural strength reached was by the PA6/S6 sample but this value did not exceed 100MPa. The relatively high strength result may be caused by the fact that the S6 filler may have plasticizing properties by reducing the density of intermolecular forces along the polymer chain.

This study has shown that different factors such as demulsifier–led surface modification of nanocomposite, thermal treatment, difference in mineral composition and presence of glass fibre reinforcement influence the mechanical properties of the nanocomposite materials. In this study, it was observed that the presence of surface modification by the demulsifier in PA6/S4 and petroleum hydrocarbon in PA6/S6 enhanced flexural modulus (Figure 6.2). Fornes et al. (2002) investigated the effect of surface modification of clay using different surfactants on PA6 nanocomposite morphology and mechanical properties. The findings indicated the use of surfactants with decreasing number of alkyl tail in moderate (not excess), led to filler exfoliation, increased modulus / strength, lower elongation at break. PA6/S3 higher chain hydrocarbon were assumed to have been removed by acid modified demulsifier, however, the sample exhibited higher flexural strength than modulus which is not fully understood, but its glass

reinforced composite (PA6/S3/GF30) showed both higher flexural modulus and strength (Figure 6.2). Similarly, PA6/S5 might have lost most of its hydrocarbon compounds due to thermal treatment used to extract petroleum hydrocarbon. However, PA6/S6/GF30 behaved differently. The presence of petroleum hydrocarbon in S6, had a plasticising effect which promoted spacing within the interlayer spaces of the nanofiller as well as exfoliation of the PA6/S6 and PA6/S6/GF30. This effectively could have contributed to their higher interfacial bonding, highest flexural strength and nanocomposite highest modulus. Zhou et al. (2005) similarly reported that the organo-modification of talc using polybutylene acrylate with SDS to enhance compatibility between talc and the polypropylene matrix and, thus, enhanced the nanocomposites mechanical properties, thus enhancing the mechanical properties of the polypropylene-talc material. In a study by Liu, Qi and Zhu (1999) on mechanical properties of PA6/montmorillonite nanocomposites filled with MMT 0.5-5%, it was observed that the flexural strength of PA6 was 64.97 MPa similar to the result obtained in this research and the flexural strength increased as MMT increased from 0.5-3% as 64.1-84.1MPa but decreased at 5% having a flexural strength of 67.60MPa. With reference to this study showing 0.5% and 1% MMT to have flexural strength of 70.95MPa and 80.85MPa respectively, it gave an indication that the manufactured nanocomposites may have had only between 0.5 and 1% MMT in the nanocomposite samples. This was because, interestingly, PA6/S2 which contained bentonite clay (MMT) of 2.5% weight had a low flexural strength of 73.2MPa below the flexural strength of 1% weight MMT as shown in Liu et al. (2011) study. In this study, PA6/S3 and PA6/S4 had flexural strength 71.4MPa and 72.1 MPa respectively. This could have been possible as they had lost colloid (froth) which could have been bentonite clay (MMT) during the demulsification/phase-separation process. On the other hand, PA6/S5 with flexural strength of 70MPa could have possibly had a lower MMT content due to its filler, S5 coming from a different drilling waste batch supplied. However, PA6/S6 of the untreated drilling fluid which had lost no colloids had a higher flexural strength of 74.6MPa compared to that of PA6/S2. This showed that the mixture of minerals in the nanofiller could have contributed to enhancing its flexural strength in PA6/S6 or in reducing its flexural strength as in PA6/S3 (for

example). PA6 hybrid nanocomposite study by Mészáros et al. (2013) was explored to understand this multi-mineral filler phenomenon. The study showed that the use of basalt, BF (volcanic rock) nanofiller (made up of SiO_2, Al_2O_3, CaO, MgO, Fe_2O_3 and FeO) in PA6 gave a higher flexural strength than PA6 and PA6/MMT of flexural stress/modulus of 33.3MPa/1189MPa and 48.2MPa/1532MPa respectively. On the other hand, PA6/BF and PA6/BF/MMT had flexural stress/modulus of 124.7MPa/4672MPa and 152.1MPa/5715MPa. This showed a mixture of minerals of known composition could increase flexural properties.

However, in the glass fibre reinforced PA6 nanocomposites, it was observed that there was no trend similar to the PA6 nanocomposites in the flexural modulus and strength. Glass fibre is known to increase the flexural modulus and strengths of PA6 composites (Njuguna, Mouti and Westwood 2015, Yan et al. 2013, Unal 2004). Flexural and compressive - strength and modulus results in Figures 6.5 and 6.10 showed that strength and modulus are influenced by glass fibre % composition by weight. PA6/S3/GF15 had low flexural and compressive - strength and modulus results compared to the other glass fibre reinforced PA6 nanocomposites. Vlasveld et al (2005) in the study on increasing PA6 composite strength using glass fibre found that flexural strength of glass fibre reinforced PA6 nanocomposite increased to >500MPa compared to PA6/glass fibre <500MPa for dry conditioned samples and the same trend for moisture conditioned samples. However, this was not the case with PA6/GF30 which had a higher flexural modulus and strength 6327MPa and 129MPa respectively than PA6/S2/GF30, PA6/S4/GF30 and PA6/S5/GF30. This reverse case was attributed to inhomogeneity in the distribution of the glass fibres in PA6 matrix of these aforementioned nanocomposites or an incompatibility in the bonding between the fillers, glass fibre and PA6 resin. In contrast, PA6/S6/GF30 may have had more exfoliated nanofiller than the other nanocomposites due to the presence of petroleum hydrocarbon oil on the surface of its nanofiller hence, its highest flexural strength (Vlasveld, Bersee and Picken 2005). However, the cause of its decrease in Flexural modulus (4667MPa) was not fully understood.

6.3.2 Compression performance

The relationship between compression properties and filler loading as obtained from compression tests on the standard compression strength and compression modulus specimens of PA6 nanocomposite materials were studied, as shown in Figures 6.7 and 6.8. Compressive strength is the property exhibited by a material or structure whereby it withstands load applied which leadings to decrease in material size. The compressive strength results gave an indication of the stress that is required to destroy the sample by crushing. Compression modulus of the nanocomposite material(s) was the ratio of the material's ability to support force at different compressive extensions in the elastic region. The compressive modulus gave an indication of the ratio of the maximum compressive stress to be applied the material compared to the resulting compression. The modulus was mainly dependent on filler type and material density.

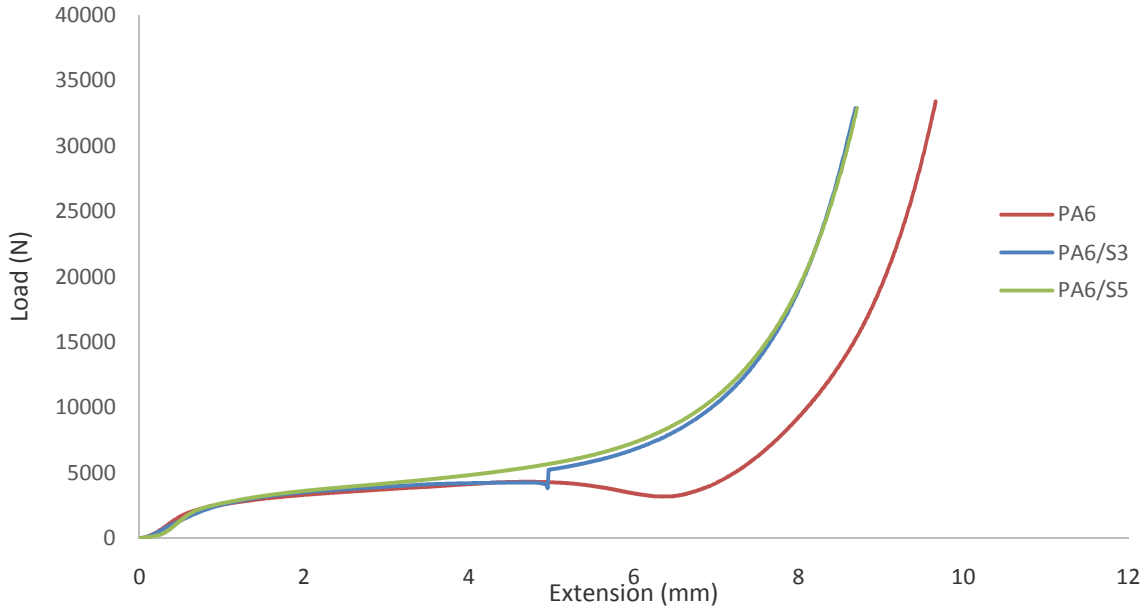

Figure 6.7 Compression strength load vs extension graph of PA6 and PA6 nanocomposites

Figure 6.7 showed a decrease in compressive extension from its initial thickness of 10mm. Figure shows that in the elastic region between 0mm and 0.9mm the samples have relatively similar compressive strength. In the plastic region as the load is applied, the nanocomposite materials PA6/S3 and PA6/S5 exhibit resistance for the load applied as shown in lower extension compared to PA6.

Therefore, the nanocomposites have a higher compressive strength than PA6 due to the presence of the fillers. The irregularity of PA6/S3 was attributed to poor interfacial bonding of the filler between 3.7mm-5.0mm compressive extension as the load applied increases or due to large standard error amongst tested specimen.

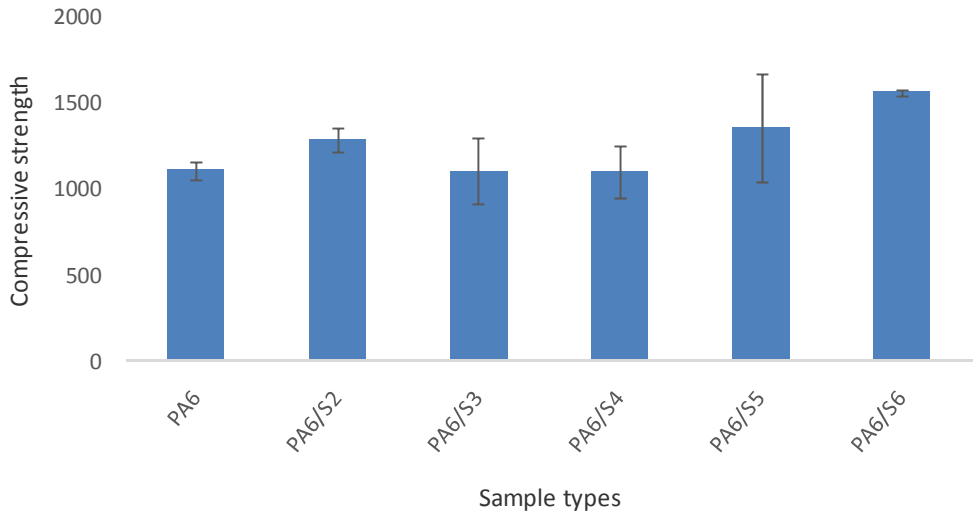

(a) Compression strength PA6 and PA6 nanocomposites

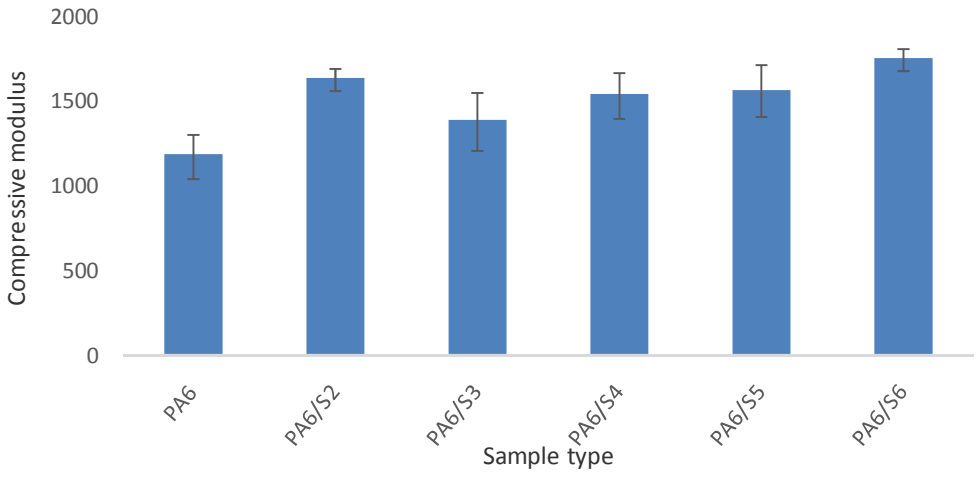

(b) Compression modulus of PA6 and PA6 nanocomposites

Figure 6.8 Effect of fillers on Compression (a) strength and (b) modulus of PA6 nanocomposites and glass reinforced PA6 nanocomposites showing the effect of nanofiller addition to increases in compression strength and modulus of PA6.

Figure 6.9 shows that in the elastic region between 0mm and 0.9mm the samples have different compressive strengths. This could be attributed to the filler type and GF distribution. PA6/S3/GF30 exhibited increased compressive strength compared to PA6/S3/GF15 and PA6/S5/GF30. In the plastic region with load applied, PA6/S3/GF30 and PA6/S3/GF15 exhibited higher resistance for the load applied as shown in lower extension compared to PA6/S5/GF30 and PA6. Therefore, the nanocomposites PA6/S3/GF30 and PA6/S3/GF15 have a higher compressive strength than PA6 due to the presence of the nanofillers and glass fibre. Figure 6.10 shows a compressive modulus test comparing load versus extension relationship of nanocomposites. The Figure 6.8 shows that in the elastic region between 0mm and 1.0mm the samples have different compressive modulus. PA6 and PA/S5 have higher compressive modulus than PA6S3 as shown in the load versus extension measurement. This could be attributed to difference in material density as shown in plasticity test (see chapter 7.3.3) where PA6/S3 is observed to the least density of 0.69 g/cm^3 compared to PA6, PA6/S2, PA6/S4, PA6/S5 and PA6/S6 with densities of 0.97 g/cm^3, 0.83 g/cm^3, 1.05 g/cm^3, 0.96 g/cm3 and 1.00 g/cm^3.

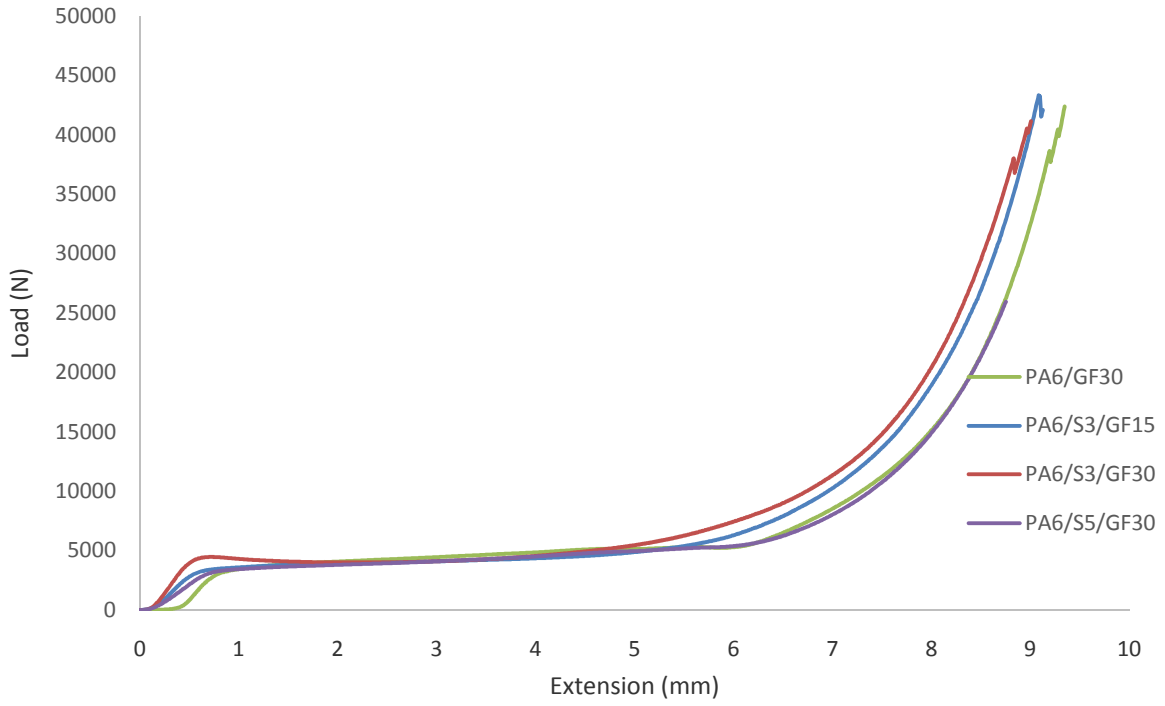

Figure 6.9 Compression strength load vs extension graph of glass reinforced PA6 nanocomposites

In the plastic region as the load is applied, the nanocomposite materials exhibit failure attributes as shown in immediate decrease in load supported by the materials as compressive extension increases. This is due to the fact that the stored energy in the material has been released. PA6/S3 offers the attributes of a lightweight material.

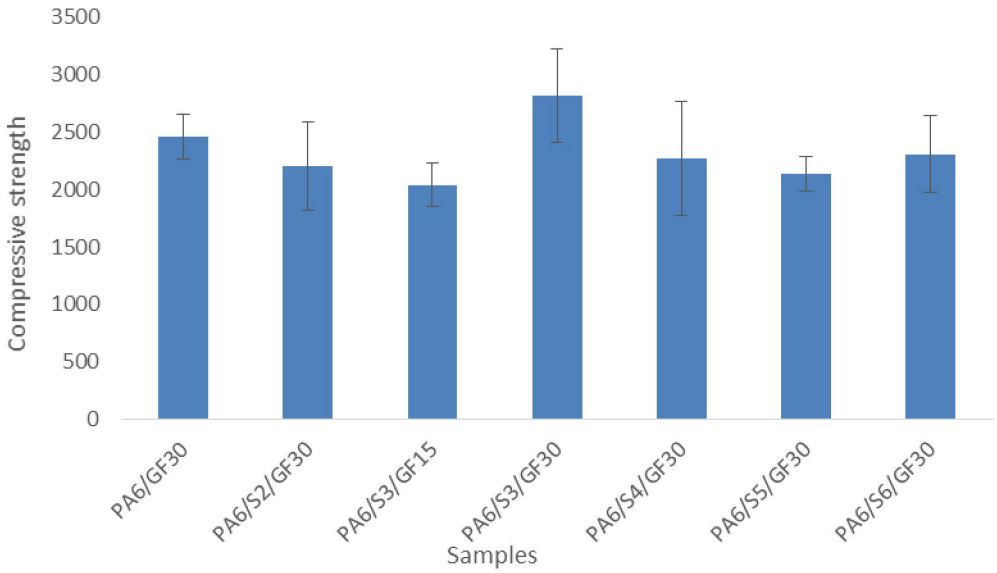

(a) Compression strength of PA6/GF30 and PA6 glass reinforced nanocomposites

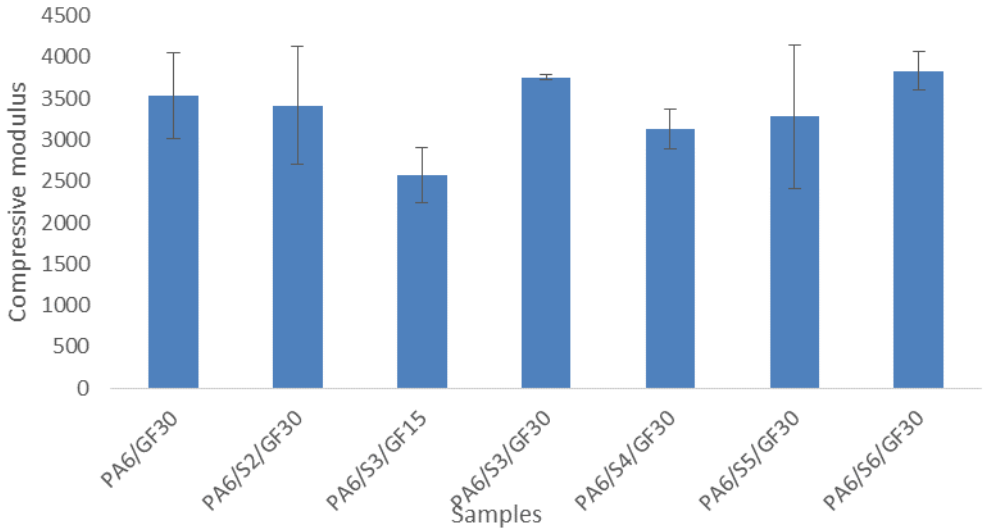

(b) Compression modulus PA6/GF30 and PA6 glass reinforced nanocomposites

Figure 6.10 Effect of filler type on PA6 compression strength and modulus

In the elastic region, it was observed that PA6/S3/GF15 showed earliest yielding, decrease in load resistance at 1550N (see Figure 6.9). This was due to the low glass fibre loading of 15% compared to the other glass fibre reinforced materials with a 30% glass fibre loading. This was followed by PA6/S4/GF30 yielding by 2000N at about 1.00mm. This could be attributed to weak interfacial bonding between fibres and resin as well as space formation due to poor compression during injection moulding of the sample. On the other hand, in the elastic region, PA6/GF30, PA6/S3/GF30, PA6/S5/GF30 and PA6/S6/GF30 show relatively similar compressive properties, and higher load resistance over 2000N. In the plastic region, PA6/S3/GF15 and PA6/S6/GF30 show better failure resistance than the other nanocomposite materials. Thus, indicating a longer lasting and failure resisting material. For PA6/S3/GF15, it is attributed to the lower GF loading which increased flexion of the material and it gives the material a ductile potential. In the case of PA6/S6/GF30, it was not attributed to the GF loading but the presence of plasticisers which gave the material its ductile attribute. This ductile and brittle characteristic of the materials was similar to the trend observed in the flexure modulus of the glass reinforced nanocomposites (see Figure 6.2). In addition, videos of compression tests showed these trends as well.

- **Stress-strain relationship for PA6 and PA6 nanocomposites**

The compression properties of the PA6 and its nanocomposites with different fillers were characterised in the 90^{o} direction. This is defined by the tips of the glass fibre in the GF nanocomposites unlike the 0^{o} direction which is parallel or side surface of fibre. During the first phase or stage of compression, the PA6 matrix (resin) transferred load to the sustaining filler. This was due to the good interface between PA6 matrix and the filler. In the second stage (plastic region), the interfaces between the PA6 matrix and the fillers were progressively destroyed. Thus, the ability to transfer load decreased and the load carried by the fillers reduced. The slope of the curve was relatively large in the first stage compared to the second stage as the curves attained maximum stress where the curve declined rapidly and showed brittle failure especially in the GF reinforced materials. Irrespective of differences in nanofiller composition, the stress-strain curves rose with increasing nanofiller and/or glass fibre content.

- **Effect of fillers on compressive strength of PA6**

The relationship between the fillers and the compression strength of the composites were shown in Figure 6.8a and Figure 6.10a. It can be seen that PA6/S6 and PA6/S5 has higher compression strength the other composites. This could be attributed to the good interface between PA6 matrix and the filler, increasing the ability of the filler to sustain the load transfer from the PA6 resin. In the glass reinforced composites, the trend was changed. The reason could be poor interfacial bonding between the glass fibre and PA6/S6. In it was obvious that the reduced GF content influenced the PA6/S3/GF15 compression strength which was the least. Thus, it confirmed that increase GF content improved compression strength as observed in PA6/GF.

- **Effect of fillers on compression modulus**

Due to the difference in compositions of minerals, surface modification and perhaps the presence of agglomeration of the nanofillers, the compression properties could not be compared directly. This could be observed the dissimilar trends of compression strength and compression modulus. However, filler S6 the untreated drilling fluid and cutting consistently proved to improve the compressive modulus and compressive strength of PA6 compared to S2 known to improve the compression properties of PA6. This could be attributed to good interface between the resin and filler (see Figure 6.8b and Figure 6.10b).

- **The effect of strain rate on compression properties**

The relationship between compression properties and filler loading as obtained from compression tests on the standard compression strength and compression modulus specimens of PA6 nanocomposite materials were studied, as shown on Table 6.1. It was observed that strain rate did not have a proportional influence on the select materials' compression strength and modulus. On addition of S5 nanofiller into PA6, the compression properties of composites increased to 1563.0 MPa from 1179.2 MPa for compression modulus, and 1353.4 MPa from 1107.7 MPa for compression strength. This characteristic material property improvement of nanofiller reinforced PA6 thermoplastics have been observed by other researchers (Vlasveld et al. 2007, Chow and Mohd Ishak 2007).

Furthermore, with the addition of 30% glass fibre (GF30) into PA6, the compression properties of nanocomposites increased more than that of the 2.5% S5 nanofiller PA6 nanocomposites to 3538.2 MPa for compression modulus, and 2457.3 MPa for compression strength. Likewise, the combination of both S5 and glass fibre fillers to PA6 in the nanocomposites (PA6/S5/GF30) was found to 0.5% increase the compression modulus and 8.5% decrease the compression strength of PA6/S5, as summarized on Table 6.1. This indicated that the introduction of S5 nanofillers into the PA6 matrix does significantly improve the compression properties of pristine PA6. However, the decrease in compression strength for PA6/S5 may probably have resulted from the use of multisized and shaped S5 nanofillers comprising of nano-sized clays, micron-sized cuttings (shale/sand) and barite in composite material.

The addition of 30% glass fibre to pure PA6 makes PA6/GF30 composite able to absorb more elastic strain energy. With the combination of S5 nanofillers and glass fibres, we can obtain a higher compression modulus of 202% for PA6 which shows this material to be tough, brittle and strong. The decrease in compression strength from 2457.3 in PA6/GF30 to 2247.4 MPa in PA6/S5/GF30 could be a reflection of glass fibre orientation or quantity differences in the tested samples. However, the synergy of S5 nanofillers and glass fibre does not have a great difference or improvement on PA6/GF30. This could be attributed to overloading of the polymer matrix which could have led to a reduction in mechanical properties. Therefore, although the nanocomposites are hard and brittle, its yielding point is lowered, and it cannot absorb much elastic strain energy and thus cracks easily.

As shown in Table 6.1 using a test rate of 2 mm/min, the results showed that the presence of nanocomposite fillers in PA6/S5 led to about a 90% and 74% increase in compression modulus and strength of PA6. Although the addition of glass fibre to pristine PA6 led to a further 251% and 134% increase in compression modulus and compression strength respectively, results showed that the synergy of glass fibre and S5 nanofiller led to a 353% increase compression modulus and 141% increase in compression strength. There was a great variation in compression modulus and compression strength of the glass reinforced materials. This showed density variation in the materials which was

attributed to errors in glass fibre addition during sample preparations or differences in glass fibre orientation or alignment in the matrix of PA6 and PA6/S5 samples as observed in microscopy (see chapter 5 and chapter 6: sample damage and failure).

The compression carried out at ISO 604 recommended rate of 1 mm/min modulus and 5 mm/min for strength as well as research test rate of 2 mm/min for modulus and strength tests gave the results on Table 6.1

Table 6.1 Compression test rates

	ISO test rate		**Research test rate**	
Sample	**Compression modulus, MPa (1mm/min)**	**Compression strength, MPa (5mm/min)**	**Compression modulus, MPa (2mm/min)**	**Compression strength, MPa (2mm/min)**
PA6	1179	1108	843.4	889.6
PA6/S5	1563	1353	1602	1544
PA6/GF30	3538	2457	2962	2080
PA6/S5/GF30	3559	2247	3817	2142

Relationships between the PA6 materials and fillers used can be easily distinguished. It was observed that the 2 mm/min test speed decreased the compressive strength compared to 5 mm/min test speed. When S5 nanoclay containing filler is added, the compressive properties at test speed 1 and 2 mm/min are relatively close while the compressive strength obtained at 5 mm/min is lower. With the addition of glass fibre to pristine PA6, a significant variation in the compressive properties is observed. It is observed that irrespective of test speed compression modulus has a higher response compared to compression strength, with ISO preferred test speed having higher responses of 3538.2 MPa and 2457.3 MPa for modulus and strength respectively. In the 3 phase nanocomposite in which S5 nanofiller and glass fibre synergies are fillers, the modulus value increases in 2mm/min tested samples while the 1 mm/min samples remain unchanged. This increase in modulus in 2 mm/min test specimen

can be attributed to the fibre alignment. The compressive strength values increase for 5 mm/min tested specimen compared to the 2 mm/min sample. In general, for all compressive response in the three phase nanocomposite sample, it suggested that the high test speed was responsible for the high compressive responses which showed that at higher test speeds, samples absorb more elastic strain energy. For PA6/S5/GF30 tested at 1mm/min, an overdose of filler loading in nanocomposites is found to decrease the compressive modulus. This indicated that the introduction of S5 nanofiller into the PA6 matrix does effectively affect the compression properties of pristine PA6. However, the decrease in compressive modulus for PA6/S5/GF30 may also probably be as a result of the aggregation of fillers in nanocomposites.

From SEM micrographs the unfilled spaces within the PA6 matrix during manufacture could result in the decrease of compressive properties. Although the addition of S5 nanofiller into the PA6 matrix has improved compressive properties of PA6, the optimum ratio of glass fibre to S5 nanofiller could be obtained in subsequent research to produce S5 nanocomposite materials of higher compressive properties. It is important to note that the S5 nanofiller encouraged shearing compression in material tested for compression strength which is an advantage in the compression performance of this novel material. This shear characteristic indicates that the material would withstand compression and not compress or crack easily.

Compression properties seemed to influence the flexural strength except in the case of PA6/S6/GF30 (Figures 6.2 and 6.6). The compressive strength of nanocomposites – PA6/S3/GF15, PA6/S4/GF30, PA6/S5/GF30 and PA6/S2/GF30 were lower than the PA6/S3/GF30, PA6/GF30 and PA6/S6/GF30 because the fibres could easily buckle under a compressive load (Vlasveld, Bersee and Picken 2005). The compressive strength of the PA6 nanocomposites depended on the compressive modulus of the PA6 matrix (see Figure 6.8). This was because the higher modulus, the higher the lateral support of the glass fibre which decreases the propensity for glass fibre to buck. PA6/S3/GF15 had lower compression properties due to lower GF% composition. Unlike the glass fibre-reinforced nanocomposites, PA6 nanocomposites have a linear increase in compressive

strength and modulus from PA6 to PA6/S6 except for PA6/S2 with a higher value than PA6/S3 and PA6/S4. It was due to the lack of filler in PA6 and perhaps a loss of clay (MMT) percentage weight composition in PA6/S3 and PA6/S4.

6.3.3 Hardness performance

Hardness is a surface property of a material used to compare the nanomaterial's resistance to plastic deformation. It cannot be compared to the modulus or strength which were bulk property (Biron 2016). PA6/S2 was the hardest nanocomposite with a hardness of 97.9 HB as shown in Figure 6.11. Decreasing hardness from PA6/S3 to PA6/S5 could be attributed to the presence of plasticizers and crosslinkers which could result in decreased interfacial bonding between polymer chains and fillers. The plasticising effect was suggested to have arisen from organo hydrocarbons and barrite contents. However, the addition of GF to PA6 as reinforcement decreased the hardness of PA6. This may be due to poor distribution of GF in the PA6 matrix, poor adherence of GF to polymer and fast cooling which could have lead to poor space creation within the matrix.The difference observed in the hardness of PA6/S3/GF15 (72 HB) and PA6/S3/GF30 (81 HB) could be as a result of incompatibility or fast cooling which resulted in lower interfacial bonding betwwen PA6/filler/GF or poor space creation respectively. On the otherhand, the increase in hardness of PA6/S4/GF30 and PA6/S5/GF30 compareed to lower performance in flexural and compression tests (compared to PA6/S3/GF30) could be as a result of presence of GF at the points of indentation.

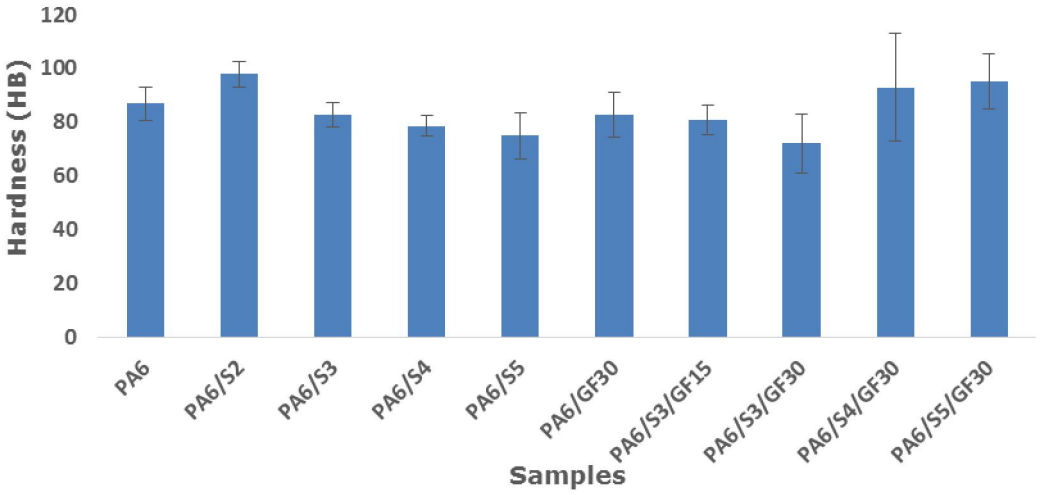

Figure 6.11 Hardness results for PA6 and PA6 nanocomposites materials

The hardness results in Figure 6.11 did not show a trend similar to the findings of Qi et al. (2013). Their study showed that as MMT increased, hardness increased. Due to lack of minerology data, it might be difficult to ascertain the effect of mineralogy on the hardness. It is however, assumed that the low hardness by glass fibre reinforced PA6 nanocomposite materials could be as a result of inner laying of the glass fibre in the PA6 matrix.

Qi et al. (2013) showed that the PA6/GF composite mechanical properties could be improved upon by the addition of solid lubricants. In their investigation, they employed graphite, ultrahigh molecular weight polyethylene (UHMWPE) and Polytetrafluoroethylene (PTFE) as solid lubricants. It was experimentally observed that 15% GF improved the hardness, tensile and impact properties of pure PA6 by 30%, 2% and 52% respectively. They found that the synergy of PA6/GF/graphite improved the tensile strength of PA6/GF composite by 5% with 5% weight of graphite added. Moreover, Qi et al. (2013) research highlighted that tensile properties in PA6/GF increased at 10% weight content of graphite. Subsequent additions of graphite content resulted in a decrease in tensile properties. However, UHMWPE gave the best impact properties of over 1% at 12% weight content compared to PA6/GF composite material. PTFE slightly improved by 5% the hardness of the composite material. They also found that inorganic filler such as graphite gave better compatibility with glass fibre.

6.3.4 Damage analysis

In sample PA6/S3/GF30 like most of the brittle samples for example, there was a break at the yield point. It led to the delamination of glass fibre from the PA6 matrix. On the other hand, samples such as PA6, PA6 2-phase composites except PA6/S6 and PA6/GF30 did not break at the yield point.

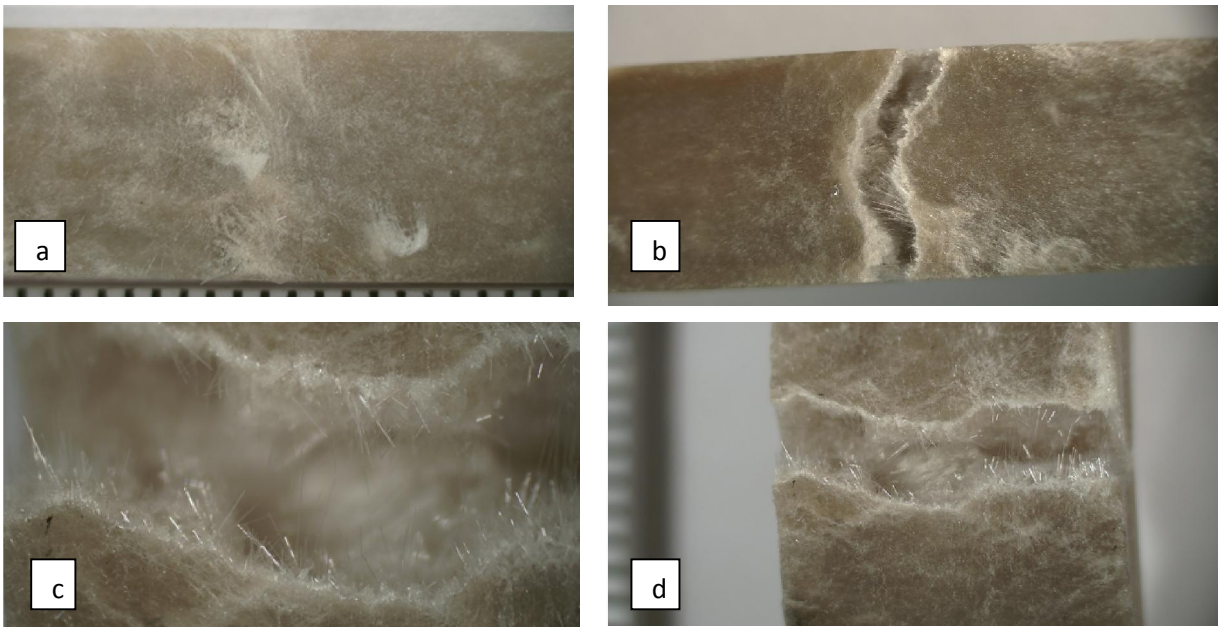

Figure 6.12 Flexural damage and failure images of PA6/S3/GF30 (a) before flexure (b-d) after flexure

The morphology of the compressive failures was studied by optical microscopy (see Figure 6.12 (a-d)). In these samples, there was a decrease in thickness and increase in average width especially at the center due to bulging and in second mode deformation double bulging. During the compression test of the PA6 and PA6 nanofiller materials, the PA6 matrix began to squash without cracking for PA6, and cracking for PA6/S3 and PA6/S5. On the other hand, for the GF reinforced PA6 materials, the PA6 matrix began to crack. The cracking was as a result of the low compression strength of the resin. PA6 and PA6/S6 were considered to be ductile because it was slowly distorted causing a phenomenon called barreling. Therefore, there is no single clear point of failure. However, PA6 composites with GFs were considered to be brittle as they snapped and broke into two or partially with clear points of failure. During the experiment, the sample, PA6/S6/GF30 suddenly fractures, quite explosively as the stored energy is released.

In some cases, delamination between the PA6 matrix and the glass fibre was observed. It was observed that the breakage due to load applied, lead to the delamination (pulling away of glass fibre from PA6 matrix). In composites,

agglomeration of nanofiller or glass fibre bundles, there is little or no space for resin to fill; thus, PA6 layers between these groups became the weak portions of the nanocomposite (Figure 6.13) and could result in reduction of compression strength (see Figure 6.8). This was similar to the experience of Pei et al 2016 investigating multilayer-connected biaxial weft knitted (MBWK) fabric reinforced Epoxy composite. Their investigation showed the tight knitting of the fibre caused fibre-bundle formation making it difficult for Epoxy resin to penetrate, therefore, the layer between the fabrics became a weak layer.

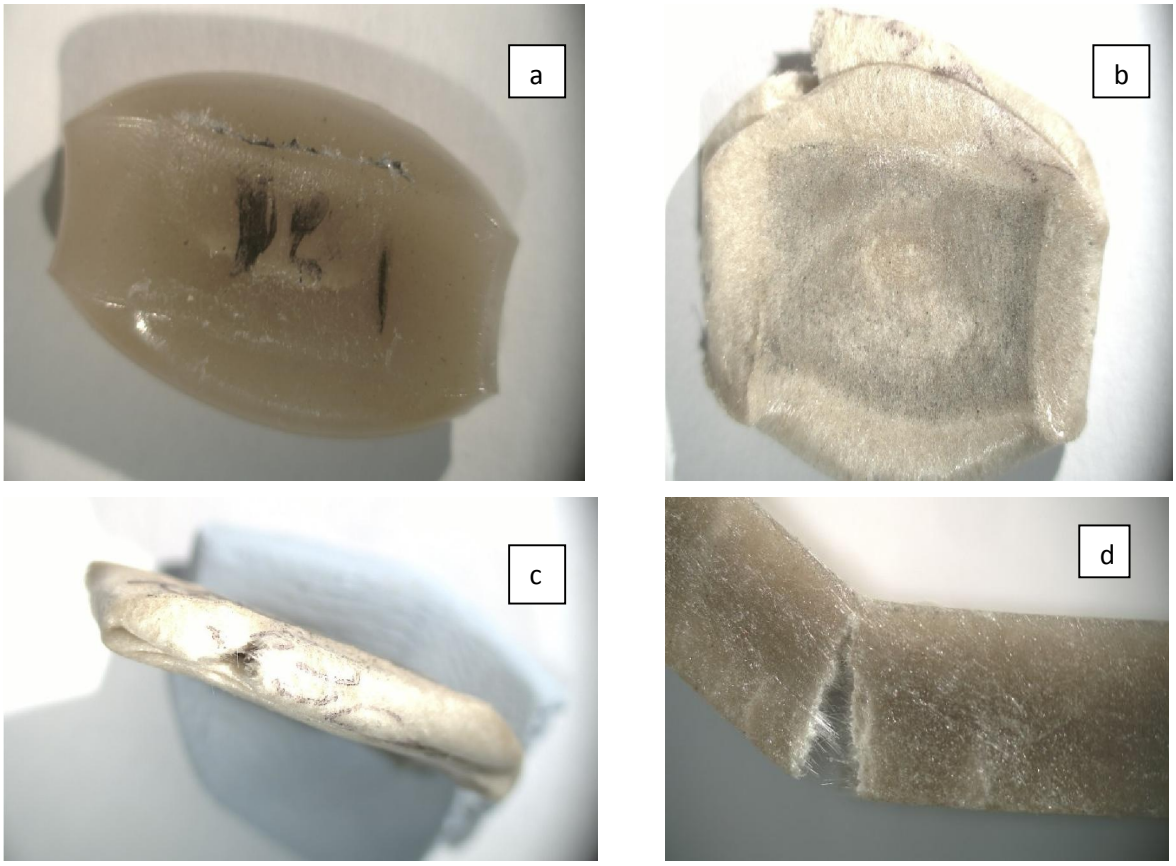

Figure 6.13 Compression damage images clockwise (a) PA6 strength sample after compression (b & c) PA6/S3/GF30 strength sample after compression, (d) PA6/S2/GF30 modulus sample after compression

6.4 Conclusion

This chapter was focused on the study of the effects of the nanofillers from the untreated and treated oil based drilling fluid and cuttings compared to S2 nanofiller on the mechanical properties of PA6 nanocomposites. Polyamide 6

composites reinforced with untreated and treated oil based mud and drill cutting showed varying mechanical properties. It was established that 2.5% wt. of fillers S3, S4, S5 and S6 in the PA6 2-phase nanocomposite samples were good fillers for improving the mechanical properties of PA6. The following conclusions were made. Firstly, flexural load bearing capacity of PA6 was improved by the nanofillers S2, S3, S4, S5, and S6 by 14, 11, 12, 8, and 16% respectively. The addition of glass fibre in PA6/GF30, PA6/S2/GF30, PA6/S3/GF15, PA6/S3/GF30, PA6/S4/GF30, PA6/S5/GF30 and PA6/S6/GF30 improved the flexural load bearing capacity of PA6 by 99, 80, 59, 104, 100, 92 and 119% respectively.

PA6/S6 improved flexural modulus and strength of PA6 by 19 and 16% respectively, which led to a 2% improvement in flexural strength compared to PA6/S2 (simulated industry polymer nanocomposite with one of the best performing industrial fillers). While PA6/S3/GF30 and PA6/S4/GF30 improved the flexural modulus of PA6 by 358 and 325% respectively and flexural strength by 107 and 101%, PA6/S2/GF30 (the commercial industrial polymer) improved PA6 flexural modulus and strength by 258 and 81% respectively. PA6/S6/GF30 showed the best PA6 flexural strength improvement of 119%. Generally, the flexural and compressive modulus and strength of the PA6 were improved by the addition of the nanofillers. This was attributed to the reinforcement, exfoliating, stiffening, rigidity effect of the nanofillers. S6 nanofillers significantly improved the mechanical properties of PA6. This was attributed to the increased interfacial bonding between the fillers and the polymer matrix as a result of the petroleum hydrocarbon present in the sample. S6 proved to be a better nanofiller than S2 nanofiller as shown in Figure 6.3.

The compressive properties (modulus and strength) of PA6 were enhanced by about 90% by the addition of the S5 nanofiller. SEM images in chapter 5 and flexural strength and modulus results for the PA6 2-phase composites suggested that the presence of layered structures such as clay in the nanofiller which has improved the intercalation of nanofiller in the PA6 matrix. The higher percentage of nanoclay increase hardness and compressive modulus of nanocomposites as observed in S2, S6 nanocomposites. It was discovered that surface modification with crude oil in untreated filler improves mechanical properties of PA6S6 and

PA6/S6/GF30 due to enhanced nanoclay and filler interaction with polyamide. Therefore, the different compositions and treatments of the nanofillers and presence of GF had impacted bonding of GF, resulting in great differences in the flexure, compression and hardness performance of the samples. The addition of 15% and 30% wt. glass fibre to the nanocomposites generally increased the flexural and compressive properties of PA6. The use of higher compression strain rates to compare the ISO test method should produce results of higher significance.

The hardness showed some lower values for the glass fibre reinforced materials which was not fully understood and requires potential future investigation. However, the flexural and compression test data showed that the untreated filler improved the mechanical properties of PA6 compared to the chemically and thermally treated fillers. The application of untreated and treated oil based mud and drill cuttings as nanofiller in plastic or elastomeric polymer has not been earlier published which make this research novel and a viable option for environmental management in oil producing and processing locations. However, ascertaining the optimum ratio of S2, S3, S4, S5 and S6 nanofillers to glass fibre, enhancing glass fibre alignment during manufacturing and application of higher temperature during injection moulding stage in the manufacture of the materials could improve the compressive properties of the three phase nanocomposite materials.

Chapter 7

Thermal Properties of Novel Nanocomposite Materials

7.1 Introduction

Polyamide 6 (PA6) is known to have high heat stability, however, the absorption of thermal, light or mechanical energy by polyamide can lead to degradation of its physical and mechanical properties (Gonçalves, Poulsen and Ogiby 2007). PA6 melt onset temperature is at about 50^{o}C and crystallizes at 180^{o}C (Holmes, Bunn and Smith 1955). Studies by Dabrowski, Bourbigot et al. (2000) showed that thermal ageing of PA6 leads to its oxidative degradation. The reduction, low percentage or absence of reinforcement materials, improper dispersion of reinforcement material and use of reinforcements of lower strength could result in thermal degradation of a composite material (Leszczyńska et al. 2007).

Factors responsible for the thermal stability and thermal degradation of PA6 are important for ascertaining the propensity of the material to exhibit different properties such as flame retardance, spark ignition and fast melting. Some factors that enhance the thermal stability of PA6 are the modification of polymer through addition of nanofiller or polymer reinforcement, the surface modification on the reinforcement materials, percentage of reinforcement materials to polymers used and sample preparation method (Leszczyńska et al. 2007). For instance, studies by Gendre et al. (2015) showed that nanosilica, glass fibre and OMMT can be used as reinforcement, and that their orientation, shape and chemical properties could influence the thermal stability of the resultant composite PA6 polymer. The investigation showed that nanosilica improved the thermal stability of PA6/GF30, hence, tensile modulus increased at 65^{o}C to 4.78GPa with nanosilica to 10%. However, at room temperature with 0-1% nanosilica, tensile modulus increases to 8.4MPa and drops with increasing nanosilica % weight. On the other hand, nanoclay (OMMT) improved the tensile modulus of PA6 as OMMT% increases from 0-10% at both room temperature and 65^{o}C. This showed thermal stability of PA6 even at high temperature such as 65^{o}C as OMMT% is increased. Therefore, from previous research, the use of two

or more reinforcement materials is generally known to improve thermal stability significantly (Silva, Sachse and Njuguna 2012; Njuguna 2011). However, the use of organic and flammable modifiers, plasticizers or coupling agents in the preparation of reinforcement materials is a possible factor that could influence thermal degradation of PA6. According to Samyn and Bourbigot (2012), the use of phosphorus chemicals in polyamide 6 showed improved thermal performances such as flame retardancy i.e. increased thermal stability. Some flame retarding formulations contained phosphorus oxynitrite (Adem et al. 2014; Bureau et al. 2002); phosphamane (Jiang et al. 2005); red phosphorus and inorganic phosphates: ammonium polyphosphate (Bureau et al. 2002); organophosphorus compounds e.g. di-melamine phosphates and melamine pyrophosphate (Holmes, Bunn and Smith 1955) and melamine polyphosphates (Özdilek et al. 2004).

Studies by Lu et al. (2015) showed that the use of phosphate modifier (ammonium polyphosphate [$(NH_4P0_3)n$, $n \leq 1500$]) enhanced the thermal property of PA6 by 46%. The use of organiphilised reinforcement resulted in the degradation of the polymer at a lower temperature compared to the pristine material. The presence of plasticisers (such as petroleum hydrocarbon) could lead to the weakening of polymer molecular forces while crosslinker (such as sodium borate) could influence material stiffness. To ascertain the effect of plasticisers and crosslinkers (processability) in the newly synthesized polymers two melt flow rate procedures were used. The Melt Mass Flow Rate (MFR) is the measure of the ability of a mass (g) of the molten form of a material to flow under pressure in 10 minutes. In addition, MFR is inversely proportional to viscosity (shear of the material) of the molten material at the conditions of the test which is dependent on the applied force while the melt volume flow rate (MVR) is the measure of the ability of a volume (cm^3) of the molten state of a material to flow under pressure in 10 minutes.

The aim of this chapter is to investigate the thermal properties such as melting point, degradation temperatures, mass flow index (MFR) and other effects of the nanofillers on the PA6 nanocomposite materials fabricated in Chapter 5.

7.2 Experiment

7.2.1 Materials

The materials used in this study were five nanofiller samples (S2-S6) and thirteen polymer samples described earlier in chapter 5 and summarised below in Table 5.1.

7.2.2 Characterisation

Four thermal analysis techniques were used in the characterisation of the nanocomposite materials. They included:

Thermogravimetric analysis (TGA): The aim of this test was to ascertain the temperature of degradation and decomposition, as well as the rate of degradation of the sample. This was carried out by measuring the weight variation of a given sample due to temperature increase and phase change as the sample degrades until it is decomposed. The TGA instrument used was a TA instrument Q500 TGA. The temperature was set on ramp mode from room temperature to 1000^0C at a rate of 10^0C per minute.

Differential Scanning Calorimetry (DSC): The aim of this test was to ascertain the melting temperatures, crystallisation temperature as well as glass transition temperature of the materials. The instrument measured the differences in heat exchange between the sample and the reference (an aluminium pan). The DSC instrument used was a TA instrument Q100. The temperature was set on heat/cool/heat procedure or mode from a temperature of -20^0C to 250^0C at a rate of 10^0C per minute. The analysis was carried out under a nitrogen environment.

Plasticity: This aim of this analysis was to determine the melt flow rate of the materials. This measured the flow properties of the samples. The analysis was carried out according to ISO 1133 for the Melt Mass-Flow Rate (MFR) expressed in g/10minute (procedure A) and Melt Volume-Flow Rate (MVR) expressed in cm^3/10minute (procedure B) of thermoplastics where the Melt Flow Rate or Melt Flow Index (MFI) was measured as the weight of the molten polymer flowing from a standard die of 2.095 x 8mm at a temperature of 230^0C with a weight of 2.16 kg applied to the piston which pushed the sample. ISO 1133 Procedure B is

recommended where MVR is used to indicate MFR when comparing samples with and without fillers or reinforcements as well as samples with different kinds of fillers and reinforcements. This experiment was carried out using Zwick Plasticizer and Figure 7.1 which illustrates the technique.

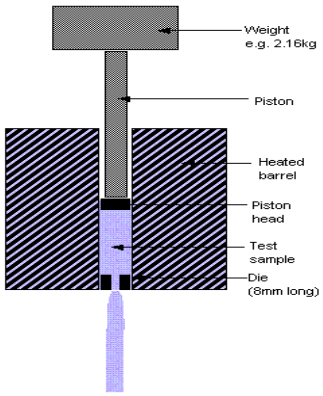

Figure 7.1 Plasticity test set up showing weight applied, heated barrel and test sample compartment.

7.3 Results and discussion

The DSC and TGA tests covered all the synthesised PA6 materials. However, the plasticity test was only conducted for the PA6 and nanofiller reinforced materials with PA6 as the experimental control.

7.3.1 TGA results

A comparison of the weight loss of the nanofillers and glass fibre was carried out in order to investigate the potential effect of the additives on the weight loss of the thermoplastic materials (Figure 7.2). In Figure 7.2, the untreated oil based mud /oil based drilling fluid (OBM) and cuttings referred to as S6, pure bentonite referred to S2, demulsifier S3 treated OBM and cuttings referred to S3 (containing phosphoric acid), demulsifier S4 treated OBM and cuttings referred to S4 and thermal treated OBM and cuttings referred S5 (thermally [thermal desorption unit] treated oil based drilling fluid).

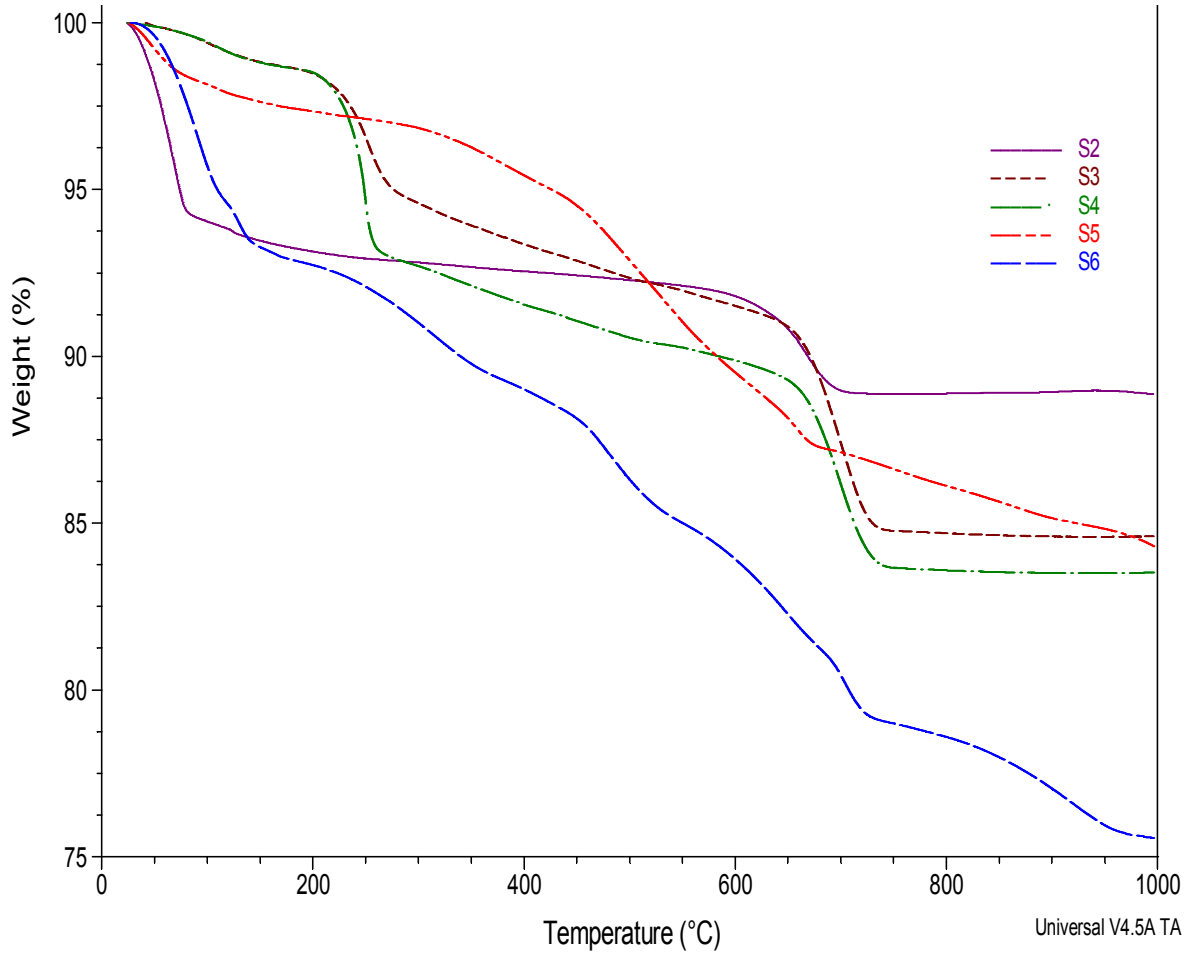

Figure 7.2 TGA of nanofillers used in the manufacture of the PA6 nanocomposite materials showing thermal degradation occurring at the rate of 10^0C/min from room temperature to 1000°C

Figure 7.3 showed that S6 (the untreated drilling mud and cuttings) had seven degradation events with the maximum weight loss of 24.44%. This was as a result of the heat related loss of moisture of equilibrium and the volatile hydrocarbons present in the filler between 25°C and 100°C. The evaporating compounds in the petroleum hydrocarbon were observed to degrade in the different degradation steps of the filler, S6.

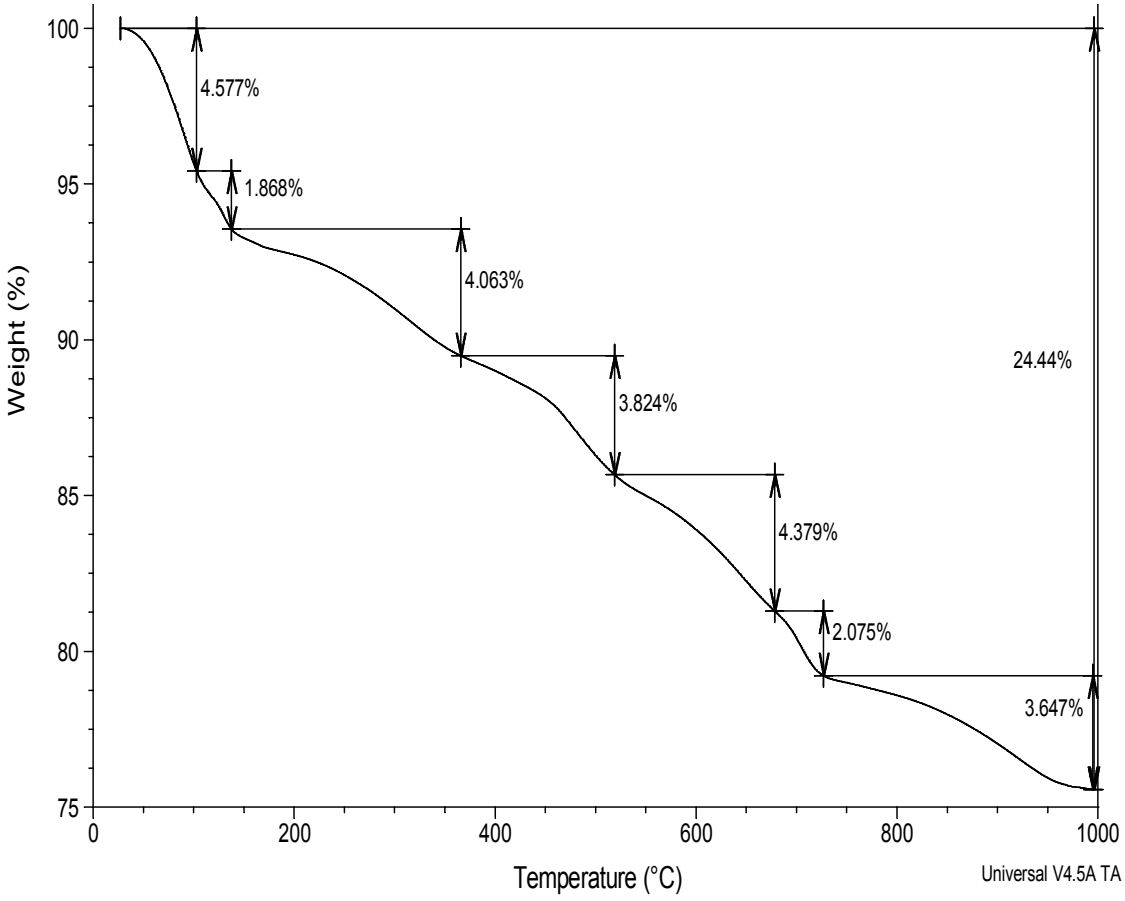

Figure 7.3 TGA of nanofiller showing S6 (the untreated oil based drilling mud and cuttings) showing the decomposition of compounds present in the oil

The TG curve of S2 was presented in Figure 7.4 as having a weight loss of 11.13%. The weight loss was a two step degradation that occurred within the range of 24.26^0C – 81.10^0C and 555.57^0C – 710.02^0C, which can be attributed to the loss of moisture associated with cations in the bentonite interlayers. This was similar to the findings of Motawie et al. (2014) where bentonite had a similar water loss at 526°C.

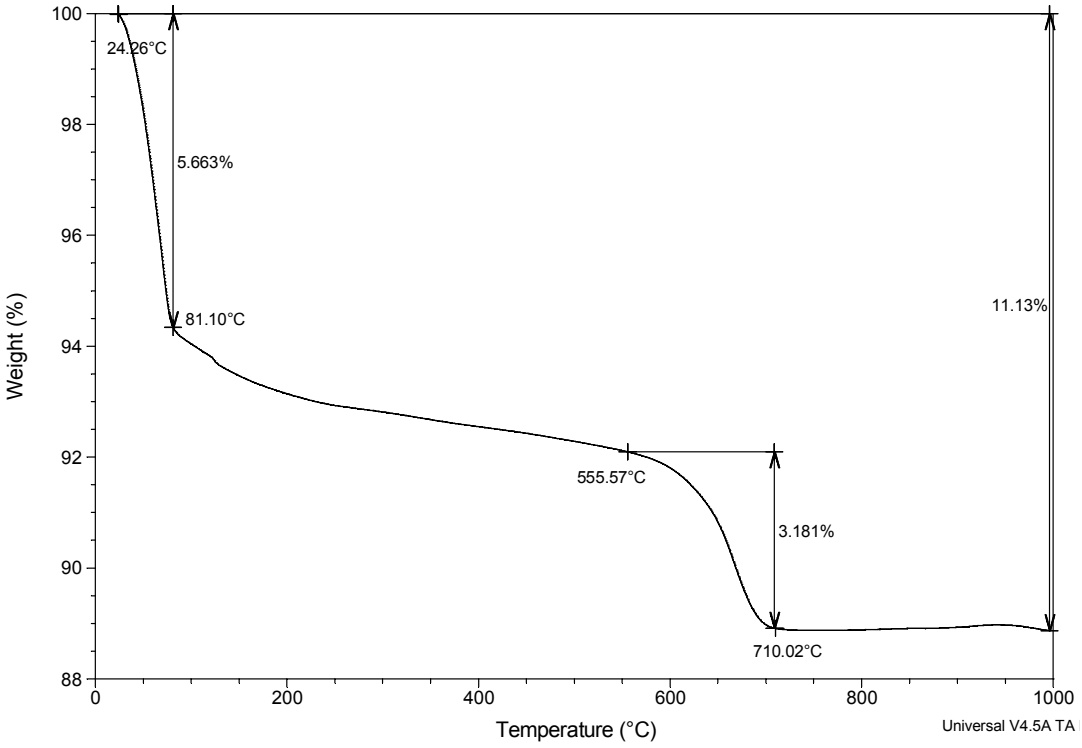

Figure 7.4 TGA of nanofillers showing S2 (experimental control) at 10^0C/min

In Table 7.1, the weight loss of S3 and S4 showed two main steps other than the initial degradation due to water loss. These degradations in S3 occurred within the range of 193.54^0C – 275.09^0C and 637.12^0C – 739.68^0C with a total weight loss of 15.39%. S4 degradation occurred within the range of 197.25^0C – 265.21^0C and 644.53^0C – 742.15^0C with a total weight loss of 16.49%. In S3 and S4, the initial degradation from about 25^0C to about 197^0C was attributed to moisture dehydration. The following degradation event from 197^0C - 260^0C was as a result of the decomposition of organic modifier which is the demulsifiers applied in chapter 4. The second degradation event was attributed to some components of the organic modifiers as well as inorganic compounds in the filler. This is similar to the work by Lu et al. (2015) where poly (styrene-co-maleic anhydride)/Clay (SMA/Clay) composites had the degradation as a result of organic modifier decomposition. S5 had an overall weight loss of 15.69% and incombustible residues of 84.31%. Its most prominent weight loss of 9.7% was between 273.85°C and 676°C. This weight loss was attributed to trapped petroleum hydrocarbon within the interlayers of filler, S5.

Table 7.1 Thermogravimetric analyses of the nanofillers and glass fibre showing the degradation events, initial degradation and end decomposition temperatures of the materials.

TGA samples	Number of Decomposition steps	Decomposition temperature ^{0}C		Mass loss (%)	Residue (%)
		Initial	Final		
S6	Total	25	1000	24.44	75.56
	1	25	102.29	4.58	
	2	102.29	136.21	1.87	
	3	136.21	366.07	4.06	
	4	366.07	519.31	3.82	
	5	519.31	678.84	4.38	
	6	678.84	726.57	2.08	
	7	726.57	1000	3.65	
S2	Total	25	1000	11.13	88.87
	1	25	555.57	5.66	
	2	555.57	710.02	3.18	
	3	710.02	1000		
S3	Total	25	1000	15.39	84.61
	1	25	193.54	1.34	
	2	193.54	275.09	3.52	
	3	637.12	739.68	6.31	
	4	739.68	1000	4.22	
S4	Total	24.26	1000	16.49	83.51
	1	24.26	199.72	1.33	
	2	199.72	265.21	5.43	
	3	644.53	742.15	5.69	
S5	Total	25	1000	15.69	84.31
	1	25	273.85	1.74	
	2	273.85	676.66	9.710	
	3	676.66	1000	4.24	

The TGA of neat PA6, PA6 nanocomposites and GF were carried out to investigate the improvement in thermal stability of PA6 with the addition of the different fillers and glass fibre (Table 7.2). This analysis elucidated the polymer chains molecular mobility restriction caused by the filler in a filled polymer such

as PA6 2-phase nanocomposites and PA6 3-phase nanocomposites. The analysis also gives evidence of the effect of these mineral fillers as well as the bond formation as a result of the adsorption of polymer on the modified surface of the fillers.

In terms of TGA generated weight loss, PA6/S3, PA6/S2 and PA6/S6 were more thermally stable than PA6/S4, PA6/S5 and PA6 (Figure 7.5). The analytical results in Figure 7.3 and Table 7.2 showed that amongst the PA6 2-phase nanocomposites, PA/S3 had the best thermal stability compared to neat PA6 samples and other PA6 2-phase nanocomposites. This quality was attributed to the phosphoric acid modified demulsifier treatment that differentiated filler S3 from S4. The acid built up H^+ ions and phosphate (PO_4^-) from phosphoric acid (a combustion-reducing element or flame retardant moiety) on nanofiller S3, which caused PA6/S3 to resist thermal degradation and burning becoming more thermal resistant than clay filled PA6/S2. However, PA6/S4 contained demulsifier-induced organophilisied S4 nanofiller (demulsifier treated filler) which had the potential to cause increased combustion of the polymer due to the presence of more volatile compounds in the filler surface coating, which resulted in a total weight loss of 98.93% (see chapter 4 FTIR TPH results). On the other hand, PA/S5 also had a high weight loss of 98.55% as a result of the petroleum hydrocarbon content of its filler which could have aided the combustion of that material (see chapter 4.3.4).

Amongst the glass reinforced nanocomposite materials, TGA results (Table 7.2) showed that PA6/GF30 had the highest percentage weight loss of 94.48%, a slight change of 5% compared to PA6. The total weight loss, PA/S3/GF30 had the least weight loss of 63.40%, followed by PA/S2/GF30 with 63.92% weight loss, while PA/S5/GF30, PA/S4/GF30, PA/S5/GF30 and PA/S6/GF30 had a weight loss of 70.71%, 74.44%, and 79.54%. On the other hand, PA6/S6/GF30 was the most thermally stable material with stability maximum of 375^0C followed by PA6/S3/GF15 (See Table 7.2). GF has a silane coating which enhances it interfacial bonding with the polymer (Gu et al. 2000).

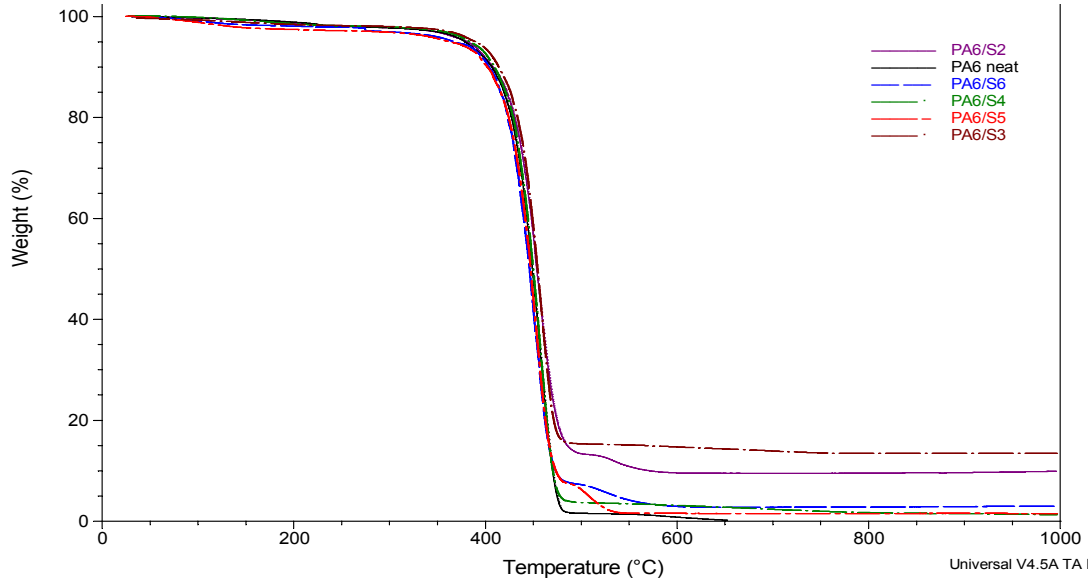

(a) Showing % weight loss of neat PA6 and PA6 nanocomposites

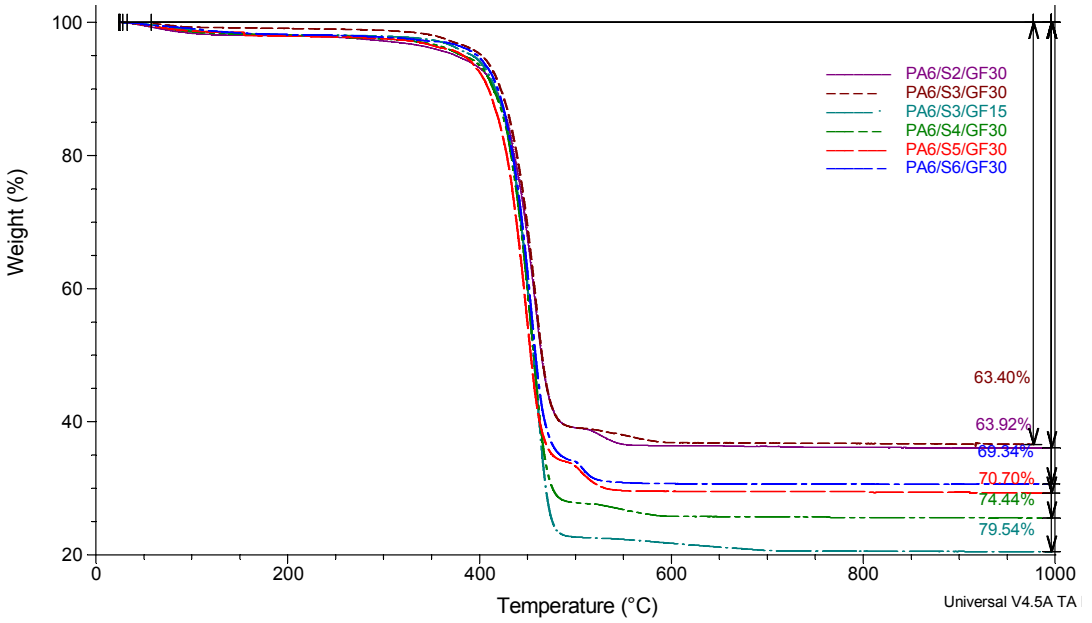

(b) Showing % weight loss of PA6 glass reinforced nanocomposites

Figure 7.5 TGA of neat PA6, PA6 nanocomposites and PA6 glass reinforced nanocomposites showing percentage weight loss of the materials at 10^0C/min from room temperature to 1000°C

The degradation of PA6, GF and PA6 nanocomposites were investigated (Fig 7.6). From observation, PA6, GF and PA6/S3 had 3 thermal degradation phases while other materials had 4 phases which is often influenced in some case by the

presence of the fillers and surface modifiers properties. In Figure 7.6, PA6/S2/GF30 it was observed that heat resistant reinforcement using glass fibre decreased the weight loss of PA6/S2 by 26.18%, while S2 with a weight loss of 11.13% and incombustible residues of 88.87% decreased the weight loss of PA6 in PA6/S2 by 9.7%.

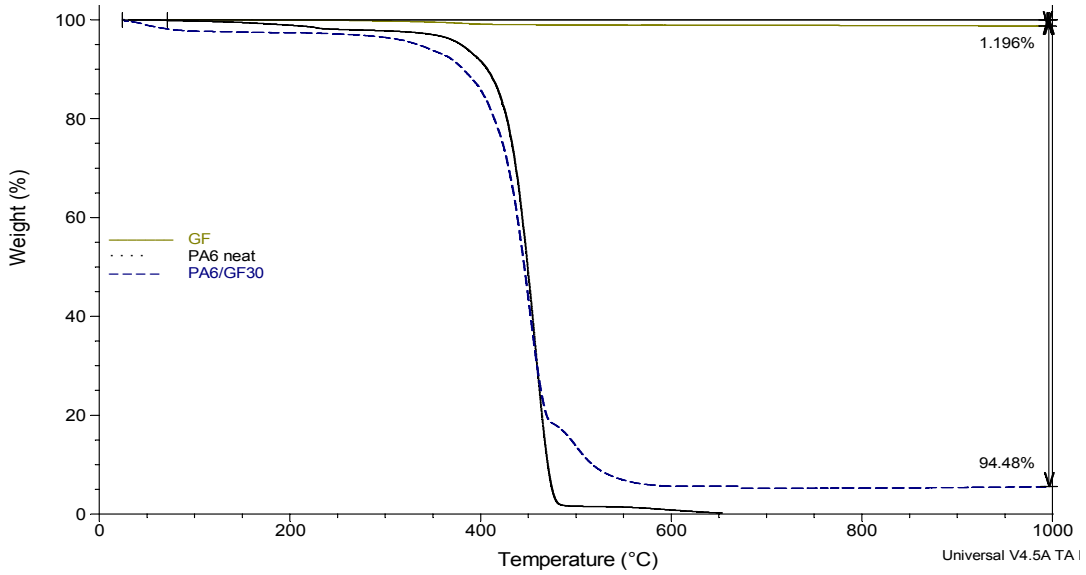

(a) Showing % weight loss of GF, PA6 nanocomposites and PA6 glass reinforced nanocomposites

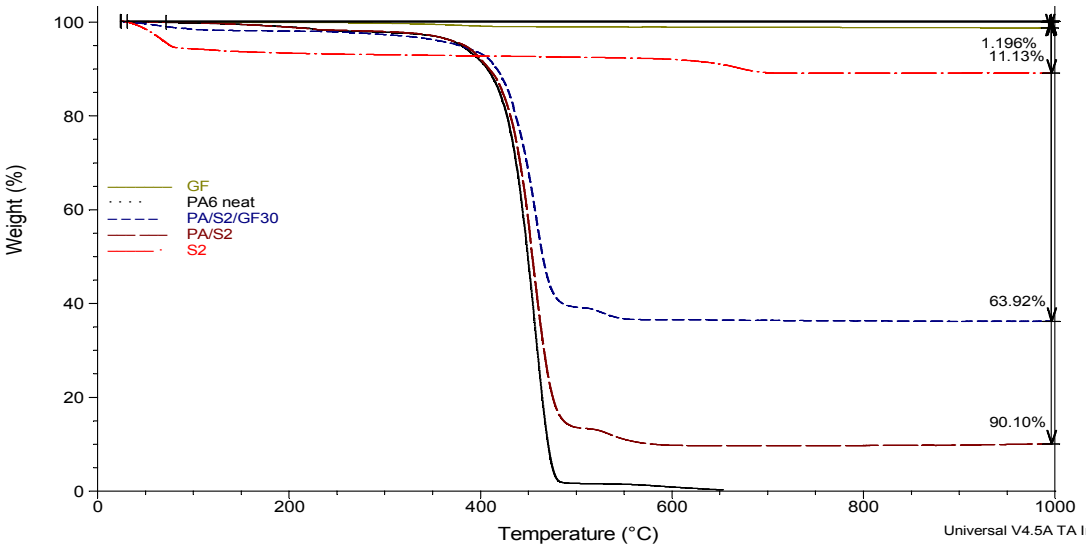

(b) Showing % weight loss of S2 and S2 related PA6 nanocomposites

Figure 7.6 TGA of neat PA6, GF, PA6/S2 and PA6/S2/GF30 nanocomposites showing percentage weight loss of the materials at 10^0C/min

For PA6/S6/GF30, it was observed that glass fibre decreased the weight loss of PA6/S6 by 27.82% while S6 with a weight loss of 24.44% and incombustible residues of 75.56%, decreased the weight loss of PA6 in PA6/S6 by 2.64% (Table 7.2). It is important to note that the weight loss observed in S6 was as a result of the drying out of the moisture and decomposition of volatile hydrocarbon on the S6 filler (see Figure 7.7).

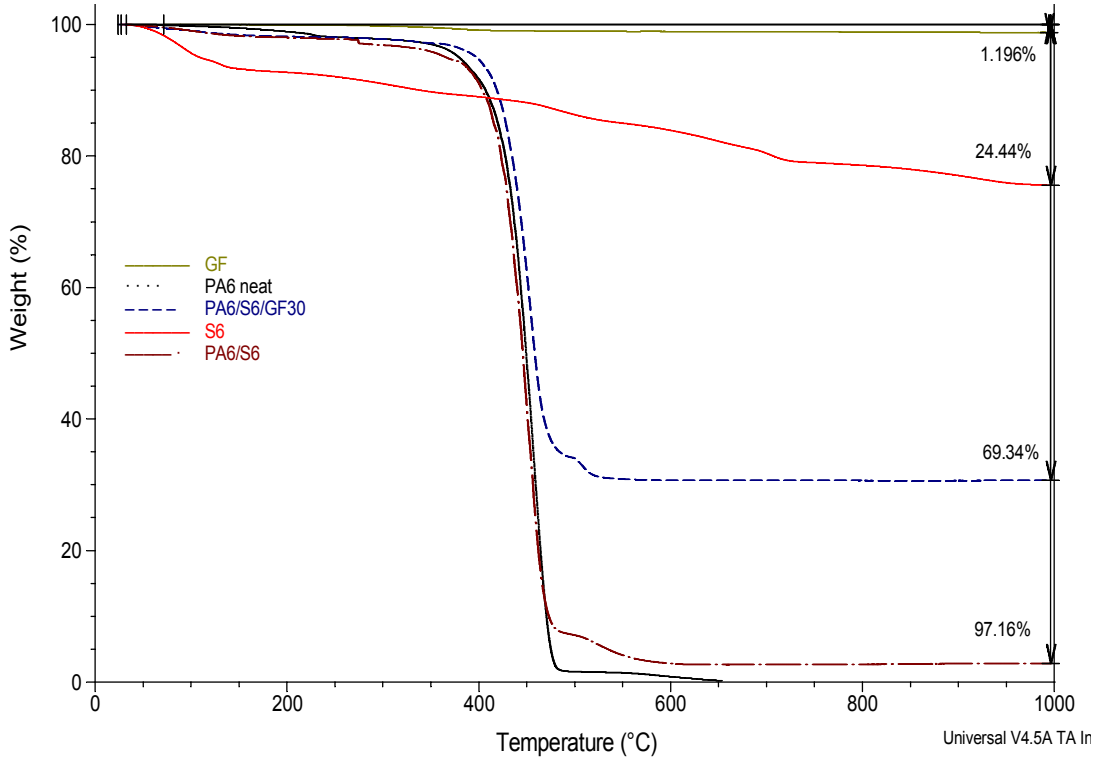

Figure 7.7 TGA of neat PA6, GF, PA6/S6 and PA6/S6/GF30 nanocomposites showing percentage weight loss of the materials at 10^0C/min

In Figure 7.8 PA6/S3/GF30 and PA6/S3/GF15, it was observed that glass fibre decreased the weight loss of PA6/S3 by 22.83% and 6.69% respectively. S3 with a weight loss of 15.21% and incombustible residues of 84.79% decreased the weight loss of PA6 in PA6/S3 by 13.51%.

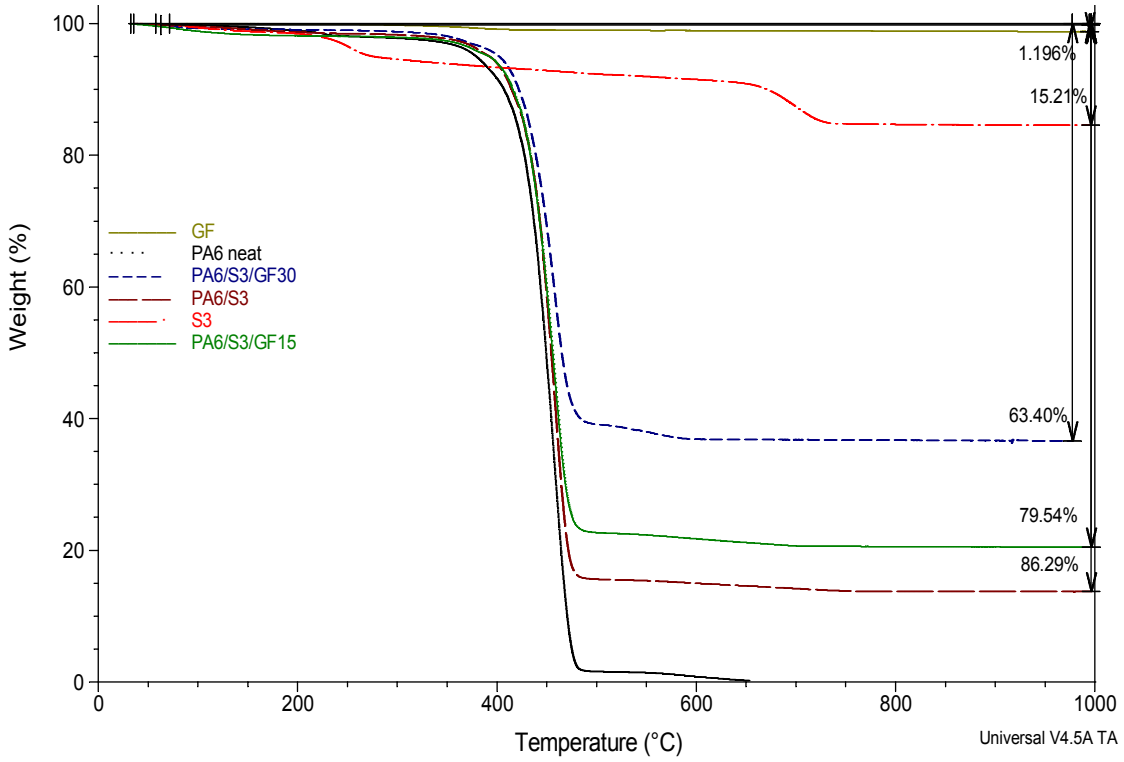

Figure 7.8 TGA of neat PA6, GF, PA6/S3 and PA6/S3/GF30 nanocomposites showing percentage weight loss of the materials at 10°C/min

Amongst the three phase composites, it was observed PA6 nanocomposite materials with organophilic fillers had a better stable thermal behaviour than the non-organophilic fillers containing PA6 materials such as PA6/S2/GF30 (Figures 7.6 a and b. From PA6/S3/GF15 and PA6/S3/GF30, it is important to note that phosphoric acid aided retarding of these materials initial degradation process as shown in Figure 7.8 compared to PA6/S4/GF30. S3 with a weight loss of 15.39% had incombustible residues of 84.61% thus, sustaining the thermal stability of the PA6/S3 and PA6/S3/GF30 materials.

In Figure 7.9 for PA6/S4/GF30, it was observed that glass fibre decreased the weight loss of PA6/S4 by 24.49%. S4 with a weight loss of 16.49% and incombustible residues of 83.51% decreased the weight loss of PA6 in PA6/S4 by 0.87%. In the first loss event, a variation of weight losses in the 2-phase materials ranged from 93.43% (PA6/S4) to 82.17% (PA6/S3). These differences in weight loss at the first degradation event within the temperature range of 324-500°C were still attributed to the fire retardant property of phosphoric acid.

However, PA6/S4 contained organic (hydrocarbon) chemical substances such as SDS and isopropanol that enhanced its degradation of 93.43% within that same temperature range. However, S4 which had a total weight loss of 16.49% and incombustible residues of 83.51% sustained the thermal stability of the PA6/S4 and PA6/S4/GF30 materials.

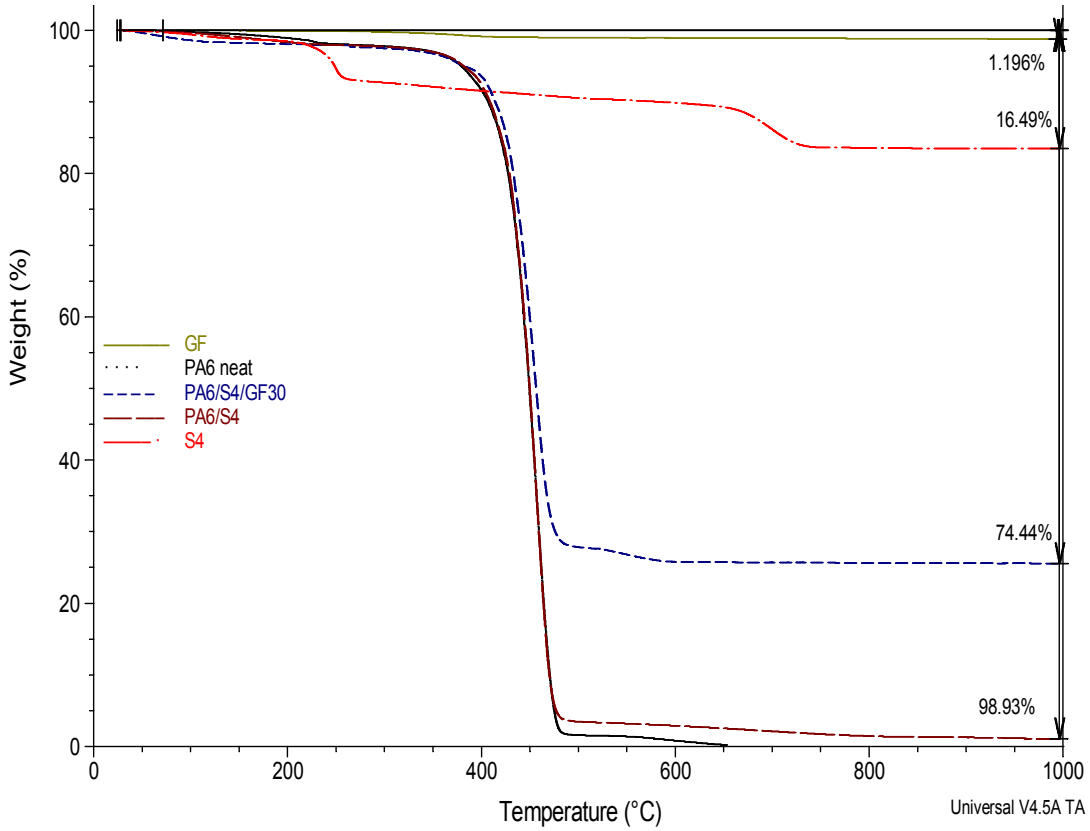

Figure 7.9 TGA of neat PA6, GF, PA6/S4 and PA6/S4/GF30 nanocomposites showing percentage weight loss of the materials at 10^0C/min

In Figure 7.10 representing PA6/S5/GF30, it was observed that glass fibre decreased the weight loss of PA6/S5 by 27.87% respectively. S5 with a weight loss of 15.69% and incombustible residues of 84.31% decreased the weight loss of PA6 in PA6/S5 by 1.23%. The PA6/S5 seems to have a lower thermal stability at its first degradation event due to the degradation of $CaCO_3$ to CaO which made the material less thermally stable and resulted in faster degradation.

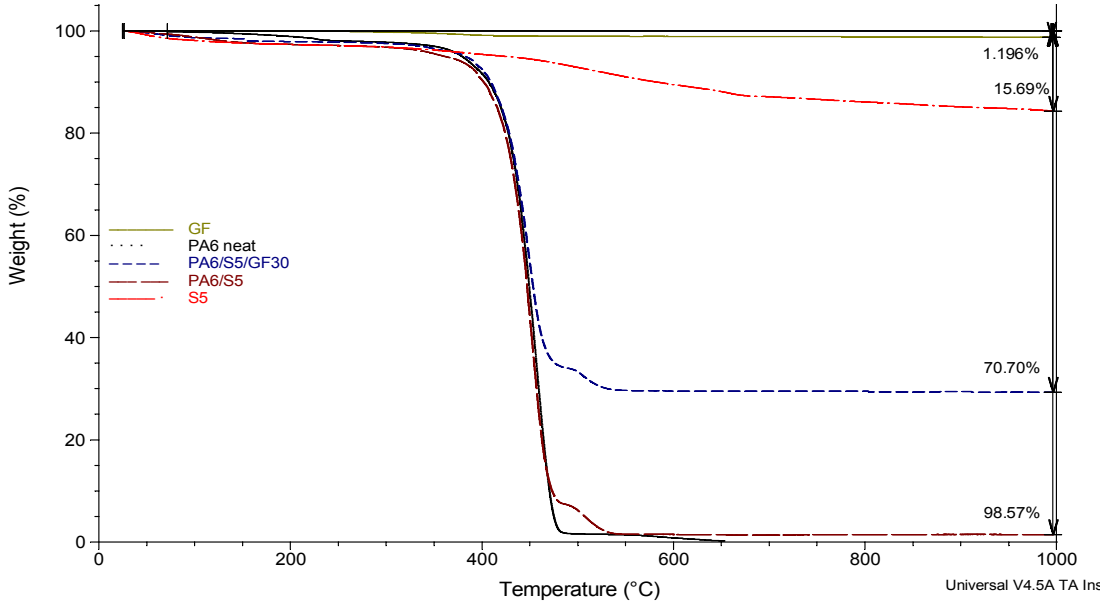

Figure 7.10 TGA of neat PA6, GF, PA6/S5 and PA6/S5/GF30 nanocomposites showing percentage weight loss of the materials at the rate of 10^0C/min

The fillers S3, S4, S5 and S6 as earlier mentioned contained barium sulphate ($BaSO_4$), sand, bentonite clay, calcium carbonate ($CaCO_3$) with melting temperatures of 1600, 1650, I500 and 825°C respectively. S6 was demulsifier washed to extract hydrocarbon resulting in the production of fillers, S3 and S4. The demulsifier S3 contained water, chitosan, poloxamer, sodium dodecyl sulphate (SDS), isopropanol and phosphoric acid - H_3PO_4 (which was used only in S3) with melting points of 0, 150-260, 53-57, 206, -88 and 42.35°C respectively. The chemical composition of the fillers and their surface modifiers had a significant impact on the weight loss of the different materials. The petroleum hydrocarbon modification on the surface of S6 was observed to increase the degradation of S6 related nanocomposites. In S2, the heating of silica in clay results in the production of vitrified glass via the partial melting of silicone dioxide or silica to increase the strength/toughness of the filler which is transferred to the PA6/S2 and perhaps other silica containing nanocomposites. Similar study results by Lu et al. (2015) of PA24/poly (styrene-co-maleic anhydride)/clay (PA24/SMA/clay) and PA6/ABS gave the same indication. The intumescent char formed by clay dispersed in PA6 in the first degradation step showed higher efficacy at decreasing thermal degradation of ABS and PA6 resulting in better combustion reduction or flame retardancy than those of PA24,

PA24/clay and PA24/SMA/clay (Lu et al. 2015). In S3, phosphoric acid was observed to help form a char that deterred burning of S3 and its related nanocomposites as earlier mention. According to Levchik, Costa and Camino (1994) the phosphate compound amidopenthyl polyphosphate (APP) catalyses the initial degradation of PA6; the thermal degradation of 5-amidopenthyl polyphosphate through constant heating resulted in the production of polyphosphoric acid and the char. In a second reaction, APP reacted with aluminum from clay to form aluminophosphate (a ceramic material at 310-560^{o}C). Thus, there was an initial degradation and weight loss caused by reactions between phosphoric acid and PA6, and phosphoric acid and clay which formed an intumescent material. The degree of first degradation step of the 3 phase nanocomposites (Figure 7.7) increased with increase in organo content from PA6/S6/GF30 (untreated oil rich filler) to PA6/S5/GF30 and then, PA6/S2/GF30 (unmodified/ no organo surface modification, see FTIR-ATR results chapter 5). The first degradation event results showed that silica has a better thermal stability than $CaCO_3$ which decomposed easily to CaO thereby distorting the thermal efficiency or stability of the composite material (Table 7.2).

PA6/S3 had a lower weight loss than PA6/S2 and PA6 due to the presence of phosphoric acid in PA6/S3. However, in Appendix D, Figure D.1 PA6/S6 and PA6/S4 had the best thermal stability before their first weight degradation event. The first degradation weight loss in the 3 phase composites was much lower compared to the 2 phase composites. This was attributed to the presence of the glass fibre (GF). The 2 phase composite of PA6/GF30 showed that the presence of the fillers had an influence on weight loss decrease/depreciation as PA6/GF30 and PA6 had the most weight loss of 76.89% and 94.48% for the first degradation event. Unlike other 2 phase composites, it was observed that the presence of GF inhibited the efficiency of fire retardant S3 in the 3-phase composite of PA6/S3/GF30 in first degradation event when compared to PA6/S2/GF30. Nevertheless, the former PA6/S3/GF30 showed decomposition at 338.11^{0}C while PA6/S2/GF30 decomposed at 322.04^{0}C. The PA6/S3/GF15 had a first degradation event with a higher weight loss of 74.41% compared to the other 3 phase composites. This was due to the lower percentage of GF it contained.

Table 7.2 Thermogravimetric analyses of the PA6, PA6 nanocomposite and Glass fibre (GF) showing the degradation events, initial degradation and end decomposition temperatures of the materials

Samples	Decomposition steps	Decomposition temperature		% Mass Loss	Residue (%)
		^{0}C Initial	^{0}C End		
PA6 resin	Total	25	1000	99.47	
(unprocessed)	1	320.83	501.46	91.17	
	2	501.46	689.57	5.153	0.53
PA6	Total	25	1000	99.80	
	1	353.44	485.77	95.13	0.2
PA6/S6	Total	25	1000	97.16	
	1	342.20	480.37	88.30	
	2	480.37	578.35	4.74	2.84
PA6/S2	Total	25	1000	90.10	
	1	334.81	499.46	83.96	
	2	499.46	581.79	3.62	9.90
PA6/S3	Total	25	1000	86.23	
	1	351.70	483.91	82.17	
	2	483.91	758.21	2.11	13.77
PA6/S4	Total	25	1000	98.93	
	1	345.74	487.76	93.43	
	2	487.76	855.26	2.364	1.07
PA6/S5	Total	25	1000	98.57	
	1	325.75	477.73	88.55	
	2	477.73	535.56	6.06	1.43
PA6/GF30	Total	25	1000	64.37	
	1	75	470	59.39	
	2	470	1000	4.69	35.63
PA6/S6/GF30	Total	25	1000	69.34	
	1	363.56	497.96	62.84	
	2	497.96	530.62	3.045	30.66
PA6/S2/GF30	Total	25	1000	63.92	
	1	322.04	488.85	55.28	
	2	488.85	555.57	2.67	36.08
PA6/S3/GF15	Total	25	1000	79.54	
	1	348.86	485.33	74.41	
	2	485.33	692.65	2.269	20.46
PA6/S3/GF30	Total	25	1000	63.40	
	1	338.11	491.32	59.02	
	2	491.32	592.64	2.383	36.60
PA6/S4/GF30	Total	25	1000	74.44	
	1	331.93	485.14	68.91	
	2	485.14	582.75	2.25	25.56
PA6/S5/GF30	Total	25	1000	70.71	
	1	320.81	485.14	63.14	
	2	485.14	539.51	4.41	29.29
GF	Total	25	1000	1.196	
	1	227.90	411.29	0.811	98.80

7.3.2 DSC results

DSC of PA6, PA6 Nanocomposites and Nanofillers

PA6 has a glass transition temperature of about 47 -50^{0}C, a melting point of 220^{0}C and a crystallisation temperature of 180^{0}C for melt compounded PA6 samples. TGA discussed earlier was used to ascertain the degradation temperature range of PA6 and its nanocomposites (see Figure 7.5). This temperature provides information required for setting DSC max temperature from about -20^{0}C below the degradation temperature of the PA6 nanocomposites (above 250^{o}C). This was carried out to prevent degradation of the PA6 nanocomposites, enable crystallisation cycle and reheating cycle for reliable DSC analysis of the PA6 nanocomposite materials as material decomposition would not permit further cooling and heating stages. The DSC analysis was carried out using a heat-cool-heat procedure.

The results of the first heating cycle could be influenced by the sample preparation and storage conditions, thus, the analysis and study of the second heating cycle is important for obtaining reproducible thermal history of the samples (Ozdilek et al 2004). Some of the PA6 nanocomposite materials had two melting events (melting points) in the endothermic phase. This section and Appendix D, Table D.1 provides information about the melting temperatures, T_m and crystallisation temperatures, T_c of the PA6 and PA6 nanocomposite materials analysed. The experimental results presented in the Figures showed that the addition of fillers increased the thermal stability of the PA6 nanocomposite materials. It was observed that the fillers generally increased the crystallisation temperature and glass transition temperatures of PA6. The differences in thermal stability of the composite materials were characteristics of the nanofiller or reinforcement type, their surface modification and percentage of glass fibre (Fu et al. 2008).

PA6 is polymorphous, possessing a stable crystalline phase called α-phase (monoclinic) which is obtainable by slow cooling the polymer from melt. On the other hand, fast cooling from the melt yields the γ-mesophase (pseudo-hexagonal). During very fast cooling also known as quenching, PA6 the amorphous phase is formed. This polymorphism is also influenced by fillers

(Jiang et al. 2005). As shown in Figure 7.11 it was observed that the melt compounded material had a single peak (dip) for each heating cycle.

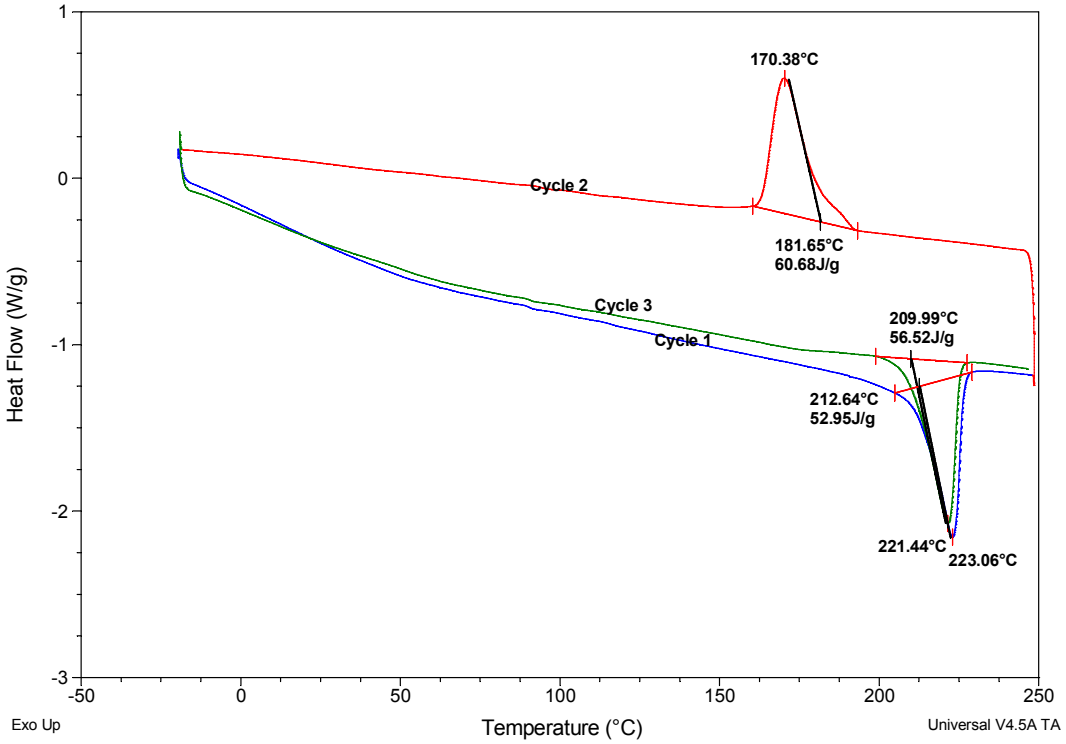

Figure 7.11 DSC thermogram of PA6 from melt compounding process showing single melting and crystallisation peaks at the rate of 10°C/min

This was opposed to the injection moulded material (Figure 7.12) which had two peaks (dips) for each melting cycle referred to as T_{m1} and T_{m2}. XRD studies showed that the injection moulded PA6 was in the γ-crystalline form (see chapter 5). Studies by Özdilek et al. (2004) showed that compression moulded neat PA6 materials produced a single α-crystalline peak during the first heating cycle. However, the second heating cycle produced two peaks, one of the γ-crystalline form and the other, an α -crystalline form. This is in contrast to Figure 7.11 where the melt compounded neat PA6 produced a single peak in the first and second heating cycles while the injection moulded (post-melt-compounded) neat PA6 produced 2 peaks in its first and second heating cycles. Hence, it was inferred that increased heating of PA6 results in γ-crystalline PA6 form. Thus, the

double heat processing of the final material by melt compounding followed by injection moulding induced the γ-crystalline PA6.

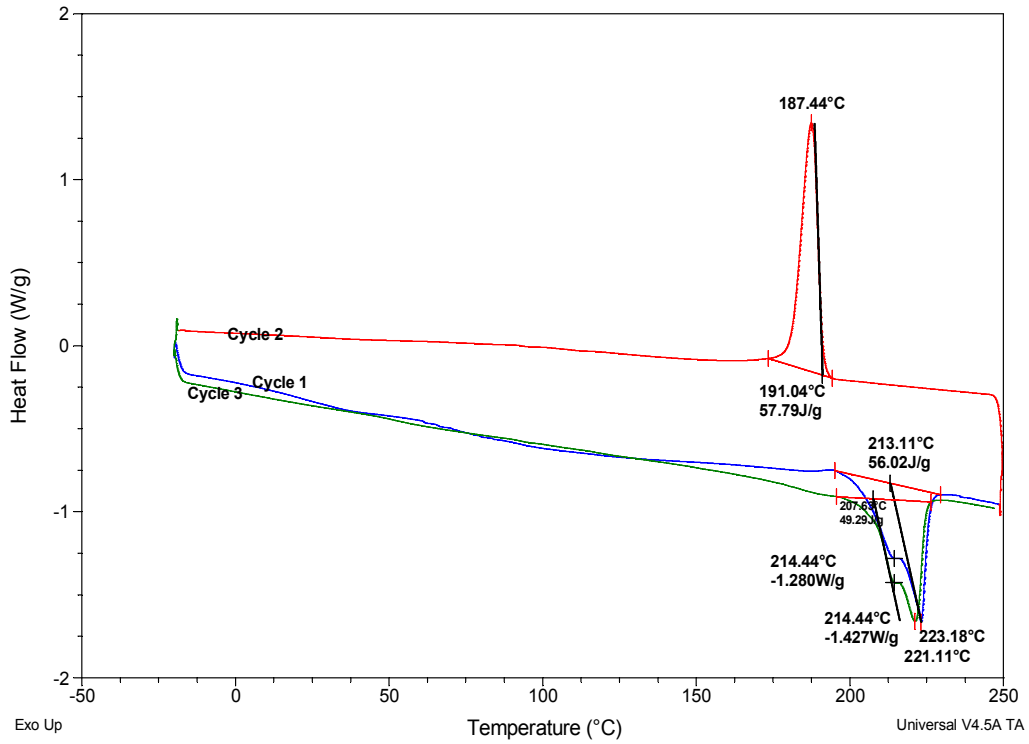

Figure 7.12 DSC thermogram of PA6 from injection moulding process showing double melting, and single crystallisation peaks at the rate of 10°C/min

From Figure 7.11 it was observed that the PA6 matrix (melt compounded) has only one melting peak at 223°C which corresponds to the α-crystalline PA6, but the glass fibre reinforced composite of injection moulding system has two melting peaks at 214.44°C and at 223.18°C (Figure 7.12). The endothermic event of the PA6/GF30, it was observed that the addition of glass fibre reduced the endothermic degradation of the material and increased the exothermic heat flow of the composite material when compared to the pristine PA6. Study of melt compounded PA6 materials by Jiang et al. (2005) showed the addition of filler/reinforcement of organophilisized montmorionite (OMMT) induced two melting peaks. According to that study, the high-temperature peak (≥220°C) relates to the α-crystalline form and the low temperature peak (≤220°C) relates to the γ-crystalline form. Subsequently, it is inferred that the addition of GF resulted in an induced γ-crystalline form as shown by XRD (see Chapter 5.5.3).

In Figure 7.13 for PA6/GF30, large portion of γ-crystalline form was formed at 220.71^{o}C in the presence of GF30 (organo modified (silane) coating). This was a similar experience to OMMT uniformly dispersed in the PA6 matrix, which has the tendency to promote the formation of smaller and numerous crystallites (Jiang et al. 2005).

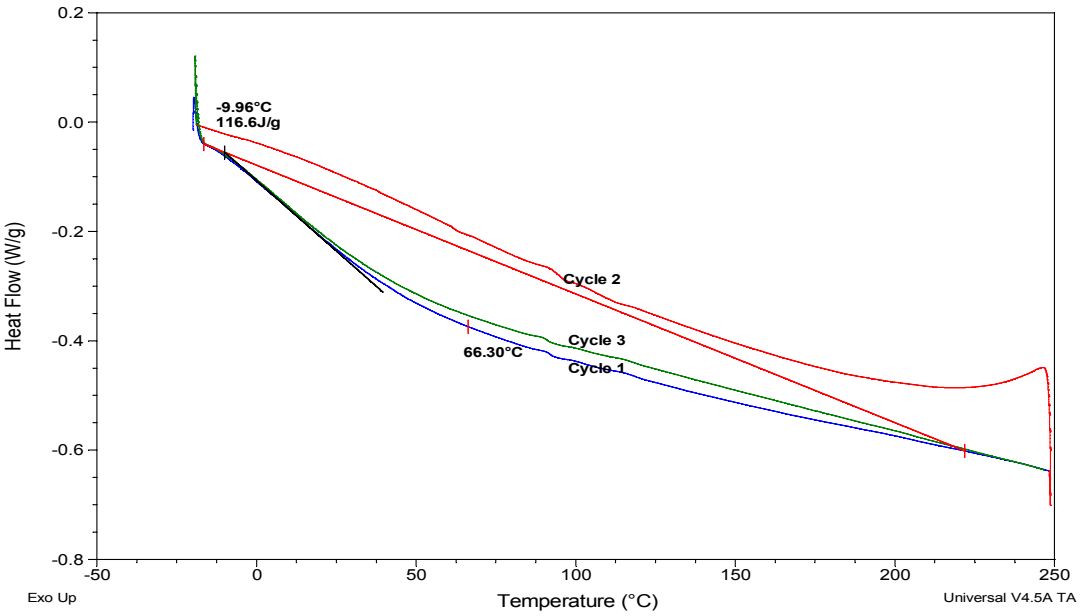

(a) Glass fibre (GF)

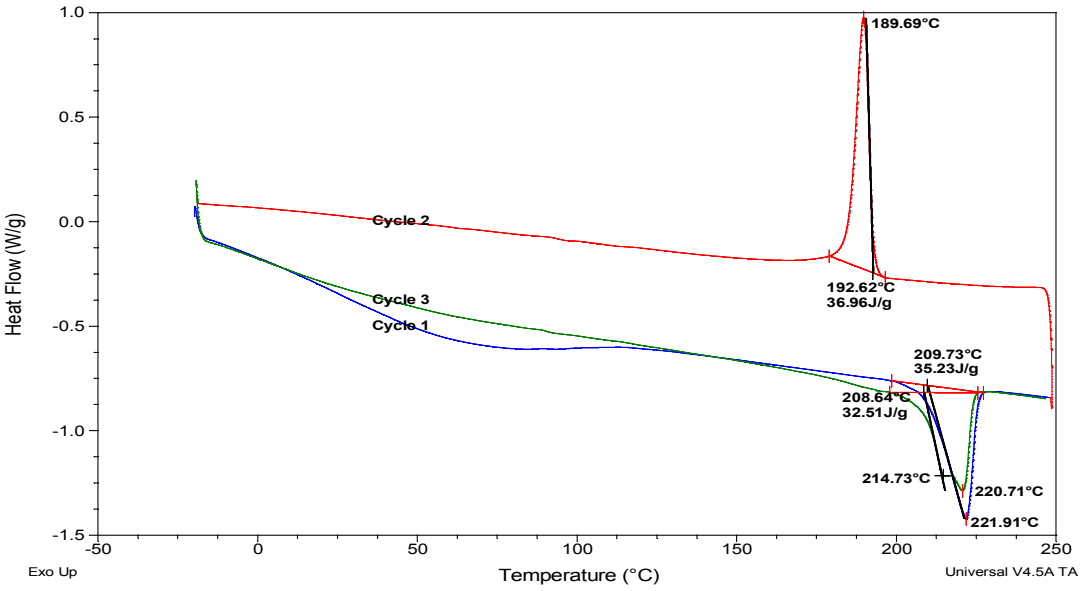

(b) PA6/GF30 composite

Figure 7.13 DSC thermogram of (a) Glass fibre (GF) and (b) PA6/GF30 composite showing melting and crystallisation peaks at the rate of 10^{o}C/min

It was observed that the addition of the filler S2 (Figure 7.14) resulted in the formation of mixed crystalline forms (α - and γ-) of PA6 as illustrated by the 2 peaks for the melting cycles in Figure 7.15.

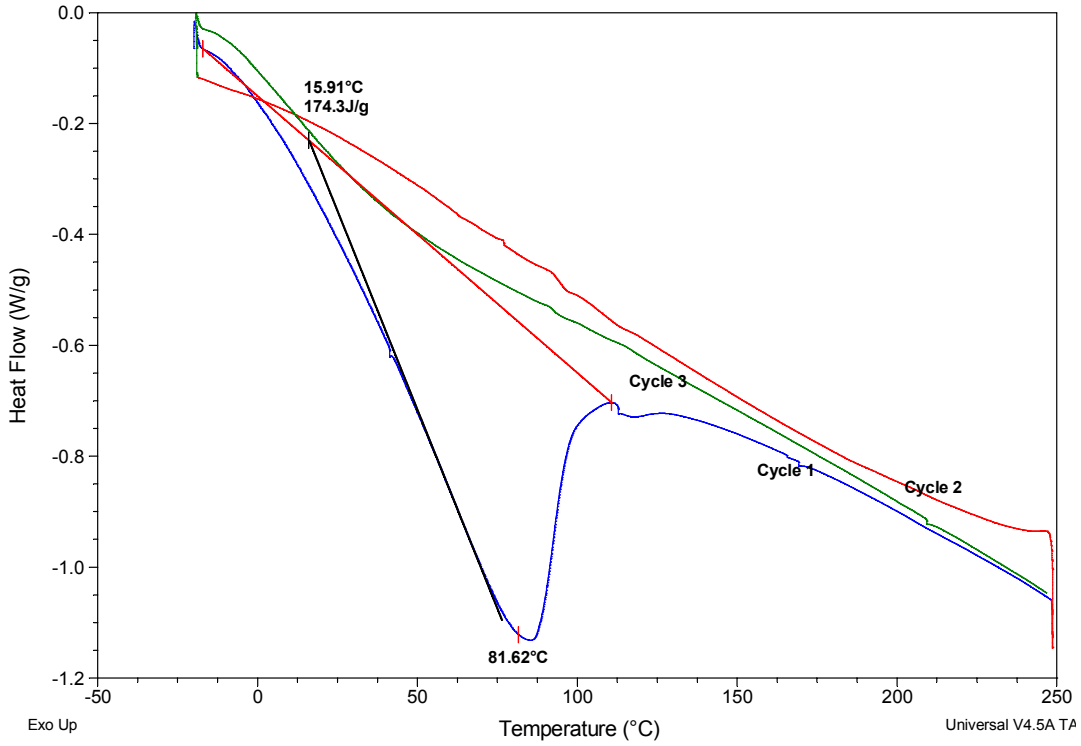

Figure 7.14 DSC thermogram of nanofiller S2 showing melting peak, no crystallisation peaks observed at the rate of 10°C/min

In Figure 7.15 the addition of filler/reinforcement (MMT) induced two different quantities of the crystalline forms of PA6 in melting cycles of PA6/S2 nanocomposite. While heating cycle 1 had a large portion α-crystalline form and a small portion of γ-crystalline form, in heating cycle 2 the reverse was the case. The reason for this is not fully understood.

On the other hand with the addition of GF to PA6/S2, it was observed that PA6/S2 had a less intense peak of γ-crystalline form (small amount of γ-crystalline form) than the α-crystalline form in the second heating cycle. This could be attributed to increase in heat and perhaps the large quantity of α-crystalline form was formed due to the presence of unmodified MMT filler homogenously dispersed in the polymer matrix (Figure 7.15).

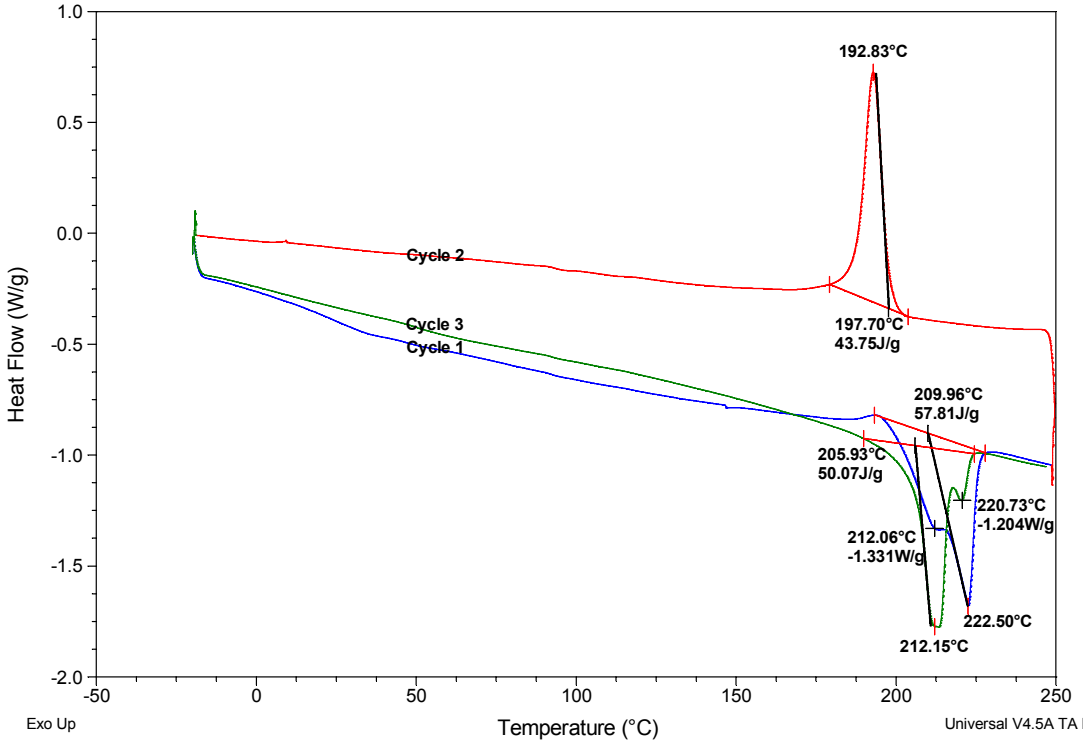

Figure 7.15 DSC thermogram of PA6/S2 composite showing melting and crystallisation peaks at the rate of 10°C/min

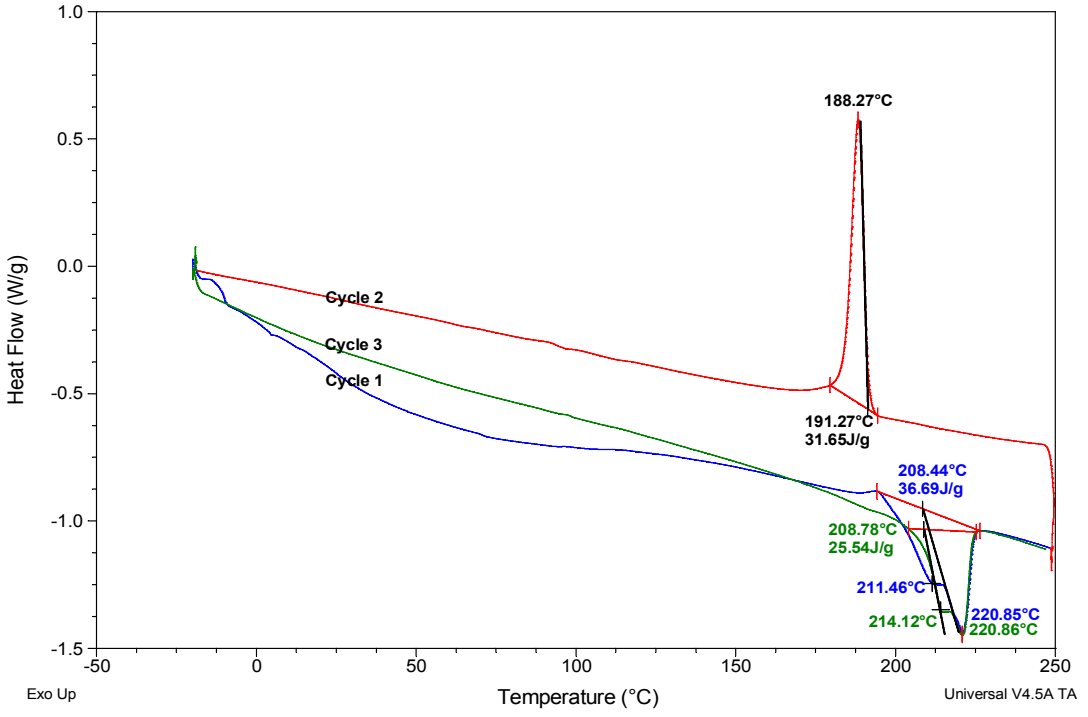

Figure 7.16 DSC thermogram of PA6/S2/GF30 composite showing melting and crystallisation peaks at the rate of 10°C/min

The DSC of the untreated drilling waste showed that it had three major endothermic events at 23°C, 86.28°C and 117.96°C. This depicted the decomposition of unknown hydrocarbon compounds within the waste sample as shown in Figure 7.17. There was no visible exothermic event for this filler.

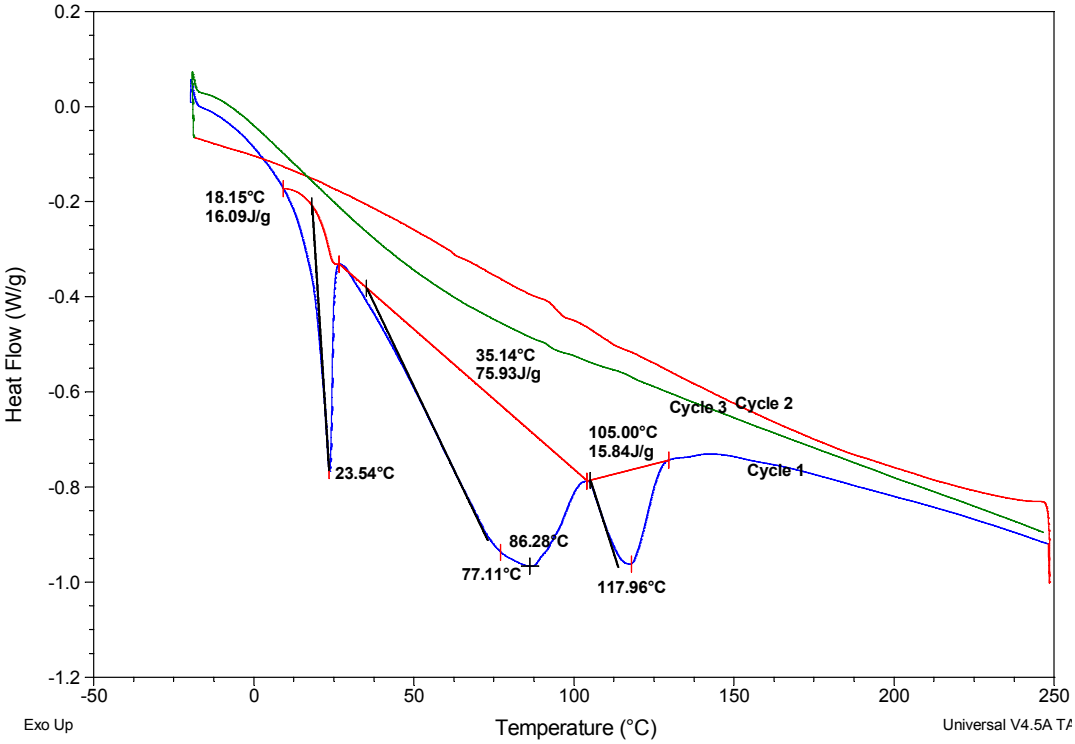

Figure 7.17 DSC thermogram of nanofiller S6 showing melting peak, no crystallisation peaks observed at the rate of 10°C/min

The DSC of the PA6/S6 in Figure 7.18 showed that it induced 2 melting peaks at 213°C and 221°C for the first heating cycle, and 207°C and 220°C for the second cycle.

However, the addition of glass fibre to the 2-phase composite, PA6/S6 yielded a material with a single melt peak at 220.56°C in the first heating cycling and double peaks in the second heating cycle (Figure 7.19).

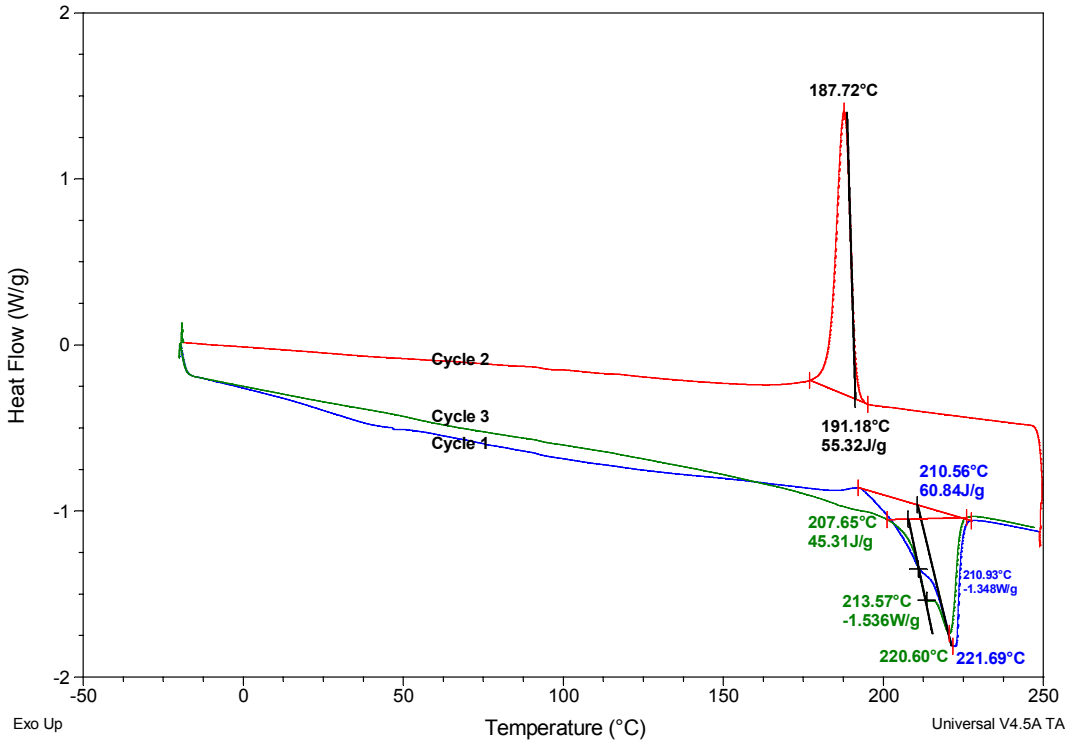

Figure 7.18 DSC thermogram of PA6/S6 nanocomposite showing melting and crystallisation peaks at the rate of 10°C/min

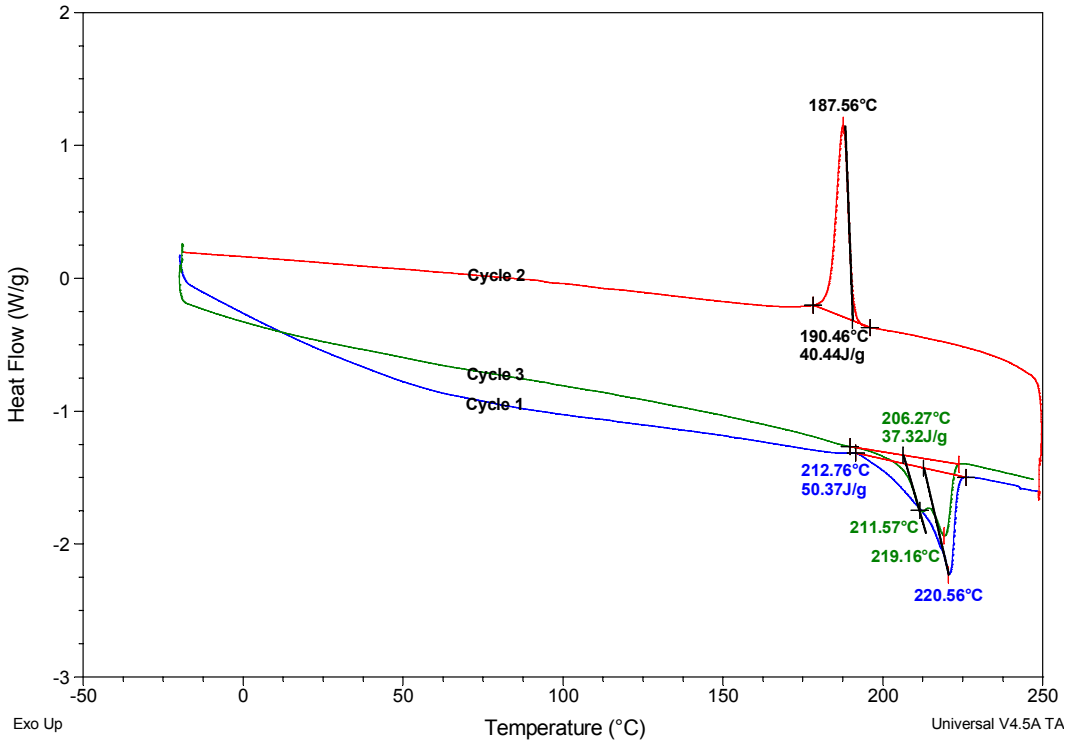

Figure 7.19 DSC thermogram of PA6/S6/GF30 nanocomposite showing melting and crystallisation peaks at the rate of 10°C/min

The change in the first heating curve (cycle 1) is attributed to the relationship between glass fibre and compound(s) in the filler (Figure 7.21), which is altered by further heating in the second heating cycle. This same characteristic single melt peak at about 220°C in the first heating cycling was observed for PA6/GF30, PA6/S3/GF15 and PA6/S3/GF30 (as seen in Figure 7.20).

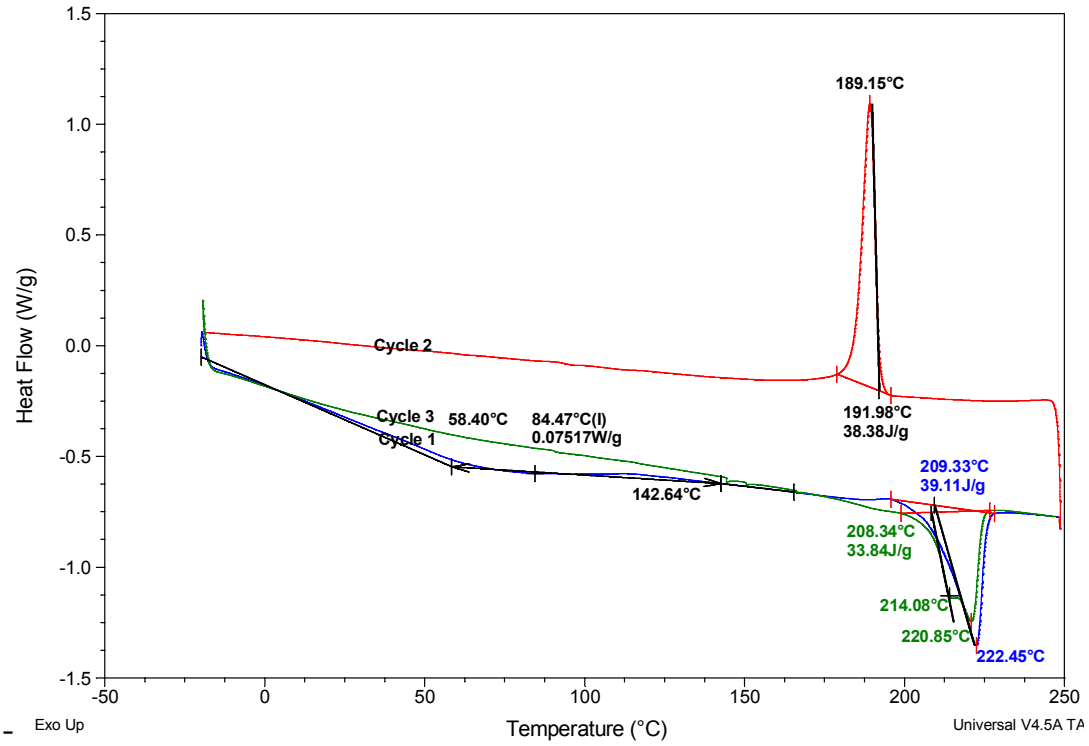

Figure 7.20 DSC thermogram of PA6/S3/GF30 nanocomposite showing melting and crystallisation peaks at the rate of 10°C/min

This is attributed to glass fibre which induces α-crystalline form of PA6 in the first heating cycle, and further heating in heating cycle 2 induced the γ-crystalline form beside the pre-existing α-crystalline form of PA6. During heating, the GF coated with an organic modifier, could have caused a faster heating (melting) of the polymer which induced the formation of only α-crystalline PA6 in PA6/GF. However, after the first heating cycle, the organo-surface modification of the glass fibre could have decomposed, thus in the second cooling stage the material melts slower therefore inducing both α- and γ- crystalline forms of PA6 (see Figure 7.13b/ Appendix D, Table D.1).

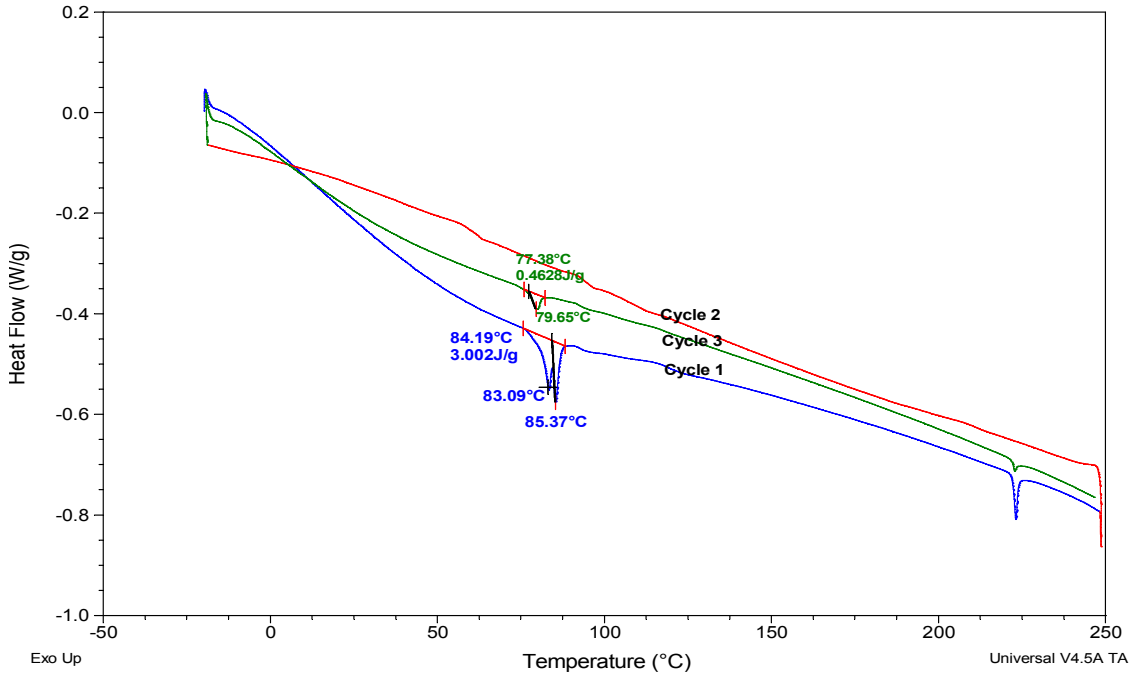

Figure 7.21 DSC thermogram of nanofiller S3 showing melting and crystallisation peaks at the rate of 10°C/min

Hence, the slight ϒ-crystalline peak for PA6/S4/GF30 in its first heating cycle (Figure 7.22). However, during the second melting cycle for PA6/S4, 3 peaks were produced: 2 α-crystalline peaks and 1 ϒ-crystalline peak. This could be due to the filler characteristic of S4 forming less stable crystallites.

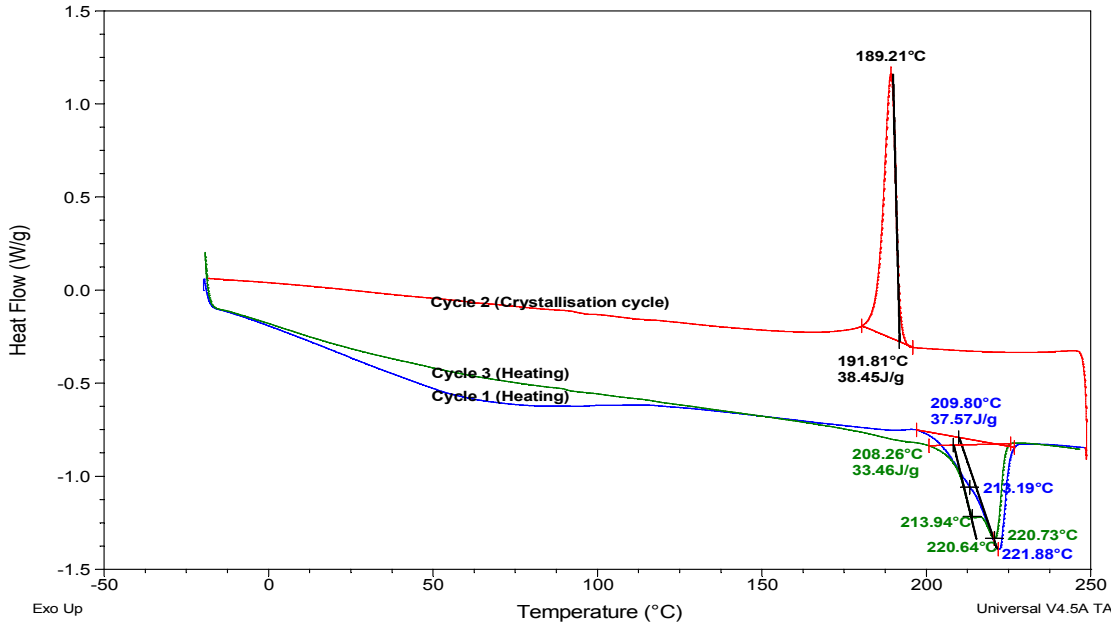

Figure 7.22 DSC thermogram of PA6/S4/GF30 showing melting and crystallisation peaks at the rate of 10°C/min

In Figure 7.22, the γ-peak being the most intense, thus, it could be attributed to the fast crystallization in the DSC. Hence, γ-crystallites could have been formed more readily since they required less reorganisation of the polymer chains. Interestingly, filler S4 (Figure 7.24) had identified compounds within it which melted at 85.9°C and 223°C, crystallised 58°C, 92°C and 211°C, thus this compound could only be decomposed at a higher temperature as shown in the DSC results. They could have influenced the high weight loss of 16.49% and 98.93% in S4 and PA6/S4 (Figure 7.24 and Figure 7.23). This unidentified compound in filler, S4 could be responsible for low stress bearing and higher strain in the PA6/S4 flexural property (Figure 6.2) as well as its ductile nature.

An assumed close similarity in filler S4 (Figure 7.24) was observed in filler S3 but with a slight difference in the first heating event (see Figure 7.21). It was observed that the peaks of unidentified compounds present in the heating cycles of S4 were present in S3, although the peaks had very low intensity in S3 compared to S4. This could be as a result of the phosphoric acid added to the demulsifier S3 used in producing S3.

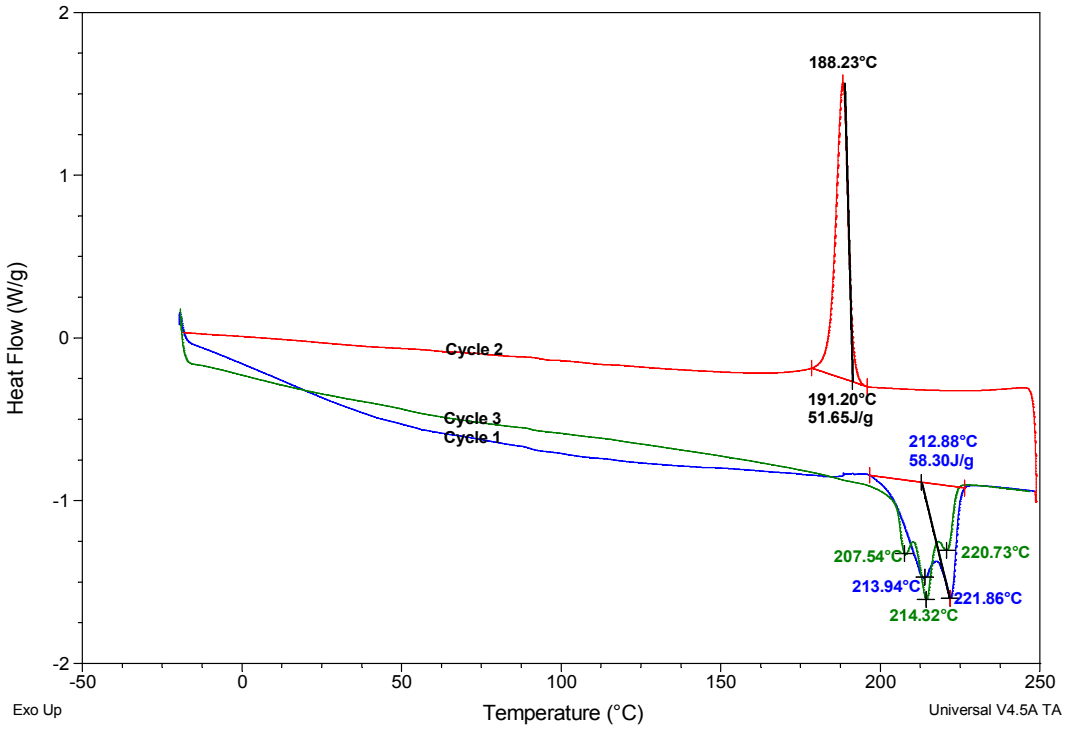

Figure 7.23 DSC thermogram of PA6/S4 showing melting and crystallisation peaks at the rate of 10°C/min

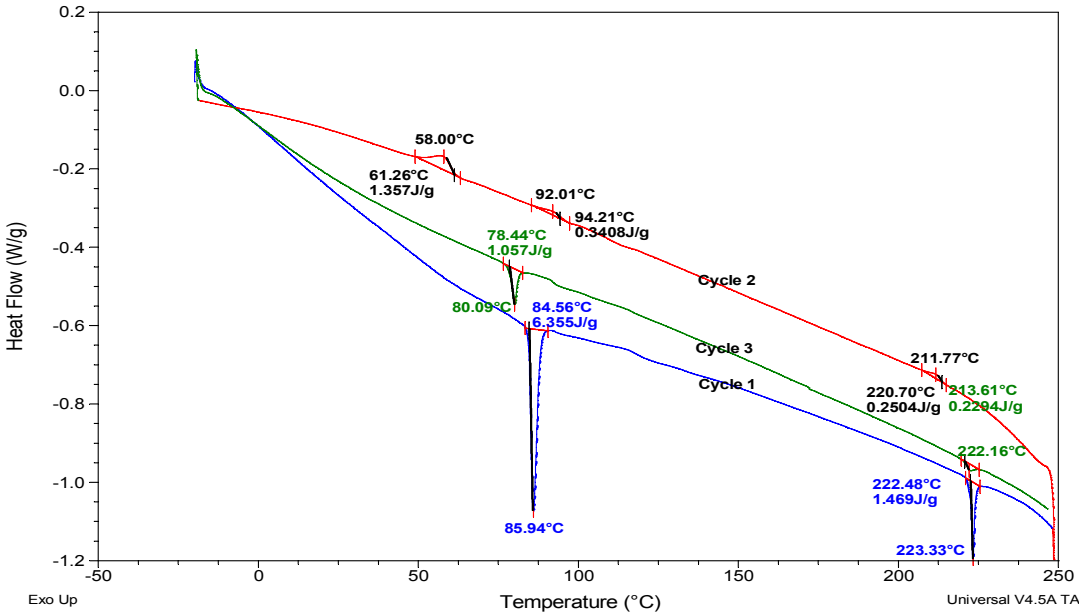

Figure 7.24 DSC thermogram of showing nanofiller S4 melting and crystallisation peaks at the rate of 10°C/min

On the other hand, nanofiller S5 which was produced from the thermal (oil extraction) treatment of ODF at 700°C produced the thermogram in Figure 7.25. The thermogram showed that there was some compound with melting point of 63°C.This compound could be hydrocarbon as shown in FTIR TPH in section 4.3.4.

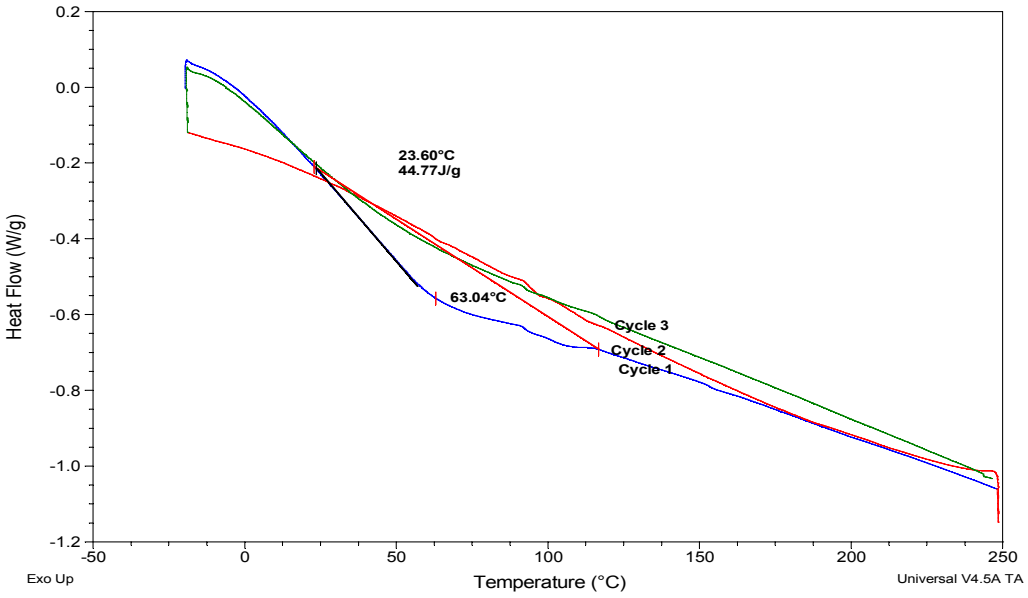

Figure 7.25 DSC thermogram of showing nanofiller S5 melting and crystallisation peaks at the rate of 10°C/min

PA6/S5 (Figure 7.26) and PA6/S5/GF30 thermal curves showed that the two melting events induced both α- and γ-crystalline forms of PA6 with the α-crystalline form being more prominent.

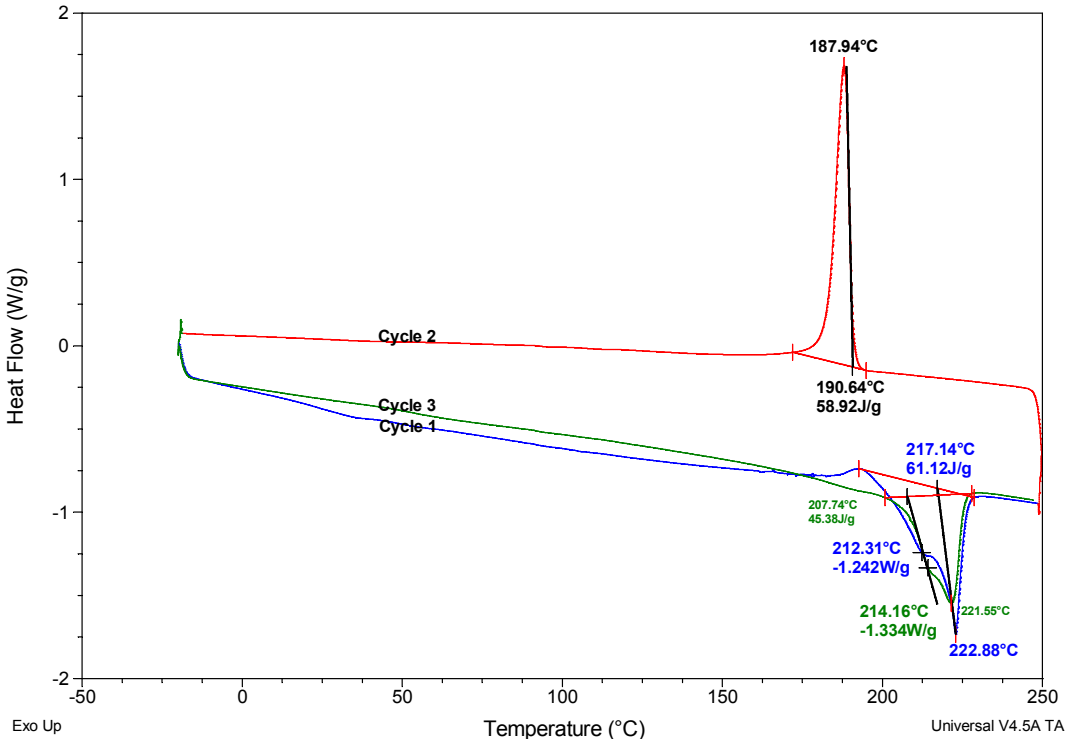

Figure 7.26 DSC thermogram of PA6/S5 showing melting and crystallisation peaks at the rate of 10°C/min

General crystallisation behaviour of the materials

The DSC thermograms in Figures 7.11-7.26 showed DSC cooling curves. The crystallisation peaks show sharp narrow peaks without signs of multiple peak formation during the crystallisation cycle. It was observed that amongst the 2 phase nanocomposite, PA6/S2 had a higher crystallisation temperature compared to other PA6 nanocomposites. This could be as a result of the absence of organo-surface modification on the filler or stronger forces of attraction between the nanofillers and PA6 matrix. The 2.5% filler addition to PA6 did not cause a great change in crystallisation temperature. This is because PA6/S2, PA6/S4, PA6/S5 and PA6/S6 had percentage change of 2.88%, 0.42%, 0.27% and 0.15% respectively, higher than PA6, the parent material. PA6/S3 had 0.17% reduction in crystallisation temperature. This was attributed to the effect of the phosphate group flame retarding component inducing a quick recrystallisation of PA6/S3.

The crystallisation temperature of this research investigated injection moulded PA6 was 187.4°C, while the nanofiller reinforced polymers PA6/S3 had crystallisation temperatures below PA6 and PA6/S2, PA6/S4, PA6/S6 and PA6/S5 had crystallisation temperature above PA6. This could be as a result of the demulsifier treatment on S3 and S4. Hence, the improved mechanical properties observed in the PA6/S3 and PA6/S4 and their glass fibre reinforced nanocomposite materials (see Chapter 6).

It was observed that GF had a marked impact on the crystallisation temperature of most of the GF reinforced composites which rose by about 2°C. However, it was observed for PA6/S6/GF30 and PA6/S2/GF30 which had lower crystallisation temperatures of 187.6°C and 188.5°C respectively; this was still above neat injection moulded PA6 at 187.4°C and neat melt compounded PA6 at 170.83°C.

7.3.3 Plasticity: Melt Flow Rate

The melt flow rate test is used as a test method for polymer quality control and assurance. It is a fast material characterisation used to assess ease of polymer flow as criteria for material quality and processability (Rides et al. 2009). There are two procedures for melt flow rate:

1. Melt Volume-Flow Rate, MVR (cm^3/10min), a measure of the ability of a volume of the molten state of a material to flow under pressure.
2. Melt Mass-Flow Rate, MFR (g/10min), a measure of the ability of a mass of the molten form of a material to flow under pressure. MFR is inversely proportional to viscosity (shear of the material) of the molten material at the conditions of the test which is dependent on the applied force.

Figure 7.27 shows the MFR and MVR results of polyamide nanocomposite materials, showing the comparison of MFR (melt mass flow rate) to MVR (melt volume flow rate) of PA6 and PA6 blends. The PA6 material had a density of 0.97 /cm^3 and melt flow index of 25.58 g/10cm^3. A closer view at the melt volume flow rate (MVR) data showed that PA6, PA6/S2, PA6/S5 and PA6/S6 have higher melt volume flow rate than PA6/S3 and PA6/S4. This could be due to easier PA6 polymer chain mobility from PA6, PA6/S2, PA6/S5, PA6/S6, PA6/S3 to PA6/S4. The mineral composition and surface modification by the demulsifier treatment

could have increased the compatibility between nanofillers (S6, S4 and S3) and PA6 matrix. Thus, resisting initial bond breaking of the nanocomposite bond unlike in the case of PA6, PA6/S2 and PA6/S5 nanocomposites.

The melt mass flow rate data showed PA6 and PA6/S2 without $BaSO_4$ had higher mass flow rates of 28.3 g/10mins and 27.9 g/10mins respectively compared to the oily drilling fluid based nanocomposites. It was observed that the melt mass flow rates of the nanocomposites PA6/S3, PA6/S4 and PA6/S6 were lower. This is due to the high melting points of 1000^{o}C and 800^{o}C for $BaSO_{4,}$ and $CaCO_3$ respectively, as well as other minerals with high melting point in the fillers which resulted in resistance to melting and flow of the molten PA6 nanocomposite material. As mentioned earlier in chapters 4 and 6, the oil extraction treatments received by the nanofillers prior to manufacture of the nanocomposites could have resulted in loss of the colloids (bentonite clay-MMT). Thus, the loss of the colloids (bentonite clay-MMT) could have increased the percentage (%) composition of $BaSO_4$ in the S3 and S4 nanofillers (see chapter 4: Figure 4.6). However, as earlier established, S5 being from a different batch of oil based drilling mud and cuttings waste could have had a different composition of minerals from S6.

MFR results suggested the possible viscosity, stiffness and curing (moulding) rate of the nanocomposites. As shown from the results, PA6 will melt and flow more than most nanocomposites. PA6/S3 and PA6/S4 would have a slow melt and flow rate, and could cure faster than the PA6 and PA6/S2.

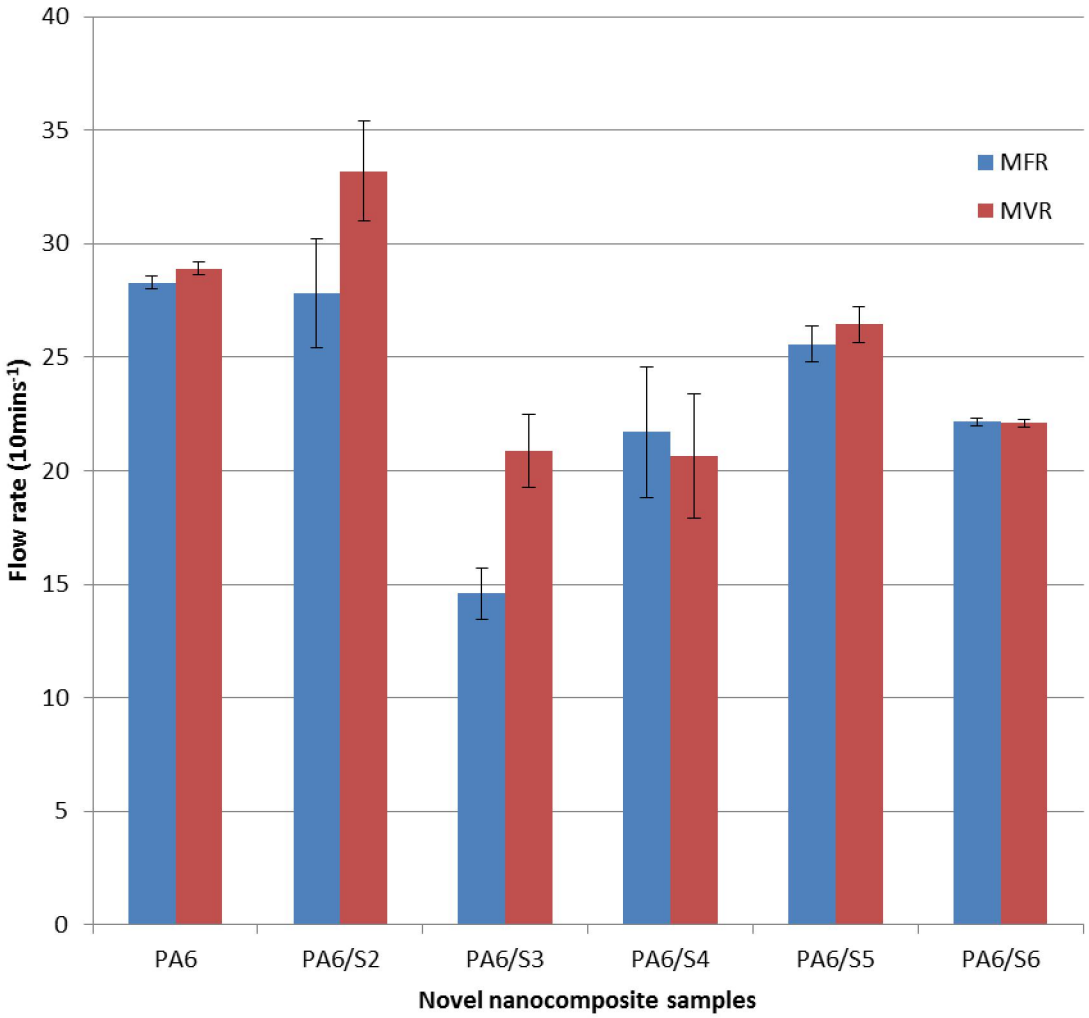

Figure 7.27 Melt mass flow rate (MFR) to melt volume flow rate (MVR) of PA6 and PA6 blends

The melt densities of PA6 and nanocomposites were obtained from the ratio of the melt mass flow rate (g/10mins) and melt volume flow rate (cm^3/10mins). Figure 7.28 showed that PA6/S2, PA6/S3 and PA6/S5 had a much lower density of 0.82g/cm^3, 0.70g/cm^3 and 0.98g/cm^3 compared to PA6/S4 and PA6/S6 with densities of 1.00g/cm^3 and 1.05g/cm^3, respectively. PA6 had a melt density of 0.97g/cm^3. It was observed generally, that the nanocomposites with lower hydrophilicity had lower densities. While the S4 and S6 containing nanocomposites were more hydrophobic fillers had higher densities (see chapter 4.3.4). The difference in the melt density PA6/S3 compared to the other nanocomposites is due to the formation of melt resistant compound during

heating which restricts the flow of PA6/S3 out of the die in given time of 10 minutes. Thus, melt volume and mass collected in 10 minutes is less compared to the other nanocomposites. It could be due to charge density of fillers and /or the forces of adhesion between the nanofillers and the polymers.

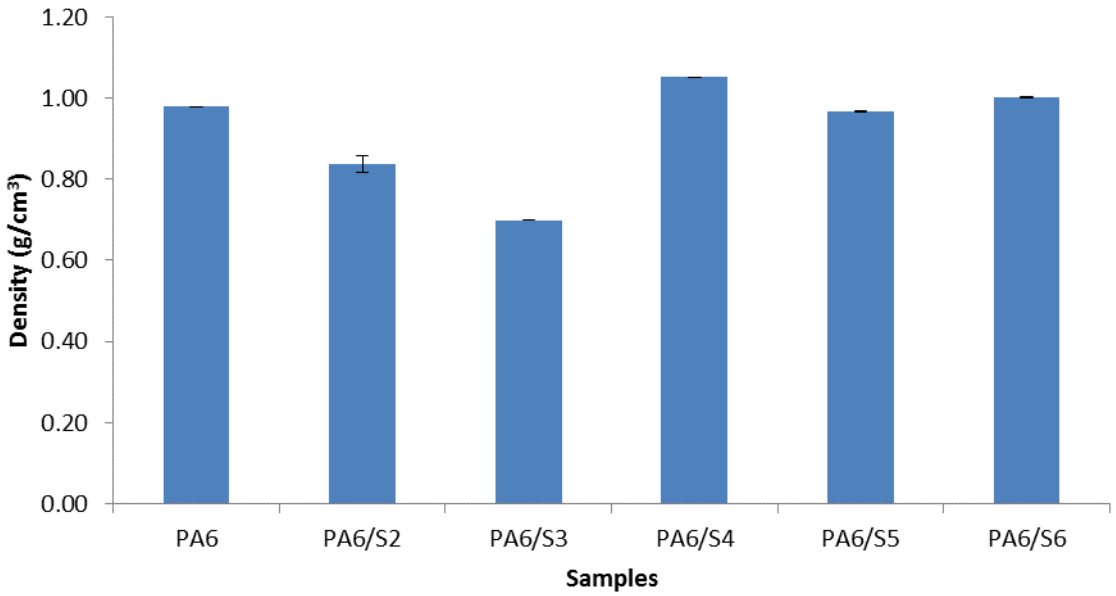

Figure 7.28 Melt densities of the PA6 and PA6 nanocomposites showing effect of filler type on melt density

7.4 Conclusion

The potential for the PA6 nanocomposites and their glass fibre nanocomposites to enhance the thermal stability of PA6 was investigated. The TGA results showed that nanofiller, S3 had improved the thermal stability of PA6 by 13.6% unlike S2 that improved PA6 by 9.7%. TGA of the glass reinforced composites showed a higher PA6 thermal stability improvement of 38.8% compared to 36.5% of PA6/S3/GF30, the best for the oil based drilling fluid and cuttings PA6 glass fibre reinforced nanocomposite. The untreated drilling fluid filled PA6 nanocomposite had the best flexural and compression properties, however, its thermal stability was about 2.7% (PA6/S6) and 30.5% (PA6/S6/GF30) compared to PA6. TGA results showed that the samples had mostly 3 levels of degradation phases which was used to assess their initial, intermediate and final thermal phase and temperature range for their stability. This information would be useful for designing potential engineering applications for the different composites. DSC

results showed that PA6 resin and PA6 injection moulded samples differed in crystallisation temperature and melting temperatures. The former and later had crystallisation temperatures of 170^{o}C and 187^{o}C respectively and melting temperatures of 212^{o}C and 223^{o}C for heating cycle 1 and melting temperatures of 221^{o}C and 221^{o}C for heating cycle 2. The 2 phase nanocomposites generally, had melting points in heating cycles 1 and 2 range between 220^{o}C and 223^{o}C while the 3-phase nanocomposites had melting points in heating cycles 1 and 2 range between 211.6^{o}C (PA6/S6/GF30) and 22.98^{o}C (PA6/S3/GF15). The plasticity and melt density results showed that PA6/S3 had the lowest MFR of 14.6 g/10mins and melt density of 0.75g/cm^{3}. Thus, PA6/S3 would melt and flow slower during processing and cure faster than the other PA6 nanocomposites. However, PA6/S3 would be a unique material for fast curing.

Chapter 8

Conclusion and future work

8.1 Conclusion

Oil based drilling fluid and drilling cuttings are oily hazardous waste that have negatively impacted flora, fauna and have a global carbon footprint . Experience has shown that some of the methods adopted by oil companies to manage these wastes are harmful and unfriendly to the environment. Research results have also shown that oil based drilling fluids and drilling cuttings can be useful if properly managed. In this research therefore, effort was made to formulate new and more ecofriendly chemical process (demulsifiers) for more effective management of oil waste. Effort was also made to recycle the solid residues after demulsification into useful engineering materials. At the end of the experiments and based on the findings of this research, it was concluded that:

- The experimental processes and procedures adopted in the conduct of this research led to a successful formulation of new and more ecofriendly demulsifiers for treatment of oil based drilling fluid. Two demulsifiers were formulated for the oil remediation of the oil based drilling fluid and cuttings. The demulsifier formula included biosurfactant (chitosan - cationic surfacatant), surfactants (sodium dodecyl sulphate - anionic surfactant, poloxamer – non-ionic surfactant), salt (sodium chloride), co-solvent (isopropanol) and an acid (phosphoric acid for demulsifier S3 only). Demulsifiers were formulated to ensure chemically enhanced phase separation of the oil based drilling fluid with cuttings into oil, water and solid components as well as surface modification of the solid residues for improved thermal stability of PA6 nanocomposite. The optimum demuisifier mixture was ISP - 2.5%v/v, SDS - 4.2 g/L, poloxamer - 1.3 g/L, NaCl - 1.7g/L, 3ppm LMWC in 0.2M acetic acid - 1.7%v/v for S3 and S4 nanofiller extraction and an addition of phosphoric acid - 2.8%v/v for S3 only.

- Demulsification of spent oil based drilling fluids and cuttings was successfully carried out using the newly formulated demulsifiers. While the pH for one of the demulsifiers was neutral, the phosphoric acid modified demulsifier was acidic with a pH of 4. The hydrocarbon reduction on the solid phase was 98.6% and 98.5% after demulsification using the demulsifier S4 and demulsifier S3 respectively. The hydrocarbon reduction could be further improved by washing of the demulsifier treated solid residues with water which was not carried out. In this study, the critical micelle concentration of the demulsifier S4 was assumed to be ~ 20 mg/L which enhanced reduction of interfacial bonding between oil and water, and, oil and solids. On the other hand, the hydrogen ions from the phosphoric acid facilitated hydrolysis of the oil from water phase and solid phase with the demulsifier not having a critical micelle concentration.

- The recovered solid phase obtained after demulsification were successfully recycled as nanofillers for PA6 nanocomposite manufacture. The use of drilling fluid and drill cutting (low-density solids) in the formulation of different blends of PA6 nanocomposite materials from untreated, chemically treated and thermally treated drilling fluid and cuttings was successfully achieved. SEM images revealed nanometer and micrometer sizes of the nanofillers in nanocomposites ranging from 249 - 790nm, and 1 - <500μm respectively. For the PA6 nanocomposites, EDXA showed presence of Ba, Al, Si, Fe and some other elements present from the nanofillers. Similarly, the XRD study of spent drilling fluid the nanofillers showed they were composed of barium sulphate, bentonite, calcium carbonate, and silica. XRD diffractograms showed that the presence of fillers produced a more amorphous material especially with the addition of 30% wt. glass fibre.

- Polyamide 6 composites reinforced with untreated and treated oil based mud and drill cutting showed varying mechanical properties. It was established that 2.5% wt. of fillers S3, S4, S5 and S6 in the PA6 2-phase nanocomposite samples were good fillers for improving the mechanical properties of PA6. The compressive properties (modulus and strength) of

PA6 were enhanced by about 90% with the addition of the S5 nanofiller. Flexural strength and modulus results for the PA6 2-phase composites suggested that the presence of layered structures such as clay in the nanofiller improved the intercalation of nanofiller in the PA6 matrix. The higher percentage of nanoclay in S2 increased hardness and compressive modulus of nanocomposites compared to S6 nanocomposites. It was discovered that surface modification with crude oil in untreated filler improved mechanical properties of PA6/S6 and PA6/S6/GF30 due to enhanced nanoclay and filler interaction with polyamide. Therefore, the different compositions and treatments of the nanofillers and presence of GF had impacted bonding of GF, resulting in great differences in the flexure, compression and hardness performance of the samples. The addition of 15% and 30% wt. glass fibre to the nanocomposites generally increased the flexural and compressive properties of PA6. However, the hardness showed some lower values for the glass fibre reinforced materials which was not fully understood and requires potential future investigation. The flexural and compression test data showed that the untreated filler improved the mechanical properties of PA6 compared to the chemically and thermally treated fillers.

Surface modification increased interfacial bonding between PA6 polymer matrix and the nanofiller; thus, produced more efficient PA6 materials.

- The TPH concentrations of the demulsifier washed solid residues S3 and S4 met the OSPAR regulations of 1%w/w, thus, conforming and complying with OSPAR standards. The elemental analysis by ICPOES showed that S3 had less of Si, Al, Mg, Fe, Mn, Zn, Cu, Cr and Ti than S4. On the other hand, S3 had more Ba, Ni, P and S of 69.4%, 57.7%, 82% and 38.6% respectively; and 23.4% less Si than S4 nanofiller, whereas As, Cd, Hg and Co were not detected in both nanofillers. S5 had much more of Al, Mg, Fe, Mn, Zn, Cu, Ni, Cr, Pb, Ti, Co, S and least Si compared to the other treated nanocomposites. All the nanofillers S2-S5 were below or within the OSPAR threshold for Zn, Cu (except S5 of 98mg/kg) and Ni. However, S2 was within OSPAR thresholds for Cr, and Pb with the exception of S3-S6.

The phosphoric acid content of demulsifier S3 treatment resulted in the surface modification of the nanofillers and enhanced thermal stability and mechanical properties of PA/S3 and PA6/S3/GF30 nanocomposite.

- It was observed that nanofillers improved the load bearing capacity of PA6. S6 nanofiller PA6 nanocomposites and glass reinforced nanocomposites had the best overall mechanical properties amongst the PA6 nanocomposites. PA6/S6 and PA6/S6/GF30 had the best flexural strength, and compression strength and modulus. This was as a result of the hydrocarbon surface modification on the untreated drilling fluid nanofiller which increased the interfacial bonding between the nanofillers and the PA6 matrix. The surface modifications on PA6/S3/GF30, PA6/S4/GF30 and PA6/S6/GF30 improved the flexural load bearing capacity of PA6 amongst the glass reinforced PA6 nanocomposites.

- The use of nanofillers and their glass fibre to enhance the thermal stability of PA6 was investigated. The TGA results showed that nanofiller, S3 had improved the thermal stability of PA6 by 13.6% unlike S2 that improved PA6 by 9.7%. This was due to the presence of the phosphoric acid surface modification on the filler. TGA of the glass reinforced nanocomposite PA6/S3/GF30 showed a higher PA6 thermal stability improvement of 36.4% compared to 35.9% of PA6/S2/GF30. The untreated drilling fluid filled PA6 nanocomposite had the best flexural and compression properties, however, its thermal stability was about 2.7% (PA6/S6) and 30.5% (PA6/S6/GF30) compared to PA6. TGA results also showed that the PA6 samples had mostly three degradation phases which were used to assess their initial, intermediate and final thermal phase and temperature ranges for their stability. DSC results showed the 2 phase nanocomposites had melting points in heating cycles 1 and 2 range between 220^{o}C and 223^{o}C, while the 3-phase nanocomposites had melting points in heating cycles 1 and 2 range between 211.6^{o}C (PA6/S6/GF30) and 222.45^{o}C (PA6/S3/GF30). The plasticity and melt density results showed that PA6/S3 had the lowest MFR of 14.6 g/10mins and melt density of 0.75g/cm^{3}. Thus, PA6/S3 would melt and flow slower during processing

and cure faster than the other PA6 nanocomposites. Therefore, PA6/S3 would be a unique material for fast curing.

The recycling of treated drilling fluid into polyamide composites has not been published. The application of untreated and treated oil based mud and drill cutting as nanofiller in plastic or elastomeric polymer has also not been (earlier) published which make this research novel and a viable option for sustainable environmental management in oil producing and processing locations.

8.2 Contribution to knowledge

Arising from the above, this research has made contributions to knowledge in the following areas:

- Formulation of a demulsifier purposeful for improving the thermal stability of PA6 nanocomposites;
- Formulation of a demulsifier purposeful for the extraction of oil water and solids; formulation of a demulsifier purposeful for the extraction of colloids;
- Method of using recycled solids from drilling fluid as a filler for PA6 nanocomposite manufacture;
- Method of extraction and surface modification of nanofillers;
- Understanding the effect of different (spent oil based drilling fluid and drill cuttings) filler type on the mechanical and thermal properties of PA6;
- Understanding the effect of the demulsifier choice on the thermal properties of PA6, and
- Provide understanding of interfacial bonding improvement between the drilling waste filler and PA6 polymer through surface modification.
- Provide evidence for the immobilisation of Pb using polyamide 6

8.3 Recommendations and future work

8.3.1 Recommendations

Based on the findings of this research, the following recommendations were made:

- Characterisation of oil recovered after treatment may be explored to ascertain degree of deviation from original state.

- Optimisation of the demulsifier perhaps through composition alteration to prevent froth production. This could improve mechanical properties of S3 nanocomposites to surpass S6 nanocomposites.
- The ratio of nano sized solid residues could be further increased by mechanical processes such as ball milling to further enhance PA6 mechanical properties.
- To ensure enhanced glass fibre alignment during manufacturing, it is recommended that a shaker feeder feed the glass fibre in the melt compounding/extrusion stage.
- Application of higher temperature during injection moulding stage of PA6 nanocomposite manufacture is recommended as this could improve melt compounded pellet melting and in the long run improve compressive and perhaps hardness properties of the glass fibre reinforced nanocomposite materials.
- Further leachability tests based on acid, base and hydrocarbon exposure for the determination of other applications of the novel nanocomposites are recommended.

8.3.2 Suggestion for future work/research

Considering the scope of this research, it is suggested that future researches should be conducted in the following areas:

- Investigations into the effect of more dilute concentrations of the demulsifiers on surface modification and hydrocarbon reduction.
- Investigation of the effects of enhancement additives and properties such as temperature and pH in optimising the efficacy of the developed demulsification process.
- Ascertaining the turbidity, TPH and ICPOES elemental concentrations of all solid and water phase obtained by individual treatment package.
- Investigation into the effect of variation of filler percentages such as 5%, 7.5%, and 10% in the manufacturing of the nanocomposites in terms of their mechanical and thermal properties would be explored.

- Improving the thermal properties of PA6/S6 and PA6/S6/GF30 is a potential future work since these polymer nanocomposites have shown the best mechanical properties amongst the investigated polymer nanocomposites. The thermal improvement of PA6/S6 and PA6/S6/GF30 could be achieved by adding a flame retardant such as phosphorous which was utilised in PA6/S3, PA6/S3/GF15 and PA6/S6/GF30.

REFERENCES

ABBE, O.E., GRIMES, S.M. and FOWLER, G.D., (2011) Decision support for the management of oil well drill cuttings, *Proceedings of the Institution of Civil Engineers-Waste and Resource Management* 2011, ICE Publishing, pp. 213-220.

ABBE, O.E., GRIMES, S.M., FOWLER, G.D. and BOCCACCINI, A.R., (2009) Novel sintered glass -ceramics from vitrified oil well drill cuttings. *Journal of Materials Science,* **44**(16), pp. 4296-4302.

ABDUL-RAHEIM, M., ABDEL-RAOUF, M., MAYSOUR, N.E., EL-KAFRAWY, A., MEHANY, A.Z. and ABDEL-AZIM, A., (2013) Some Sugar Fatty Ester Ethoxylates as Demulsifiers for Petroleum Sludge. *Journal of Surfactants and Detergents,* **16**(3), pp. 377-387.

ABEND, S., BONNKE, N., GUTSCHNER, U. and LAGALY, G., (1998) Stabilization of emulsions by heterocoagulation of clay minerals and layered double hydroxides. *Colloid and Polymer Science,* **276**(8), pp. 730-737.

ADEGBOTOLU, U., NJUGUNA, J., POLLARD, P. and YATES, K., (2014) Waste to Want: Polymer nanocomposites using nanoclays extracted from Oil based drilling mud waste. *IOP Conference Series: Materials Science and Engineering,* **64**(1).

ADEM, E., BURILLO, G., DEL CASTILLO, L., VÁSQUEZ, M., AVALOS-BORJA, M. and MARCOS-FERNÁNDEZ, A., (2014) Polyamide-6: The effects on mechanical and physicochemical properties by electron beam irradiation at different temperatures. *Radiation Physics and Chemistry,* **97**, pp. 165-171.

ADEWOLE, G.M., ADEWALE, T.M. and UFUOMA, E., (2010) Environmental aspect of oil and water-based drilling muds and cuttings from Dibi and Ewan off-shore wells in the Niger Delta, Nigeria. *African Journal of Environmental Science and Technology,* **4**(5), pp. 284-292.

AGUILERA, M.A., BROITMAN, B.R. and THIEL, M., (2016) Artificial breakwaters as garbage bins: Structural complexity enhances anthropogenic litter accumulation in marine intertidal habitats. *Environmental Pollution,* **214**, pp. 737-747.

AL-ANSARY, M.S. and AL-TABBAA, A., (2007) Stabilisation/solidification of synthetic petroleum drill cuttings. *Journal of hazardous materials,* **141**(2), pp. 410-421.

ALI, H.A.A., (2012) Preparation and evaluation of demulsifiers agents for Basra crude oil. *Applied Petrochemical Research,* **1**(1), pp. 29-33.

ALMERAS, X., LE BRAS, M., HORNSBY, P., BOURBIGOT, S., MAROSI, G., KESZEI, S. and POUTCH, F., (2003) Effect of fillers on the fire retardancy of intumescent polypropylene compounds. *Polymer Degradation and Stability,* **82**(2), pp. 325-331.

ANDRADE, P.F., AZEVEDO, T.F., GIMENEZ, I.F., FILHO, A.G.S. and BARRETO, L.S., (2009) Conductive carbon–clay nanocomposites from petroleum oily sludge. *Journal of hazardous materials,* **167**(1–3), pp. 879-884.

AZIM, A.A.A., ABDUL-RAHEIM, A.M., KAMEL, R.K. and ABDEL-RAOUF, M.E., (2011) Demulsifier systems applied to breakdown petroleum sludge. *Journal of Petroleum Science and Engineering,* **78**(2), pp. 364-370.

BALSON, T.G., 2003. Something old, something new: a discussion about demulsifiers, *Chemistry in the oil industry VIII* 2003, Royal Society of Chemistry, pp. 226.

BANSAL, A., YANG, H., LI, C., CHO, K., BENICEWICZ, B.C., KUMAR, S.K. and SCHADLER, L.S., (2005) Quantitative equivalence between polymer nanocomposites and thin polymer films. *Nature materials,* **4**(9), pp. 693-698.

BANSAL, K. and SUGIARTO, S., (1999) Exploration and Production Operations-Waste Management A Comparative Overview: US and Indonesia Cases. *SPE Asia Pacific Oil and Gas Conference and Exhibition* 1999, Society of Petroleum Engineers.

BARKER, S.A., (2013) Suspensions. In: M.E. AULTON and K.M.G. TAYLOR, eds, *Aulton's Pharmaceutics. The design and manufacture of medicines.* pp. 416-434.

BECKETT, A. and STENLAKE, J., (1976) *Practical pharmaceutical chemistry: Part two.* Athlone Press University of London, London, UK.

BENKA-COKER, M. and OLUMAGIN, A., (1996) Effects of waste drilling fluid on bacterial isolates from a mangrove swamp oilfield location in the Niger Delta of Nigeria. *Bioresource technology,* **55**(3), pp. 175-179.

BENKA-COKER, M.O. and OLUMAGIN, A., (1995) Waste drilling-fluid-utilising microorganisms in a tropical mangrove swamp oilfield location. *Bioresource technology,* **53**(3), pp. 211-215.

BHATNAGAR, A., KHANDELWAL, M. and RAO, K.U.M., (2010). Enhancing diamond drilling performance by the addition of non-ionic polymer to the flushing media. *Mining Science and Technology (China),* **20**(3), pp. 400-405.

BILLANY, M.R., (2007) Suspensions and emulsions. In: M.E. AULTON, ed, *Aulton's pharmaceutics: the design and manufacture of medicines.* 3rd edn. Churchill Livingstone Elsevier, pp. 383-405.

BIN MERDHAH, A., (2010). Inhibition of Calcium Sulfate and Strontium Sulfate Scale in Waterflood. *SPE Production & Operations,* **25**(04), pp. 545-552.

BIRON, M., (2016) 5 - Avoid Some Pitfalls. In: M. BIRON, ed, *Material Selection for Thermoplastic Parts.* Oxford: William Andrew Publishing, pp. 209-230.

BOURBIGOT, S., DEVAUX, E. and FLAMBARD, X., (2002) Flammability of polyamide-6/clay hybrid nanocomposite textiles. *Polymer Degradation and Stability,* **75**(2), pp. 397-402.

BROOKFIELD, (2001)-last update, Brookfield Viscometer Manual | Brookfield Rheometer Manual [Homepage of Brookfield], [Online]. Available: http://www.brookfieldengineering.com/ support/documentation/ operator-manuals.asp [Feb, 2013].

BRUGNEROTTO, J., LIZARDI, J., GOYCOOLEA, F., ARGÜELLES-MONAL, W., DESBRIERES, J. and RINAUDO, M., (2001) An infrared investigation in relation with chitin and chitosan characterization. *Polymer,* **42**(8), pp. 3569-3580.

BUREAU, M., DENAULT, J., COLE, K. and ENRIGHT, G., (2002) The role of crystallinity and reinforcement in the mechanical behavior of polyamide-6/clay nanocomposites. *Polymer Engineering & Science,* **42**(9), pp. 1897-1906.

CAENN, R. and CHILLINGAR, G.V., (1996) Drilling fluids: State of the art. *Journal of petroleum science and engineering,* **14**(3), pp. 221-230.

CAENN, R., DARLEY, H.C. and GRAY, G.R., (2011) Drilling and Drilling Fluids Waste Management. *Composition and properties of drilling and completion fluids.* Gulf professional publishing, pp. 617-654.

CEFAS (2013) OSPAR List of Substances Used and Discharged Offshore which re Considered to Pose Little or No Risk to the Environment (PLONOR)(Revised at OIC 2013) [Online]. Available: https://www.cefas.co.uk/media/1384/13-06e_plonor.pdf [May, 2017]

CEFAS (2010) United Kingdom National Plan for the phase-out of substances identified as candidates for substitution [Online]. Available: https://www.cefas.co.uk/media/52537/uk-national-substitution-plan-5-dec-2010.pdf [May, 2017].

CHABRAND, R.M. and GLATZ, C.E., (2009) Destabilization of the emulsion formed during the enzyme-assisted aqueous extraction of oil from soybean flour. *Enzyme and microbial technology,* **45**(1), pp. 28-35.

CHEN, Y. and WANG, Q., (2006) Preparation, properties and characterizations of halogen-free nitrogen–phosphorus flame-retarded glass fibre reinforced polyamide 6 composite. *Polymer Degradation and Stability,* **91**(9), pp. 2003-2013.

CHIN, K. and WONG, K., (1981) Palm oil refinery wastes treatment. *Water research,* **15**(9), pp. 1087-1092.

CHILDS, J.D., ACOSTA, E., SCAMEHORN, J.F. and SABATINI, D.A., (2005) Surfactant-enhanced treatment of oil-based drill cuttings. Journal of Energy Resources Technology, **127**(2), pp.153-162.

CHOW, W. and MOHD ISHAK, Z., (2007). Mechanical Morphological And Rheological Properties Of Polyamide 6 Organo-Montmorillonite Nanocomposites. *Express Polymer Letters,* **1**(2), pp. 77-83.

CHRISTIAN, C., ELLIS, D., BREGE, J., QUINTERO, L. and CLARK, D., (2009) The development of an effective water-wetting cement spacer for the displacement of non-aqueous fluids (NAF), *AADE Technical Conference and Exhibition* 2009, AADE, pp. 1-5.

CIWM, (2014) *The Circular Economy: what does it mean for the waste and resource management sector?* United Kingdom: The Chartered Institution of Wastes Management.

DABROWSKI, F., BOURBIGOT, S., DELOBEL, R. and LE BRAS, M., (2000) Kinetic modelling of the thermal degradation: of polyamide-6 nanocomposite. *European Polymer Journal,* **36**(2), pp. 273-284.

DAHIYA, J.B., MULLER-HAGEDORN, M., BOCKHORN, H. and KANDOLA, B.K., (2008) Synthesis and thermal behaviour of polyamide 6/bentonite/ammonium polyphosphate composites. *Polymer Degradation and Stability,* **93**(11), pp. 2038-2041.

DARLEY, H.C. and GRAY, G.R., (1988) *Composition and properties of drilling and completion fluids.* Gulf Professional Publishing. Houston, USA.

DAS, A., STÖCKELHUBER, K.W., JURK, R., JEHNICHEN,D., and HEINRICH, G., (2011) A general approach to rubber–montmorillonite nanocomposites: Intercalation of stearic acid. *Applied Clay Science*, (51), 1–2, pp. 117–125

DECC, (2014)-last update, Methodology for the Sampling and Analysis of Produced Water and Other Hydrocarbon Discharges [Homepage of Crown copyright Department of Energy and Climate Change], [Online]. Available: https://www.gov.uk/.../Methodology_for_the_Sampling_and_Analysis_of_Produced_Water_and_Other_Hydrocarbon_Discharges [June, 2012].

DEGUCHI, R., NISHIO, T. and OKADA, A., (1993) *Process for preparing a polyamide composite material. Ube Industries, Ltd., Toyota Jidosha Kabushiki Kaisha and Kabushiki Kaisha Toyota Chuo Kenkyusho.* Washington, DC, Google US Patents.

DEMIRBAS, A., SARI, A. and ISILDAK, O., (2006) Adsorption thermodynamics of stearic acid onto bentonite. *Journal of hazardous materials,* **135**(1–3), pp. 226-231.

DENISON, R. and RUSTON, J., (1990) *Recycling and incineration: evaluating the choices.* Island Press.Washington D.C.

DUKE, R.B., (1983) *Mineral acid demulsification of surfactant-containing emulsion.* shington D.C., US: Google Patents.

EKE, P.E. and SCHOLZ, M., (2008) Benzene removal with vertical-flow constructed treatment wetlands. *Journal of chemical technology and biotechnology,* **83**(1), pp. 55-63.

EKEH-ADEGBOTOLU, U., EKEH, O. and WEGWU, M., (2012) Cleanup of Crude Oil Polluted Sites Using Arachis hypogaea L.(Groundnut) and Biostimulants, *Nigeria Annual International Conference and Exhibition* 2012, SPE-162968-MS Society of Petroleum Engineers.

ELSHORBAGY, W. and ALKAMALI, A., (2005) Solid waste generation from oil and gas industries in United Arab Emirates. *Journal of hazardous materials,* **120**(1), pp. 89-99.

EMUCHAY, D., ONYEKONWU, M.O., OGOLO, N.A. and UBANI, C., (2013) Breaking of Emulsions Using Locally Formulated Demusifiers, August, 5 2013, Society of Petroleum Engineers.

ESE, M., SJÖBLOM, J., DJUVE, J. and PUGH, R., (2000) An atomic force microscopy study of asphaltenes on mica surfaces. Influence of added resins and demulsifiers. *Colloid and Polymer Science,* **278**(6), pp. 532.

EUR-LEX, (2013)-last update, Dangerous substances directive [Homepage of HSE Books], [Online]. Available: http://www.legislation.gov.uk/uksi/2002/2776/pdfs/uksi_20022776_en.pdf. [7 January, 2013].

EUROPEAN UNION, (2002)-last update, Consolidated European waste catalogue [Homepage of European Union], [Online]. Available: https://www.sepa.org.uk/media/139107/euro_waste_catalogue.pdf [September, 2016].

EUROPEAN UNION, (2014)-last update, EU Waste Framework Directive [Homepage of gov.uk Department for Environment, Food & Rural Affairs], [Online]. Available: https://www.gov.uk/guidance/waste-legislation-and-regulations#eu-waste-framework-directive [Sept, 2016].

FALCIGLIA, P.P., CANNATA, S., ROMANO, S. and VAGLIASINDI, F.G.A., (2014) Stabilisation/solidification of radionuclide polluted soils — Part I:

Assessment of setting time, mechanical resistance, γ-radiation shielding and leachate γ-radiation. *Journal of Geochemical Exploration,* **142**, pp. 104-111.

FELL, J.T., (2007). Surface and interfacial phenomena. In: M.E. AULTON, ed, *Aulton's pharmaceutics: the design and manufacture of medicines.* 3rd edition edn. Churchill livingstone, Elsevier, pp. 59-69.

FERNANDEZ, L.C., ZEGARRA, H., BACA, G. and TORRES, L.G., (2008) Characterization and surfactant-enhanced washing treatability of drilling fluids stored for more than 20 years. *Journal of surfactants and detergents,* **11**(4), pp. 307-314.

FERREIRA, J. and BRANCO, F., (2007) Structural application of GRC in telecommunication towers. *Construction and Building Materials,* **21**(1), pp. 19-28.

FINK, J., (2012) *Petroleum Engineer's guide to oil field chemicals and fluids.Waltham, MA: Gulf Professional Pub,* Houston, UK.

FINK, J., (2015) Chapter 16 - Enhanced oil recovery. In: J. FINK, ed, *Petroleum Engineer's Guide to Oil Field Chemicals and Fluids (Second Edition).* Boston: Gulf Professional Publishing, pp. 477-565.

FITZ, W.J. and WENZEL, W.W., (2002) Arsenic transformations in the soil–rhizosphere–plant system: fundamentals and potential application to phytoremediation. *Journal of Biotechnology,* **99**(3), pp. 259-278.

FITZER, E., KLEINHOLZ, R., TIESLER, H., STACEY, M.H., BRUYNE, R., LEFEVER, I., FOLEY, A., FROHS, W., HAUKE, T. and HEINE, M., (2000) Fibres, 5. Synthetic Inorganic. *Ullmann's encyclopedia of industrial chemistry*. John Wiley and Sons.

FOGG, D., (2011) Umbilical Technology for Arctic Projects. Offshore Technology Conference. OTC 22129 Arctic Technology Conference. Houston, Texas, USA. 7–9 February, 2011

FORNES, T., YOON, P., HUNTER, D., KESKKULA, H. and PAUL, D., (2002) Effect of organoclay structure on nylon 6 nanocomposite morphology and properties. *Polymer,* **43**(22), pp. 5915-5933.

FU, S., FENG, X., LAUKE, B. and MAI, Y., (2008) Effects of particle size, particle/matrix interface adhesion and particle loading on mechanical properties of particulate–polymer composites. *Composites Part B: Engineering,* **39**(6), pp. 933-961.

GALIMBERTI, M., CIPOLLETTI, V. and COOMBS, M., (2013) Application of clay polymer nanocomposites. *Handbook of Clay Science, 2nd edition.Elsevier, Amsterdam,* (Part B).

GAN, S., LAU, E. and NG, H., (2009) Remediation of soils contaminated with polycyclic aromatic hydrocarbons (PAHs). *Journal of hazardous materials,* **172**(2), pp. 532-549.

GARLAND, E., KERR, J.M., MUNDY, K., MASON, M., YOUNG, S., PEGORS, S., SEDLOCK, E.R., BARRETT, J., CAMPBELL, J.A. and EYGUN, C., (2008) OGP Exploration & Production Waste Management Guidelines. *SPE International Conference on Health, safety and Environment in OGP exploration and Production.*

GBADEBO, A., TAIWO, A. and EGHELE, U., (2010) Environmental impacts of drilling mud and cutting wastes from the Igbokoda onshore oil wells, Southwestern Nigeria. *Indian Journal of Science and Technology,* **3**(5), pp. 504-510.

GENDRE, L., NJUGUNA, J., ABHYANKAR, H. and ERMINI, V., (2015) Mechanical and impact performance of three-phase polyamide 6 nanocomposites. *Materials & Design,* **66**, pp. 486-491.

GHAZI, M., QUARANTA, G., DUPLAYA, J., HADJAMORA, R., KHODJAB, M., AMAR, H.A. and KESSAISSIA, Z., (2011) Life-Cycle Impact Assessment of oil drilling mud system in Algerian arid area. Resources, Conservation and Recycling. **55**, pp. 1222– 1231.

GONÇALVES, E.S., POULSEN, L. and OGILBY, P.R., (2007) Mechanism of the temperature-dependent degradation of polyamide 66 films exposed to water. *Polymer Degradation and Stability,* **92**(11), pp. 1977-1985.

GONZALEZ, L., LAFLEUR, P., LOZANO, T., MORALES, A. B., GARCIA, R., ANGELES, M., RODRIGUEZ, F. AND SANCHEZ, S. (2014), Mechanical and thermal properties of polypropylene/montmorillonite nanocomposites using stearic acid as both an interface and a clay surface modifier. Polymer Composites, 35: 1–9. doi:10.1002/pc.22627

GONZALEZ, M.F., CRAWLEY, W. and PATTON, D., (2008) New Treatment Technologies and Programs to Reduce, Reuse, and Recycle Drilling Waste, *Transportation Research Board 87th Annual Meeting* 2008.

GU, W., WU, H.F., KAMPE, S.L. and LU, G., (2000) Volume fraction effects on interfacial adhesion strength of glass -fibre-reinforced polymer composites. *Materials Science and Engineering: A,* **277**(1–2), pp. 237-243.

HANRAHAN, G., (2012) Chapter 9 - Environmental Toxicology and Hazardous Waste Characterization. In: G. HANRAHAN, ed, *Key Concepts in Environmental Chemistry.* Boston: Academic Press, pp. 265-293.

HARGREAVES, T., (2003) Chemical formulation. An overview of surfactant-based preparations used in everyday life. First edn. *Royal Society of Chemistry.* Cambridge, UK.

HENCKENS, M., DRIESSEN, P. and WORRELL, E., (2015) Towards a sustainable use of primary boron. Approach to a sustainable use of primary resources. *Resources, Conservation and Recycling,* **103**, pp. 9-18.

HERMOSO, J., MARTINEZ-BOZA, F. and GALLEGOS, C., (2014) Influence of viscosity modifier nature and concentration on the viscous flow behaviour of oil-based drilling fluids at high pressure. *Applied Clay Science,* **87**, pp. 14-21.

HEWAK, D., NETO, J.M., SAMSON, B., BROWN, R., JEDRZEJEWSKI, K., WANG, J., TAYLOR, E., LAMING, R., WYLANGOWSKI, G. and PAYNE, D., (1994) Quantum-efficiency of praseodymium doped Ga: La: S glass for 1.3/spl mu/m optical fibre amplifiers. *IEEE photonics technology letters,* **6**(5), pp. 609-612.

HOLDWAY, D.A., (2002) The acute and chronic effects of wastes associated with offshore oil and gas production on temperate and tropical marine ecological processes. *Marine pollution bulletin,* **44**(3), pp. 185-203.

HOLLIDAY, G. and DEUEL, L., (1990) A Statistical Review of API and EPA Sampling and Analysis of Oil and Gas Field Wastes, *SPE Annual Technical Conference and Exhibition* 1990, Society of Petroleum Engineers.

HOLMES, D., BUNN, C. and SMITH, D., (1955) The crystal structure of polycaproamide: Nylon 6. *Journal of Polymer Science,* **17**(84), pp. 159-177.

HOSNY, R., FATHY, M., RAMZI, M., ABDEL MOGHNY, T., DESOUKY, S.E.M. and SHAMA, S.A., (2016) Treatment of the oily produced water (OPW) using coagulant mixtures. *Egyptian Journal of Petroleum,* **25**(3), pp. 391-396.

HUANG, X., EL-ALAWI, Y., GURSKA, J., GLICK, B.R. and GREENBERG, B.M., (2005) A multi-process phytoremediation system for decontamination of persistent total petroleum hydrocarbons (TPHs) from soils. *Microchemical Journal,* **81**(1), pp. 139-147.

ITO M. and NAGAI, K., (2008) Degradation issues of polymer materials used in railway field Polymer Degradation and Stability 93 (2008) 1723–1735

JHA, A.K., SHARMA, C., SINGH, N., RAMESH, R., PURVAJA, R. and GUPTA, P.K., (2008) Greenhouse gas emissions from municipal solid waste management in Indian mega-cities: A case study of Chennai landfill sites. *Chemosphere,* **71**(4), pp. 750-758.

JIANG, T., WANG, Y., YEH, J. and FAN, Z., (2005) Study on solvent permeation resistance properties of nylon6/clay nanocomposite. *European Polymer Journal,* **41**(3), pp. 459-466.

JIAOJIAO, G., JIENIAN, Y., MING, C., XIANGSHUANG, B. and HAIMIN, S., (2011). Scale deposition mechanism and low-damage underbalanced drilling

fluids for high CO2 content gas reservoirs. *Petroleum Exploration and Development,* **38**(6), pp. 750-755.

JIMENEZ, J., AEMIG, Q., DOUSSIET, N., STEYER, J., HOUOT, S. and PATUREAU, D., (2015) A new organic matter fractionation methodology for organic wastes: Bioaccessibility and complexity characterization for treatment optimization. *Bioresource technology,* **194**, pp. 344-353.

JONES, T., SANDERS, M. and CHAMBERS, B., (2002) Improvements in the analysis of thermally recovered drilling fluid base oils from drilled cuttings, *SPE International Conference on Health, Safety and Environment in Oil and Gas Exploration and Production* 2002, Society of Petroleum Engineers.

KATOH, Y. and OKAMOTO, M., (2009) Crystallization controlled by layered silicates in nylon 6–clay nano-composite. *Polymer,* **50**(19), pp. 4718-4726.

KENNEDY, C.J., (2011) TOXICOLOGY | The Toxicology of Organics in Fishes. In: A.P. FARRELL, ed, *Encyclopedia of Fish Physiology.* San Diego: Academic Press, pp. 2069-2077.

KHALLADI, R., BENHABILES, O., BENTAHAR, F. and MOULAI-MOSTEFA, N., (2009) Surfactant remediation of diesel fuel polluted soil. *Journal of hazardous materials,* **164**(2), pp. 1179-1184.

KHAN, A.G., (2005) Role of soil microbes in the rhizospheres of plants growing on trace metal contaminated soils in phytoremediation. *Journal of Trace Elements in Medicine and Biology,* **18**(4), pp. 355-364.

KHAN, A.N. and AHMED, B.A., (2015) Comparative study of Polyamide 6 reinforced with glass fibre and montmorillonite. *Polymer Bulletin,* **72**(5), pp. 1207-1216.

KHATUA, B., LEE, D.J., KIM, H.Y. and KIM, J.K., (2004) Effect of organoclay platelets on morphology of nylon-6 and poly (ethylene-r an-propylene) rubber blends. *Macromolecules,* **37**(7), pp. 2454-2459.

KISIC, I., MESIC, S., BASIC, F., BRKIC, V., MESIC, M., DURN, G., ZGORELEC, Z. and BERTOVIC, L., (2009) The effect of drilling fluids and crude oil on some chemical characteristics of soil and crops. *Geoderma,* **149**(3), pp. 209-216.

KODEL, K.A., ANDRADE, P.F., VALENÇA, J.V.B. and SOUZA, D.D.N., (2012) Study on the composition of mineral scales in oil wells. *Journal of Petroleum Science and Engineering,* **81**, pp. 1-6.

KOSHELEV, V.N., KLIMOVA, L.Z., STARIKOV, V.V. and NIZOVA, S.A., (2000) New Demulsifiers for Petroleum Preparation Processes, *Ecology, Chemistry and Technology of Fuel and Oils*. **36**(2), pp. 97 – 100.

KUSUM, R. and BOMMAYYA, H., (2011) Palm oil and rice bran oil: Current status and future prospects. *International Journal of Plant Physiology and Biochemistry,* **3**(8), pp. 125-132.

LADOUSSE, A., TALLEC, C., CHAINEAU, C. and VIDALIE, J., (1996) Landfarming of drill cuttings, *SPE Health, Safety and Environment in Oil and Gas Exploration and Production Conference* 1996, Society of Petroleum Engineers.

LAGALY, G., REESE, M. and ABEND, S., (1999a) Smectites as colloidal stabilizers of emulsions: I. Preparation and properties of emulsions with smectites and nonionic surfactants. *Applied Clay Science,* **14**(1), pp. 83-103.

LAGALY, G., REESE, M. and ABEND, S., (1999b) Smectites as colloidal stabilizers of emulsions: II. Rheological properties of smectite-laden emulsions. *Applied Clay Science,* **14**(5), pp. 279-298.

LAHA, S., TANSEL, B. and USSAWARUJIKULCHAI, A., (2009) Surfactant–soil interactions during surfactant-amended remediation of contaminated soils by hydrophobic organic compounds: a review. *Journal of environmental management,* **90**(1), pp. 95-100.

LANGE, J. and WYSER, Y., (2003) Recent innovations in barrier technologies for plastic packaging—a review. *Packaging Technology and Science,* **16**(4), pp. 149-158.

LANGEVIN, D. and ARGILLIER, J., (2016) Interfacial behavior of asphaltenes. *Advances in Colloid and Interface Science,* **233**, pp. 83-93.

LEE, S.M. and TIWARI, D., (2012) Organo and inorgano-organo-modified clays in the remediation of aqueous solutions: an overview. *Applied Clay Science,* **59**, pp. 84-102.

LEONARD, S.A. and STEGEMANN, J.A., (2010a) Stabilization/solidification of petroleum drill cuttings. *Journal of hazardous materials,* **174**(1), pp. 463-472.

LEONARD, S.A. and STEGEMANN, J.A., (2010b) Stabilization/solidification of petroleum drill cuttings: Leaching studies. *Journal of hazardous materials,* **174**(1), pp. 484-491.

LESZCZYŃSKA, A., NJUGUNA, J., PIELICHOWSKI, K. and BANERJEE, J., (2007) Polymer/montmorillonite nanocomposites with improved thermal properties: Part II. Thermal stability of montmorillonite nanocomposites based on different polymeric matrixes. *Thermochimica Acta,* **454**(1), pp. 1-22.

LEVCHIK, S.V., COSTA, L. AND CAMINO, G., (1994) Effect of the fire-retardant ammonium polyphosphate on the thermal decomposition of aliphatic polyamides. Part III—Polyamides 6.6 and 6.10. Polymer degradation and stability, 43(1), pp.43-54.

LEWIS, M.A., (1995) Use of freshwater plants for phytotoxicity testing: a review. *Environmental Pollution,* 87(3), pp. 319-336.

LI, Q., KANG, C. and ZHANG, C., (2005) Waste water produced from an oilfield and continuous treatment with an oil-degrading bacterium. *Process Biochemistry,* **40**(2), pp. 873-877.

LI, T., ZHU, J. and ZHANG, W., (2012) Cascade utilization of low temperature geothermal water in oilfield combined power generation, gathering heat tracing and oil recovery. *Applied Thermal Engineering,* **40**, pp. 27-35.

LI, M., OU, H., LI, Z., GU, T., LIU, H. and GUO, X., (2015) Contamination of cement slurries with diesel-based drilling fluids in a shale gas well. *Journal of Natural Gas Science and Engineering,* **27, Part 3**, pp. 1312-1320.

LI, Y. and SHIMIZU, H., (2004) Novel morphologies of poly(phenylene oxide) (PPO)/polyamide 6 (PA6) blend nanocomposites. *Polymer,* **45**(22), pp. 7381-7388.

LIN, Q. and MENDELSSOHN, I.A., (2009) Potential of restoration and phytoremediation with Juncus roemerianus for diesel-contaminated coastal wetlands. *Ecological Engineering,* **35**(1), pp. 85-91.

LIU, L., QI, Z. and ZHU, X., (1999) Studies on nylon 6/clay nanocomposites by melt-intercalation process. *Journal of Applied Polymer Science,* **71**(7), pp. 1133-1138.

LIU, C., HOTTA, Y., SANTO, A., HENGESBAUGH, M., WATABE, A., TOTOKI, Y., ALLEN, D. and BENGTSSON, M., (2016) Food waste in Japan: Trends, current practices and key challenges. *Journal of Cleaner Production,* **133**, pp. 557-564.

LIU, J., HUANG, X., LU, L., LI, M., XU, J. and DENG, H., (2011) Turbiscan Lab® Expert analysis of the biological demulsification of a water-in-oil emulsion by two biodemulsifiers. *Journal of hazardous materials,* **190**(1–3), pp. 214-221.

LIU, S., HWANG, S., YEH, J. and HUNG, C., (2011) Mechanical properties of polyamide-6/montmorillonite nanocomposites — Prepared by the twin-screw extruder mixed technique. *International Communications in Heat and Mass Transfer,* **38**(1), pp. 37-43.

LIU, L., BARBER, A.H., NURIEL, S. and WAGNER, H.D., (2005) Mechanical Properties of Functionalized Single-Walled Carbon-Nanotube/Poly (vinyl alcohol) Nanocomposites. *Advanced Functional Materials*, **15**(6), pp.975-980

LIU, X. and WU, Q., (2002) Phase transition in nylon 6/clay nanocomposites on annealing. *Polymer,* **43**(6), pp. 1933-1936.

LU, C., LIU, L., CHEN, N., WANG, X., YANG, D., HUANG, X. and YAO, D., (2015) Influence of clay dispersion on flame retardancy of ABS/PA6/APP blends. *Polymer Degradation and Stability,* **114**, pp. 16-29.

LUO, J. and DANIEL, I.M., (2003) Characterization and modeling of mechanical behavior of polymer/clay nanocomposites. *Composites Science and Technology,* **63**(11), pp. 1607-1616.

MACEK, T., KOTRBA, P., SVATOS, A., NOVAKOVA, M., DEMNEROVA, K. and MACKOVA, M., (2008) Novel roles for genetically modified plants in environmental protection. *Trends in biotechnology,* **26**(3), pp. 146-152.

MAKHONIN, G.M., PETROV, A.A. and BORISOV, S.I., (1982) Effects of crude oil components on demulsifier efficiency. *Chemistry and Technology of Fuels and Oils,* **18**(8), pp. pp 410-413.

MARI, M., NADAL, M., SCHUHMACHER, M. and DOMINGO, J.L., (2009) Exposure to heavy metals and PCDD/Fs by the population living in the vicinity of a hazardous waste landfill in Catalonia, Spain: Health risk assessment. *Environment international,* **35**(7), pp. 1034-1039.

MATHIAS, L.J., DAVIS, R.D. and JARRETT, W.L., (1999) Observation of r and γ Crystal Forms and Amorphous Regions of Nylon 6-Clay Nanocomposites Using Solid-State 15N Nuclear Magnetic Resonance. *Macromolecules*. **32**, pp. 23.

MCCOSH, K., ADDICKS, G.A. and GALLO, D., (2008) Oil recovery form production waste reduces environmental impact, *AADE Fluids conference and exhibition*, 8-9 April 2008, AADE.

MCCOSH, K., KAPILA, M., DIXIT, R., WAY, P.W. and PHIPPS, J., (2009) Continuous Improvement in Slop-Mud Treatment Technology. *SPE Drilling & Completion,* **24**(03), pp. 418-423.

MCCOSH, K.L., KAPILA, M., DIXIT, R., WAY, P.W. and PHIPPS, J., (2007) Continuous Improvement in Slop-Mud Treatment Technology. *SPE Drilling & Completion,* **24**(03), pp. 418-423.

MCPHEE, C., REED, J. and ZUBIZARRETA, I., (2015) Core Analysis: A Best Practice Guide. *Developments in Petrolueum Science.* First Edn. Vol 64. Elsevier.

MECKING, S., (2004) Nature or Petrochemistry Biologically Degradable Materials. *Angewandte Chemie International Edition,* **43**(9), pp. 1078-1085.

MÉSZÁROS, L., DEÁK, T., BALOGH, G., CZVIKOVSZKY, T. and CZIGÁNY, T., (2013) Preparation and mechanical properties of injection moulded polyamide 6 matrix hybrid nanocomposite. *Composites Science and Technology,* **75**, pp. 22-27.

MILLAR, A., GOODMAN, S. and DOBRAI, N., (2013) Application of molecular techniques for the detection, testing and evaluation of microbial diversity in the oil and gas industry. In: Chemistry in the oil industry XIII, *Oilfield Chemistry - New frontiers.* First edn. Vol 1. Royal Society of Chemistry and European oilfield speciality chemicals association, Suffolk, UK pp. 445-458.

MISHRA, S., SONAWANE, S. and SHIMPI, N., (2009) Influence of organo-montomorillonite on mechanical and rheological properties of polyamide nanocomposites. *Applied Clay Science,* **46**(2), pp. 222-225.

MISHRA, S., CHATTERJEE, A. and SINGH, R., (2011) Novel synthesis of nano-calcium carbonate (CaCO3)/polystyrene (PS) core–shell nanoparticles by atomized microemulsion technique and its effect on properties of polypropylene (PP) composites. *Polymers for Advanced Technologies,* **22**(12), pp. 2571-2582.

MOISEEV, Y.V. and ZAIKOV, G.E., (1987) *Chemical resistance of polymers in aggressive media.* Springer Science & Business Media.

MONTAÑO, M., ZIMMER, K.E., DAHL, E., BERG, V., OLSAKER, I., SKAARE, J.U., MURK, A.J., ROPSTAD, E. and VERHAEGEN, S., (2011) Effects of mixtures of persistent organic pollutants (POPs) derived from cod liver oil on H295R steroidogenesis. *Food and Chemical Toxicology,* **49**(9), pp. 2328-2335.

MORGAN, A.B. and WILKIE, C.A., (2007) *Flame retardant polymer nanocomposites.* John Wiley & Sons.

MOTAWIE, A.M., MADANY, M.M., EL-DAKRORY, A.Z., OSMAN, H.M., ISMAIL, E.A., BADR, M.M., EL-KOMY, D.A. and ABULYAZIED, D.E., (2014) Physico-chemical characteristics of nano-organo bentonite prepared using different organo-modifiers. *Egyptian Journal of Petroleum,* **23**(3), pp. 331-338.

MOUTI, Z., WESTWOOD, K., LONG, D. and NJUGUNA, J., (2012) Finite Element Analysis of Glass Fibre-Reinforced Polyamide Engine Oil Pan Subjected to Localized Low Velocity Impact from Flying Projectiles. *Steel research international,* **83**(10), pp. 957-963.

MUKHERJEE, S. and SRIVASTAVA, S.K., (2006) Minerals transformations in northeastern region coals of India on heat treatment. *Energy & Fuels,* **20**(3), pp. 1089-1096.

MULLIGAN, C.N., YONG, R.N. and GIBBS, B.F., (2001) Heavy metal removal from sediments by biosurfactants. *Journal of hazardous materials,* **85**(1–2), pp. 111-125.

NEWMAN, K., LOMOND, P. and MCCOSH, K., (2009) Advances in mixing technology improve drilling fluid preparatiion and properties, *National technical conference and exhibition-08-02* 2009, American Association of Drilling Engineers, pp. 1-5.

NFON, E., COUSINS, I.T. and BROMAN, D., (2008) Biomagnification of organic pollutants in benthic and pelagic marine food chains from the Baltic Sea. *Science of the total environment,* **397**(1), pp. 190-204.

NGUYEN, T.T., YOUSSEF, N.H., MCINERNEY, M.J. and SABATINI, D.A., (2008) Rhamnolipid biosurfactant mixtures for environmental remediation. *Water research,* **42**(6), pp. 1735-1743.

NJUGUNA, J., MOUTI, Z. and WESTWOOD, K., (2015) 8 - Toughening mechanisms for glass fibre-reinforced polyamide composites. In: Q. QIN and J. YE, *Toughening Mechanisms in Composite Materials.* Woodhead Publishing, pp. 211-232.

NJUGUNA, J., (2011) The application of energy-absorbing structures on side impact protection systems. *International Journal of Computer Applications in Technology,* **40**(4), pp. 280-287.

OGP, (2009) Drilling fluids and health risk management. A guide to drilling personnel, managers and health professionals in the oil and gas industry. *Oil and gas producers.*

OGP, (2005) Fate and effect of naturally occurring substance in produced water on the marine environment. *Oil and gas producers*.

OGP, (2003) Environmental aspects of the use and diusposal of non aqeous drilling fluids associated with offshore oil and gas operations. **Report 342**.

OKADA, A. and USUKI, A., (2006) Twenty Years of Polymer-Clay Nanocomposites. *Macromolecular Materials and Engineering,* **291**(12), pp. 1449-1476.

ORMELOH, J., (2014) Thermomechanical cuttings cleaner–qualification for offshore treatment of oil contaminated cuttings on the Norwegian continental shelf and martin linge case study.

OSPAR COMMISSION, (2013a) Background Document Concerning Techniques for the Management of Produced Water from Offshore Installations. *Offshore Industry Series*.

OSPAR COMMISSION, (2013b) OSPAR List of Substances Used and Discharged Offshore which Are Considered to Pose Little or No Risk to the Environment (PLONOR). OSPAR Agreement 2013-06. *OSPAR Commission*

OSPAR COMMISSION, (2010a) Overview assessment of the implementation of OSPAR recommendation 2001/1 for the management of produced water from offshore installations. *London: OSPAR Commission*.

OSPAR COMMISSION, (2010b) The North-East Atlantic Environment Strategy; Strategy of the OSPAR Commission for the Protection of the Marine Environment

of the North-East Atlantic 2010-2020 (OSPAR Agreement 2010-3). *London: OSPAR Commission*.

OSPAR COMMISSION, (2007) Litter, Monitoring Marine Beach.

ÖZDILEK, C., KAZIMIERCZAK, K., VAN DER BEEK, D. and PICKEN, S.J., (2004) Preparation and properties of polyamide-6-boehmite nanocomposites. *Polymer,* **45**(15), pp. 5207-5214.

PABON, M. and CORPART, J., (2002) Fluorinated surfactants: synthesis, properties, effluent treatment. *Journal of Fluorine Chemistry,* **114**(2), pp. 149-156.

PAGE, P.W., GREAVES, C., LAWSON, R., HAYES, S. and BOYLE, F., (2003) Options for the recycling of drilling cuttings. *SPE/EPA/DOE Exploration and Production Environmental Conference, San Antonio, TX, USA,* Soc. Petrol. Eng(Paper SPE 80583).

PARIA, S., (2008) Surfactant-enhanced remediation of organic contaminated soil and water. *Advances in Colloid and Interface Science,* **138**(1), pp. 24-58.

PAVLIDOU, S. and PAPASPYRIDES, C., (2008) A review on polymer–layered silicate nanocomposites. *Progress in polymer science,* **33**(12), pp. 1119-1198.

PEI, X., SHANG, B., CHEN, L., LI, J. and TANG, Y., (2016) Compression properties of multilayer-connected biaxial weft knitted carbon fibre fabric reinforced composites. Composites Part B: Engineering, 91, pp.296-305

PEKDEMIR, T., COPUR, M. and URUM, K., (2005) Emulsification of crude oil–water systems using biosurfactants. *Process Safety and Environmental Protection,* **83**(1), pp. 38-46.

PENG, S., ZHOU, Q., CAI, Z. and ZHANG, Z., (2009) Phytoremediation of petroleum contaminated soils by Mirabilis Jalapa L. in a greenhouse plot experiment. *Journal of hazardous materials,* **168**(2), pp. 1490-1496.

PERRY, M.L. and GRIFFIN, J.M., (2001) Chemical Treatment of Cuttings Drilled With Oil-Based Mud Employing a Laboratory Simulated Soil Washing Procedure, , Feburary 23 2001, Society of Petroleum Engineers.

PHAM, H. and NGUYEN, Q.P., (2014) Effect of silica nanoparticles on clay swelling and aqueous stability of nanoparticle dispersions. *Journal of Nanoparticle Research,* **16: 2137**(16).

PIELICHOWSKI, K., MAJKA, T. M., LESZCZYŃSKA, A. and GIACOMELLI, M., (2013) Optimization and Scaling up of the Fabrication Process of Polymer Nanocomposites: Polyamide-6/Montmorillonite Case Study. In: J. Njuguna ed, *Structural Nanocomposites*. Engineering Materials. Springer Berlin Heidelberg pp 75-103

QI, W., YU, Z., LIU, Y. and LI, Y., (2013) Removal of emulsion oil from oilfield ASP wastewater by internal circulation flotation and kinetic models. *Chemical Engineering Science,* **91**, pp. 122-129.

QUINTAVALLA, S. and VICINI, L., (2002) Antimicrobial food packaging in meat industry. *Meat Science,* **62**(3), pp. 373-380.

QUINTERO, L., CHRISTIAN, C., HALLIDAY, W., WHITE, C., DEAN, D. and COURTNEY, G., (2008) New spacer technoloy for cleaning and water wetting of casing and riser, *AADE Fluids conference and exhibition, Texas.*, 8-9, April 2008 2008, AADE.

QUINTERO, L., JONES, T.A. and PIETRANGELI, G.A., (2012) Proper Design Criteria of Microemulsion Treatment Fluids for Enhancing Well Production, *SPE Europec/EAGE Annual Conference* 2012, Society of Petroleum Engineers.

QUINTERO, L. and PIETRANGELI, G.A., (2013) Enhanced Oil Solubilization Using Microemulsions With Linkers, *SPE International Symposium on Oilfield Chemistry* 2013, Society of Petroleum Engineers.

RADWAN, S., AL-AWADHI, H., SORKHOH, N. and EL-NEMR, I., (1998) Rhizospheric hydrocarbon-utilizing microorganisms as potential contributors to phytoremediation for the oil Kuwaiti desert. *Microbiological research,* **153**(3), pp. 247-251.

RAFIZUL, I.M. and ALAMGIR, M., (2012) Characterization and tropical seasonal variation of leachate: Results from landfill lysimeter studied. *Waste Management,* **32**(11), pp. 2080-2095.

RAY, M.R., ROYCHOUDHURY, S., MUKHERJEE, G., ROY, S. and LAHIRI, T., (2005) Respiratory and general health impairments of workers employed in a municipal solid waste disposal at an open landfill site in Delhi. *International journal of hygiene and environmental health,* **208**(4), pp. 255-262.

REIS, D.J.C., (1996) *Environmental control in petroleum engineering.* Gulf Professional Publishing.

RIDES, M., MORIKAWA, J., HALLDAHL, L., HAY, B., LOBO, H., DAWSON, A. and ALLEN, C., (2009) Intercomparison of thermal conductivity and thermal diffusivity methods for plastics. *Polymer Testing,* **28**(5), pp. 480-489.

RONG, M., ZHANG, M. and RUAN, W., (2006) Surface modification of nanoscale fillers for improving properties of polymer nanocomposites: a review. *Materials science and technology,* **22**(7), pp. 787-796.

SADIQ, R., HUSAIN, T., VEITCH, B. and BOSE, N., (2004) Risk-based decision-making for drilling waste discharges using a fuzzy synthetic evaluation technique. *Ocean Engineering,* **31**(16), pp. 1929-1953.

SALAGER J., (2006) Emulsion phase inversion phenomena. In: J. SJOBLOM, ed, *Emulsions and Emulsion stability.* Second edition edn. Vol 132. CRC press Taylor and Francis, pp. 185-244.

SAMYN, F. and BOURBIGOT, S., (2012) Thermal decomposition of flame retarded formulations PA6/aluminum phosphinate/melamine polyphosphate/organomodified clay: Interactions between the constituents. *Polymer Degradation and Stability,* **97**(11), pp. 2217-2230.

SÁNCHEZ-CHARDI, A. and NADAL, J., (2007) Bioaccumulation of metals and effects of landfill pollution in small mammals. Part I. The greater white-toothed shrew, Crocidura russula. *Chemosphere,* **68**(4), pp. 703-711.

SEATON, S., MORRIS, R., BLONQUIST, J. and HOGAN, B., (2006) Analysis of Drilling Fluid Base Oil Recovered from Drilling Waste by Thermal Desorption, *International Petroleum Environmental Conference* 2006.

SEDMAN, A., TALVISTE, P., MÕTLEP, R., JÕELEHT, A. and KIRSIMÄE, K., (2012) Geotechnical characterization of Estonian oil shale semi-coke deposits with prime emphasis on their shear strength. *Engineering Geology,* **131**, pp. 37-44.

SEPA, (2016 a)-last update, Flytipping [Homepage of Scottish Environment Protection Agency], [Online]. Available: http://www.sepa.org.uk/regulations/waste/flytipping/ [July/26, 2016].

SEPA, (2016 b)-last update, Waste [Homepage of Scottish Environment Protection Agency], [Online]. Available: http://www.sepa.org.uk/regulations/waste/ [July/26, 2016].

SEPA, (2016 c)-last update, Special Waste [Homepage of Scottish Environment Protection Agency], [Online]. Available: http://www.sepa.org.uk/regulations/waste/special-waste [July/26, 2016].

SHIVER, C., (1984) *Continuous process for the reclamation of waste drilling fluids*.

SHON, C., ESTAKHRI, C.K., LEE, D. and ZHANG, D., (2016) Evaluating feasibility of modified drilling waste materials in flexible base course construction. *Construction and Building Materials,* **116**, pp. 79-86.

SHUIXIANG, X., GUANCHENG, J., MIAN, C., HAO, D., GUANGQUAN, L., YU, X., JIANHUA, W. and KANG, Q., (2011) An environment friendly drilling fluid system. *Petroleum Exploration and Development,* **38**(3), pp. 369-378.

SILVA, F., NJUGUNA, J., SACHSE, S., PIELICHOWSKI, K., LESZCZYNSKA, A. and GIACOMELLI, M., (2014) The influence of multiscale fillers reinforcement into impact resistance and energy absorption properties of

polyamide 6 and polypropylene nanocomposite structures.Materials & Design. **50**, pp. 244-252.

SILVA, F., NJUGUNA, J., SACHSE, S., PIELICHOWSKI, K., LESZCZYNSKA, A. and GIACOMELLI, M., (2013) The influence of multiscale fillers reinforcement into impact resistance and energy absorption properties of polyamide 6 and polypropylene nanocomposite structures. *Materials & Design,* **50**, pp. 244-252.

SILVA, F., SACHSE, S. and NJUGUNA, J., (2012) Mechanical properties and impact-energy absorption of injection moulded nanocomposites structures, *ECCM15-15th European Conference on Composite Materials, Venice, Italy* 2012.

SJOBLOM, J., FORDEDAL, H. AND SKODVIN, T., (1996) Flocculation and coalescence in Emulsions as studied by dielectric spectroscopy. In: J. SJOBLOM, ed, *Emulsions and Emulsion stability.* First edition edn. Vol 61. CRC press Taylor and Francis, pp. 393-435.

STEPHENSON, R.L., SEATON, S., MCCHAREN, R., HERNANDEZ, E. and PAIR, R.B., (2004) Thermal desorption of oil from oil-based drilling fluids cuttings: processes and technologies, *SPE Asia Pacific Oil and Gas Conference and Exhibition* 2004, Society of Petroleum Engineers.

STEVENS, T., BODEN, A., ARTHUR, J.M., SCHLACHER, T.A., RISSIK, D. and ATKINSON, S., (2012) Initial effects of a moderate-sized oil spill on benthic assemblage structure of a subtropical rocky shore. *Estuarine, Coastal and Shelf Science,* **109**, pp. 107-115.

SUN, T., CANG, L., WANG, Q., ZHOU, D., CHENG, J. and XU, H., (2010) Roles of abiotic losses, microbes, plant roots, and root exudates on phytoremediation of PAHs in a barren soil. *Journal of hazardous materials,* **176**(1), pp. 919-925.

TAN, Y., WANG, X. and WU, D., (2015) Preparation, microstructures, and properties of long-glass -fibre-reinforced thermoplastic composites based on polycarbonate/poly (butylene terephthalate) alloys. *Journal of Reinforced Plastics and Composites,* **34**(21), pp. 1804-1820.

TEHRANI, A., CHAPMAN, J. and FRASER, A., (2003) Reducing barite sag in oil-based drilling fluids. **8**, pp. 284.

TERZAGHI, C., BUFFAGNI, M., CANTELLI, D., BONFANTI, P. and CAMATINI, M., (1998) Physical-chemical and ecotoxicological evaluation of water based drilling fluids used in Italian off-shore. *Chemosphere,* **37**(14), pp. 2859-2871.

THENG, B.K. and YUAN, G., (2008) Nanoparticles in the soil environment. *Elements,* **4**(6), pp. 395-399.

TRUSH, M.A., (2008)-last update, Xenobiotics Biotransformation. [Homepage of John Hopkins University], [Online]. Available: http://ocw.jhsph.edu/courses/publichealthtoxicology/PDFs/Lecture2_Trush.pdf. [6 January, 2013].

TYRONE, D.V. and ULYASHEVA, N., (2016) The research phase of the evaporation process in drilling fluids oil-based. *Bulletin of the Tomsk Polytechnic University of,* **327**(4), pp. 97-107.

UNAL, H., (2004) Morphology and mechanical properties of composites based on polyamide 6 and mineral additives. *Materials & Design,* **25**(6), pp. 483-487.

URUM, K., PEKDEMIR, T. and GOPUR, M., (2003) Optimum conditions for washing of crude oil-contaminated soil with biosurfactant solutions. *Process Safety and Environmental Protection,* **81**(3), pp. 203-209.

URUM, K., GRIGSON, S., PEKDEMIR, T. and MCMENAMY, S., (2006) A comparison of the efficiency of different surfactants for removal of crude oil from contaminated soils. *Chemosphere,* **62**(9), pp. 1403-1410.

URUM, K. and PEKDEMIR, T., (2004) Evaluation of biosurfactants for crude oil contaminated soil washing. *Chemosphere,* **57**(9), pp. 1139-1150.

URUM, K., PEKDEMIR, T., ROSS, D. and GRIGSON, S., (2005) Crude oil contaminated soil washing in air sparging assisted stirred tank reactor using biosurfactants. *Chemosphere,* **60**(3), pp. 334-343.

VAIA, R.A. and WAGNER, H.D., (2004) Framework for nanocomposites. *Materials Today,* **7**(11), pp. 32-37.

VILAVERT, L., NADAL, M., FIGUERAS, M.J., KUMAR, V. and DOMINGO, J.L., (2011) Levels of chemical and microbiological pollutants in the vicinity of a waste incineration plant and human health risks: Temporal trends. *Chemosphere,* **84**(10), pp. 1476-1483.

VLASVELD, D., DAUD, W., BERSEE, H.E. and PICKEN, S., (2007) Continuous fibre composites with a nanocomposite matrix: Improvement of flexural and compressive strength at elevated temperatures. *Composites Part A: Applied Science and Manufacturing,* **38**(3), pp. 730-738.

VLASVELD, D., PARLEVLIET, P., BERSEE, H. and PICKEN, S., (2005) Fibre–matrix adhesion in glass -fibre reinforced polyamide-6 silicate nanocomposites. *Composites Part A: applied science and manufacturing,* **36**(1), pp. 1-11.

VLASVELD, D., BERSEE, H.E.N. and PICKEN, S.J., (2005) Nanocomposite matrix for increased fibre composite strength. *Polymer,* **46**(23), pp. 10269-10278.

WAN, T., LIAO, S., WANG, K., YAN, P. and CLIFFORD, M., (2013) Multi-scale hybrid polyamide 6 composites reinforced with nano-scale clay and micro-scale short glass fibre. *Composites Part A: Applied Science and Manufacturing,* **50**, pp. 31-38.

WANG, Y.C., FAN, S.C., LEE, K.R., LI, C.L., HUANG, S.H., TSAI, H.A., and LAI, J.Y., (2004) Polyamide/SDS–clay hybrid nanocomposite membrane application to water–ethanol mixture pervaporation separation. *Journal of membrane science*, *239*(2), pp.219-226

WANG, J., HU, F., LI, C., LI, J. and YANG, Y., (2010) Synthesis of dendritic polyether surfactants for demulsification. *Separation and Purification Technology,* **73**(3), pp. 349-354.

WHITLOW, R., (1995) Basic soil mechanics. Harlow: Longman, pp. 1-30.

WILKINSON, A., LAUGEL, L., CLEMENS, M., HARDING, V. and MARIN, M., (1999) Phase structure in polypropylene/PA6/SEBS blends. *Polymer,* **40**(17), pp. 4971-4975.

WILLS, J., (2000) Muddied Waters A Survey of Offshore Oilfield Drilling Wastes and Disposal Techniques to Reduce the Ecological Impact of Sea Dumping.

WU, J., XU, Y., DABROS, T. and HAMZA, H., (2005) Effect of EO and PO positions in nonionic surfactants on surfactant properties and demulsification performance. *Colloids and Surfaces A: Physicochemical and Engineering Aspects,* **252**(1), pp. 79-85.

WU, S., WANG, F., MA, C.M., CHANG, W., KUO, C., KUAN, H. and CHEN, W., (2001) Mechanical, thermal and morphological properties of glass fibre and carbon fibre reinforced polyamide-6 and polyamide-6/clay nanocomposites. *Materials Letters,* **49**(6), pp. 327-333.

WYPYCH, G., (2016) 2 - FILLERS – ORIGIN, CHEMICAL COMPOSITION, PROPERTIES, AND MORPHOLOGY. In: G. WYPYCH, ed, *Handbook of Fillers (Fourth Edition).* ChemTec Publishing, pp. 13-266.

XIA, W., SHEN, W., YU, L., ZHENG, C., YU, W. and TANG, Y., (2016) Conversion of petroleum to methane by the indigenous methanogenic consortia for oil recovery in heavy oil reservoir. *Applied Energy,* **171**, pp. 646-655.

YAN, X., WEI, Z., WANG, D., ZHANG, G. and WANG, J., (2015) Phosphorus status and its sorption-associated soil properties in a paddy soil as affected by organic amendments. *Journal of Soils and Sediments,* **15**(9), pp. 1882-1888.

YAN, C., LI, H., ZHANG, X., ZHU, Y., FAN, X. and YU, L., (2013) Preparation and properties of continuous glass fibre reinforced anionic polyamide-6 thermoplastic composites. *Materials & Design,* **46**, pp. 688-695.

YAN, P., LU, M., YANG, Q., ZHANG, H., ZHANG, Z. and CHEN, R., (2012) Oil recovery from refinery oily sludge using a rhamnolipid biosurfactant-producing Pseudomonas. *Bioresource technology,* **116**, pp. 24-28.

YANG, Q., WANG, H., LIU, Y. and LI, Z., (2010) Solid/liquid separation performance of hydrocyclones with different cone combinations. *Separation and purification Technology,* **74**(3), pp. 271-279.

YOSHIOKA, H., MOCHIMARU, H., SAKATA, S., TAKEDA, H. and YOSHIDA, S., (2015) Methane production potential of subsurface microbes in Pleistocene sediments from a natural gas field of the dissolved-in-water type, central Japan. *Chemical Geology,* **419**, pp. 92-101.

ZHANG, X., HE, Q., GU, H., COLORADO, H.A., WEI, S. and GUO, Z., (2013) Flame-retardant electrical conductive nanopolymers based on bisphenol F epoxy resin reinforced with nano polyanilines. *ACS applied materials & interfaces,* **5**(3), pp. 898-910.

ZHANG, A., LI, M., LV, P., ZHU, X., ZHAO, L. and ZHANG, X., (2016) Disposal and Reuse of Drilling Solid Waste from a Massive Gas Field. *Procedia Environmental Sciences,* **31**, pp. 577-581.

ZHANG, J., TIAN, D., LIN, M., YANG, Z. and DONG, Z., (2016) Effect of resins, waxes and asphaltenes on water-oil interfacial properties and emulsion stability. *Colloids and Surfaces A: Physicochemical and Engineering Aspects,* **507**, pp. 1-6.

ZHANG, Z., XU, G., WANG, F., DONG, S. and CHEN, Y., (2005) Demulsification by amphiphilic dendrimer copolymers. *Journal of colloid and interface science,* **282**(1), pp. 1-4.

ZHONG, L., MAYER, A.S. and POPE, G.A., (2003) The effects of surfactant formulation on nonequilibrium NAPL solubilization. *Journal of contaminant hydrology,* **60**(1–2), pp. 55-75.

ZHOU, Y., RANGARI, V., MAHFUZ, H., JEELANI, S. and MALLICK, P., (2005) Experimental study on thermal and mechanical behavior of polypropylene, talc/polypropylene and polypropylene/clay nanocomposites. *Materials Science and Engineering: A,* **402**(1), pp. 109-117.

ZHOU, S., LUO, W., ZOU, H., LIANG, M. and LI, S., (2015) Enhanced thermal conductivity of polyamide 6/polypropylene (PA6/PP) immiscible blends with high loadings of graphite. *Journal of Composite Materials*.

ZHU, J., ZHU, H., NJUGUNA, J. and ABHYANKAR, H., (2013) Recent Development of Flax Fibres and Their Reinforced Composites Based on Different Polymeric Matrices, *Materials*, **6**(11), pp. 5171-5198

ZOLFAGHARI, R., FAKHRU'L-RAZI, A., ABDULLAH, L.C., ELNASHAIE, S.S.E.H. and PENDASHTEH, A., (2016) Demulsification techniques of water-in-oil and oil-in-water emulsions in petroleum industry. *Separation and Purification Technology,* **170**, pp. 377-407.

Publications:

The following publications have been produced during this research.

Urenna V. Adegbotolu, Kyari Yates, Kerr Matthews, Krzysztof Pielichowski, Agnieszka Leszczynska, Thomsz Majak, James Njuguna (2016) Waste to Want: Polymer nanocomposites using nanoclays extracted from Oil based drilling mud waste: Part II – Abstract

Adegbotolu, U. V., Pollard, P., Yates, K. and Njuguna, J. (2016). Waste to Want: Polymer nanocomposites using nanoclays extracted from Oil based drilling mud waste: Part II. *Materials Science and Engineering* (in view)

James Njuguna, Urenna V. Adegbotolu, Kerr Matthews and Kyari Yates. (2015). A study on polyamide nanocomposite using nanoclays nanofillers reclaimed from oil and drilling fluids and cuttings waste. *Energy challenges and mechanics - Abstract*

Adegbotolu, U. V., Pollard, P., Yates, K. and Njuguna, J. (2014). Waste to Want: Polymer nanocomposites using nanoclays extracted from Oil based drilling mud waste. *Materials Science and Engineering* 64 (2014) 012023 DOI:10.1088/1757-899X/64/1/012023.

Ekeh-Adegbotolu U V, Ekeh O M and Wegwu M O (2012). Cleanup of Crude Oil Polluted Sites. Using Arachis hypogaea L. (Groundnut) and Biostimulants. SPE-162968-MS

Media release:

Urenna Ekeh-Adegbotolu (2014) Demulsification and the benefits of eco-friendly offshore waste management. Available at http://www.offshore-technology.com/features/featuredemulsification-and-the-benefits-of-eco-friendly-offshore-waste-management-4379573/. Accessed online: 27/04/2016

Jenny Rush (2014) Research seeks to turn drilling mud green. Available at http://www.rgu.ac.uk/news/research-seeks-to-turn-drilling-mud-green/. Accessed online: 19/09/2016

Presentations:

Adegbotolu, U. V., Njuguna, J., Yates, K. and Matthews, K. H. (Nanostruc 2016). Waste to Want: Polymer nanocomposites using nanoclays extracted from Oil based drilling mud waste. Aberdeen, United Kingdom (Paper presentation)

Urenna V. Adegbotolu, James Njuguna, Kerr Matthews and Kyari Yates. Marine Alliance for Science and Technology for Scotland (MAST) *Polymer*

particles release from consumer nanoproducts and oil & gas production processes (Sept, 2015) (Paper presentation)

Urenna V. Adegbotolu, James Njuguna, Kerr Matthews and Kyari Yates*. 4th international Symposium on Energy Challenges and Mechanics by North Sea Journals and conferences. A study on polyamide nanocomposite using nanoclays nanofillers reclaimed from oil and drilling fluids and cuttings waste*. Nanocomposite International conference Hilton Tree Tops, Aberdeen (Aug 2015) (Paper presentation)

Urenna V. Adegbotolu and Kyari Yates. Robert Gordon University, Aberdeen IDEAS symposium 2014. Chitosan: A begnin and cheap crude oil remedial treatment for North Sea derived produced water (Paper presentation)

Urenna V. Ekeh-Adegbotolu. Institute of Minerals, Mining and Materials Women in Materials Seminar. Shell Aberdeen, UK. *Women in material research. 29 Apr 2014* (Paper presentation)

Ekeh-Adegbotolu U V, Ekeh O M and Wegwu M O (2012). Cleanup of Crude Oil Polluted Sites. Using Arachis hypogaea L. (Groundnut) and Biostimulants. SPE Abuja, Nigeria (Paper presentation)

Adegbotolu, U. V., Pollard, P., Yates, K. and Njuguna, J. (Nanostruc 2014). Waste to Want: Polymer nanocomposites using nanoclays extracted from Oil based drilling mud waste. Madrid, Spain. (Poster presentation)

Adegbotolu, U. V., Yates, K., Njuguna, J. (Nanostruc 2016). Waste to Want: Polymer nanocomposites using nanoclays extracted from Oil based drilling mud waste. Aberdeen, United Kingdom (Poster presentation)

Ekeh-Adegbotolu, U. V., Pollard, P., Yates, K. and Njuguna, J. Waste to Want: Polymer nanocomposites using nanoclays extracted from Oil based drilling mud waste. 8th Annual Environmental and Clean Technology Conference 2014 Scottish Environmental Technology Network

Urenna V. Adegbotolu, Pat Pollard and Kyari Yates. Robert Gordon University, Aberdeen IDEAS symposium 2013. New Demulsifier for produced water and oil based drilling fluid treatment to reduce hydrocarbon discharge (Poster presentation)

Urenna V. Adegbotolu, Pat Pollard and Kyari Yates. RSC Early Analytical Professionals 4-6th of April, 2014 ETP sponsored in Penrith, United Kingdom New Demulsifier for oil based drilling fluid treatment to reduce hydrocarbon discharge (Poster presentation)

Urenna V. Adegbotolu, Pat Pollard and Kyari Yates. RSC Environmental Group Conference 2013, New Demulsifier for produced water and oil based drilling fluid treatment. University of Glasgow. (Poster presentation)

Awards:

Won the first place in the Scottish Environmental Technology Network (SETN) Student Poster Contest (PhD Division), for "Waste to Want: Polymer nanocomposites using nanoclays extracted from Oil based drilling mud waste" **Ekeh-Adegbotolu, U. V., Pollard, P., Yates, K. and Njuguna, J.** The award was presented at the 8th Annual Environmental and Clean Technology Conference 2014 Scottish Environmental Technology Network held on Thursday 26th June, 2014 in Radisson BLU Hotel, Glasgow, Scotland, United Kingdom. Scottish Environmental Technology Network (SETN) http://www.setn.org.uk/wordpress/setnconference.

Appendix A

Table A.1 Summary of international and regional agreements pertaining to offshore oil and gas industry

International agreement	Authority	Year of enactment
Convention on the prevention of marine pollution by dumping of waste and other matter	IMO	1972
International convention for the prevention of pollution from ships (MARPOL 78/79)	IMO	1978
United Nations convention on the law of the Sea	UN	1982
United Nations conference on environment and development	UN	1992
Integrative Pollution Prevention control directive	European Union Directives 96/61/EC	1996
European Hazardous Waste Directive (91/689/EEC)	European Union Directives	1991
Registration, evaluation, authorisation and restriction of chemicals (REACH) EU Regulation 1907/2006 - information on substances notified under Directive 67/548/EEC	European Union Directives	2006
Dangerous substance and explosives atmosphere regulation (DSEAR, 2006)	European Union Directives	2006
European Union (EU) directive of dangerous substances (Directive 79/831/EEC)	European Union Directives	
Landfill directive 1999/31/EC	European Union Directives	1999

International agreement	Authority	Year of enactment
Waste Framework Directive 2008/98/EC	European Union Directives	2008
Waste Incineration Directive 2000/76/EC	European Union Directives	2000
Environmental Impact Assessment Directive 2011/92/EU	European Union Directives	2011
Regional agreement	**Authority**	**Year of enactment**
Convention for the protection of the North East Atlantic marine environment Oslo-Paris (OSPAR) convention	Member countries (Belgium, Denmark, Finland, France, Germany, Iceland, Ireland, the Nertherlands, Noorway, Portugal, Spain, Sweden and United Kingdom	1992

Table A. 2 Comparison of regulation pertaining to oil and gas industry which affect waste management. Source: UK Department of Trade and industry (DTI), API Guidance document E5: waste management in E&P operations.

Regulatory topic	UK		
	Legislation	Regulatory authority	Description of Legislation
Exploration and production waste	Petroleum act, 1988	DTI	Requires operators to possess a license for exploration, development, production and abandonment of oil fields. To ensure that all available practises and methods must be used to prevent waste discharge into the environment
Environmental impact assessment/ Environmental impact statement and Air quality	Environmental impact assessment (Scotland) Regulations 1999; Town and county planning (England and Wales) regulations 1999	Local authorities	To assess impact of future developments on the environment; For air quality: create air quality objectives as well as improvement plans with regards to air po pollutants such as Nitrogen dioxide, Sulphur dioxide, carbon monoxide, lead and particulates.

Transport (hazardous waste)	EC regulation (259/93), Trans frontier shipment of waste, 1994	DEFRA, EA, SEPA	Requirement of license for waste shipment and disposal
Transport (non-hazardous waste)/ Pipelines	Pipelines Act, 1962 (amended 2000); Works Regulations, 2000; Gas Act, 1986, Public Gas Transporter Pipeline Works Regulations, 1999	DTI	Regulates petroleum products transport via pipelines, requirement, reporting and inspections, prevention and avoidance of Environmental impacts
Ground water	EC Directive (80/68/EEC); Groundwater regulations, 1998	EA, SEPA	To protect groundwater from discharge, regulate injection well.
Surface water impact/ Spill planning and response	Pollution prevention and control act, 1999, and Regulations, 2000	EA, SEPA, Local authority	
Hazardous waste control and disposal /Hazardous waste cleanup	Waste management licensing regulations, 1994	EA, SEPA	Stipulates that hazardous wastes management and disposal must be carried out using safe, acceptable and environmentally sound procedures. Under the Environmental Waste catalogue, hazardous waste is classified as toxic, poisonous explosive, corrosive, flammable, infectious, or eco-toxic.

Table A. 3 Ecotoxicological assessment criteria (EAC) as determined at the Workshop on Ecotoxicological Assessment Criteria for biota (November 1995, Berlin, Germany) and reported to the OSPAR Environmental and Assessment and Monitoring Committee (ASMO) (Ref: ASMO 96/9/11-E(L))

Substance	Water (µg/l)	Sediment (mg/kg	Fish (mg/kg	Mussel (mg/kg
TRACE METALS				
As	1-10	1-10 (p)	n.r.	n.r.
Cd	0,01-0,1 (f)	0,1-1 (p)	f.c.	f.c.
Cr	1-10	10-100 (p)	n.r.	n.r.
Cu	0,005-0,05 (f)[1]	5-50 (p)	f.c.	f.c.
Hg	0,005-0,05 (f)	0,05-0,5 (p)	f.c.	f.c.
Ni	0,1-1	5-50 (p)	n.r.	n.r.
Pb	0,5-5	5-50 (p)	f.c.	f.c.
Zn	0,5-5	50-500 (p)	n.r.	n.r.
ORGANOCHLORINE PESTICIDES				
DDE	n.r.	0,0005-0,005 (p)	0,005-0,05	0,005-0,05 (f)
Dieldrin	n.r.	0,0005-0,005 (p)	0,005-0,05	0,005-0,05 (f)
Lindane	0,0005-0,005	n.r.	0,0005-	n.r.
PAHs				
Naphthalene	5-50	0,05-0,5 (f)	n.r.	0,5-5 (p)
Phenanthrene	0,5-5	0,1-1 (f)	n.r.	5-50 (p)
Anthracene	0,001-0,01 (p)	0,05-0,5 (f)	n.r.	0,005-0,05 (p)
Fluoranthene	0,01-0,1 (p)	0,5-5 (p)	n.r.	1-10 (p)
Pyrene	0,05-0,5 (p)	0,05-0,5 (p)	n.r.	1-10 (p)
Benz[*a*]anthracene	n.d.	0,1-1 (p)	n.r.	n.d.
Chrysene	n.d.	0,1-1 (p)	n.r.	n.d.
Benzo[*k*]fluoranthen	n.d.	n.d.	n.r.	n.d.
Benzo[*a*]pyrene	0,01-0,1 (p)	0,1-1 (p)	n.r.	5-50 (p)
Benzo[*ghi*]perylene	n.d.	n.d.	n.r.	n.d.
Indeno[123-	n.d.	n.d.	n.r.	n.d.
ΣPCB_7	n.r.	0,001-0,01 (p)	0,001 – 0,01	0,005-0,05 (f)
TBT	0,00001-	0,000005-	n.r.	0,001-0,01 (f)

f = firm p = provisional f.c. = for future consideration dw = dry weight fw = fresh weight

n.r. = not relevant in relation to the current monitoring programme n.d. = no data available or insufficient data available [1]this range is within the background range for natural water. This value should be compared to the bioavailable fraction of Cu in seawater

Appendix B

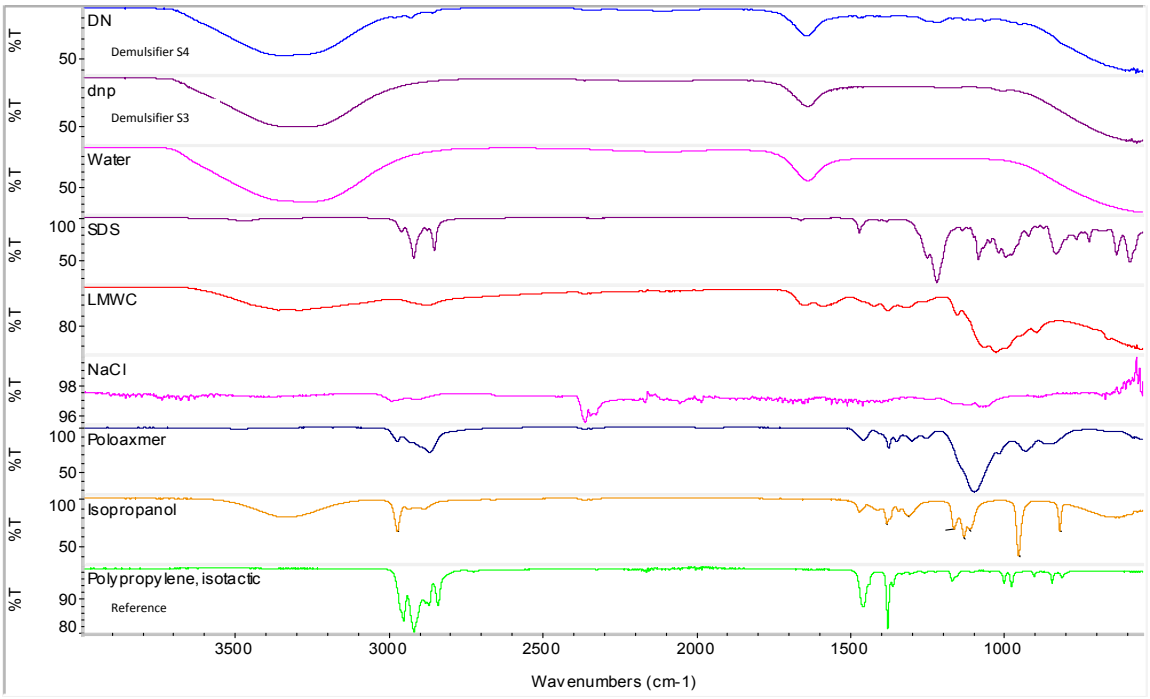

Figure B. 1 Stacked FTIR-ATR of demulsifier component

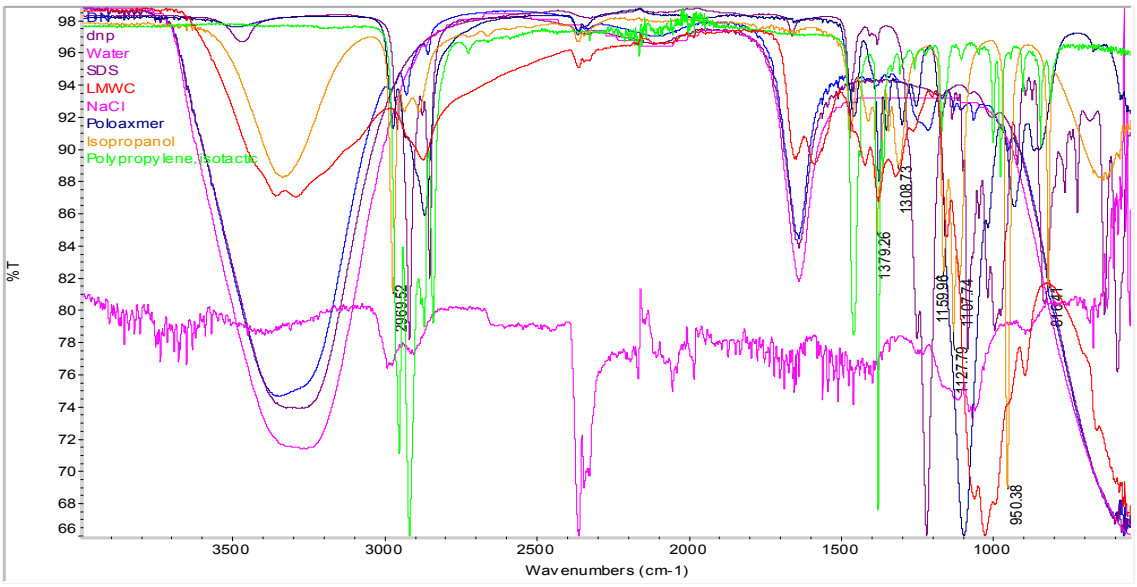

Figure B. 2 Overlayed FTIR-ATR of demulsifier component

Appendix C

Table C. 1 Leaching test (1 hour)

	Leaching test 1 hour (mg/L)							
Elements	**P**	**Cd**	**Cr**	**Ni**	**Pb**	**Zn**	**Cu**	**Ba**
PA6	nd	nd	nd	nd	nd	nd	nd	nd
PA6/S2	nd	nd	nd	nd	nd	0.082	nd	nd
PA6/S3	nd	nd	nd	nd	nd	0.183	nd	nd
PA6/S4	nd	nd	nd	nd	nd	0.106	nd	nd
PA6/S5	nd	nd	nd	nd	nd	nd	nd	nd
PA6/S6	nd	nd	nd	nd	nd	nd	nd	nd
PA6/GF30	nd	nd	nd	nd	nd	nd	nd	nd
PA6/S2/GF30	nd	nd	nd	nd	nd	0.118	nd	nd
PA6/S3/GF15	nd	nd	nd	nd	nd	nd	nd	nd
PA6/S3/GF30	nd	nd	nd	nd	nd	0.053	nd	nd
PA6/S4/GF30	nd	nd	nd	nd	nd	nd	nd	nd
PA6/S5/GF30	nd	nd	nd	nd	nd	1.132	nd	nd
PA6/S6/GF30	nd	nd	nd	nd	nd	0.878	nd	nd

Table C. 2 Leaching test (24 hours)

	Leaching test 24 hours (mg/L)							
Elements	**P**	**Cd**	**Cr**	**Ni**	**Pb**	**Zn**	**Cu**	**Ba**
PA6	nd	nd	nd	nd	nd	0.073	nd	nd
PA6/S2	nd	nd	nd	nd	nd	0.018	nd	nd
PA6/S3	nd	nd	nd	nd	nd	0.005	nd	nd
PA6/S4	nd	nd	nd	nd	nd	0.027	nd	nd
PA6/S5	nd	nd	nd	nd	nd	0.16	nd	nd
PA6/S6	nd	nd	nd	nd	nd	0.096	nd	0.13
PA6/GF30	nd	nd	nd	nd	nd	0.082	nd	nd
PA6/S2/GF30	nd	nd	nd	nd	nd	0.376	nd	nd
PA6/S3/GF15	nd	nd	nd	nd	nd	0.043	nd	nd
PA6/S3/GF30	nd	nd	nd	nd	nd	0.025	nd	nd
PA6/S4/GF30	nd	nd	nd	nd	nd	nd	nd	0.055
PA6/S5/GF30	nd	nd	nd	nd	nd	0.056	nd	nd
PA6/S6/GF30	nd	nd	nd	nd	nd	0.342	nd	0.055

Appendix D

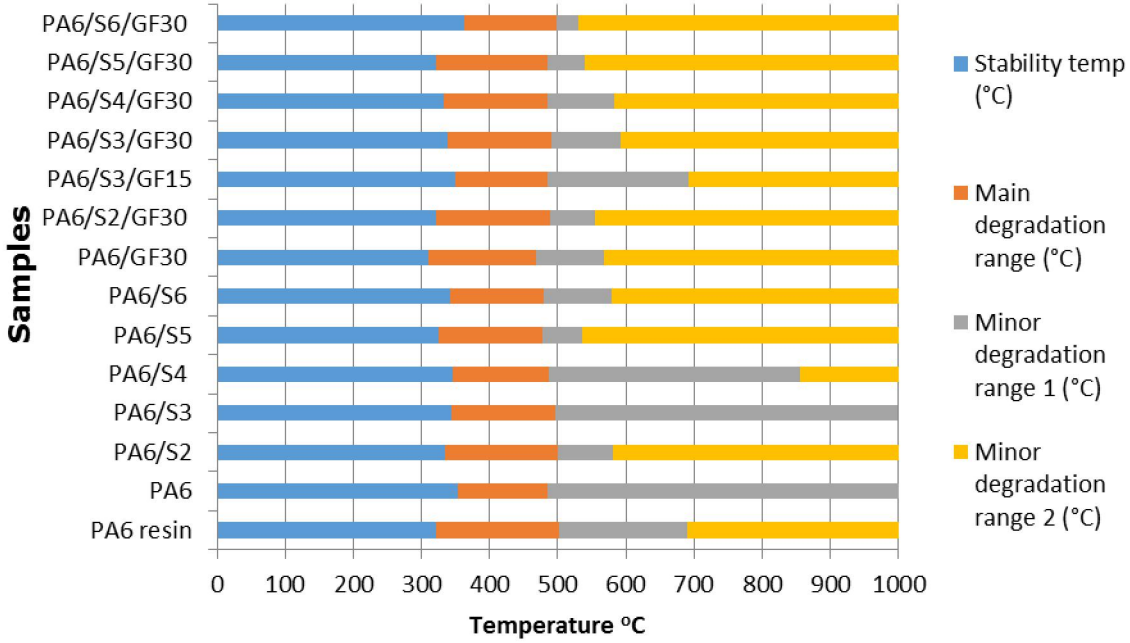

Figure D. 1 TGA Phase stability and degradation of PA6 and PA6 nanocomposite

Table D. 1 DSC data of PA6 and its nanocomposite materials at 10°C/min

	Process	Heating 1			Cooling		Heating 2			
	Samples	T_m1 (°C)	T_m2 (°C)	Enthalpy ΔH_m []	T_c (°C)	Enthalpy ΔH_m [	T_m1 (°C)	T_m2 (°C)		Enthalpy ΔH_m []
n.	PA6 melt comp'd	223.06		52.95	170.83	60.68	221.44			56.52
1.	PA6	214.44	223.18	56.02	187.44	57.79	214.44	221.11		49.29
2.	PA6/S6	210.93	221.69	60.84	187.72	55.32	213.57	220.60		45.31
3.	PA6/S2	212.06	222.50	57.81	192.83	43.75	212.15	220.73		50.07
4.	PA6/S3	213.19	223.08	55.56	187.11	51.52	214.70	221.49		43.63
5.	PA6/S4	213.94	221.86	58.30	188.23	51.65	207.54	214.44	220.73	48.01
6.	PA6/S5	212.31	222.88	61.12	187.94	58.92	214.16	221.55		45.38
7.	PA6/GF30	0	221.91	35.23	189.69	36.96	214.73	220.98		32.51
8.	PA6/S6/GF30	0	211.57	50.37	187.56	40.44	211.57	219.16		37.32
9.	PA6/S2/GF30	212.17	221.32	39.69	188.51	35.47	209.60	213.59	220.01	32.32
10.	PA6/S3/GF15	0	221.74	41.40	189.	44.42	214.73	220.98		38.59
11.	PA6/S3/GF30	0	222.45	38.87	189.	38.55	214.44	220.85		33.70
12.	PA6/S4/GF30	213.19	222.23	37.57	189.15	38.45	213.94	220.73		33.46
13.	PA6/S5/GF30	210.93	221.48	40.94	189.55	35.36	213.94	220.35		33.10
14.	PA6 unprocessed pellet	0	212.64	52.95	170.38	60.68	0	221.44		56.52

Appendix E

This is the free Material Data Center Datasheet of Tarnamid® T-30 - PA6 - Grupa Azoty S.A.

Material Data Center offers the following functions for **Tarnamid® T-30**:
unit conversion, PDF datasheet print, comparison with other plastics, snap fit calculation, beam deflection calculation, CAE interfaces

Check here, which other Tarnamid datasheets, application examples or technical articles are available in Material Data Center

Use the following short links to get directly to the properties of interest in this datasheet:
Rheological properties - Mechanical properties - Thermal properties - Electrical properties - Other properties - Material specific properties

Any use of this information falls under the rules of our disclaimer.

Rheological properties	dry / cond	Unit	Test Standard
ISO Data			
Melt volume-flow rate, MVR	25 / *	cm³/10min	ISO 1133
Temperature	275 / *	°C	-
Load	5 / *	kg	-
Molding shrinkage, parallel	1.4 / *	%	ISO 294-4, 2577
Molding shrinkage, normal	1.4 / *	%	ISO 294-4, 2577

Mechanical properties	dry / cond	Unit	Test Standard
ISO Data			
Tensile Modulus	2800 / 1100	MPa	ISO 527-1/-2
Yield stress	78 / 45	MPa	ISO 527-1/-2
Strain at break	>50 / >50	%	ISO 527-1/-2
Charpy impact strength, +23°C	N / N	kJ/m²	ISO 179/1eU
Charpy impact strength, -30°C	N / N	kJ/m²	ISO 179/1eU
Charpy notched impact strength, +23°C	6 / 13	kJ/m²	ISO 179/1eA
Charpy notched impact strength, -30°C	3 / 3	kJ/m²	ISO 179/1eA
Flexural modulus, 23°C	2400 / 900	MPa	ISO 178
Izod impact notched, 23°C	4 / 10	kJ/m²	ISO 180/1A
Ball indentation hardness	140 / 60	MPa	ISO 2039-1

Thermal properties	dry / cond	Unit	Test Standard
ISO Data			
Melting temperature, 10°C/min	221 / *	°C	ISO 11357-1/-3
Temp. of deflection under load, 1.80 MPa	60 / *	°C	ISO 75-1/-2
Vicat softening temperature, 50°C/h 50N	195 / *	°C	ISO 306
Coeff. of linear therm. expansion, parallel	110 / *	E-6/K	ISO 11359-1/-2
Coeff. of linear therm. expansion, normal	120 / *	E-6/K	ISO 11359-1/-2
Burning behav. at thickness h	HB / *	class	IEC 60695-11-10
Thickness tested	3.2 / *	mm	-

Electrical properties	dry / cond	Unit	Test Standard
ISO Data			
Relative permittivity, 1MHz	3.5 / 4.2	-	IEC 60250
Dissipation factor, 1MHz	220 / 2000	E-4	IEC 60250
Volume resistivity	1E13 / 1E10	Ohm*m	IEC 60093
Surface resistivity	* / 1E13	Ohm	IEC 60093
Electric strength	21 / 24	kV/mm	IEC 60243-1
Comparative tracking index	600 / 600	-	IEC 60112

Other properties	dry / cond	Unit	Test Standard
ISO Data			
Water absorption	9.5 / *	%	Sim. to ISO 62
Humidity absorption	3 / *	%	Sim. to ISO 62
Density	1140 / -	kg/m³	ISO 1183

Material specific properties	dry / cond	Unit	Test Standard
ISO Data			
Viscosity number	240 / *	cm³/g	ISO 307, 1157, 1628

Characteristics

Processing
Injection Molding, Profile Extrusion, Other Extrusion, Blown Film Extrusion
Delivery form
Granules, Natural Color
Features
Barrier Properties
Applications
Packaging
Regional Availability
Europe

Disclaimer

Figure E. 1 Tarnamid PA6 MSDS

Table E. 1 Effects of 2.5% nanofiller and 15 and 30% glass fibre on percentage (%) improvement on PA6 flexural properties.

Samples	flexural load-extension (maximum load) (%)	flexural stress-strain (Peak stress) %	flexural load-extension (max extension) %	flexural modulus (%)	flexural strength (%)
PA6/S2	14	14	0.9	19	14
PA6/S3	11	nc	2.8	10	11
PA6/S4	12	nc	3.8	15	12
PA6/S5	8	8.4	-1.9	12	9
PA6/S6	16	nc	-2.83	19	16
PA6/GF30	99	97	nc	328	100
PA6/S2/GF30	80	80	nc	258	81
PA6/S3/GF15	59	56	nc	182	61
PA6/S3/GF30	104	102	nc	358	107
PA6/S4/GF30	100	-15	nc	325	101
PA6/S5/GF30	92	92	nc	276	93
PA6/S6/GF30	119.3	119	nc	216	119

nc= not calculated

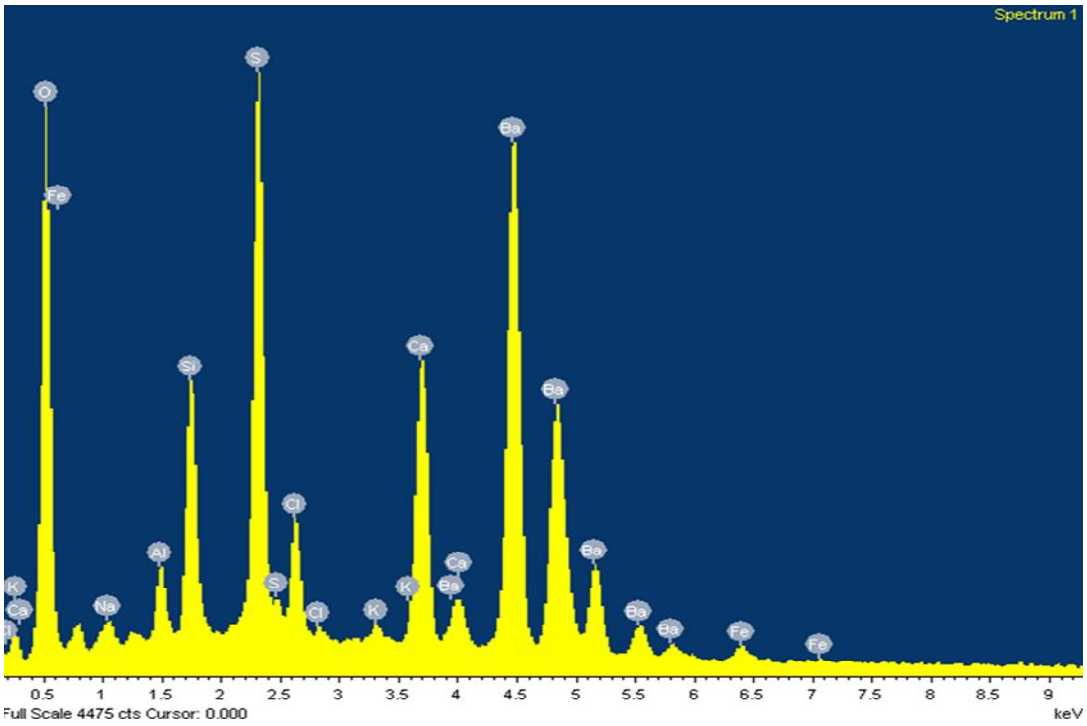

Figure E. 2 EDXA graph of thermally treated oil based drilling fluid (Bakah-Kwoffie 2016)

FTIR-ATR

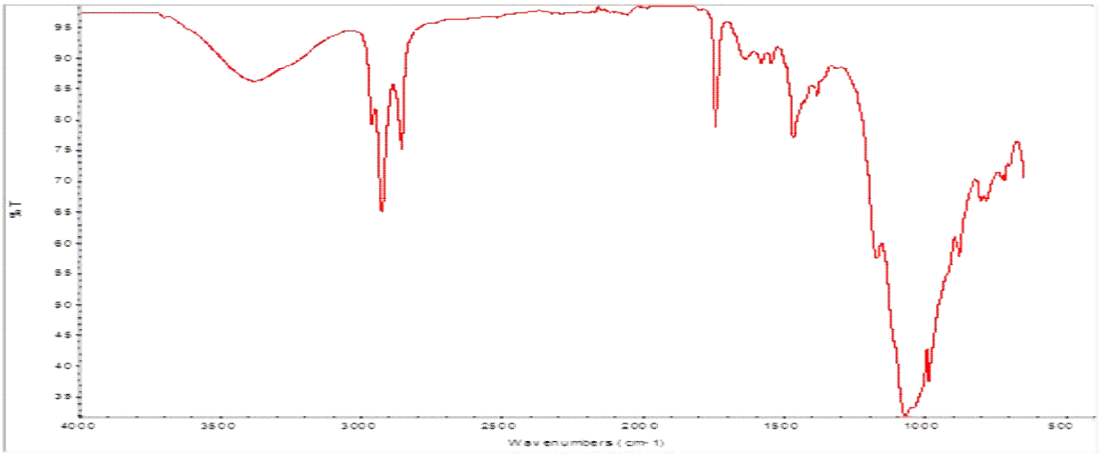

Figure E. 3 FTIR-ATR spectrum of oil based drilling fluid for thermal treatment with TPH concentration of 218,750 mg/kg (Bakah-Kwoffie 2016)

Mechanical results

Combined graphs for compression strength

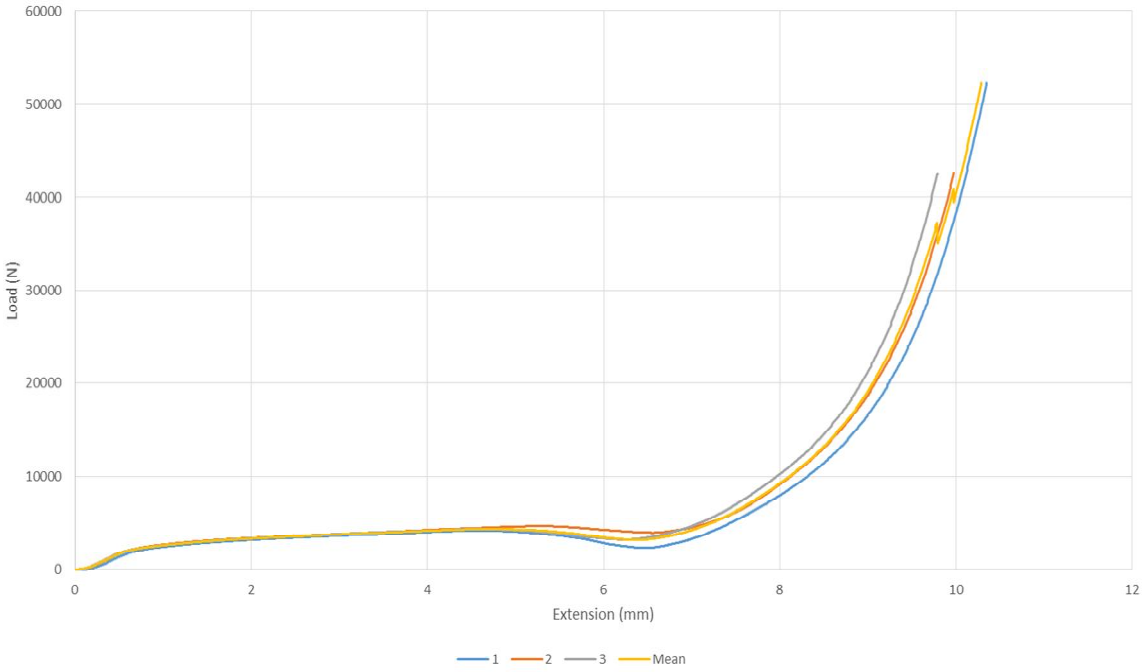

Figure E. 4 Compression strength load vs extension graph of PA6 and PA6 nanocomposites

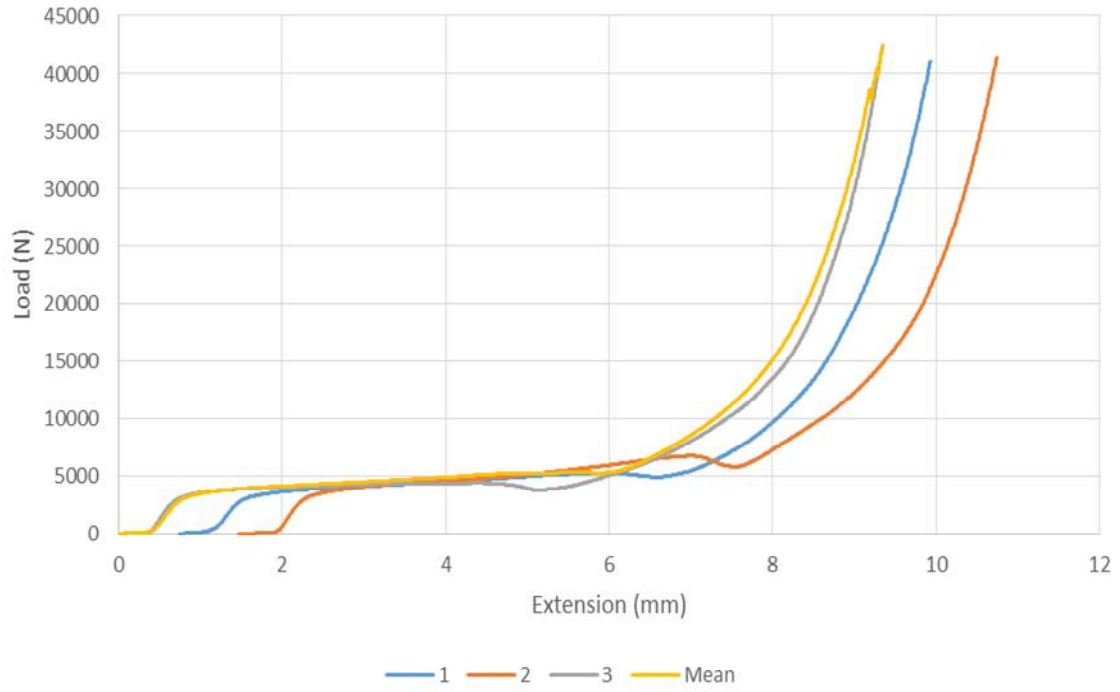

Figure E. 5 Compression strength load vs extension graph of PA6/GF30

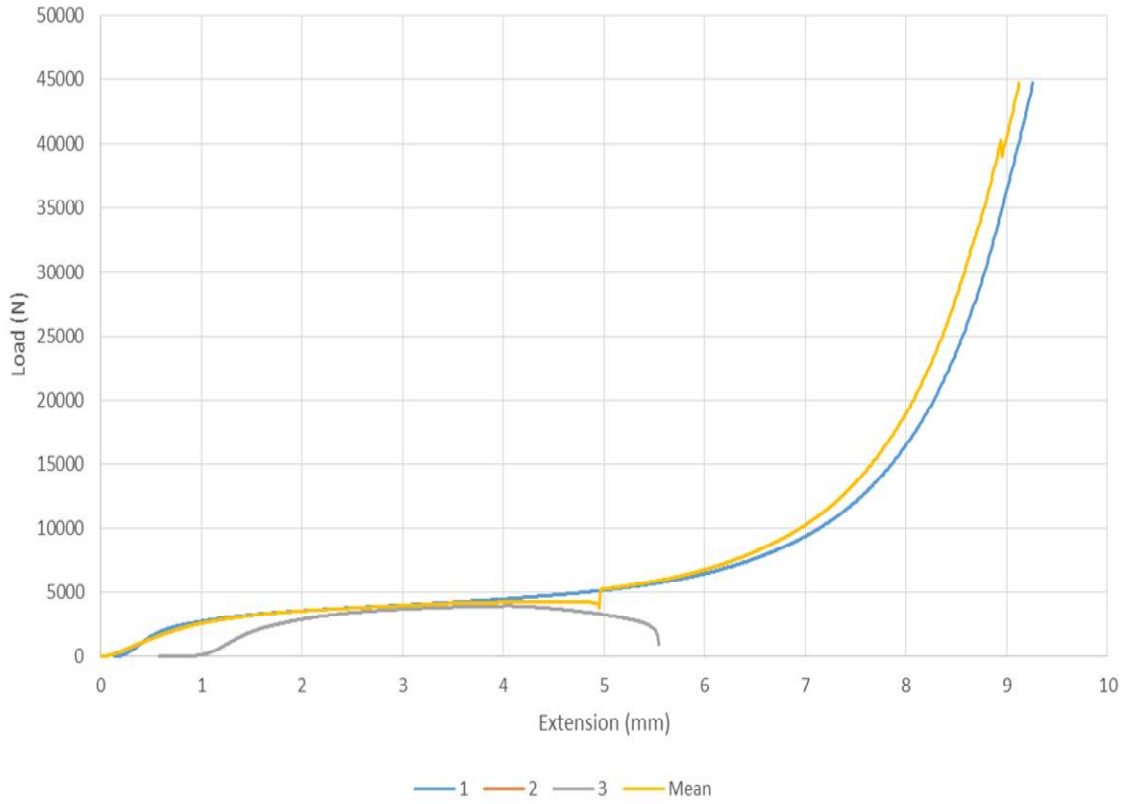

Figure E. 6 Compression strength load vs extension graph of PA6/S3

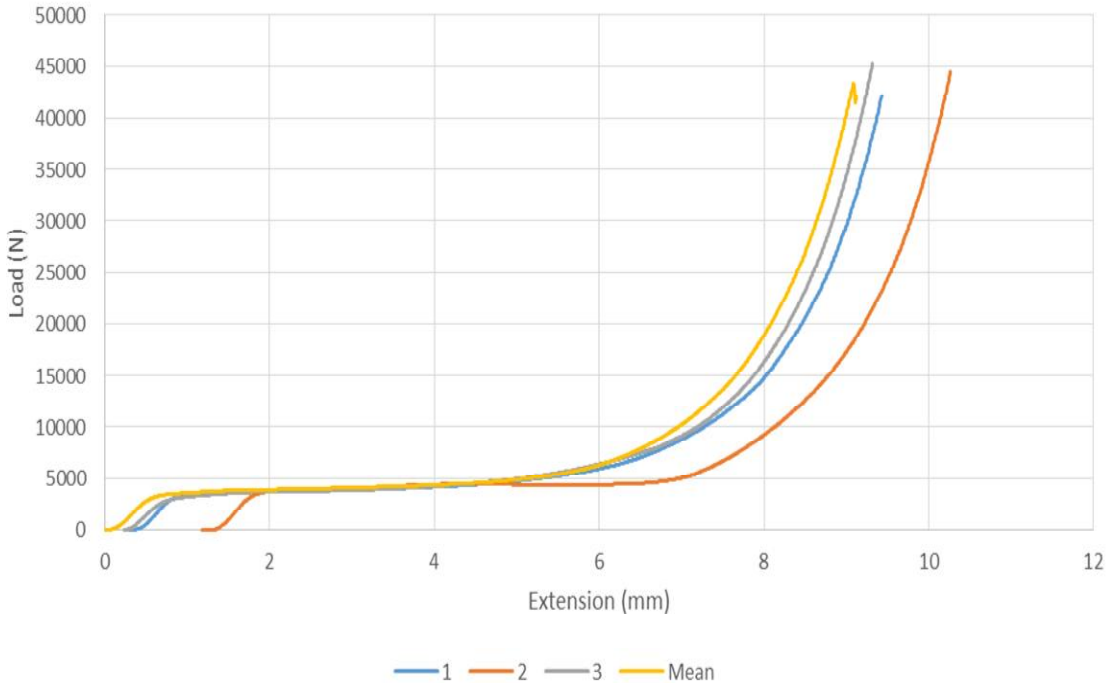

Figure E. 7 Compression strength load vs extension graph of PA6/S3/GF15

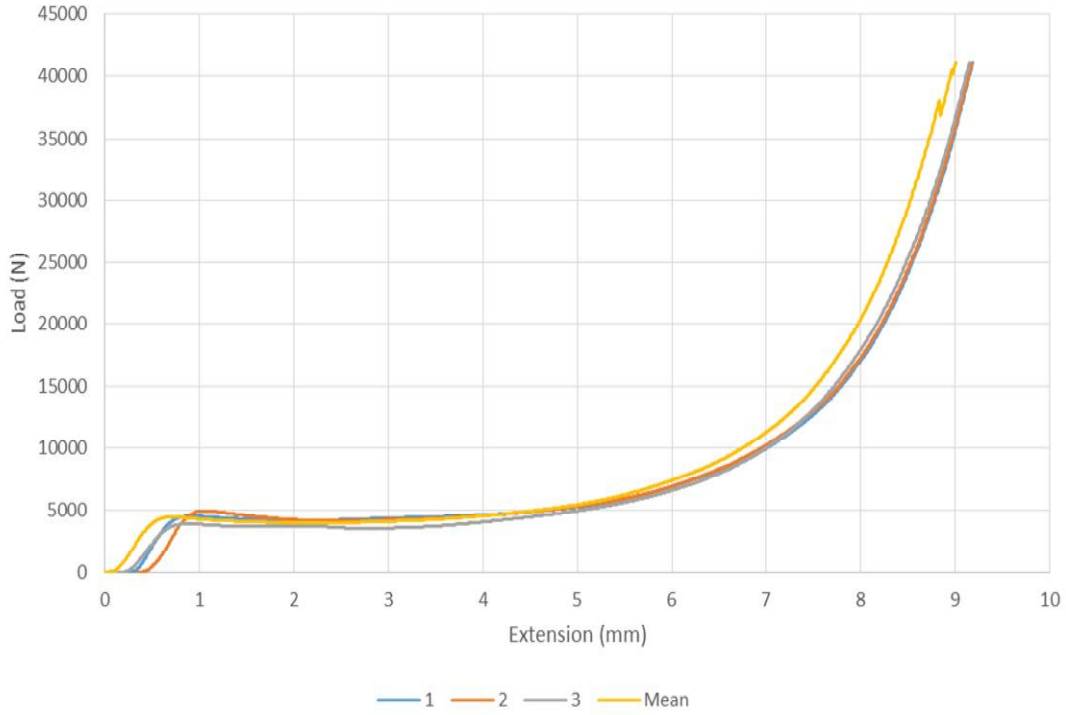

Figure E. 8 Compression strength load vs extension graph of PA6/S3/GF30

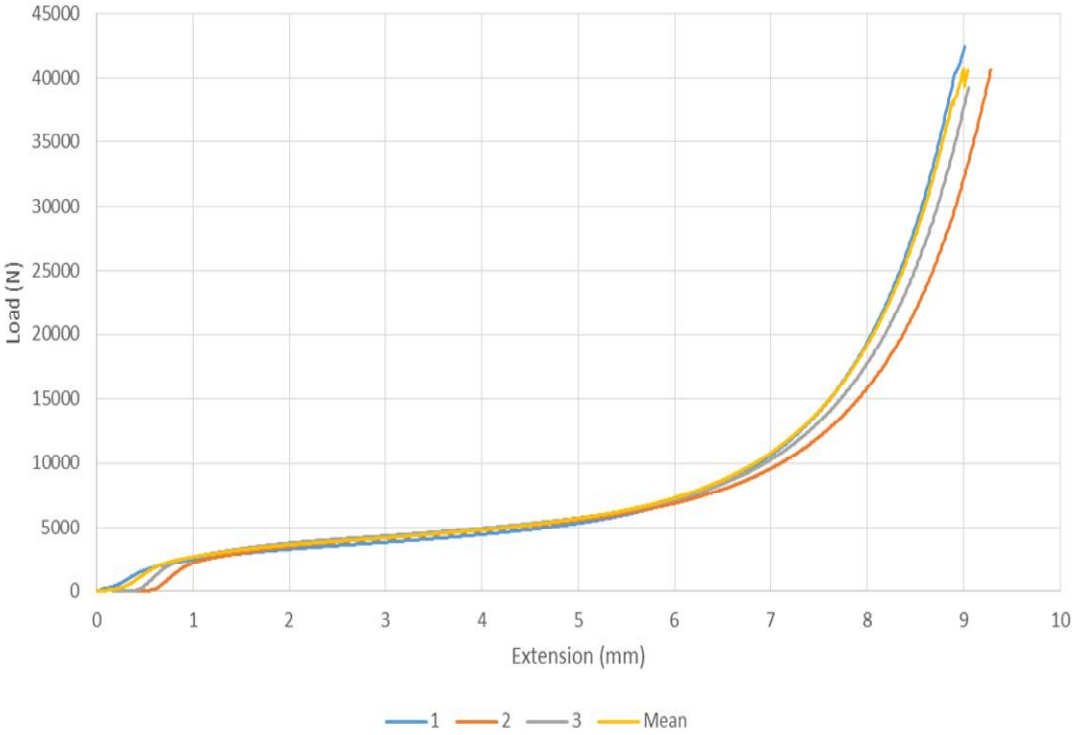

Figure E. 9 Compression strength load vs extension graph of PA6/S5

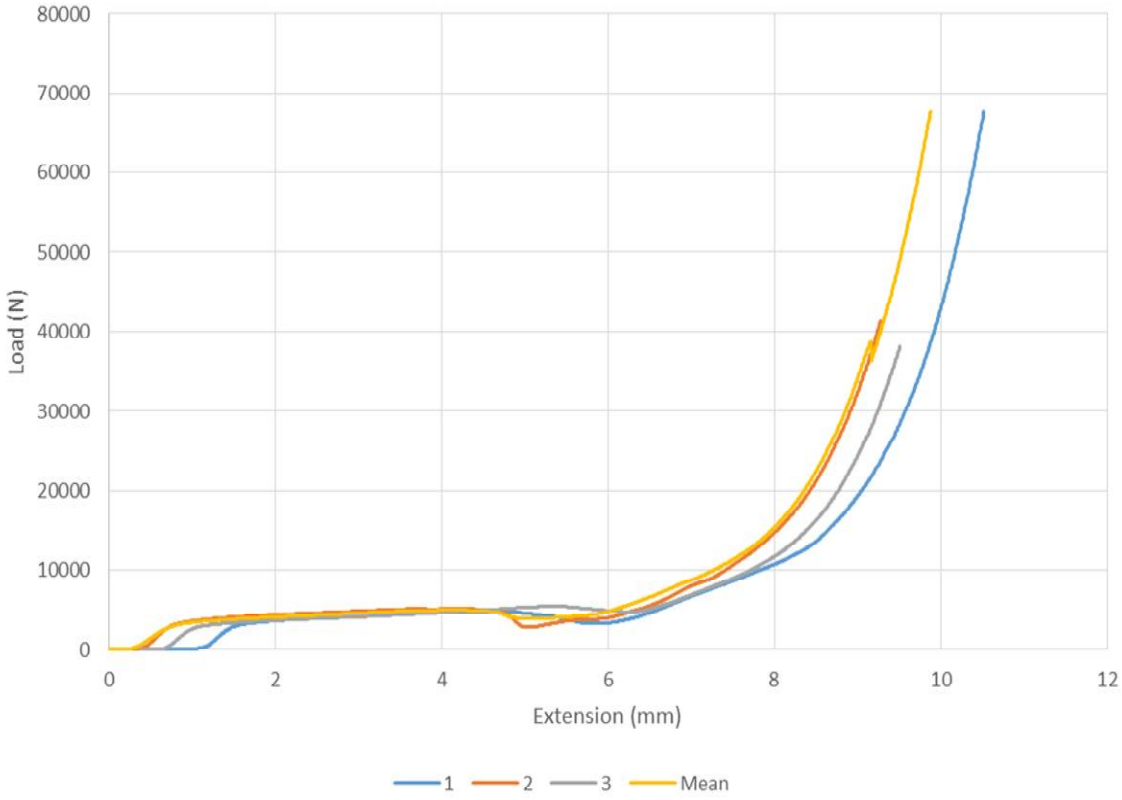

Figure E. 10 Compression strength load vs extension graph of PA6/S5/GF30

Combined graphs for compression Modulus

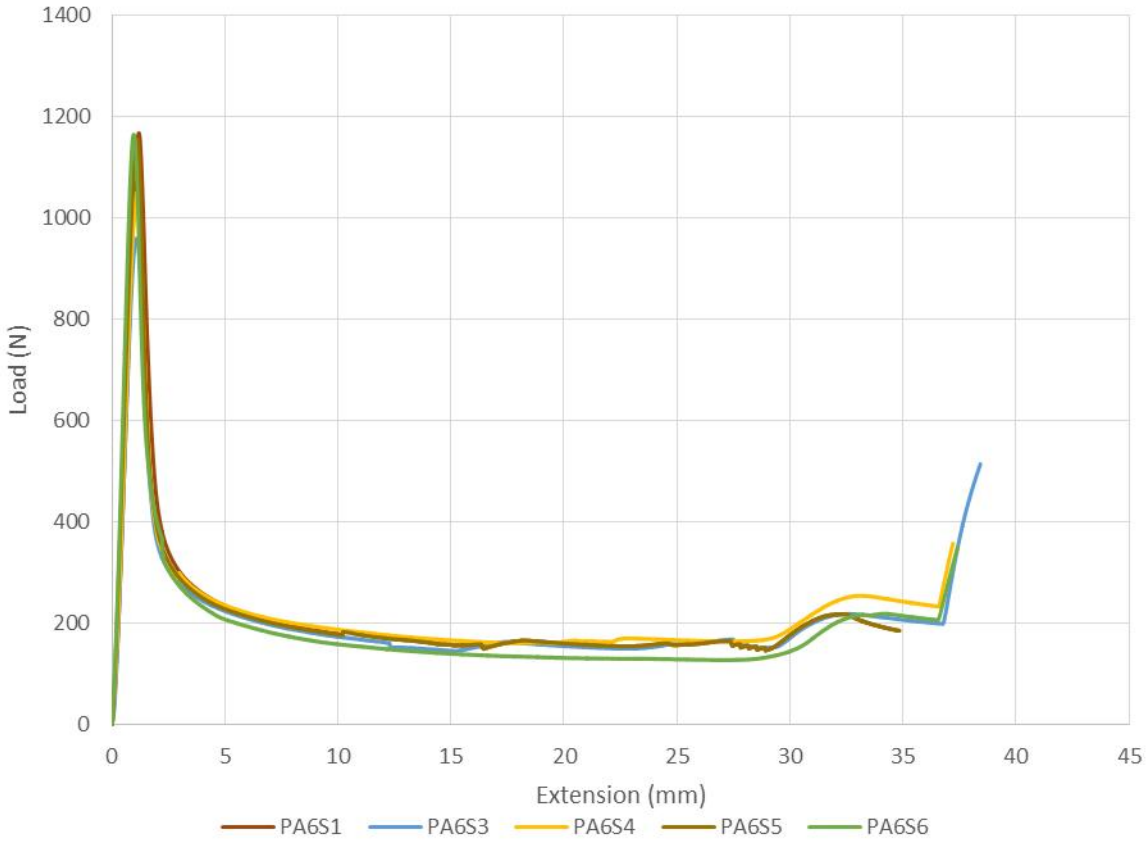

Figure E. 11 Compression modulus load vs extension of PA6 and PA6 nanocomposites

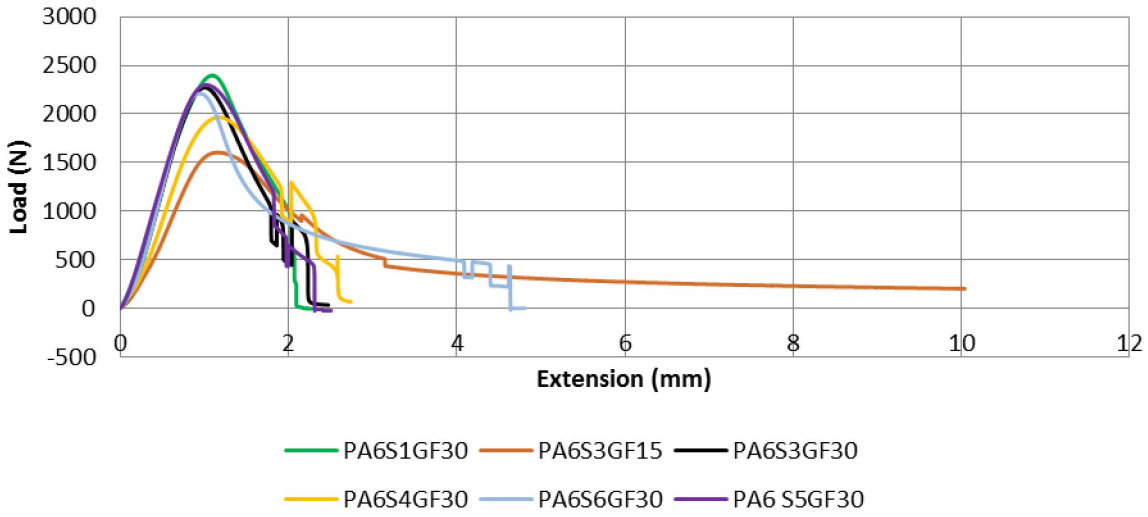

Figure E. 12 Compression modulus load vs extension of PA6

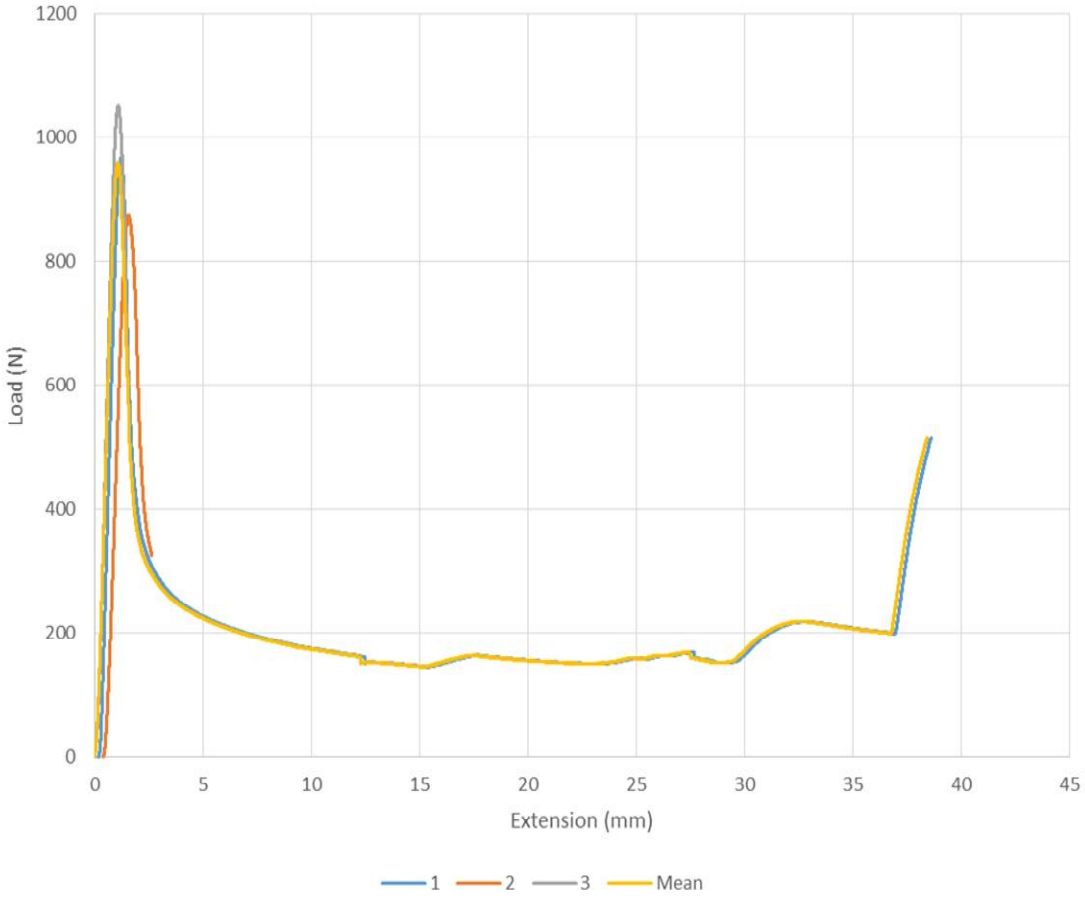

Figure E. 13 Compression modulus load vs extension of PA6/S3

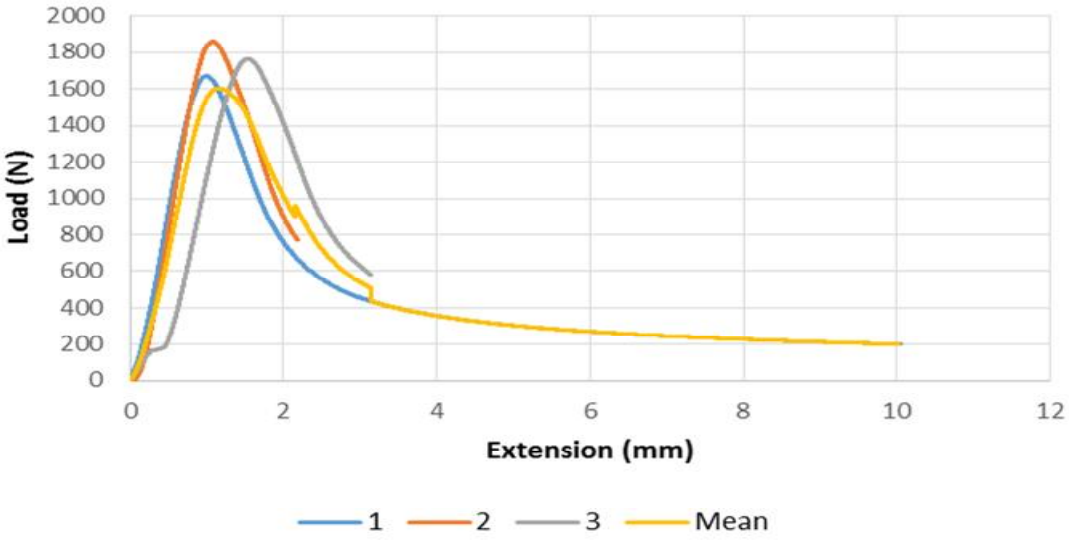

Figure E. 14 Compression modulus load vs extension of PA6/S3/GF15

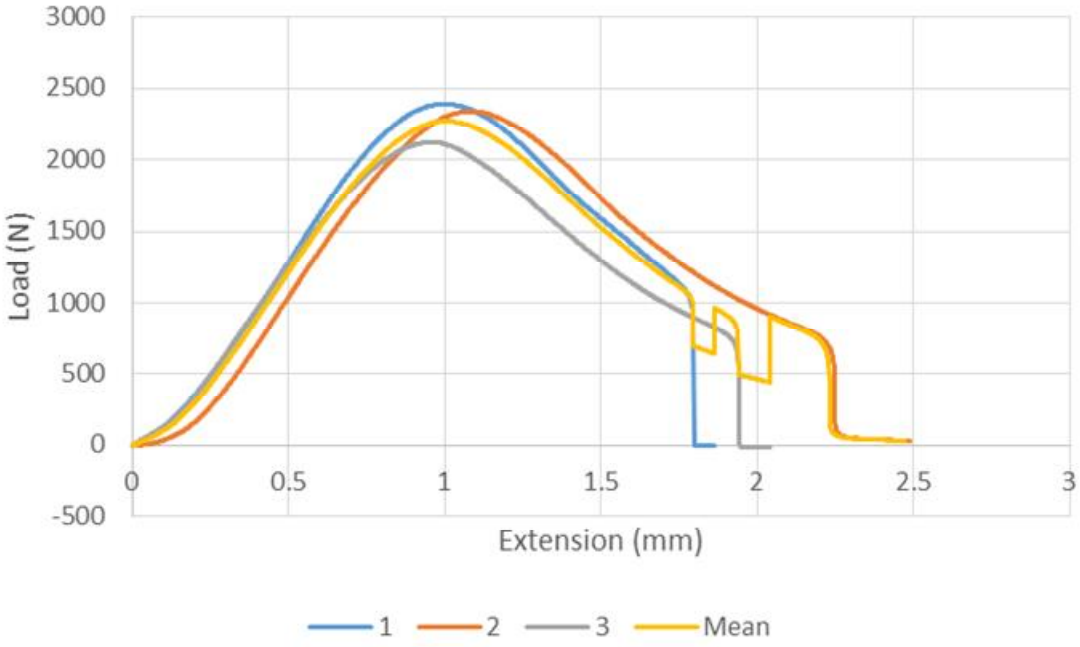

Figure E. 15 Compression modulus load vs extension of PA6/S3GF/30

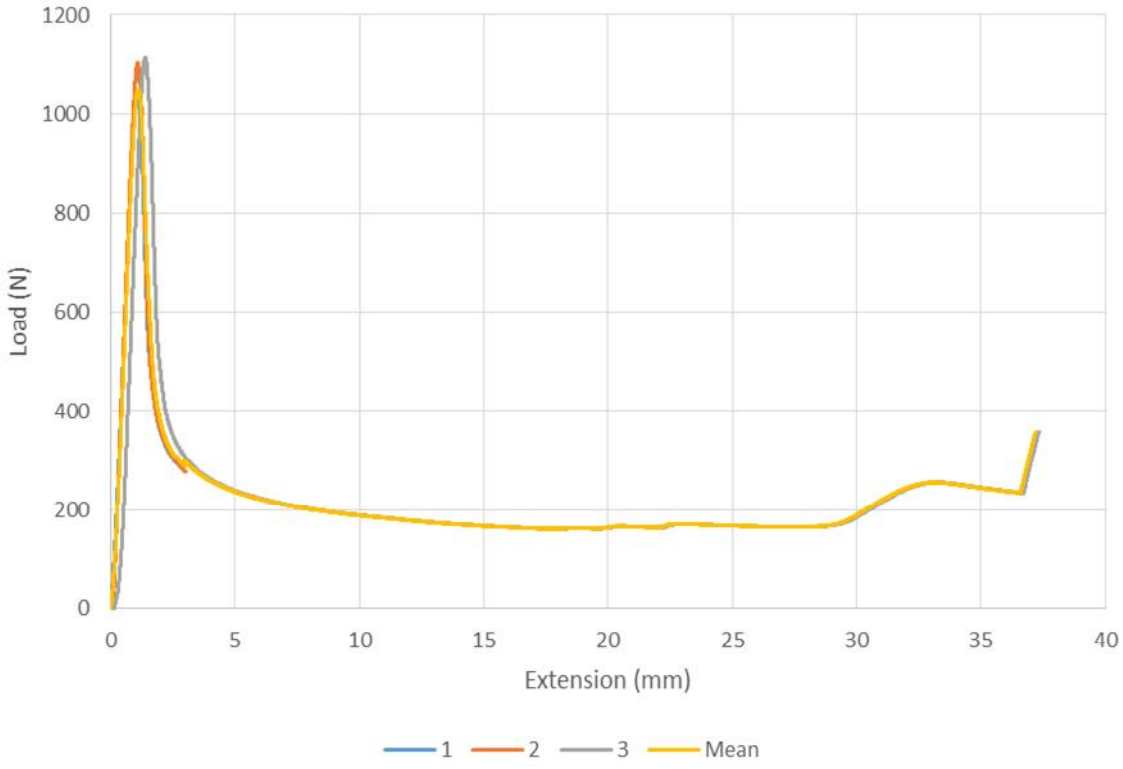

Figure E. 16 Compression modulus load vs extension of PA6/S4

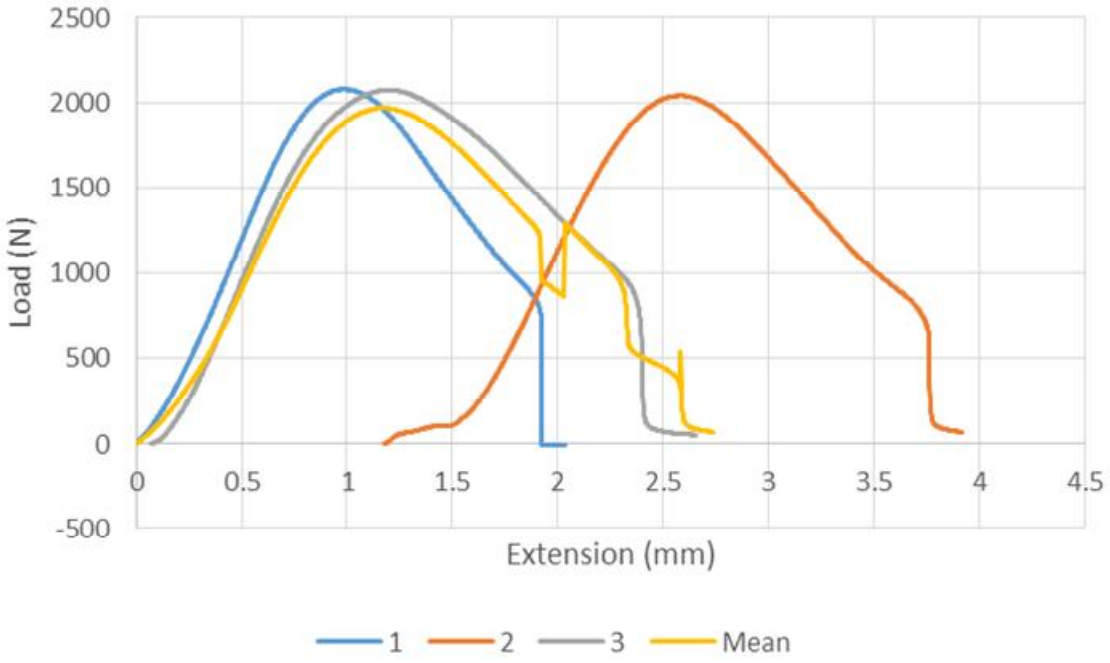

Figure E. 17 Compression modulus load vs extension of PA6/S4/GF30

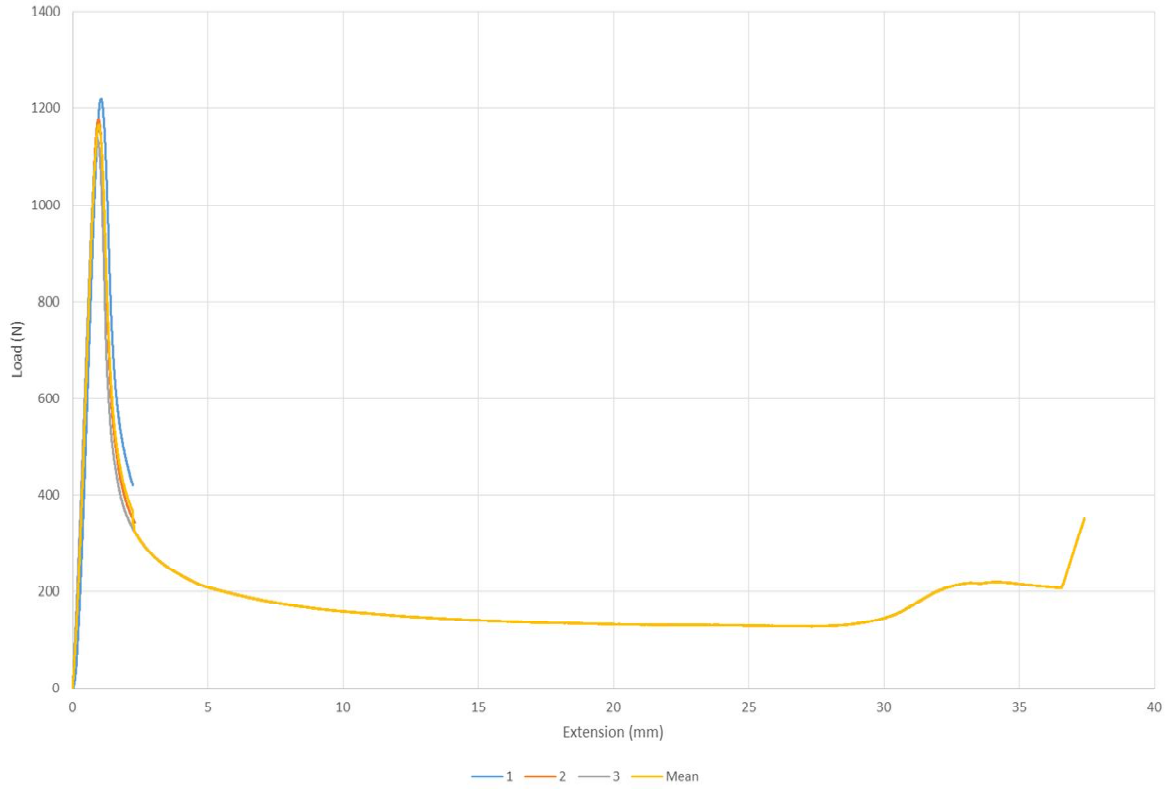

Figure E. 18 Compression modulus load vs extension of PA6/S6

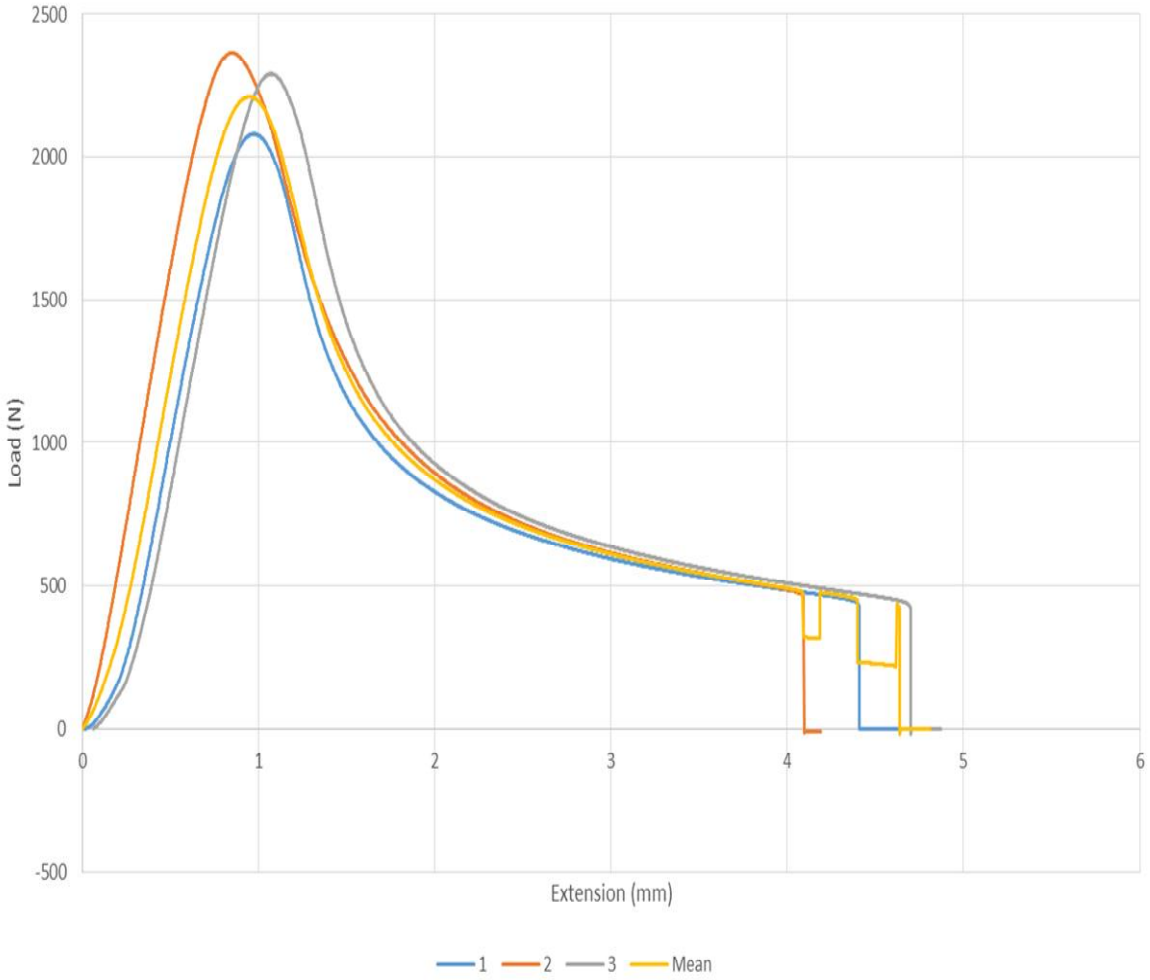

Figure E. 19 Compression modulus load vs extension of PA6/S6/GF30